Effect of top-casting defects and transverse cracks on the corrosion behavior of steel in reinforced concrete exposed to chloride environment

Wulong Zhang

Université Fédérale

Toulouse Midi-Pyrénées

THÈSE

En vue de l'obtention du

DOCTORAT DE L'UNIVERSITÉ DE TOULOUSE

Délivré par l'Institut National des Sciences Appliquées de Toulouse

---

Présentée et soutenue par

WULONG ZHANG

Le 9 avril 2020

Influence des défauts de mise en place du béton et des fissures fonctionelles transversales sur la corrosion des armatures des structures en béton exposées aux chlorures

---

Ecole doctorale : **MEGEP - Mécanique, Energétique, Génie civil, Procédés**

Spécialité : **Génie civil**

Unité de recherche :

LMDC - Laboratoire Matériaux et Durabilité des Constructions de Toulouse

Thèse dirigée par

Raoul FRANCOIS

Jury

M. Kefei LI, Rapporteur
M. Wenjun ZHU, Rapporteur
M. Linwen YU, Examinateur
Mme Zhaohui CHEN, Examinatrice
M. Jean-Philippe CHARRON, Examinateur
Mme Myriam CARCASSES, Examinatrice
M. Raoul FRANCOIS, Directeur de thèse

INSA-TOULOUSE

Département de Génie Civil

Influence des défauts de mise en place du béton et des fissures fonctionelles transversales sur la corrosion des armatures des structures en béton exposées aux chlorures

Thèse de doctorant

Spécialité: Génie Civil

Wulong ZHANG

Jury

M. Kefei LI, Rapporteur

M. Wenjun ZHU, Rapporteur

M. Linwen YU, Examinateur

Mme Zhaohui CHEN, Examinateur

M. Jean-Philippe CHARRON, Examinateur

Mme Myriam CARCASSES, Examinateur

M. Raoul FRANCOIS，Directeur de thèse

Toulouse France April 2020

Auteur: Wulong ZHANG

Titre: Influence des défauts de mise en place du béton et des fissures fonctionelles transversales sur la corrosion des armatures des structures en béton exposées aux chlorures

Thèse de doctorat de l'Institut National des Sciences Appliquées de Toulouse

Spécialité: Génie Civil

Résumé

Le but de la thèse est d'étudier le comportement à la corrosion des armatures dans le béton sous environnement de chlorures, en relation avec l'impact couplés ou non des défauts due au coulage à l'interface acier-béton (nommé «top-casting defects»), de la présence d'une fissure transversale artificielle ou des fissures transversales induites par le chargement mécanique.

Quatre parties principales sont incluses dans cette thèse. La première partie étudie les caractéristiques de l'interface acier-béton, y compris la distribution des bulles d'air à l'interface acier-béton, les propriétés des vides dus au ressuage et la microstructure des produits d'hydratation du ciment à l'interface acier-béton, et l'effet des défauts de coulage sur la pénétration des ions chlorures à l'interface acier-béton. La deuxième partie étudie l'effet des «top-casting defects» et des fissures artificielles sur le comportement à la corrosion des armatures en acier au début de la période de corrosion sous environnement de chlorures, incluant la distribution de la corrosion par piqûres et l'analyse du processus cinétique de corrosion des armatures dans le béton. La troisième partie discute de l'influence des «top-casting defects» sur le comportement à la corrosion des armatures de poutres naturellement corrodées sous une charge maintenue pour une durée d'exposition relativement longue, y compris les cartes de fissuration des poutres, les profils de chlorures, les pertes de section d'acier due à la corrosion et la répartition de la corrosion le long des armatures. La dernière partie s'est intéressée au comportement à la corrosion des étriers utilisés dans les poutres en béton armé sous charge maintenue exposées dans un environnement chloruré depuis plus de 9 ans. Elle se compose des cartes de fissuration des poutres, des cartes de corrosion des étriers et de la perte de section d'acier due à la corrosion des étriers et des barres d'armature principales.

Selon les résultats expérimentaux de la première partie, il a été constaté que des bulles d'air sont principalement apparues à l'emplacement de la zone de nervure du côté inférieur de l'acier Haute

Adhérence (HA) selon la direction de coulage. Des vides dus au ressuage sont toujours apparus à l'interface inférieure de l'acier-béton, tandis que l'interface supérieure de l'acier-béton était plus dense que celle de l'interface inférieure. Des cristaux de Portlandite et d'Ettringite sont principalement formés à l'interface inférieure acier-béton. La présence de vides de ressuage facilite le transport des ions chlorures le long de l'interface acier-béton.

Dans le cas de la deuxième partie, la corrosion s'est amorcée principalement à l'emplacement de la zone de nervure du côté inférieur des armatures selon la direction de coulage en raison de la présence de «top-casting defects». Les barres d'acier dans le béton avec fissure artificielle présentaient un taux de corrosion plus élevé que les barres d'acier dans le béton sans fissure artificielle jusqu'à ce que les chlorures traversent le béton d'enrobage. Ensuite, après cette période, un taux de corrosion similaire a été identifié pour les armatures dans le béton avec ou sans fissure artificielle.

Pour la troisième partie, les «top-casting defects» sont le facteur d'impact le plus significatif accélérant la détérioration du béton armé. Dans le cas des barres de compression, présentant des «top-casting defects», bien que la distribution de la corrosion soit aléatoire, la corrosion était susceptible de se produire du côté inférieur des barres. Sans défauts «top-casting defects», la corrosion était plus importante sur la partie extérieure des barres d'armature faisant face à la surface du béton exposée à la pénétration des chlorures. Après la formation des fissures induites par la corrosion, la corrosion s'est progressivement développée tout autour du périmètre des armatures, de sorte que les défauts «top-casting defects» n'ont plus affecté le processus de corrosion. Dans le cas des barres de traction, avec des défauts «top-casting defects», la corrosion commence au niveau des fissures de service puis se développe préférentiellement à la surface inférieure de la barre de traction. Sans «top-casting defects», la corrosion commence aux fissures de service mais ne se développe pas le long des barres. Ce n'est que lorsque la teneur en chlorure à la profondeur de l'armature atteint une valeur critique que la corrosion se développe le long de l'armature, de préférence à la surface extérieure de la barre en raison de sa teneur en chlorure probablement plus élevée.

Dans le cas de la dernière partie, les parties horizontales des étriers se sont corrodées principalement à mi-portée de la zone de traction (en face des fissures de service) et aux extrémités de la zone de compression des poutres en béton armé quelles que soient les conditions d'exposition,

tandis que les parties horizontales opposées étaient protégées. La corrosion des parties verticales des étriers, qui était légère, n'a pas été affectée par les fissures de service. Il n'y avait pas de corrélation entre la corrosion des étriers et celles des armatures principales. Le comportement à la corrosion de l'intersection entre les étriers et les barres principales a été contrôlé par les conditions de l'interface acier-béton. Le processus de corrosion est influencé par la formation de zones cathodiques et anodiques liées au processus de macro-piles. Dans la première étape de la corrosion, la zone de protection cathodique est principalement située à mi-portée des armatures comprimées. Dans la deuxième période de corrosion, outre la précédente cathode en zone de compression, l'emplacement de la protection cathodique se situe également aux extrémités des armatures tendues.

Mots clés: béton armé, corrosion, chlorures, interface acier-béton, fissure artificielle, fissures de service, étriers d'effort tranchant

Thèse soutenu le 09 Avril 2020 à l'Institut National des Sciences Appliquées devant la commission d'examen composée de:

M. Raoul François (Directeur de these, INSA-Toulouse)

M. Kefei LI (Rapporteur, Tsinghua University)

M. Wenjun ZHU, (Rapporteur, Tongji University)

M. Linwen YU, (Examinateur, Chongqing University)

Mme Zhaohui CHEN, (Examinateur, Chongqing University)

M. Jean-Philippe CHARRON, (Examinateur, Polytechnique Montréal)

Mme Myriam CARCASSES, (Examinateur, Paul Sabatier: Université Toulouse Ⅲ)

Author: Wulong ZHANG

Title: Effect of top-casting defects and cracks on the corrosion behavior of reinforcing steel in concrete under chloride environment

Thèse de doctorat de l'Institut National des Sciences Appliquées de Toulouse

Specialty: Civil Engineering

Abstract

The purpose of the thesis is to investigate the corrosion behavior of reinforcing steel in concrete under chloride environment, in relation to the impact of top-casting-induced defects in the steel-concrete interface, artificial transverse crack and load-induced transverse cracks.

Four main parts are included in this thesis. The first part investigates the characteristics of steel-concrete interface, including the distribution of air bubbles at steel-concrete interface, the properties of bleed water voids and the microstructure of cement hydration products at steel-concrete interface, and the effect of top-casting defects on the chloride ions penetration at steel-concrete interface. The second part studies the effect of top-casting defects and artificial crack on the corrosion behavior of steel rebars in early corrosion period under chloride environment, containing the pitting corrosion distribution and the kinetic process analysis of steel rebar in concrete. The third part discusses the influence of top-casting-induced defects on the corrosion behavior of reinforcing steel of naturally corroded beams under sustained loading in a relative long exposure term, including the cracking maps of RC beams, the chloride profiles, the cross-sectional loss of reinforcing steel and the distribution of corrosion on steel rebars. The last part answered the corrosion behavior of stirrups used in reinforced concrete beams under sustained load exposed in a chloride environment for more than 9 years. It consists of the cracking maps of reinforced beams, the corrosion maps of stirrups and the cross-sectional loss of stirrups and main rebars.

According to the experimental results from the first part, it was found that, air bubbles mainly appeared at the location of the rib zone of the bottom side of deformed steel according to the casting direction. Bleed water voids always appeared at the bottom interface of steel-concrete, while the top interface of steel-concrete was denser compared to that of the bottom interface. Portlandite crystals and ettringites mainly nucleated and grown at the bottom interface of steel-concrete. The presence

of bleed water voids facilitated the transportation of chloride ions at the steel-concrete interface.

In the case of the second part, corrosion mainly initiated at the location of rib zone of the bottom side of steel rebar according to the casting direction due to the presence of top-casting defects. The steel bars in concrete with artificial crack exhibited a higher corrosion rate corrosion compared to the steel bars in concrete without artificial crack in early period. However, after this period, a similar corrosion rate was identified for steel rebars in concrete with or without artificial crack.

For the third part, top-casting defects are the most significantly impacting factor accelerating the deterioration of reinforced concrete. In the case of compressive bars, with top-casting defects, although the distribution of corrosion was random, corrosion was manly prone to occur at the bottom side of compressive bars facing top-casting defects. Without top-casting defects, the corrosion was more prominent on the outside part of rebars facing the concrete surface exposed to chloride ingress. After the presence of corrosion-induced cracks, corrosion gradually developed all around the perimeter of rebars, with the result that top-casting defect no longer affected the corrosion process. In the case of tensile bars, with top-casting-induced defects, corrosion starts at service cracks and then develops preferentially at the bottom surface of the tensile bar. Without top-casting defects, corrosion starts at service cracks but does not develop along the tensile bars. It is only when the chloride content at the depth of reinforcement reaches a critical value that corrosion develops along the tensile bar-preferentially at the outside surface of the rebar because of its probable higher chloride content.

In the case of last part, the horizontal legs of stirrups mainly corroded at the mid span of the tensile zone and at the ends of the compressive zone of the reinforced concrete beams regardless of the exposure conditions, while the opposite horizontal legs were protected. The corrosion of vertical legs of stirrups, which was slight, was not impacted by the load-induced cracks. There was no correlation between stirrups and the main reinforcing steels in the concrete in terms of corrosion. The corrosion behavior of the intersection between stirrups and main bars was controlled by the interfacial conditions between them. The location of cathodic protection area was affected by the corrosion process. In the first stage of corrosion, the area of cathodic protection mainly located at the mid span of top cast rebars in compressive side. In the second period of corrosion, apart from the previous cathode in compressive zone, the location of cathodic protection also located at the ends of

bottom cast rebars in tensile zone.

Key words: reinforced concrete; corrosion; chloride; steel-concrete interface; artificial crack; load-induced cracks; corrosion of stirrup; vertical leg of stirrup; horizontal legs of stirrup

I would like to dedicate the thesis to my beloved parents and wife

谨以此论文献给我的父母与妻子!

Acknowledgement

I would like to express my sincere appreciation to my supervisor, Prof. Raoul François. I can successfully manage to complete my thesis, for I obtained my supervisor's guidance, advice and support. And thanks to his encouragement, I kept motivated all the time. It is really a pleasure to work under his supervision.

I would like to extend my gratitude to my senior fellow apprentice, Doctor Linwen Yu. With his advice and assistance on my work, the way of my thesis become expedite.

I appreciate the help from my colleague, Doctor Xiaoxiao Gao. Thanks for your help on my live and work.

I feel grateful to the engineers, technicians and office staff of LMDC for their kind help. Without their support, I would not have enough power to complete my experiments.

The financial support from China Scholarship Council (CSC) for my study in France is acknowledged gratefully. I would like to thank the staff of Education Office in Embassy of China in France for their help.

My eternal thankfulness is extended to my parents. Without their support, I would not have embarked on this venture.

致　　谢

春去秋来,三年半的博士生涯即将画上句号.回顾三年多的博士时光,尝尽了酸甜苦辣,这些宝贵的经历都已融入我身体,进入我血液,已化为我人生的动力,去为将来的幸福生活而打拼.

首先，感谢我的父亲张世君先生,龚光明先生,感谢我的母亲,陈平女士,黄彦彦女士,感谢我外公黄荣安先生，外婆唐光素女士，感谢他们对我三十年来的养育,也感谢他们在我博士期间的鼓励与支持.

其次,我要感谢我的导师, Raoul François 教授.多谢导师三年多以来的照顾.导师治学态度严谨,是我研究道路上的明灯,在他的指导下,我的论文得以顺利完成. 同时导师为人幽默风趣,从他身上我学到微笑面对一切困难的态度. 同时也感谢蒙特利尔工程学院 Jean-Philippe Charron 教授对我实验和论文的指导。

同时,我要感谢我的导师杨长辉教授.在杨老师的提点与鼓励之下,我才下定决定出国留学,感谢他对我出国留学的支持.同时,感谢导师丛钢教授及师母陈德玲老师在我办理留学事宜中的帮助。

再次,我要感谢我的师兄余林文副教授和傅博博士,感谢他们在我论文修改中所付出的辛苦.我与师兄相识多年,感谢师兄指路,我才有到法国深造师的机会,同时也是在师兄们的帮助下,我的论文才得以顺利完成.师兄们工作态度认真严谨,为人仗义,与我亦师亦友,感谢师兄多年来的帮助与照顾。

我要感谢高小小师姐.初到法国之时，背井离乡加上语言不通,心中难免产生负面情绪在高师姐的帮助下,我快速地适应了实验室的工作环境与生活环境.同时,我也要感谢我的师弟蔡渝新在实验方面对我的帮助。

我要感谢我的妻子李春雪女士，感谢她对我学业上的支持、理解与等待。在我余下的人生中，我会好好爱她，好好为我们的小家奋斗！

最后,感谢各位评审老师,感谢国家留学基金委为我提供经费去完成我的学业,我将用我所学去回报我的国家,去回报社会.感谢所有帮助过我的朋友与家人！

张武龙

2020 年 2 月 17 日

Laboratoire Matériaux et Durabilité des Constructions

Contents

List of figures

List of tables

Résumé

Selon les prévisions des Nations Unies, en 2019, la population totale mondiale était de plus de 7,7 milliards et en 2100, elle dépassera 11,2 milliards [1]. La croissance rapide de la population mondiale entraîne un énorme défi pour les ressources limitées de terres. Il est bien connu que la superficie totale de l'océan représente plus de 70% de la Terre, par conséquent, encercler la mer pour faire des îles artificielles et implanter des villes est considéré comme le moyen le plus efficace pour résoudre les ressources terrestres limitées [2].

Au cours des dernières décennies, de plus en plus de structures en béton armé ont été construites dans un environnement océanique [3-6]. Cependant, une corrosion induite par les chlorures, en raison d'une exposition à long terme à un environnement marin, pourra se développer sur les constructions océaniques [7]. Généralement, la corrosion peut entraîner des fissures et des écaillages, et entraîner la perte de section transversale des barres d'armature en acier et, enfin, endommager la liaison entre le béton et les barres d'armature en acier [7]. Afin de réduire la menace de détérioration des constructions en béton armé pour la société humaine, il est donc nécessaire d'étudier la corrosion de l'acier dans le béton.

Selon les recherches publiées, le processus de corrosion peut généralement être divisé en deux phases pour le béton armé non fissuré [8] ou en quatre phases pour le béton armé fissuré [7].

Pour le béton armé non fissuré, le processus de corrosion comporte successivement l'amorçage de la corrosion et la propagation de la corrosion. Pour l'initiation de la corrosion, cela correspond au temps nécessaire aux chlorures pour pénétrer de l'environnement extérieur à travers le béton d’enrobage et pour s'accumuler au niveau de l'acier en concentration suffisante pour détruire localement la couche de protection passive sur la surface de l'acier et ainsi provoquer une corrosion active. Pour la propagation de la corrosion, cela correspond à la période pendant laquelle le taux de corrosion et la quantité cumulée de produits de corrosion augmentent progressivement jusqu'à ce qu'un niveau de dommages inacceptable se soit produit. L'illustration schématique a été montrée sur la Figure 1 (a).

Pour le béton armé fissuré, le processus de corrosion consiste successivement en l'incubation, l'initiation, l'induction et la propagation. Dans l'incubation de corrosion, les agents agressifs

pénètrent à travers les fissures primaires pour atteindre rapidement les barres d'armature en acier. Lors de l'initiation de la corrosion, les barres d'armature en acier situées au niveau des fissures primaires ont été dépassivées, tandis que les barres d'armature en acier entre les fissures primaires restent protégées par un revêtement en béton. Les barres d'armature en acier ont été corrodées sous la forme d'une corrosion par macro piles. Lors de l'induction de la corrosion, les produits de corrosion obturent les fissures primaires ce qui ralentit fortement le développement de la corrosion. La durée de cette période est liée au temps mis par les ions chlorure pour pénétrer à travers la structure poreuse de la couverture en béton. Dans la propagation de la corrosion, lorsque toute la couverture de béton est contaminée par des chlorures, la corrosion redémarre. Ensuite, le développement des produits de rouille induit une fissuration secondaire de la couverture en béton. Le modèle a été illustré à la Figure 1 (b).

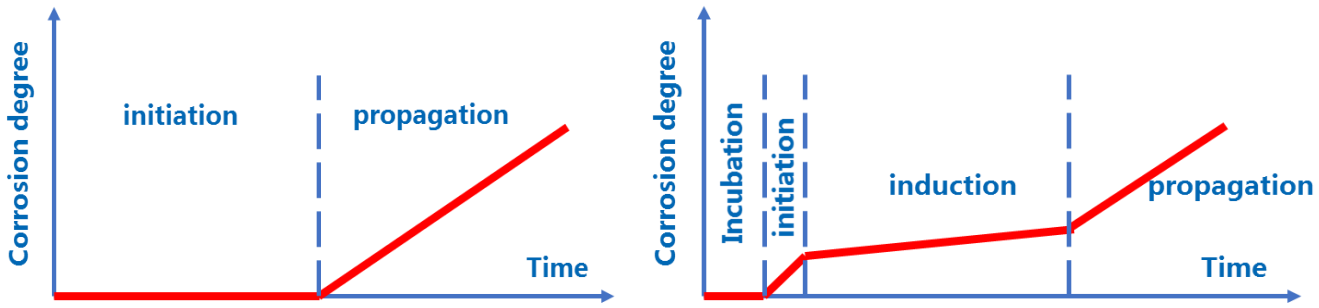

(a) Corrosion model of uncracked reinforced concrete (b) Corrosion model of cracked reinforced concrete

Figure 1 Modèles de corrosion du béton armé [7, 8]

La fissuration est une caractéristique intrinsèque des structures en béton armé [9]. Il a été confirmé que les fissures accéléraient l'initiation de la corrosion de l'acier dans le béton en raison de la facilité d'accès des agents agressifs [10-13]. Cependant, on ne comprend pas bien comment les fissures affectent la propagation de la corrosion. Certains chercheurs [14-16] ont rapporté que les fissures accélèrent la propagation de la corrosion en augmentant la pénétration des divers ingrédients de la corrosion du béton. Cependant, d'autres recherches publiées ont indiqué que les fissures n'ont aucun effet sur la propagation de la corrosion [10, 17-20]. Une explication possible de ces contradictions est que les fissures ne sont pas en mesure de décrire les défauts d'interface réalistes entre l'acier et le béton [21].

Généralement, les défauts d'interface acier-béton courants sont les défauts de coulage sous les barres supérieures (qu'on appellera dans la suite « top-casting defects »), formés par le ressuage, la

ségrégation et le tassement du béton frais lorsque la hauteur du béton sous armature est supérieure à 15 cm [22, 23]. Les “top-casting defects”, sont constitués principalement de bulles d'air et de vides de ressuage [24], et essentiellement localisés à l'interface inférieure acier-béton selon la direction de coulage du béton frais [23-25].

Il a été rapporté que les “top-casting defects” accéléraient l'initiation de la corrosion des armatures dans le béton [26]. Cependant, l'emplacement des points initiaux de corrosion par piqûres n'est pas bien compris. Certaines études ont rapporté [27, 28] que les points initiaux de corrosion par piqûres sont apparus aux endroits des vides dans l'interface acier-béton. Tandis que d'autres études ont indiqué [29] que l'emplacement de l'initiation de la corrosion était lié aux conditions de l'acier (la métallurgie et la géométrie des barres d'armature). Cependant, certains chercheurs ont considéré [30-33] que les points initiaux étaient liés aux conditions locales de saturation au niveau de l'interface acier-béton. A contrario, il n'existe pratiquement aucune littérature concernant l'effet des “top-casting defects” sur la propagation de la corrosion des armatures dans le béton. Hormis les armatures principales en acier, les étriers peuvent être considérés comme une partie non négligeable du ferraillage et de la structure en béton armé [34]. Selon les résultats publiés [35, 36], des “top-casting defects” sont apparus principalement sous parties horizontales des étriers perpendiculaire au sens de la coulage et provoquent une corrosion par piqûres sévère. Cependant, la microstructure du béton entourant les parties verticales étaient denses et aucune corrosion ne s’y produisait. Pour les coins de l'étrier, l'interface entre le coin et le béton apparait être plus poreuse et moins dense et le taux de corrosion du coin de l'étrier est plus élevé [37].

Pour la corrélation entre les étriers et les barres d'armature en acier en termes de corrosion, certains chercheurs [38, 39] ont estimé que les étriers peuvent aider à former de la corrosion par macro piles importante des barres d'armature en acier en reliant les zones anodiques et cathodiques distantes. Cependant, d'autres études [40, 41] ont indiqué que les étriers peuvent protéger les armatures principales contre la corrosion selon les principes fondamentaux de la corrosion galvanique complétée par une possible différence de métallurgie entre étriers et barres HA principales.

Le but de cette thèse est d'étudier l'effet couplé des “top-casting defects” et de la fissuration sur le comportement à la corrosion des armatures dans le béton sous un environnement de chlorures. La

thèse comprend cinq chapitres.

Le chapitre Ⅰ présente le contexte, énonce les enjeux et propose les objectifs de la recherche. Selon les objectifs de la thèse, trois thèmes de recherche ont été proposés: 1). Étudier l'effet des "top-casting defects" et les fissures transversales sur le comportement à la corrosion de l'acier d'armature dans le béton sous environnement de chlorures lors de **l'amorçage de la corrosion**. 2). Etudier l'impact des "top-casting defects" et / ou des fissures induites par le chargement sur le développement de la corrosion et le comportement du béton armé dans la phase de **propagation de la corrosion**. 3). Etudier le comportement à la corrosion des étriers dans une poutre en béton armé. Afin de répondre à ces questions, trois expériences différentes ont été conçues et réalisées.

Le chapitre Ⅱ, en tant que revue de la littérature, comprend sept sections. La section 1 est une introduction. La section 2 passe en revue la littérature concernant les principes fondamentaux de la corrosion de l'acier dans le béton. La section 3 discute des sources de présence des chlorures dans le béton, du mécanisme de transport des chlorures dans le béton et des facteurs ayant une incidence sur le transport des chlorures dans le béton et présente la pénétration des chlorures dans le béton fissuré. La section 4 examine la formation des fissures du béton et le processus de corrosion dans le béton fissuré et l'effet des fissures lors de l'amorçage et de la propagation de la corrosion. La section 5 présente la formation et les caractéristiques des "top-casting defects" dans l'interface acier-béton et examine l'effet "top-casting defects" sur la corrosion des armatures dans le béton lors de l'amorçage et de la propagation de la corrosion. La section 6 passe en revue la corrosion des étriers dans le béton et la corrélation entre la corrosion des étriers et des armatures principales. La partie 8 correspond aux références bibliographiques.

Le chapitre Ⅲ présente des informations détaillées sur trois programmes expérimentaux démarrés respectivement en 2010, 2013 et 2017.

Pour l'expérience de 2017, correspondant au premier thème, deux groupes de blocs de béton armé, labellisés Groupe A et Groupe B, ont été préparés. Tous les blocs de béton armé A et B ont des dimensions de 210×150×280mm. Le diamètre des barres d'armature et des étriers en acier utilisés ici est respectivement de 12 mm et 6 mm. Le ferraillage des blocs A et B a été montré dans la Figure 2. Une barre d'armature en acier HA (la barre rouge sur la Figure 2), d'une longueur de 160 mm, a été fixée au centre de l'ossature en acier avec un fil de pêche. L'armature centrale (Témoin

Métallique - TM) avait un enrobage de béton d'environ 69 mm par rapport aux surfaces latérales. Il doit être considéré comme étant dans un état passif permanent en raison de son enrobage important. Ainsi, le courant électrique circulant entre chaque armature longitudinale et le TM peut être utilisé pour caractériser leur taux de corrosion. Des fils électriques ont été soudés sur les quatre barres d'armature longitudinales et sur le TM afin de mesurer le courant de corrosion. Des tuyaux thermoplastiques isolants (zones jaunes sur la Figure 1) ont été positionnés sur les étriers au contact avec les quatre armatures longitudinales en acier afin d'empêcher les connexions électriques entre les barres principales.

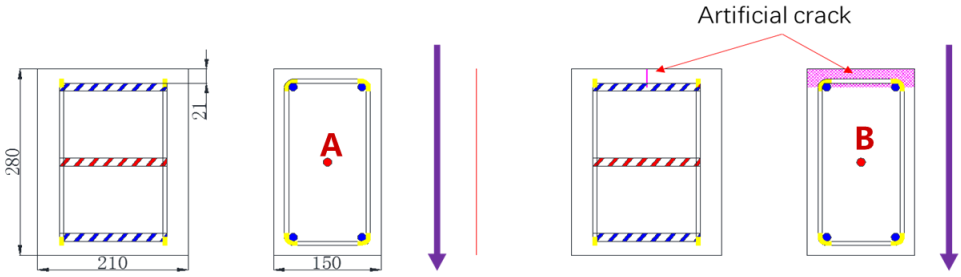

Figure 2 Géométrie et Ferraillage des blocs A et B

(Les barres bleues indiquent les armatures longitudinales HA; la barre rouge correspond au témoin métallique TM; la zone jaune à chaque coin des étriers représente les tuyaux isolants; les flèches violettes indiquent la direction de coulage)

Trois échantillons ont été coulés pour chaque groupe. Dans le cas du groupe B, une fissure artificielle d'une largeur de 1 mm et d'une profondeur de 27 mm a été réalisée. Il convient de noter que certaines études publiées [10, 17, 42] ont rapporté qu'une largeur de fissure supérieure à 0,5 mm n'affecte pas la propagation de la corrosion, par conséquent, une largeur de 1 mm a été choisie pour la fissure artificielle. Pour la réalisation de la fissure artificielle, une cale a été fixée à l'emplacement central du ferraillage avant le coulage du béton et a été retirée après la prise initiale du béton. Il n'y avait pas de fissure artificielle dans les échantillons du groupe A.

Pour l'expérience de 2013, correspondant au deuxième thème, quatre poutres en béton armé avec différentes directions de coulage et conditions d'exposition ont été préparées. Toutes les poutres ont été coulées avec une dimension de 3000×280×150mm. L'épaisseur d'enrobage du béton autour des étriers est de 20 mm. Les diamètres de la barre de compression, de la barre de traction et de l'étrier utilisés ici sont de 6 mm, 12 mm et 6 mm, respectivement. La disposition et la section

transversale des poutres en béton armé sont illustrées aux Figure 3 and Figure 4.

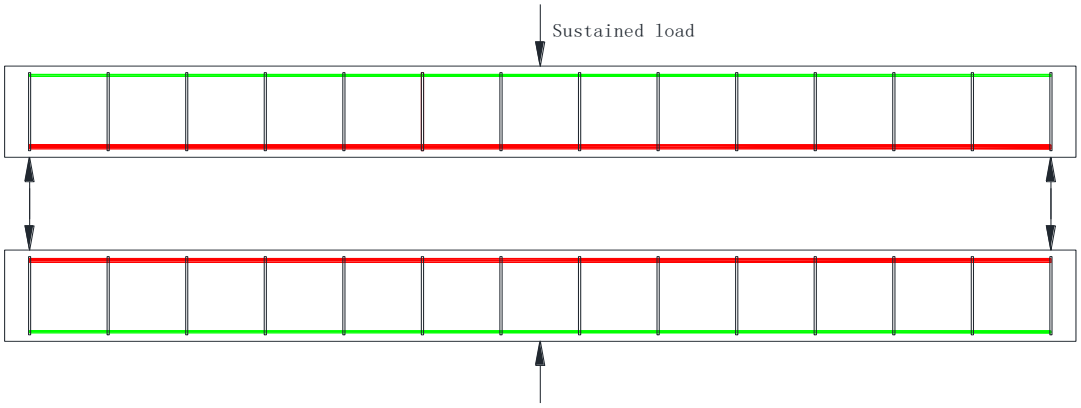

Figure 3 Géométrie et Ferraillage des poutres C

(Les lignes vertes représentent les barres de compression; les lignes rouges signifient les barres de traction et les lignes noires correspondent aux étriers. Les flèches représentent le chargement externe)

Selon la Figure 4, quatre poutres en béton armé ont été divisées en deux groupes. Le groupe 1 contient la poutre C1 et la poutre C2, tandis que le groupe 2 se compose de la poutre C3 et de la poutre C4. Dans le cas de la poutre C1, la face comprimée correspond à la surface supérieure (par rapport au sens de coulage) et également à la surface exposée au brouillard salin. Pour la poutre C2, la face comprimée correspond également à la surface supérieure (par rapport au sens de coulage) mais est à l'opposé de l'exposition au brouillard salin. Au contraire, dans le cas de la poutre C3, , la face comprimée correspond à la surface inférieure (par rapport au sens de coulage) et également à la surface exposée au brouillard salin. Pour la poutre C4, la face comprimée correspond également à la surface inférieure (par rapport au sens de coulage) mais est à l'opposé de l'exposition au brouillard salin.

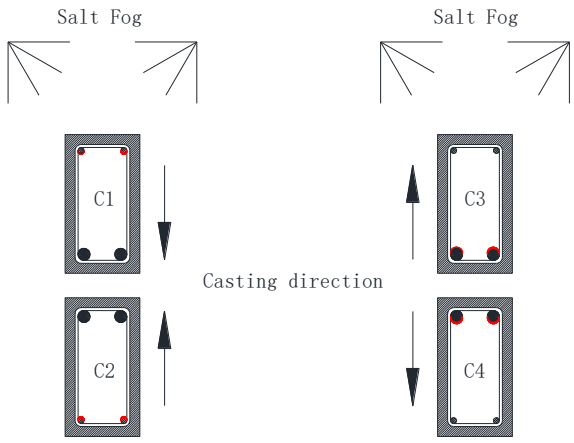

Figure 4 section transversal des différentes poutres C

Pour l'expérience de 2010, correspondant au troisième thème, deux poutres en béton armé,

labellisées poutre As01 et poutre As02, exposées pendant 9 ans ont été étudiées. Les dimensions des deux poutres As était les mêmes que pour les poutres C, mais l'enrobage du béton autour des étriers était de 40 mm. Le diamètre de la barre de compression, de la barre de traction et de l'étrier utilisé ici est de 8 mm, 16 mm et 8 mm, respectivement. La disposition et la section transversale des poutres en béton armé sont indiquées dans la figure 5.

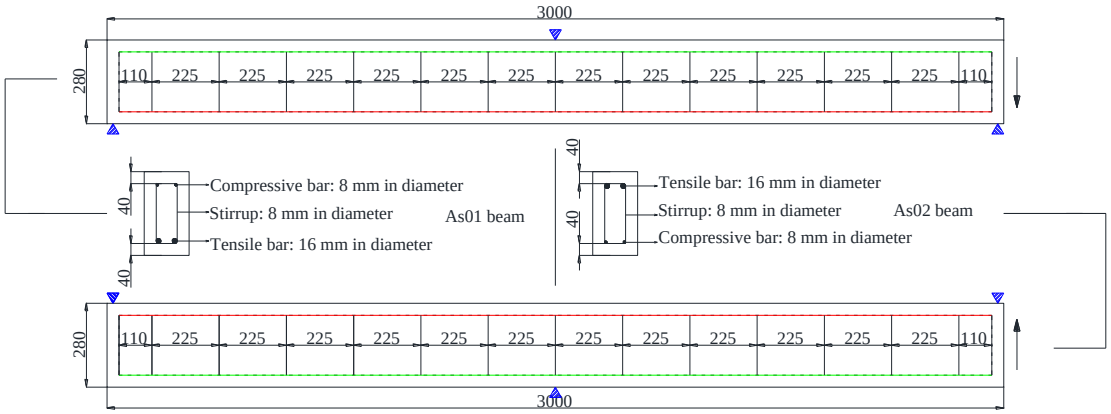

Figure 5 Layout of As beams (all dimensions in mm)

(Les lignes vertes représentent les barres de compression; les lignes rouges signifient les barres de traction et les lignes noires correspondent aux étriers. Les flèches représentent le chargement externe)

Selon la Figure 6, la poutre As01 et la poutre As02 ont été chargées ensemble. Pour la poutre As01, la face comprimée correspond à la surface supérieure (par rapport au sens de coulage) et également à la surface exposée au brouillard salin. Cependant, pour la poutre As02, la face comprimée correspond à la surface supérieure (par rapport au sens de coulage) mais à la surface opposée à l'exposition au brouillard salin.

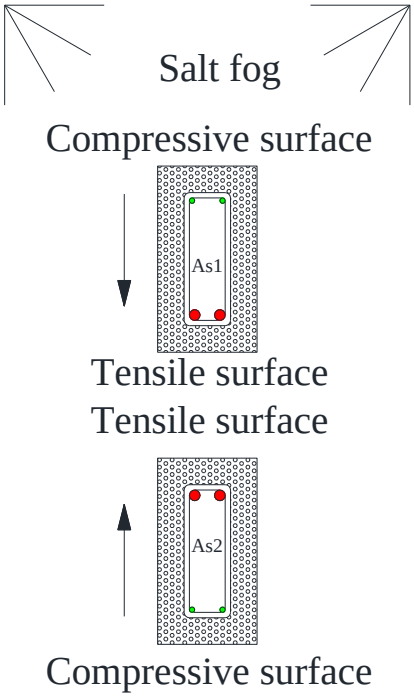

Figure 6 section transversale des poutres As et direction de coulage

Du ciment (CEM Ⅰ, grade 52.5 R) fabriqué par le Groupe Lafarge Ciment, ayant une densité de 3,15 g / cm^3 et une surface spécifique Blaine de 415 m^2 / kg, a été utilisé pour préparer le béton utilisé dans cette étude. La composition chimique est donnée en Table 1.

Table 1 Composition chimique du ciment (%)

	SiO_2	**Al_2O_3**	**Fe_2O_3**	**CaO**	**MgO**	**SO_3**	**Na_2O**
Weight （%）	21.4	6.0	2.3	63.0	1.4	3.0	0.5

Les proportions du mélange de béton sont données dans la Table 2, qui maintient la cohérence des propriétés du béton avec les recherches antérieures de l'auteur [17, 20, 22, 26]. L'affaissement du béton était de 70 mm. Sa résistance moyenne à la compression à 28 jours (testée sur des éprouvettes cylindriques de 110x220 mm) était de 45 MPa. Le module d'élasticité était de 32 GPa et la résistance à la traction, testée par essai de fendage sur les éprouvettes cylindriques, était de 4,7 MPa. La porosité était d'environ 15,2%..

Table 2 Proportions de la composition de béton

Mix composition		
Rolled gravel (silica+limestone)	5-15mm	1109 kg/m^3
Sand	0-5mm	745 kg/m^3
Portland cement: OPC (high performance)		364 kg/m^3
Water		182 kg/m^3

Après durcissement, pour les poutres C et les poutres As, un système de flexion à trois points a été appliqué pour induire les fissures de flexion. Dans le cas des poutres C, deux valeurs de charge ont été utilisées: Mser1 = 21,2 kN • m (poutres C1 ou C2) et Mser2 = 14,1 kN • m (poutres C3 et C4). Pour les poutres As, Mser = 20 kN • m a été appliqué.

Tous les échantillons de béton armé ont été stockés dans un environnement agressif. L'environnement agressif était un brouillard salin (35 g / l de NaCl correspondant à la concentration en chlorure de l'eau de mer). Tous les échantillons ont été soumis à des cycles de mouillage / séchage avec deux jours de mouillage et cinq jours de séchage. La température était la température ambiante du sud-ouest de la France, avec une moyenne mensuelle allant de 5,1 ℃ à 21,3 ℃ et l'humidité relative de la valeur moyenne mensuelle varie de 50% à 84%.

Afin de mesurer le courant galvanique des groupes A et B, une mesure a été conçue selon la norme ASTM G71 (2003). Pour les armatures HA en position haute, lorsque la corrosion induite par les chlorures a eu lieu, le potentiel de l'acier diminue puis conduit à une différence de potentiel avec le témoin métallique. En conséquence, lors de la connexion électrique du témoin métallique à la barre d'acier corrodée, la différence de potentiel conduit à un courant qui est directement mesuré avec un ampèremètre (voir Figure 7). Le courant galvanique a été mesuré chaque semaine.

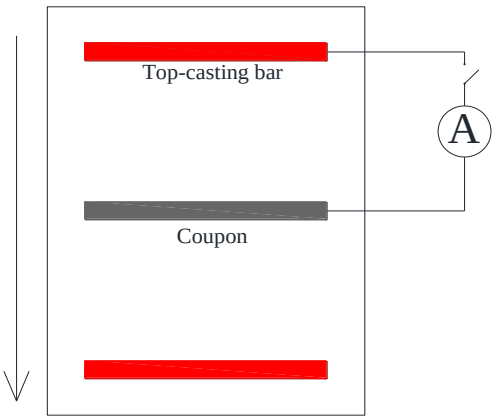

Figure 7 Mesure du courant de corrosion galvanique

Afin de mesurer les profils de chlorures, des prélèvements en béton ont été obtenus à partir d'échantillons broyés en poudre, puis les chlorures ont été extraits de l'acide nitrique à 80 ℃ et dosés par titrage potentiométrique. Ensuite, les ions chlorure ont été calculés et les profils de chlorure ont été tracés.

La distribution des « top-casting defects » a été observée par BSE autour des armatures en acier ainsi que la microstructure et la composante chimique des produits d'hydratation du ciment dans l'interface acier-béton ont été mesurées et analysées par SEM et EDS, respectivement.

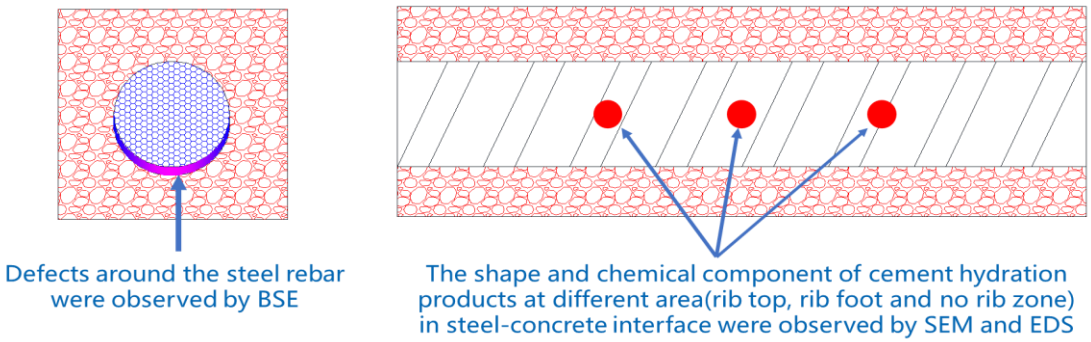

Figure 8 Caractérisation de l'interface acier-béton

Le chapitre Ⅳ examine l'effet des "top-casting defects" et fissures sur le comportement à la corrosion des armatures dans le béton lors de l'amorçage et de la propagation de la corrosion. Ce chapitre comprend cinq sections.

La section 1 de ce chapitre propose une introduction aux quatre autres sections suivantes.

La section 2 étudie les caractéristiques de l'interface acier-béton et l'effet des "top-casting defects" et d'une fissure artificielle sur le comportement à la corrosion des armatures au début de la période de corrosion sous environnement de chlorures. Dans cette section, tout d'abord, les

caractéristiques de l'interface acier-béton sont analysées. Deuxièmement, la pénétration des ions chlorure le long de l'interface acier-béton est étudiée. Enfin, le taux de corrosion et la distribution de la corrosion de l'acier dans le béton non fissuré et fissuré sont déterminés. Un bref résumé est donné (voir ci-dessous).

Dans la Figure 9 (a), on peut constater que la couleur de l'interface supérieure était plus profonde que celle de l'interface inférieure. Cette différence est attribuée à la couche de produits d'hydratation du ciment plus dense ainsi qu'à la différence de microstructure entre l'interface supérieure et l'interface inférieure. La Figure 9 (b) présente la distribution des bulles d'air dans l'interface acier-béton. Il convient de noter qu'empreinte des armatures HA en acier sur le béton est divisée en trois zones différentes: sommet de la nervure, pied de nervure et zone entre deux nervures selon la forme de la barre d'armature en acier. Sur la figure, on peut observer que la plupart des bulles d'air sont apparues au pied des nervures, un quart des bulles d'air situées sur la zone sans nervures, pas plus de 10% ont été trouvées au sommet des nervures.

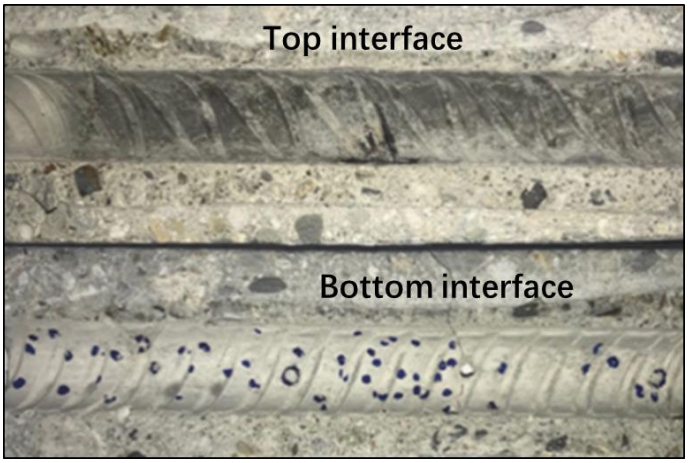

Figure 9 (a) Conditions of steel-concrete interface

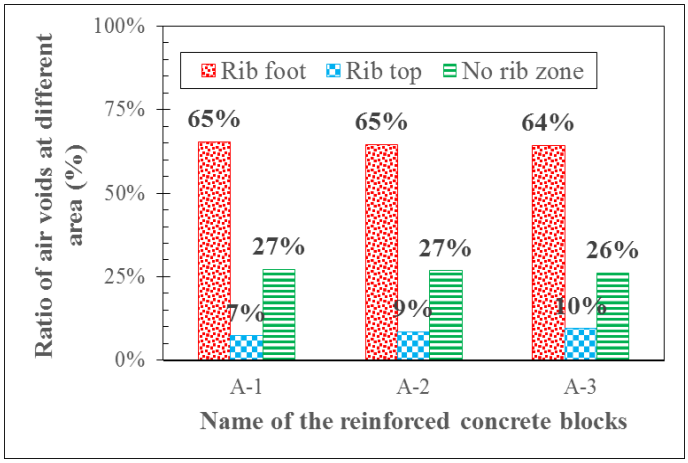

Figure 9 (b) Distribution of air bubbles in steel-concrete interface

Figure 9 Distribution des bulles d'air le long de l'interface acier-béton

Dans le cas de la formation de bulles d'air sous l'armature, lors du compactage du béton frais, les bulles d'air ont migré simultanément vers la surface inférieure de l'armature HA. Lorsque les vides d'air ascendants étaient en contact avec la zone supérieure des nervures, la plupart des bulles d'air ne pouvaient pas adhérer à cette petite surface pointue, alors elles ont continué à migrer le long du contour de la nervure et se sont accumulées à l'emplacement du pied de la nervure. Ainsi, les bulles d'air dans la zone du pied de nervures avaient deux origines: certaines provenaient du sommet des nervures et d'autres provenaient directement du béton frais. Pour la zone sans nervure, les vides

d'air ascendants pourraient migrer jusqu'à cette zone directement, puis se mélanger pour former un grand vide d'air à la surface de la zone sans nervures des barres d'armature en acier. Par conséquent, la quantité de bulles d'air était la plus basse au sommet de la nervure et la plus élevé au pied de la nervure, et la quantité dans la zone sans nervures étant comprise entre celle du pied et somment de la nervure.

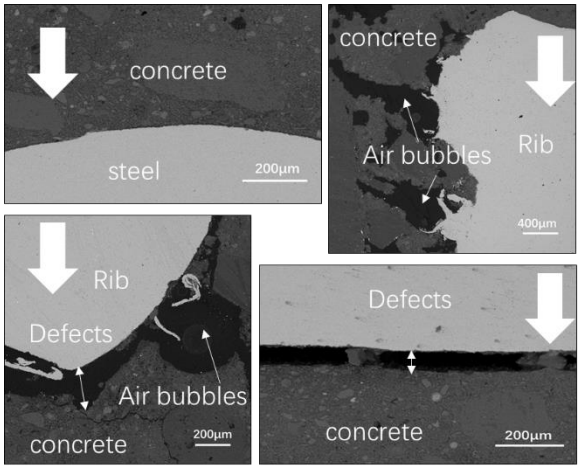

Figure 10 Vues BSE de l'interface acier-béton

La Figure 10 montre la distribution des "top-casting defects", on peut observer que l'interface acier-béton supérieure était relativement parfaite, cependant, certains défauts évidents sont apparus à l'interface inférieure et aux zones de nervure même dans l'interface supérieure. Cela signifie que la qualité de l'interface acier-béton était contrôlée par la direction de coulage et par la forme de l'armature.

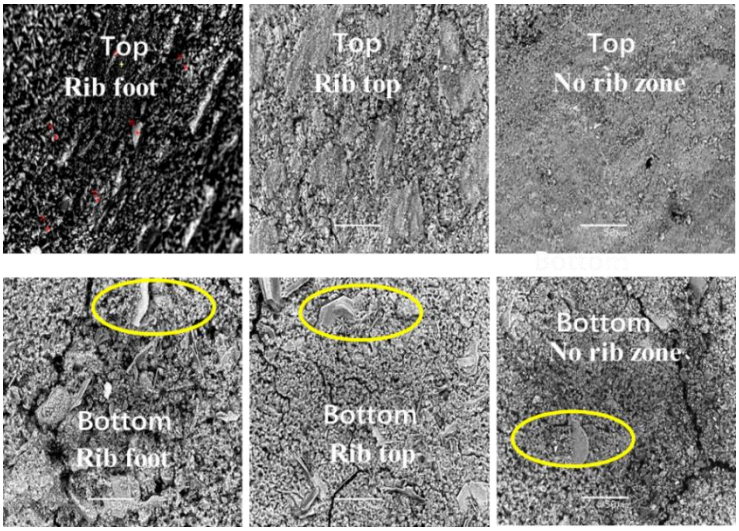

Figure 11(a) Results of SEM

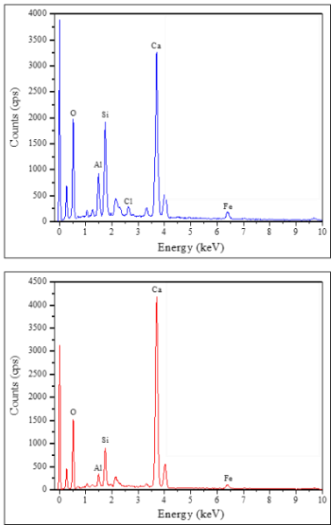

Figure 11 (b) Results of EDS

Figure 11 Microstructures des produits d'hydratation du ciment dans l'interface acier-béton

Les microstructures des produits d'hydratation du ciment dans l'interface acier-béton ont été représentées sur la Figure 11. Sur la Figure 11 (a), il peut être constaté qu'aucun cristal évident ne peut être observé dans l'interface supérieure, mais certaines grosses particules peuvent être repérées. Cependant, dans l'interface inférieure, certains cristaux évidents en forme de plaques ou en forme d'aiguilles peuvent être trouvés. D'après les résultats de l'EDS (Figure 11 (b)), les particules et les cristaux étaient de Portlandite, de l'ettringite et du gel de C-S-H. D'après la Figure 10, on peut savoir que l'interface supérieure était trop dense pour fournir suffisamment d'espace pour la croissance des cristaux, cependant, en présence de "top-casting defects",, il y a suffisamment d'espaces pour la croissance des cristaux. Par conséquent, on peut en déduire que les "top-casting defects", n'affectent pas les types de produits d'hydratation du ciment, mais cela affecte leurs structures.

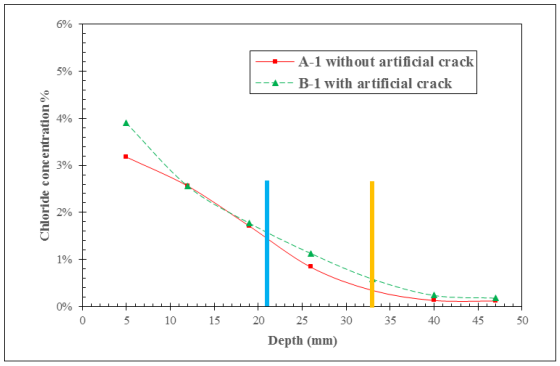

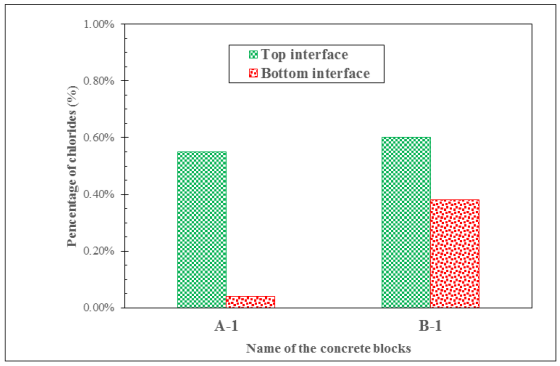

Figure 12 (a) Chloride profiles of A-1 and B-1 Figure 12(b) Chloride contents in steel-concrete interface

Figure 12 Pénétration des chlorures à l'interface acier-béton

La Figure 12(a) montre les profils en chlorures de A-1 et B-1. La teneur en chlorures d'A-1 est similaire à celle de B-1. Il est facile de comprendre que tous les échantillons étaient les mêmes indépendamment du béton fissuré ou du béton non fissuré, par conséquent, à une profondeur donnée, la teneur en chlorure était similaire. D'après la Figure 12(b), il peut être constaté que la teneur en chlorures dans l'interface inférieure de B-1 était beaucoup plus élevée que celle de A-1. Cela signifie que les chlorures ont d'abord pénétré dans la fissure artificielle et ont migré le long de l'interface acier-béton. Étant donné que l'interface supérieure était plus dense, les chlorures ont préférentiellement migré le long de l'interface inférieure le long des "top-casting defects".

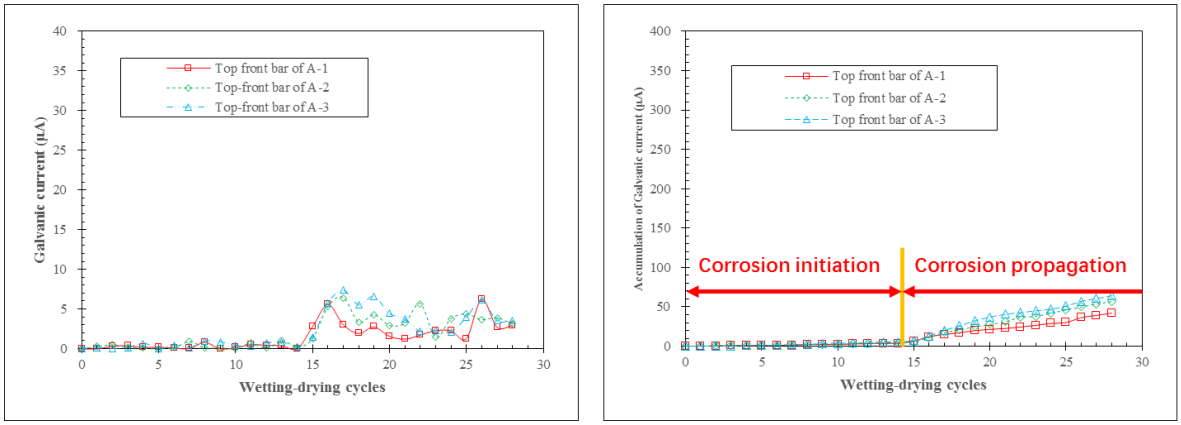

Figure 13 Courant de corrosion galvanique dans les barres supérieures des blocs A

La Figure 13 montre le courant de corrosion galvanique et son accumulation en fonction du temps pour les barres supérieures de trois échantillons du groupe A sans fissure artificielle. On peut constater que la corrosion des armatures en l'absence de fissure artificielle est conforme au modèle proposé par Tuutti [8]. La période de 0 à 14 cycles de mouillage-séchage correspond à l'amorçage de la corrosion, et la propagation de la corrosion a lieu après le 14ème cycle de mouillage-séchage. Après le début de la corrosion, le taux de corrosion des armatures en acier a tendance à être stable.

Figure 14 faciès de corrosion de la barre supérieure de A-1

La Figure 14 montre que les taches de rouille se situent principalement au pied des nervures de la barre HA l'interface inférieure. Bien que les emplacements des taches de rouille ne puissent pas être considérés comme des lieux de corrosion par piqûres. Cependant, après avoir enregistré les taches de rouille de la surface, les barres d'armature en acier ont été brossées et on a vérifié que les emplacements de la rouille sur la surface de l'acier représentent bien les endroits de corrosion par piqûres. En outre, selon la répartition de la corrosion par piqûres, les points initiaux de corrosion par piqûres n'étaient pas liés à l'emplacement des vides d'air, par ex. la corrosion a eu lieu au pied d'une nervure sans vide d'air, ou aucune corrosion ne s'est produite dans la zone sans nervure en présence de bulles d'air.

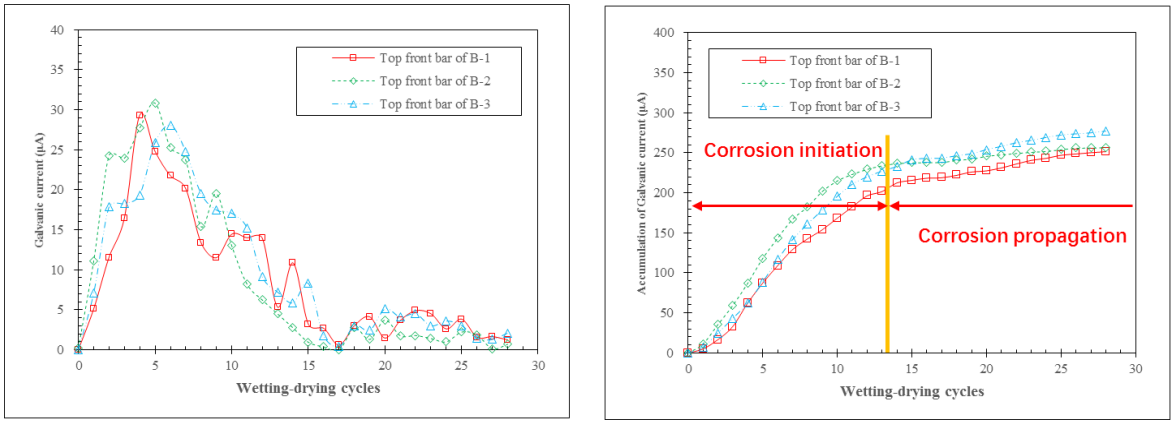

Figure 15 Courant de corrosion galvanique pour les barres supérieurs des blocs B

En présence de fissure artificielle, les armatures supérieures de tous les blocs B présentaient un taux de corrosion plus élevé que celles de tous les blocs A. Cependant, après le 15e cycle de mouillage-séchage, un taux de corrosion similaire a été identifié pour les barres d'armature en acier supérieures dans les blocs A et les blocs B.

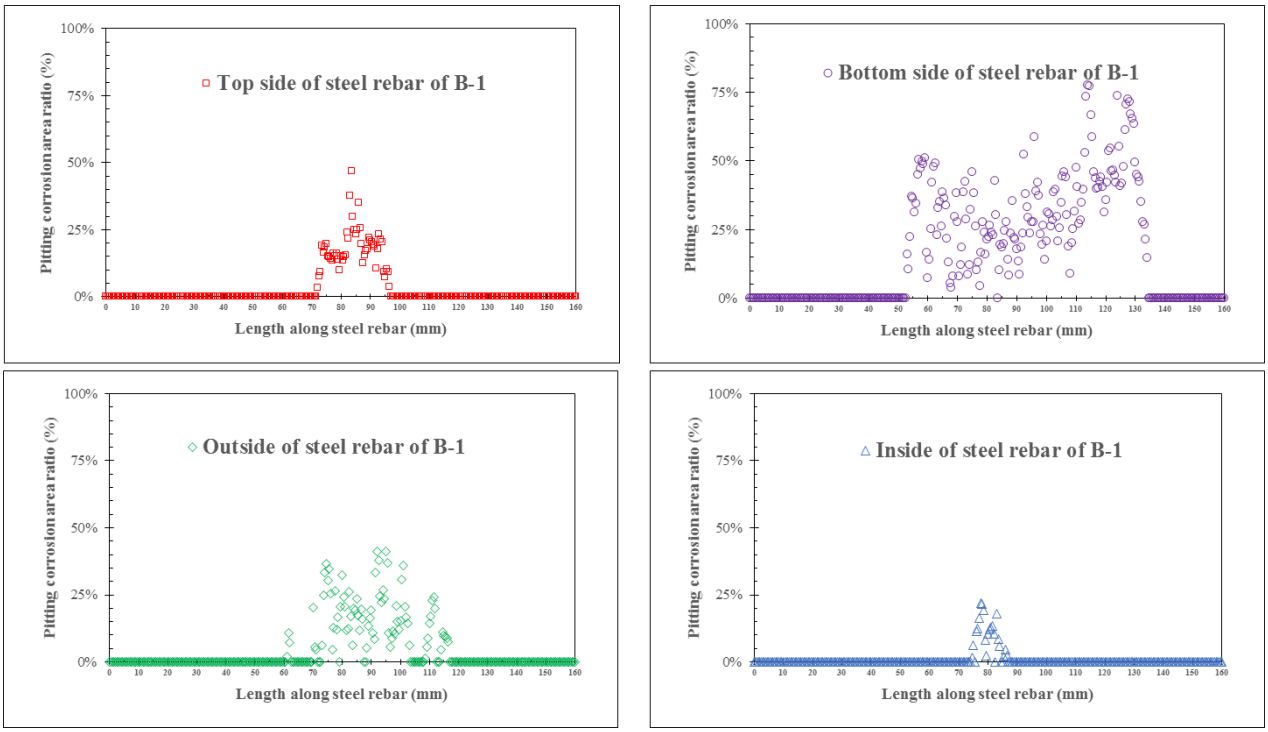

Figure 16 distribution de la corrosion localisée le long de l'armature supérieure du bloc B-1

En présence de fissures artificielles et de "top-casting defects", chaque côté de l'armature était soumis à une corrosion par piqûres différente. Pour la surface supérieure, la corrosion par piqûres s'est principalement accumulée autour de la fissure artificielle et la plus importante a été trouvée dans la largeur de la fissure. En effet, l'ouverture de la fissure artificielle était large, 1 mm, et

permettait ainsi à la solution de chlorures d'entrer en contact avec la surface de l'acier. Pour le côté inférieur, la corrosion par piqûres s'est principalement produite à des endroits éloignés de la fissure artificielle. Les ions chlorures pénètrent à partir de la fissure artificielle et migrent le long de l'interface inférieure acier-béton. Pour la surface extérieure, à part la fissure artificielle, les ions chlorures pouvaient pénétrer depuis la surface latérale extérieure de la couverture en béton, et ainsi, le champ de corrosion était plus large que celui du côté supérieur. Pour la surface intérieure, les ions chlorures ne pouvaient pas se rendre facilement à la surface de l'acier, donc un plus petit nombre de sites de corrosion par piqûres sont apparus près de la fissure artificielle.

La section 3 du chapitre Ⅳ présente l'impact des “top-casting defects” sur les caractéristiques de corrosion de la zone de compression de quatre poutres C pour un relativement long terme d'exposition dans un environnement de chlorures. Les cartes de fissuration, les profils de chlorures, la répartition des piqûres et la perte de section transversale des barres d'armature en acier ont été mesurés à 38 et 48 mois. La relation entre la corrosion par piqûres et les fissures induites par la corrosion a été discutée.

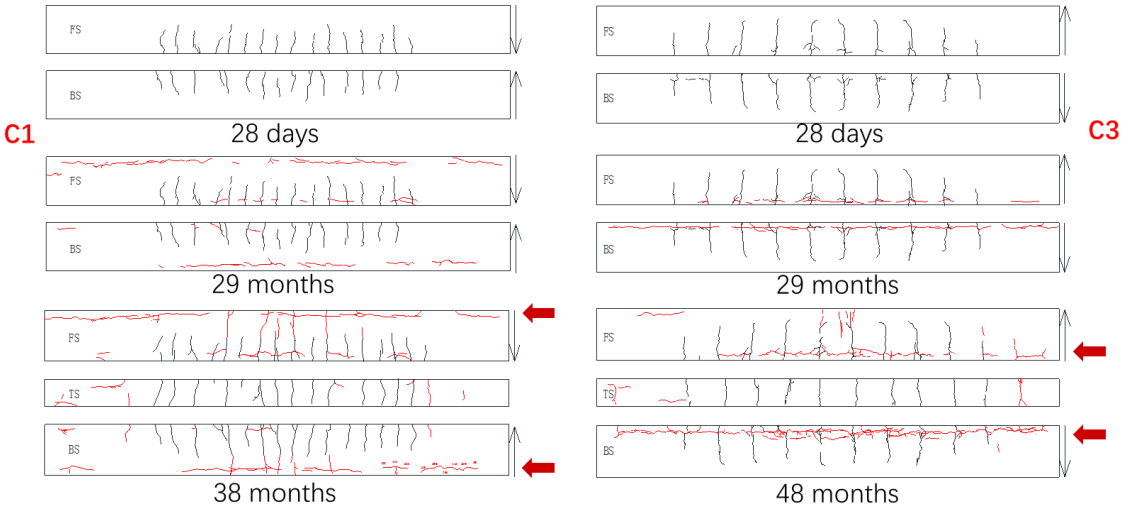

Figure 17 Carte de fissuration des poutres C1 et C3

La Figure 17 montre les cartes de fissuration des poutres C1 et C3. On peut constater que des fissures continues induites par la corrosion sont apparues principalement aux l'endroit correspondant à la présence des “top-casting defects” quel que soit le côté de la poutre : zone de compression ou de traction.

Table 3 Longueur des fissures induites par la corrosion des poutres C à différentes échéances

	Interfacial state	Exposure conditions	Length of corrosion-induced cracks (mm)						
			Exposure time (month)	0	8	24	29	38	48
C1	Defects	Top exposure	Front side	0	692.8	1194.5	2140.3	2388.9	
			Bottom side	0	0	897.4	1509.4	1812.6	
C2	Defects	Bottom exposure	Front side	0	0	0	1542.6	1598	
			Bottom side	0	0	0	0	1168.9	
C3	No defects	Top exposure	Front side	0	0	0	0		303
			Bottom side	0	0	0	0		0
C4	No defects	Bottom exposure	Front side	0	0	0	0		0
			Bottom side	0	0	0	0		0

La Table 3 présente l'évolution de la longueur des fissures induites par la corrosion le long des barres comprimées des poutres C à différents échéances de corrosion. On peut observer que les fissures induites par la corrosion les plus longues sont apparues dans la zone de compression des poutres C1 et C2 et que le développement en longueur des fissures induites par la corrosion a été significatif pendant la période de 29 à 38 mois d'exposition. Il convient de noter que de minuscules fissures induites par la corrosion sont apparues sur la face avant de la poutre C2 après 24 mois d'exposition. En revanche, si la zone de compression était sans défauts, comme dans les zones de compression des poutres C3 et C4, l'apparition de fissures induites par la corrosion a été retardée à 48 mois pour C3 et ne s'est produite pour C4 qu'à 48 mois. Cela signifie que les défauts induits par le sens de coulage du béton ont favorisé le développement de la corrosion et l'apparition de fissures induites par la corrosion.

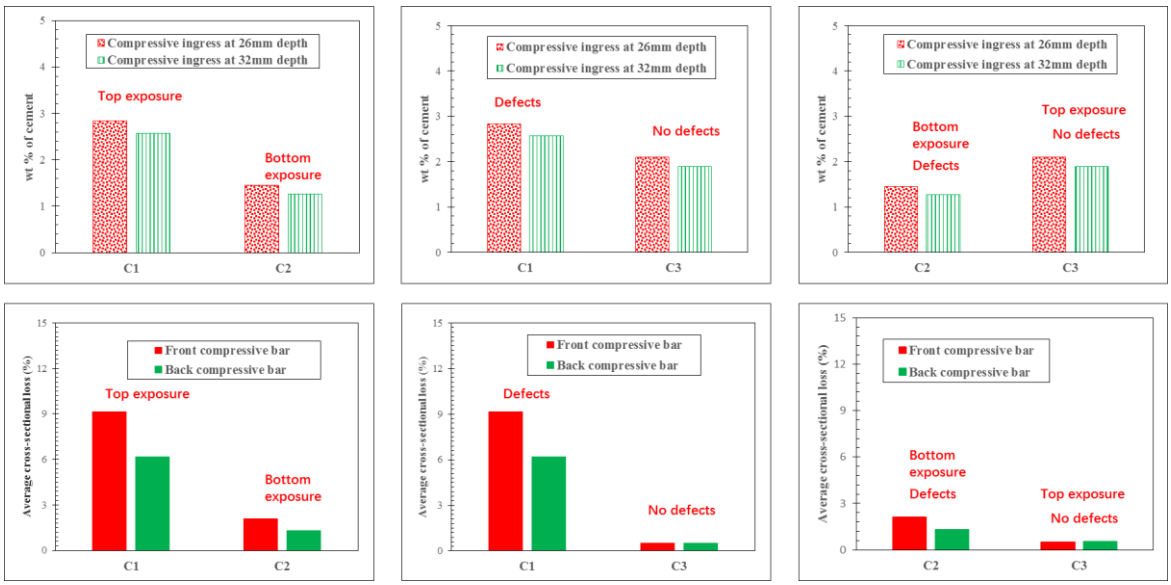

Figure 18 Pénétration des chlorures et perte moyenne de section due à la corrosion pour les barres comprimées

L'impact de la direction de coulage du béton et des conditions d'exposition sur la pénétration de chlorures et sur la perte moyenne de section transversale des barres comprimées ont été comparés à la Figure 18. On peut constater que les “top-casting defects” et les conditions d'exposition (face exposée à la pulvérisation) peuvent accélérer la pénétration de chlorures et la perte de section des armatures. Cependant, les “top-casting defects” entraînent une plus grande perte moyenne de section transversale des armatures de compression même pour une pénétration de chlorures plus faible.

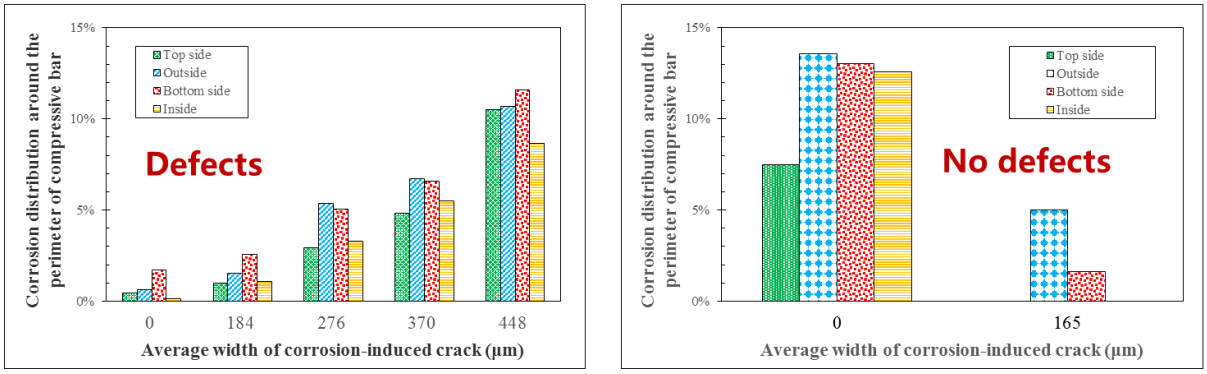

Figure 19 Corrélation entre la corrosion des barres comprimées et l’ouverture moyenne de fissures induites par la corrosion

La relation entre la corrosion de l'acier et la largeur moyenne des fissures induites par la corrosion a été analysée à la Figure 19. En présence de “top-casting defects”, avant l’apparition des fissures induites par la corrosion, la corrosion a principalement eu lieu à l'interface inférieure de a liaison acier-béton. Après l'apparition des fissures induites par la corrosion, la corrosion s'est

progressivement développée autour du périmètre des barres comprimées. Ce résultat est conforme à ceux obtenus sur les blocs de béton armé (Figure 14). Lorsque la largeur des fissures induites par la corrosion dépasse une certaine valeur, on peut considérer que les “top-casting defects” n'affectent plus le processus de corrosion des armatures. En l'absence de “top-casting defects”, la corrosion s'est amorcée et s'est développée préférentiellement à la surface extérieure de l'acier, plus près de la surface du béton exposée à l'environnement de chlorures.

La section 4 du chapitre Ⅳ examine l'effet des fissures dues au chargement mécanique associées ou non à des “top-casting defects” sur les caractéristiques de corrosion de la zone tendue des poutres C à relativement court terme (moins de 4 ans). La corrélation entre les fissures de service et la corrosion des barres tendues a été discutée et le modèle phénoménologique du processus de corrosion des barres d'armature de traction a été établi.

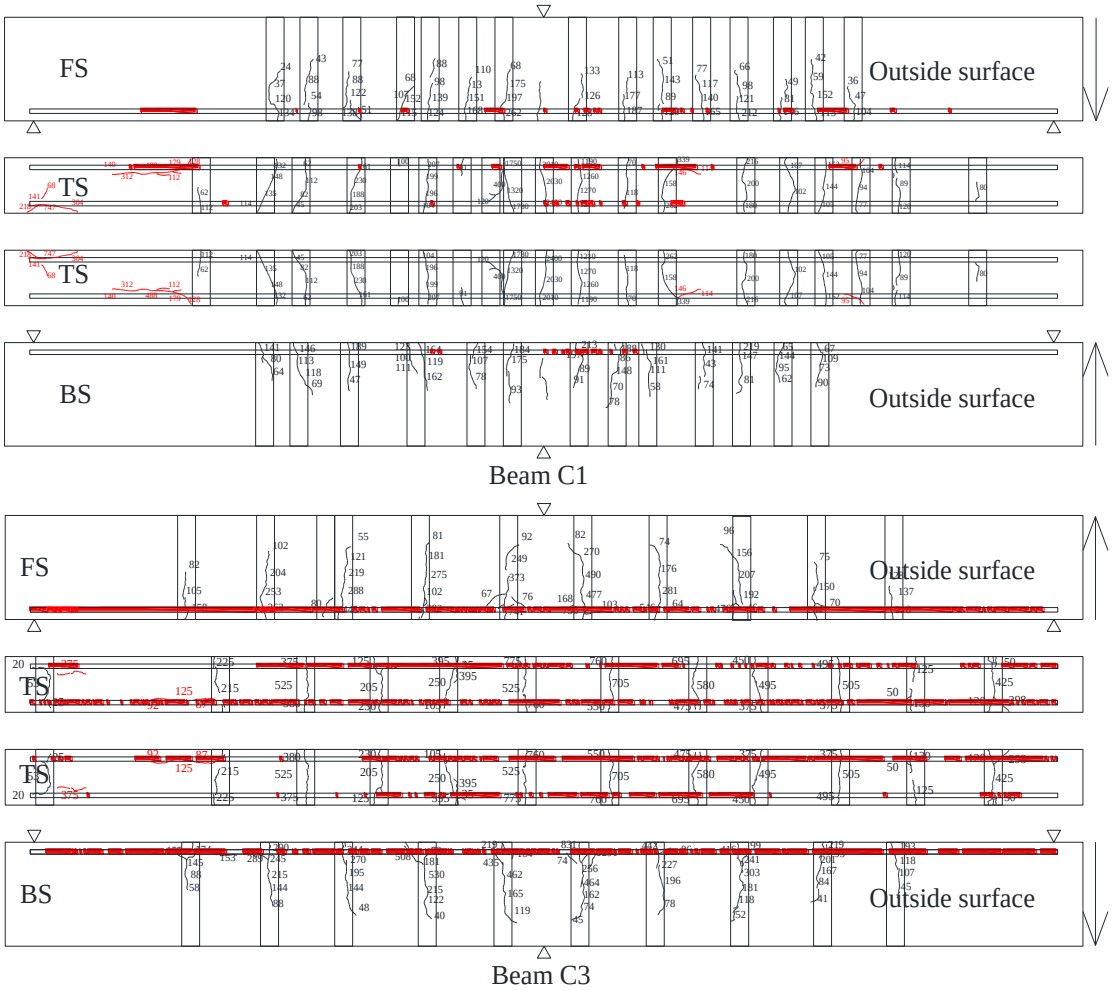

Figure 20 Superposition de la carte de corrosion et de fissuration pour les poutres C1 et C3

La Figure 20 présente la superposition des cartes de fissuration et des cartes de corrosion des

poutres C1 et C3. Il est clair qu'il n'y a pas de corrélation entre elles. Ce résultat est conforme aux résultats précédemment publiés [22].

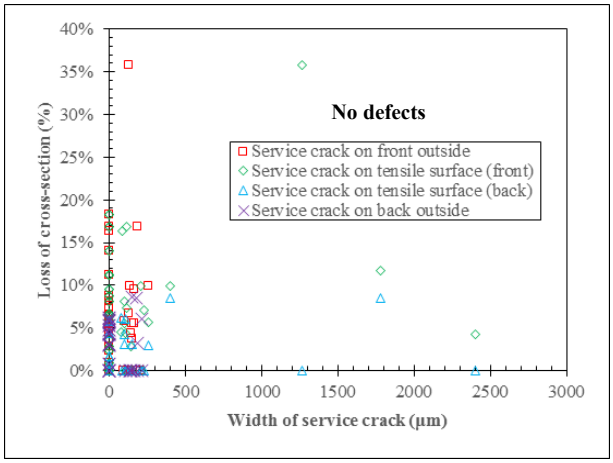

Figure 21 (a) C1 beam

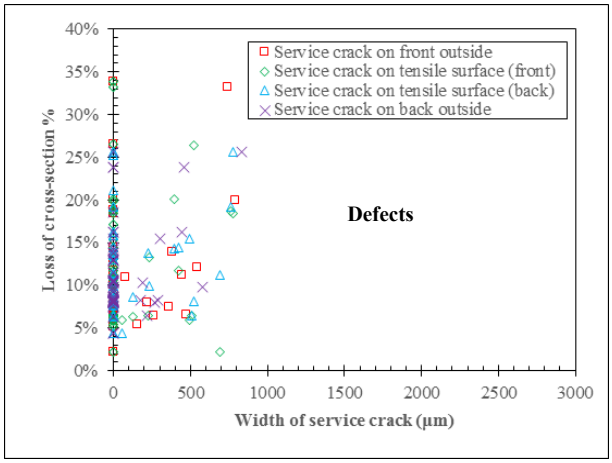

Figure 21 (b) C3 beam

Figure 21 Corrélation entre les ouvertures des fissures de service et la perte de section des armatures tendues

La Figure 21 ne montre aucune corrélation entre la largeur des fissures transversales et la perte de section transversale des armatures tendues, indépendamment de la présence ou de l'absence de “top-casting defects”. De plus, les zones éloignées des fissures transversales et les zones sans fissures transversales présentent la même perte de section que les zones fissurées.

Pour la poutre C1 sans “top-casting defects”, on s'attendrait à ce que la corrosion se développe d'abord à proximité des fissures de service mais ne se propage pas tant que la pénétration des chlorures à travers l’enrobage de béton n'est pas suffisante pour initier la corrosion. En conséquence, des fissures induites par la corrosion sont apparues après 24 mois d'exposition. Pour la poutre C3 avec présence de “top-casting defects”, les chlorures ont pénétrés par les fissures et ont migrés le long des défauts dus au sens de coulage vers les points les plus faibles de l'acier pour initier la corrosion. Ce résultat a été confirmé dans la Figure 12 et dans la Figure 16.

Le processus de corrosion des barres tendues des quatre poutres en C est présenté à la Figure 22 en fonction de la perte de section moyenne des barres tendues. En présence de “top-casting defects”, l'étape de propagation suit directement l'étape d'amorçage, la période d'induction est nulle. En l'absence de “top-casting defects”, l'amorçage à l'emplacement de la fissure est suivi d'une période d'induction correspondant au temps nécessaire à la pénétration de chlorures à travers l’enrobage de béton dans les zones non fissurées. Lorsque suffisamment de chlorures atteignent les

barres, la phase de propagation commence. Il y a un effet des conditions d'exposition pour la pénétration de chlorures: une surface de traction exposée à la pulvérisation par le haut conduit à une pénétration de chlorure plus élevée qu'une surface de traction opposée.

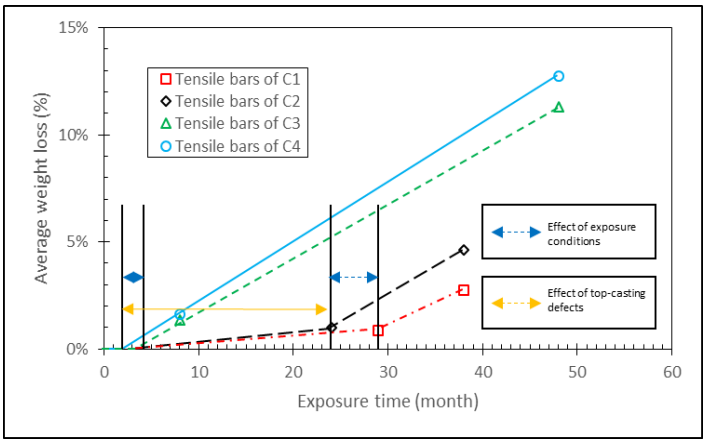

Figure 22 Processus de corrosion des poutres C fissurées

La section 5 du chapitre Ⅳ étudie le comportement à la corrosion des étriers extraits des poutres As qui ont été exposés à un environnement de chlorures sous une charge maintenue pendant 9 ans. Le comportement à la corrosion de différentes zones d'étriers est analysé et, enfin, la relation entre la corrosion des étriers et les aciers principaux de renforcement dans les poutres en béton est discutée.

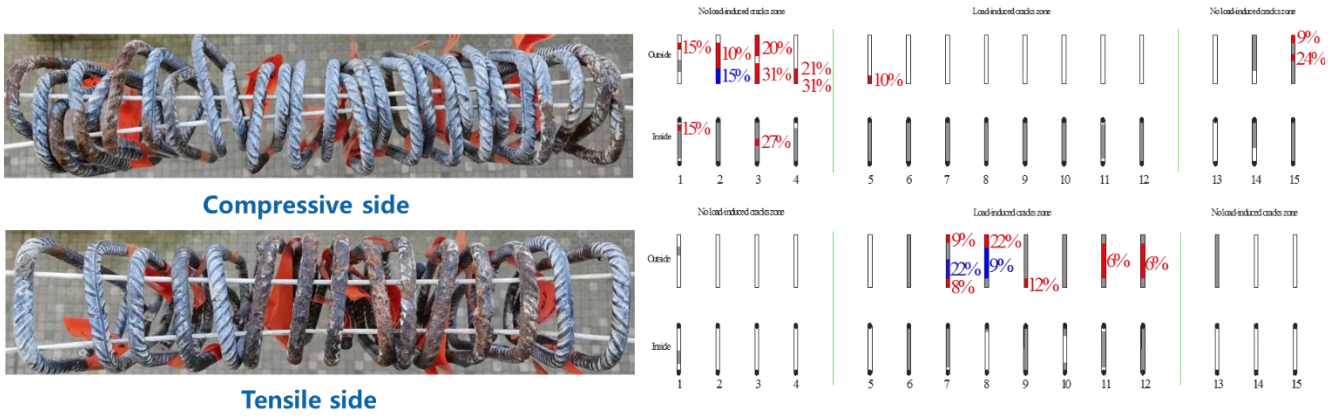

Figure 23 Corrosion des parties horizontales des étriers

Selon la distribution des fissures dues au chargement mécanique sur la poutre As01, les étriers ont été divisés en deux groupes: les étriers dans la zone non fissurée et ceux dans la zone fissurée.

Pour les parties horizontales des étriers, du côté de la zone comprimée, l'intérieur des parties horizontales a souffert d'une légère corrosion due aux défauts de coulage, cependant, une corrosion par piqûres sévère s'est principalement produite à l'extérieur des parties horizontales situées au deux

extrémités de la poutre. Au contraire, du côté de la zone tendue, la corrosion par piqûres s'est principalement accumulée au milieu de la poutre (Figure 23). Le phénomène similaire peut également être observé sur les barres principales (Figure 24).

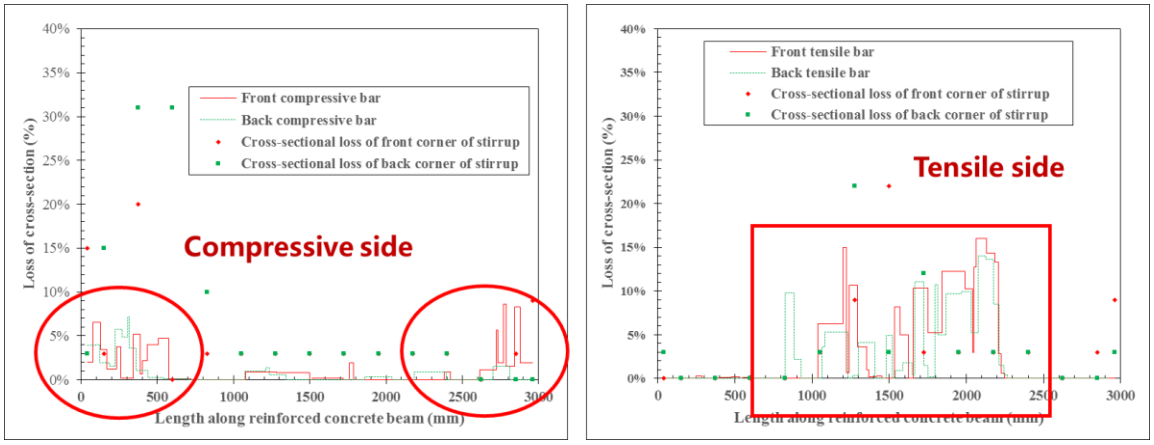

Figure 24 perte de section due à la corrosion pour les barres principales et pour les étriers d'effort tranchant des poutres As

Selon le faciès de corrosion, le processus de corrosion des barres d'armature en acier peut être divisé en deux étapes. Les illustrations schématiques sont présentes dans la Figure 25.

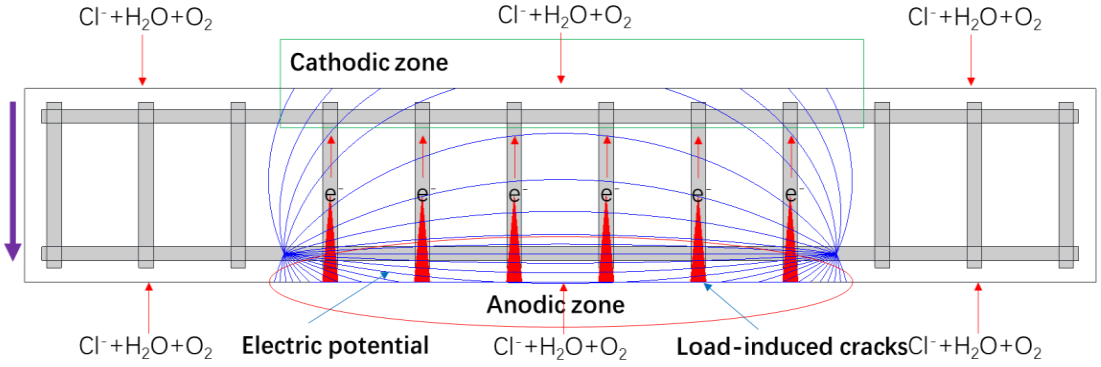

Figure 25 (a) Macrocell corrosion of stirrups in RC in first step of corrosion

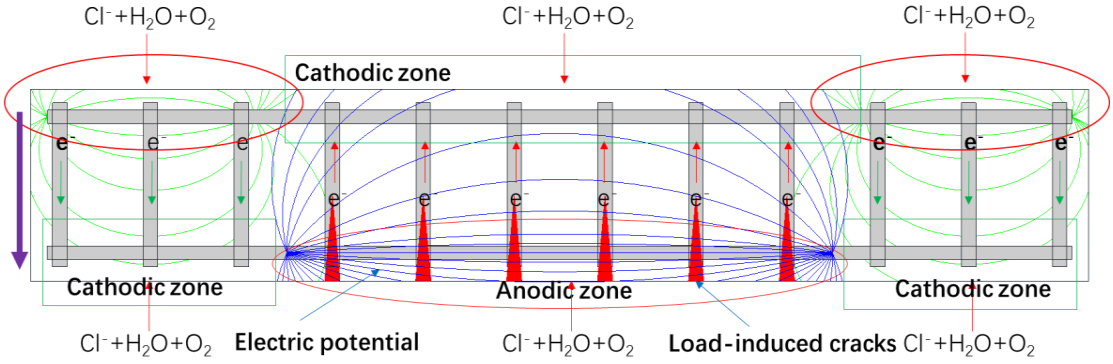

Figure 25 (b) Macrocell corrosion of stirrups in RC in second step of corrosion

Figure 25 Mécanisme de corrosion par macro-piles des poutres en béton armé fissures en service

Après l'application de la charge mécanique à la poutre en béton armé (As), des fissures se sont formées longeant les parties verticales des étriers dans la zone de traction. Dans l'environnement du brouillard salin, les ions chlorures et l'humidité pénètrent d'abord à la profondeur des armatures dans la zone de traction à travers les fissures induites par la charge, attaquant la couche passive formée sur la surface extérieure des armatures. Une fois la couche passive localement détruite, la corrosion commence et la zone active sert d'anode. Pendant ce temps, les armatures situées dans la zone de compression sont restées dans un état passif en raison de la protection de la couverture de béton épaisse. En raison de la connexion électrique entre les deux parties, les barres d'armature en zone comprimée ont agi comme une cathode et ont été protégées, car les zones cathodiques sont plus polarisées et actives à proximité de la zone anodique. Ainsi, les électrons ont migré dans les étriers de la zone tendue fissurée vers la zone de comprimée.

Dans un second temps, le processus de corrosion a été modifié, après que les ions chlorures ont pénétré la couverture de béton non fissurée des zones situées à l'extrémité de la poutre, car plus éloignée des zones anodiques initiales, elles étaient moins protégées de la corrosion par le processus de macro-pile. La nouvelle zone anodique ainsi crée a protégé catholiquement les armatures tendues situées en regard aux deux extrémités de la poutre.

Selon la Figure 24, on peut constater qu'une corrosion sévère s'est produite sur certaines barres HA horizontales alors les coins des étriers n'étaient que légèrement corrodés, et que certaines barres HA horizontales en contact avec des coins d'étriers fortement corrodés n'ont souffert que d'une légère corrosion au niveau de leurs intersections. . On peut donc en déduire que la corrosion des étriers n'est pas corrélée à celle des armatures principales HA.

Le chapitre Ⅴ présente les conclusions de ces expériences et les perspectives pour les futures recherches.

Les bulles d'air sont principalement situées à l'interface inférieure acier-béton selon la direction de coulage du béton frais et sa distribution est affectée par la forme des barres HA (crénelures). La plupart des bulles d'air sont situées dans la zone de pied de nervure des aciers HA. Les microstructures des produits d'hydratation du ciment autour des armatures ont été affectées par la direction de coulage. Des cristaux évidents de Portlandite et d'Ettringite peuvent se développer dans l'interface inférieure, mais ils ne peuvent pas être observés dans l'interface supérieure.

Pour le béton armé non fissuré, en l'absence de “top-casting defects”, la corrosion s'est amorcée préférentiellement à l'extérieur des barres d'armature en acier. En présence de “top-casting defects”, la corrosion a principalement eu lieu au pied des nervures des barres HA dans l'interface inférieure. Les points initiaux de corrosion par piqûres n'étaient pas liés aux vides d'air. Dans la phase de propagation, la corrosion s'est développée progressivement autour du périmètre des barres en acier, et après un certain temps, les “top-casting defects” n'ont plus d'incidence sur le processus de corrosion.

Pour le béton armé fissuré, en l'absence de “top-casting defects”, la corrosion s'est d'abord amorcée au niveau des fissures transversales, mais ne s'est pas propagée et ceux jusqu'à ce que la pénétration des chlorures à travers la couverture de béton soit suffisante pour initier la corrosion. En revanche, en présence de “top-casting defects”, les chlorures peuvent pénétrer à partir des fissures transversales et migrer le long des défauts jusqu'aux points les plus faibles pour initier la corrosion loin des fissures. De même, dans la propagation de la corrosion, l'effet des “top-casting defects”, sur la corrosion des barres d'armature en acier a progressivement diminué puis a disparu. Aucune corrélation entre la largeur des fissures transversales et la propagation de la corrosion n’a pu être trouvée.

Pour la corrosion des étriers, quelles que soient les conditions d'exposition, une corrosion par piqûres s'est toujours produite sur les parties horizontales des étriers situés à mi-portée de la zone de tendue (en face des fissures de service) et aux extrémités de la poutre en béton armé dans la zone de compression, tandis que les parties horizontales opposées étaient protégés. Aucune corrélation n’a été trouvée entre la corrosion des étriers et celles des armatures principales de flexion. L’état de corrosion à l'intersection entre les étriers et les barres principales est principalement lié aux conditions à l’interface acier-béton.

[1] U.U.N.E.S. Aff, World population prospects: The 2015 revision, 33 (2015) 1-66.
[2] S.J.U.R.B. Guihua, F. Control, Application of Plastic Drainage Plate Subgrade Treatment and Stage Loading Technique in Project of Encircling Sea to Make Land, 9 (2008).
[3] L.C.F. Guang-de, Economics, A Study of the Construction of Hong Kong-Zhuhai-Macao Bridge, Decrease of Transportation Cost and Industrial Transfer of Greater Pearl River Delta: An Analytic Framework of New Economic Geography [J], 8 (2011).
[4] W.F. Baker, D.S. Korista, L.C.J.T.s.d.o.t. Novak, s. buildings, Burj Dubai: Engineering the world's tallest building, 16 (2007) 361-375.

[5] D.C. Wallace, J Chesapeake Science, Age, growth, year class strength, and survival rates of the white perch, Morone americana (Gmelin) in the Delaware River in the vicinity of Artificial Island, 12 (1971) 205-218.
[6] D.A. Jay, K. Leffler, H.L. Diefenderfer, A.B.J.E. Borde, Coasts, Tidal-fluvial and estuarine processes in the lower Columbia River: I. Along-channel water level variations, Pacific Ocean to Bonneville Dam, 38 (2015) 415-433.
[7] R. François, S. Laurens, F. Deby, Corrosion and Its Consequences for Reinforced Concrete Structures, Elsevier2018.
[8] K.S. Tuutti, Corrosion of steel in concrete, (1982).
[9] P.K. Mehta, P.J. Monteiro, Concrete Microstructure, Properties and Materials, 2017.
[10] R. François, G. Arliguie, Influence of service cracking on reinforcement steel corrosion, Journal of Materials in Civil Engineering, 10 (1998) 14-20.
[11] R. Francois, J. Maso, Effect of damage in reinforced concrete on carbonation or chloride penetration, Cement and Concrete Research, 18 (1988) 961-970.
[12] C. Arya, F. Ofori-Darko, Influence of crack frequency on reinforcement corrosion in concrete, Cement and Concrete Research, 26 (1996) 345-353.
[13] S.C. Das, H.S. Pouya, E. Ganjian, Corrosion mitigation of chloride-contaminated reinforced concrete structures: a state-of-the-art review, Proceedings of the Institution of Civil Engineers-Construction Materials, 164 (2010) 21-28.
[14] M.B. Otieno, The development of empirical chloride-induced corrosion rate prediction models for cracked and uncracked steel reinforced concrete structures in the marine tidal zone, University of Cape Town, 2014.
[15] M. Otieno, H. Beushausen, M. Alexander, Towards incorporating the influence of cover cracking on steel corrosion in RC design codes: the concept of performance-based crack width limits, Materials and Structures, 45 (2012).
[16] M. Otieno, M. Alexander, H.-D. Beushausen, Corrosion in cracked and uncracked concrete-influence of crack width, concrete quality and crack reopening, Magazine of Concrete Research, 62 (2010) 393-404.
[17] W. Zhang, R. François, L. Yu, Influence of load-induced cracks coupled or not with top-casting-induced defects on the corrosion of the longitudinal tensile reinforcement of naturally corroded beams exposed to chloride environment under sustained loading, Cement and Concrete Research, 129 (2020) 105972.
[18] C. Fu, N. Jin, H. Ye, X. Jin, W. Dai, Corrosion characteristics of a 4-year naturally corroded reinforced concrete beam with load-induced transverse cracks, Corrosion Science, 117 (2017) 11-23.
[19] R. François, G. Arliguie, Effect of microcracking and cracking on the development of corrosion in reinforced concrete members, Magazine of Concrete Research, 51 (1999) 143-150.
[20] L. Yu, R. François, V.H. Dang, V. L'Hostis, R. Gagné, Development of chloride-induced corrosion in pre-cracked RC beams under sustained loading: Effect of load-induced cracks, concrete cover, and exposure conditions, Cement and Concrete Research, 67 (2015) 246-258.
[21] A. Michel, A.O.S. Solgaard, B.J. Pease, M.R. Geiker, H. Stang, J.F. Olesen, Experimental investigation of the relation between damage at the concrete-steel interface and initiation of reinforcement corrosion in plain and fibre reinforced concrete, Corrosion Science, 77 (2013) 308-321.

[22] L. Yu, R. François, R. Gagné, Influence of steel-concrete interface defects induced by top-casting on development of chloride-induced corrosion in RC beams under sustained loading, Materials and Structures, 49 (2016) 5169-5181.
[23] F. Chen, C.-Q. Li, H. Baji, B. Ma, Effect of design parameters on microstructure of steel-concrete interface in reinforced concrete, Cement and Concrete Research, 119 (2019) 1-10.
[24] U.M. Angst, M.R. Geiker, A. Michel, C. Gehlen, H. Wong, O.B. Isgor, B. Elsener, C.M. Hansson, R. François, K. Hornbostel, The steel-concrete interface, Materials and Structures, 50 (2017) 143.
[25] R. Zhang, A. Castel, R. François, Influence of steel-concrete interface defects owing to the top-bar effect on the chloride-induced corrosion of reinforcement, Magazine of Concrete Research, 63 (2011) 773-781.
[26] W. Zhang, L. Yu, R. François, Influence of top-casting-induced defects on the corrosion of the compressive reinforcement of naturally corroded beams under sustained loading, Construction and Building Materials, 229 (2019) 116912.
[27] J. Ryou, K. Ann, Variation in the chloride threshold level for steel corrosion in concrete arising from different chloride sources, Magazine of Concrete Research, 60 (2008) 177-187.
[28] W.H. Hartt, J. Nam, Effect of cement alkalinity on chloride threshold and time-to-corrosion of reinforcing steel in concrete, Corrosion, 64 (2008) 671-680.
[29] I. Zafar, T. Sugiyama, Laboratory investigation to study the corrosion initiation of rebars in fly ash concrete, Magazine of Concrete Research, 66 (2014) 1051-1064.
[30] U.M. Angst, M.R. Geiker, M.C. Alonso, R. Polder, O.B. Isgor, B. Elsener, H. Wong, A. Michel, K. Hornbostel, C. Gehlen, The effect of the steel–concrete interface on chloride-induced corrosion initiation in concrete: a critical review by RILEM TC 262-SCI, Materials and Structures, 52 (2019) 88.
[31] S.K. Goudar, B. Das, S. Arya, Microstructural Study of Steel-Concrete Interface and Its Influence on Bond Strength of Reinforced Concrete, Advances in Civil Engineering Materials, 8 (2019) 171-189.
[32] U.M. Angst, B. Elsener, C.K. Larsen, Ø. Vennesland, Chloride induced reinforcement corrosion: Electrochemical monitoring of initiation stage and chloride threshold values, Corrosion Science, 53 (2011) 1451-1464.
[33] C. Andrade, M. Alonso, J.J.E.A.S. Gonzalez, Similarity between atmospheric/underground corrosion and reinforced concrete corrosion, (1990) 39-48.
[34] P. Bhatt, T.J. MacGinley, B.S. Choo, Reinforced concrete design: Design theory and examples, CRC Press2006.
[35] T.U. Mohammed, N. Otsuki, H. Hamada, T. Yamaji, Chloride-induced corrosion of steel bars in concrete with presence of gap at steel-concrete interface, Materials Journal, 99 (2002) 149-156.
[36] T.U. Mohammed, N. Otsuki, M. Hisada, T. Shibata, Effect of Crack Width and Bar Types on Corrosionof Steel in Concrete, Journal of Materials in Civil Engineering, 13 (2001) 194-201.
[37] A. Alhozaimy, R.R. Hussain, R. Al-Zaid, A. Al Negheimish, Investigation of severe corrosion observed at intersection points of steel rebar mesh in reinforced concrete construction, Construction and Building Materials, 37 (2012) 67-81.
[38] N. Otsuki, S.-i. Miyazato, N.B. Diola, H. Suzuki, Influences of bending crack and water-cement ratio on chloride-induced corrosion of main reinforcing bars and stirrups, Materials Journal, 97 (2000) 454-464.

[39] T.U. Mohammed, N. Otsuki, M. Hisada, Corrosion of steel bars with respect to orientation in concrete, ACI Materials Journal, 96 (1999) 154-159.
[40] O. Geng, Reinforcement corrosion and degradation rate of concrete members China railway publishing house2010.
[41] L. Tong, Research on the damage of concrete and the influence for the longitudinal reinforcement corrosion by stirrup corrosion Structural Engineering, Xi'an University of Architecture and Technology, 2013.
[42] C. Boschmann Kathler, U.M. Angst, M. Wagner, C.K. Larsen, B. Elsener, Effect of cracks on chloride-induced corrosion of steel in concrete-a review: Etatsprogrammet Varige konstruksjoner 2012-2015, ETH Zurich, 2017.

I. Introduction

1 Background

Concrete is one of the most widely used building materials around the world owning to its excellent compressive strength, versatility, low cost and widely distributed raw materials[1]. Concrete, however, is a typical quasi-brittle material because the tensile strength of which is markedly relatively lower in comparison with its compressive strength. Thus, reinforcing steels are used to reinforce concrete in most of concrete constructions. As reinforced concrete exhibited excellent physical performances and mechanical properties, it has become one of the uppermost building materials in the world which cannot be replaced in this century[1].

Generally, the serviceability and the durability of reinforced concrete are quite remarkable in-service as the reinforcing steel used in concrete can be protected well by the concrete cover from both physical and chemical points of view. From the physical point of view, steel reinforcement can be protected well by concrete cover through preventing the access of aggressive substances, such as carbon dioxide, moisture and chloride ions due to the dense and relatively impermeable concrete cover. From the chemical point of view, a passive layer formed on the surface of steel reinforcement in a high alkaline environment formed by the hydration of cement which can protect steel from corrosion[2].

Nowadays, encircling the sea to make land or city is regarded as the most way to resolve the limited land resources due to the rapid growth of world population. Therefore, more and more reinforced concrete structures or elements are constructed in ocean environment. However, when the reinforced concrete constructions or members are long-term exposed to a chloride environment, such as in an ocean environment, the passive layer of reinforcing steel in concrete would be destroyed to result in the corrosion of steel reinforcement which would be maintained for a long term[3, 4]. The corrosion of steel in concrete accelerates the deterioration of reinforced concrete construction, and threatens human safety.

Each year, considerable natural and social resources are consumed to repair and rehabilitate deteriorated reinforced concrete structures. In 2004, United States spent $5 billion on the remediation of concrete bridges affected by corrosion of the reinforcing steel[5]. In UK, billions of pounds, equivalent to around 4% to 6% of gross domestic product (GDP), are spent on the rehabilitating of corroded reinforced concrete structures[6]. In China, the loss caused by the

deterioration of reinforced concrete structures is more than ￥100 billion each year[7]. The cost of repair a rehabilitation of reinforced concrete structures in the other countries of the world is not very well documented, but undoubtedly, considerable resources had to be allocated towards restoring the useful service life of deteriorating concrete structures. Therefore, to find a proper method to protect steel corrosion in concrete and to accurately predict the service life of reinforced concrete structures by studying the corrosion behavior of steel in concrete under a chloride environment possesses obvious benefits both in society and economy for the guarantees of the safety and durability of ocean engineering.

Corrosion process of reinforced concrete is commonly composed of two phases the initiation phase and the propagation phase[8]. In a chloride environment, during the initiation phase, the chlorides can penetrate from the environment and reach the level of reinforcing steel. When chloride concentration at the surface of the reinforcing steel reaches a certain value (chloride threshold level, or critical chloride content), the protective layer breaks down and the corrosion of steel in concrete takes place locally. Then, the propagation phase begins. During the propagation phase, the cross-sectional loss of steel reinforcement would gradually rise and the bearing capacity of reinforced concrete gradually reduced and then the cracking and spalling of concrete cover would appear due to the generation of volumetric corrosion products. When the reduction of the bearing capacity of corroded reinforced concrete structures reaches the maximum acceptable damage level, service life of reinforced concrete structures is end.

According to the previous investigations, the starting time of corrosion initiation is affected by the diffusion rate of chloride ions in concrete and the critical chloride ions content near the steel surface[9]. Since the 1950s, numerous studies aimed at measuring the critical chloride content and accordingly a large amount of results were published. Different literature reviews show[10-13] that the reported values for critical chloride content scatter over a large range, that is, from virtually 0 up to > 3% chloride by mass of cement. No general trends could be identified regarding certain types of binder, concrete mix proportions, etc. So, it is hard to establish an accurate model to predict the initiation of steel corrosion in concrete.

In the past decade, more and more investigations reported that the steel-concrete interface has a particular influence on the corrosion of steel in concrete in chloride exposure environment[14-18]

and in the case of carbonation[19]. It also influences certain aspects of the bond between steel and concrete such as adhesion between steel and concrete[20-23]. Therefore, in 2014, TC 262-SCI, one of the Technical Committees of RILEM, was established to research the characteristics of steel-concrete interface and the impact of steel-concrete interface on the corrosion of reinforced concrete under chloride environment.

According the present documents, most of these studies focused on the properties of interfacial defects and the effect of it on the critical chloride threshold of steel in concrete or mortar[24, 25]. However, the impact of interfacial defects on the corrosion behavior of steel reinforcement itself in corrosion initiation and propagation has received very little research attention[18, 26]. Apart from this, there were hardly any literatures concerning the corrosion of stirrups used in reinforced concrete buildings, which can be regarded as an important part of reinforced concrete constructions.

In order to establish a reliable prediction model of service life considering corrosion behavior of steel reinforcement in concrete, we firstly must clarify the characteristics of steel-concrete interface and the effect of it on the corrosion behavior of reinforced concrete should be understood more completely.

2 Statement of the problem

Cracking is a common damage of concrete and is inevitable during the whole service life. A lot of researchers have reached a consensus that cracks accelerate corrosion initiation because they provide the aggressive agents with preferential pathways[27-30]. However, it is not well understood how cracks affect the propagation phase. Some researchers consider that cracks accelerate chloride-induced corrosion by increasing concrete penetrability and the corrosion rate also increases with increased crack width in the propagation phase[30, 31]. However, other researchers[27, 32-34] hold the view that crack width has no effect on corrosion propagation kinetics. One possible explanation for this contradiction is that the surface cracks width alone does not reliably describe the condition of the steel-concrete interface.

Various interfaces widely exist in the structure of concrete material[1]. Generally, at the macroscopic level, reinforced concrete mainly contains two phases aggregate-paste phase and steel-concrete phase. For the latter one, some interfacial defects, containing, air bubbles, bleed water

defects and voids, would be formed at the interface of steel-concrete due to bleeding, segregation and settlement of fresh concrete[16, 18]. According to the fundamentals of thermodynamics, due to the existence of these defects, the micro-environment around steel bar will no longer to be perfect, a macro-cell would be established between the side of steel bar with a dense concrete cover and the side of reinforcement facing towards the defects when reinforced concrete elements exposed to a chloride environment[14]. Ryou and Ann[35] observed that corrosion initiated in the voids at the steel-concrete interface, regardless of whether the chlorides were of external or internal origin. Hartt and Nam[36] found that corrosion initiated preferentially at air voids of diameter larger than 2.5 mm. However, recent studies reported that defects at the steel-concrete interface did not have any influence on corrosion initiation under certain environmental conditions[37, 38]. Angst et al[37] observed by visual inspections that the location of corrosion onset did not coincide with the location of interfacial air voids.

Furthermore, just several studies have been found on the effect of top-casting defects on corrosion behavior of reinforced concrete in corrosion propagation. Yu et al[18] found that corrosion-induced cracks always developed much more quickly along top-cast steel bars, owing to the existence of top-casting-induced defects, and they were favorable to both the initiation and the propagation of corrosion. However, the studies of the effect of top-casting defects on the corrosion behavior of steels in concrete can be hardly found. Thus, there is an eager demand for investigations on the effect of interfacial defects of steel-concrete on the corrosion behavior of reinforcing steels in concrete constructions.

Apart from the main reinforcing steels in concrete, stirrups used in concrete can be regarded as an important part for the reinforced concrete structures. Generally, stirrups are used for fixing the location of main deformed steel bars during manufacturing and installing steel frame and for bearing the shear stress during the service life of reinforced concrete structure[2]. Recently, most published documents concerning the stirrups mainly focus on the shear capacity. However, the corrosion behavior of stirrups used in reinforced concrete has received very little research attention. In the case of the relationship between stirrups and the main steel rebars, some investigations[39, 40] reported that the stirrups can protect the main rebars against corrosion, however, other studies[41, 42] indicated that stirrups do not protect main bars, but accelerate the corrosion rate of reinforcing

steels. So, it is necessary to research the corrosion behavior of stirrups in concrete for the establishment of prediction model of reinforced concrete elements.

Summary, although many studies have been conducted on the influence of interfacial defects for chloride-induced corrosion[24, 25], on-going investigations and discussions on the topic highlights the importance to clarify if, and how, interfacial defects may effect initiation and propagation of corrosion of steel in concrete.

3 Objectives of the research

The main objectives of this research are

1. To study the top-casting-induced defects and transverse crack on the corrosion behavior of reinforcing steel in concrete under chloride environment in corrosion initiation. In details, this research investigates the interfacial conditions of steel-concrete, the chloride penetration in steel-concrete interface and the effect of top-casting-induced defects and/or artificial crack on the corrosion behavior of steel rebars in corrosion initiation.

2. To study the impact of top-casting defects and/or load-induced cracks on the corrosion development and corrosion behavior of corroded reinforced concrete in corrosion propagation. In details, the impact of top-casting-induced defects and/or load-induced cracks on the development of corrosion-induced cracking on concrete beams, the chloride ingress, the cross-sectional loss of steel rebars and the distribution of pitting corrosion around the perimeter of steel is measured, compared and analyzed.

3. To study the corrosion behavior of stirrups in reinforced concrete beam. In details, the cracking maps of reinforced concrete beams were recorded firstly. Then, the microstructure of steel-concrete interface was studied. The third, the cross-sectional loss of stirrups and the distribution of corrosion on stirrups were measured and compared. The corrosion behavior of different legs of stirrups were analyzed. Finally, the relationship between stirrups and main reinforcing steels in concrete beams was discussed.

4 Thesis outline

This thesis has five chapters

Chapter Ⅱ reports a literature review including the fundamentals of steel corrosion in concrete and the formation and characteristics of top-casting defects in steel-concrete interface. Subsequently, some published researches concerning the effect of top-casting defects on the corrosion process and corrosion behaviors of steel reinforcement in concrete are reviewed. Finally, the corrosion behavior of stirrups in concrete is reviewed.

Chapter Ⅲ presents detailed information of three experimental programs started in 2010, 2013 and 2017 respectively. All the details of the reinforced concrete blocks and/or beams concerned in this thesis can be found in this chapter.

Chapter Ⅳ investigates the corrosion behavior of reinforcing steel in concrete in different corrosion period, including the characteristics of steel-concrete interface and the effect of artificial crack and/or top-casting defects on the initial corrosion behavior of reinforced concrete blocks; the effect of load-induced crack and top-casting defects on the corrosion behaviors of different steel reinforcement in concrete beams in corrosion propagation; the corrosion of stirrups in corroded reinforced concrete beam.

Chapter Ⅴ summarizes the conclusions and perspective of this work.

Chapter Ⅳ consists of several research papers, which are either already published in an international journal or in the process of publication. In order to keep their original format in this thesis, there are some repetitions in some sections, e.g. experimental context, exposure conditions etc.

5 Reference

[1] P.K. Mehta, P.J. Monteiro, Concrete Microstructure, Properties and Materials, 2017.

[2] A.H. Nilson, G. Winter, L.C. Urquhart, O.R. Charles Edward, Design of concrete structures, McGraw-Hill New York, USA1991.

[3] D. Coronelli, P. Gambarova, Structural assessment of corroded reinforced concrete beams: modeling guidelines, Journal of structural engineering, 130 (2004) 1214-1224.

[4] Y. Auyeung, P. Balaguru, L. Chung, Bond behavior of corroded reinforcement bars, Materials Journal, 97 (2000) 214-220.

[5] M. O'Connell, C. McNally, M.G. Richardson, Biochemical attack on concrete in wastewater applications: A state of the art review, Cement and Concrete Composites, 32 (2010) 479-485.

[6] S.C. Das, H.S. Pouya, E. Ganjian, Corrosion mitigation of chloride-contaminated reinforced concrete structures: a state-of-the-art review, Proceedings of the Institution of Civil Engineers-Construction Materials, 164 (2010) 21-28.

[7] B. Hou, D. Zhang, P. Wang, Marine Corrosion and Protection: Current Status and Prospect, Bulletin of Chinese Academy of Sciences, 31 (2016) 1326-1331.

[8] K.S. Tuutti, Corrosion of steel in concrete, (1982).

[9] U.M. Angst, Predicting the time to corrosion initiation in reinforced concrete structures exposed to chlorides, Cement and Concrete Research, 115 (2019) 559-567.

[10] W. Breit, Critical corrosion inducing chloride content–State of the art and new investigation results, Betontechnische Berichte 1998-2000, (2001) 631-637.

[11] K.Y. Ann, H.-W. Song, Chloride threshold level for corrosion of steel in concrete, Corrosion science, 49 (2007) 4113-4133.

[12] M. Alonso, M. Sanchez, Analysis of the variability of chloride threshold values in the literature, Materials and Corrosion, 60 (2009) 631-637.

[13] U. Angst, B. Elsener, C.K. Larsen, Ø. Vennesland, Critical chloride content in reinforced concrete—a review, Cement and concrete research, 39 (2009) 1122-1138.

[14] R. Zhang, A. Castel, R. François, Influence of steel-concrete interface defects owing to the top-bar effect on the chloride-induced corrosion of reinforcement, Magazine of Concrete Research, 63 (2011) 773-781.

[15] A. Castel, T. Vidal, R. François, G. Arliguie, Influence of steel-concrete interface quality on reinforcement corrosion induced by chlorides, Magazine of Concrete Research, 55 (2003) 151-159.

[16] T.A. Soylev, R. François, Quality of steel-concrete interface and corrosion of reinforcing steel, Cement and Concrete Research, 33 (2003) 1407-1415.

[17] T.U. Mohammed, N. Otsuki, H. Hamada, T. Yamaji, Chloride-induced corrosion of steel bars in concrete with presence of gap at steel-concrete interface, Materials Journal, 99 (2002) 149-156.

[18] L. Yu, R. François, R. Gagné, Influence of steel-concrete interface defects induced by top-casting on development of chloride-induced corrosion in RC beams under sustained loading, Materials and Structures, 49 (2016) 5169-5181.

[19] R.M. Ghantous, R. François, S. Poyet, V. L'hostis, F. Bernachy-Barbe, D. Meinel, L. Portier, N.-C. Tran, Relation between crack opening and extent of the damage induced at the steel/mortar interface, Construction and Building Materials, 193 (2018) 97-104.

[20] T.A. Söylev, R. Francois, Effects of bar-placement conditions on steel-concrete bond, Materials and structures, 39 (2006) 211-220.

[21] A. Castel, T. Vidal, K. Viriyametanont, R. François, Effect of reinforcing bar orientation and location on bond with self-consolidating concrete, ACI Structural Journal, 103 (2006) 559.
[22] M. Hoshino, Relation between bleeding, coarse aggregate, and specimen height of concrete, Materials Journal, 86 (1989) 185-190.
[23] G.B. Welch, B.J. Patten, Bond strength of reinforcement affected by concrete sedimentation, Journal Proceedings, 1965, pp. 251-264.
[24] U.M. Angst, M.R. Geiker, M.C. Alonso, R. Polder, O.B. Isgor, B. Elsener, H. Wong, A. Michel, K. Hornbostel, C. Gehlen, The effect of the steel–concrete interface on chloride-induced corrosion initiation in concrete: a critical review by RILEM TC 262-SCI, Materials and Structures, 52 (2019) 88.
[25] U.M. Angst, M.R. Geiker, A. Michel, C. Gehlen, H. Wong, O.B. Isgor, B. Elsener, C.M. Hansson, R. François, K. Hornbostel, The steel-concrete interface, Materials and Structures, 50 (2017) 143.
[26] W. Zhang, L. Yu, R. François, Influence of top-casting-induced defects on the corrosion of the compressive reinforcement of naturally corroded beams under sustained loading, Construction and Building Materials, 229 (2019) 116912.
[27] R. François, G. Arliguie, Influence of service cracking on reinforcement steel corrosion, Journal of Materials in Civil Engineering, 10 (1998) 14-20.
[28] R. Francois, J. Maso, Effect of damage in reinforced concrete on carbonation or chloride penetration, Cement and Concrete Research, 18 (1988) 961-970.
[29] C. Arya, F. Ofori-Darko, Influence of crack frequency on reinforcement corrosion in concrete, Cement and Concrete Research, 26 (1996) 345-353.
[30] M. Otieno, M. Alexander, H.-D. Beushausen, Corrosion in cracked and uncracked concrete-influence of crack width, concrete quality and crack reopening, Magazine of Concrete Research, 62 (2010) 393-404.
[31] M. Otieno, H. Beushausen, M. Alexander, Towards incorporating the influence of cover cracking on steel corrosion in RC design codes: the concept of performance-based crack width limits, Materials and Structures, 45 (2012).
[32] P. Schieβl, M. Raupach, Laboratory studies and calculations on the influence of crack width on chloride-induced corrosion of steel in concrete, Materials Journal, 94 (1997) 56-61.
[33] D. Darwin, Crack Width, Cover, and Corrosion, Farmington Hills, (1985).
[34] R. Oesterle, The Role of Concrete Cover in Crack Control Criteria and Corrosion Protection, RD serial, (1997).
[35] J. Ryou, K. Ann, Variation in the chloride threshold level for steel corrosion in concrete arising from different chloride sources, Magazine of Concrete Research, 60 (2008) 177-187.
[36] W.H. Hartt, J. Nam, Effect of cement alkalinity on chloride threshold and time-to-corrosion of reinforcing steel in concrete, Corrosion, 64 (2008) 671-680.
[37] U.M. Angst, B. Elsener, C.K. Larsen, Ø. Vennesland, Chloride induced reinforcement corrosion: Electrochemical monitoring of initiation stage and chloride threshold values, Corrosion Science, 53 (2011) 1451-1464.
[38] U. Angst, Chloride induced reinforcement corrosion in concrete, Doctoral theses, Norwegian University of Science and Technology, Trondheim, (2011).
[39] O. Geng, Reinforcement corrosion and degradation rate of concrete members China railway publishing house2010.

[40] L. Tong, Research on the damage of concrete and the influence for the longitudinal reinforcement corrosion by stirrup corrosion Structural Engineering, Xi'an University of Architecture and Technology, 2013.
[41] N. Otsuki, S.-i. Miyazato, N.B. Diola, H. Suzuki, Influences of bending crack and water-cement ratio on chloride-induced corrosion of main reinforcing bars and stirrups, Materials Journal, 97 (2000) 454-464.
[42] T.U. Mohammed, N. Otsuki, M. Hisada, Corrosion of steel bars with respect to orientation in concrete, ACI Materials Journal, 96 (1999) 154-159.

II. Literature review

1 Introduction

Cracking and interfacial defects of steel-concrete are two inevitable characters in the entire life cycle of reinforced concrete. As mentioned above, both the two characters would induce the deterioration of steel reinforced concrete. Therefore, in order to get an overall understanding on the effect of interfacial defects and cracks on the steel corrosion in concrete, it is necessary to make a review of the previous published researches concerning the effect of cracks and interfacial defects on the steel corrosion in concrete, respectively.

This chapter consists of three parts 1). The fundamentals of steel reinforcement corrosion in concrete; 2). Chloride ions ingress in cracked concrete; 3). Effect of cracks on steel corrosion in concrete; 4). Impact of interfacial defects on the deterioration of steel reinforcement in concrete; 5). Corrosion of stirrups in reinforced concrete.

2 Fundamentals of chloride-induced steel corrosion in concrete

Reinforcing steel can be protected by concrete in terms of both physical and chemical methods. From the physical protection perspective, concrete limits the penetration of aggressive agents (chloride ions, carbon dioxide and moisture), which are necessary to initiate and maintain corrosion process. From the chemical point of view, a thin, dense and passive film is formed on the surface of steel rebar by the high alkalinity formed by the $Ca(OH)_2$ generated by the hydration of cement, which can enhance the corrosion potential and resist against the corrosion of steel. The main compositions of this thin layers are mixed oxides and hydrated oxides of iron[1-3], which will be detailedly reviewed in section Ⅱ-5.1.

It is well known that the corrosion of steel in concrete is a classic electrochemical process, including anodic reaction and cathodic reaction, which takes place as follow

Anodic reaction $Fe \rightarrow Fe^{2+} + 2e^-$

Cathodic reaction $O_2 + 2H_2O + 4e^- \rightarrow 4OH^-$

At the anode of this electrochemical process, iron is oxidized. Corrosion products form and precipitate on or not far from the anode sites. Electrons released at the anode are consumed in the cathodic reaction, where hydroxyls form through the reaction between moisture and oxygen. The cathodic reaction is not harmful to the steel. The whole corrosion process is presented in the

schematic presented in Figure II-1.

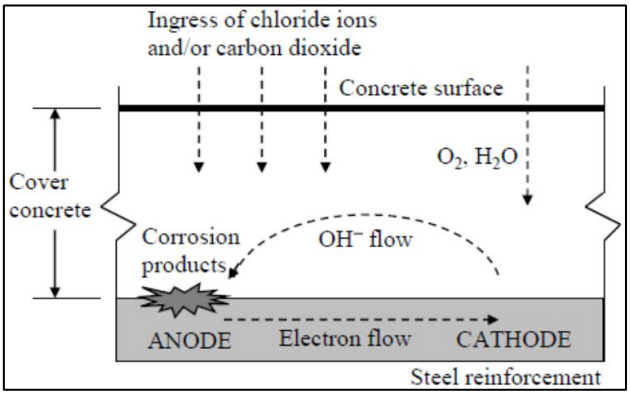

Figure II-1 A schematic of corrosion process in concrete [4]

There are four conditions that must be fulfilled to initiate and maintain the corrosion process

a. an anodic reaction;

b. a cathodic reaction;

c. a conductor for the flux of ions between anode and cathode;

d. a conductor for the flux of electrons.

These conditions are summarized in Figure II-2[5]. Normally, steel bar in concrete acts as electron conductor and the pore solution of concrete works as the conductor of the flux of ions[6].

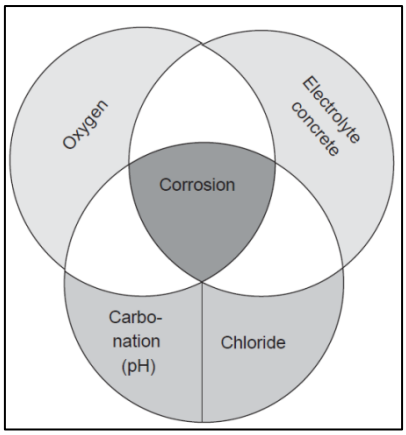

Figure II-2 Necessary conditions for corrosion of steel in concrete [5]

Corrosion of steel reinforcement in concrete structures can be classified as micro-cell corrosion and macro-cell corrosion. In micro-cell corrosion, anodic and cathodic sites are adjacent to each other, small and inseparable. Generally, micro-cell corrosion is induced by carbonation of concrete cover[7]. But even in the case of corrosion induced by carbonation, macro-cell corrosion appears due to multi-layers of steel (Figure II-3). And the appearance of micro-cell corrosion is usually uniform. While in macro-cell corrosion, anode and cathode are clearly separated in different areas

and one of the most import features of macro-cell corrosion is a real big cathode/anode area ratio. Macro-cell corrosion occurs frequently in concrete contaminated by chlorides or cracked concrete[7, 8]. The distribution of macro-cell corrosion is usually heterogeneous or even in the form of pitting corrosion.

Macro-cell corrosion is usually found in corroded reinforced concrete structures in-service. As illustrated in Figure II-3, the reinforcements of the top layer are contaminated by chlorides or depassivated by carbonation and they become active, while the reinforcements of the bottom layer are still in passive state and water and oxygen are available there. The active and passive parts are connected electrically by stirrups, then macro-cell corrosion form between them.

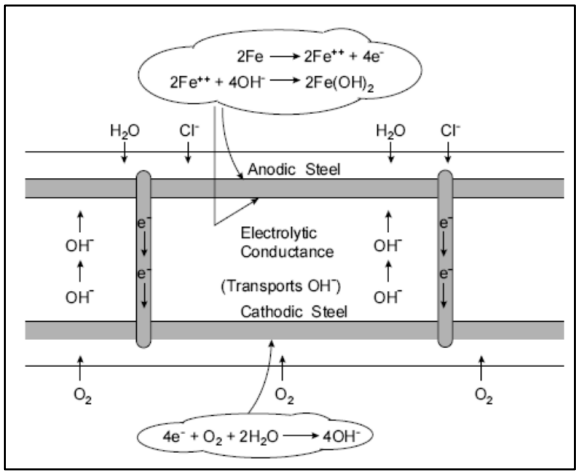

Figure II-3 Macro-cell corrosion in reinforced concrete structures in-service [9]

Corrosion of steel in concrete gives up to the formation of corrosion products, which consist of iron oxides and iron hydroxides. The exact compositions of corrosion products depend on oxygen availability, pH value, temperature, the presence of chloride and carbon dioxide and so on. Normally, the volume of corrosion products is several times bigger than original steel and the expand factors depend on their chemical compositions. The expand factors of different corrosion products area presented in Figure II-4[10] and rang from 1.8 to 6.2.

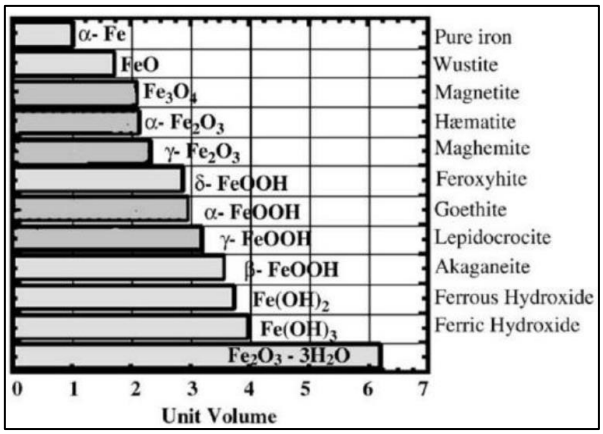

Figure II-4 Corrosion products and their expand factors [10]

3 Chloride ingress in cracked concrete

Chloride content in reinforced concrete is an important parameter to predict the corrosion initiation of reinforcement steel in concrete, which has led to the concept of a chloride threshold level (or critical chloride threshold) [11]. In this section, the source of chlorides in concrete and the mechanisms of chloride ingress in concrete will be reviewed.

3.1 Source of chloride

Generally, according to the nature of concrete in different period, that is, the fresh concrete and hardened concrete, two major sources of chloride ions in concrete can be found[12] 1). Chlorides incorporated in the fresh concrete during mixing, e.g. contaminated mixing water, salty aggregates or admixtures. 2). Chloride ions penetrating in the hardened concrete from the environment, e.g. from seawater, salty groundwater, de-icing salts, industrial process and so on.

In the past, Calcium chloride was commonly used as an accelerating admixture in fresh concrete. Chloride additions ranging from 0.5% to 2% by mass of cement have given up to extensive corrosion damage[13]. However, chloride content in admixtures is limited today. Ingress of chloride ions from environment is thus a primary concern.

Seawater is aggressive against reinforcing steel in concrete. Generally, the content of salt, mainly including Na^+, Mg^{2+}, Cl^- and SO_4^{2-}, is 3.5% per weight in seawater. Ocean structures can be affected by reinforcement corrosion. The de-icing salt will be used largely when bridge decks and road structures were built in cold region. Not all de-icing salts contain chloride. The sodium chloride,

however, is one of the cheapest and most efficient in the family of de-icing salts. When ice is removed from the surface of a structure using de-icing salts, the structure is exposed to melt water containing a high concentration of chloride. The melt water can be transported by vehicles from the roads to car parks. These structures are then very vulnerable since they can be exposed to dynamic loads and chlorides, which can increase the ingress of chloride ions in cracked concrete[14], as will be elaborated later.

3.2 Mechanisms of chloride transport and binding in concrete

3.2.1 Chloride transport in uncracked concrete

Chloride penetration in uncracked concrete is managed by three mechanisms, namely, capillary suction, diffusion and permeation [15]. However, the cracking of concrete cover, such as load-induced cracks or shrinkage, can alter the mechanism of chloride ingress significantly[16]. In order to understand the mechanisms of the ingress of chloride in cracked concrete, firstly, the basic transport mechanisms of chloride in uncracked concrete should be reviewed completely.

Transport mechanisms of chloride in uncracked concrete can be categorized as[12] 1). Capillary suction, where the chloride transport is caused by a difference in moisture content. In non-saturated concrete, water containing chloride ions moves towards zones with lower moisture content due to surface tension in the capillary pores; 2). Diffusion, where ionic transport is driven by a concentration difference in various zones. Chloride ions move from zones with higher concentration to zones with lower concentration; 3). Permeation, where a difference in hydraulic pressure in various zones drives the movement of chloride ions.

For these three given mechanisms, a brief introduction from the point of physical chemistry is presented respectively[17]

- **Capillary suction**

Capillary suction takes place in dry or partly saturated porous materials. If a liquid gets in touch with a porous material, it is absorbed rapidly by the under-pressure in the pores caused by capillary action. The action depends on the surface tension, viscosity and density of a liquid, contact angle between the liquid and solid phases, and on the pore radius. It can be described by the Young-

Laplace equation, assuming an idealized pore

$$P = -\frac{2\gamma\cos\theta}{r} \quad (1)$$

Where P is the pore pressure pulling chloride contaminated water, γ liquid-vapor surface tension of fluid, θ the contact angle between liquid and solid phases, and r the pore radius.

Capillary suction is an important mechanism leading to ingress of chloride ions into non-saturated concrete.

➢ **Diffusion**

For the diffusion of chloride ions in concrete to take place, the concrete must have a continuous liquid phase and there must be a chloride concentration gradient. Degree of pore saturation is thus an important parameter influencing diffusion of ions in concrete; the diffusion process is most effective when the concrete is fully saturated, although it can also occur in partially saturated concrete. Therefore, ionic diffusion of chloride is the controlling transport process when concrete is fully saturated; in a partially saturated condition, chlorides are transported by means of several combined mechanisms. However, it is usually assumed that diffusion is the predominant transport mechanism of chloride ions in concrete in uncracked concrete, even if in the outermost zone, capillary suction can play a major role.

The theory of diffusion is based on Fick's laws of diffusion[18]. Chloride diffusion into concrete can be described by Fick's first law, which relates the diffusive flux to the concentration field. It assumes that the flux goes from regions of high concentration to regions of low concentration, with a magnitude proportional to the concentration gradient. For one-dimensional diffusion, this is[12]

$$J = -D\frac{\partial C}{\partial x} \quad (2)$$

Where,

J is the diffusion flux in dimensions of [(amount of substance) length^{-2} time^{-1}], e.g. (mol/m^{2}s).

D is the diffusion coefficient in dimensions [length^2 time^{-1}], e.g. (m^2/s).

C is the chloride concentration in dimensions [(amount of substance) length^{-3}], e.g. (mol/m^3).

x is the position in dimensions [length], e.g. (m).

Fick's first law is used to derive the relevant equation for a case when concentration is time

dependent, i.e. Fick's second law

$$\frac{\partial C}{\partial t} = \frac{\partial}{\partial x}\left(D\frac{\partial C}{\partial x}\right) \quad (3)$$

If the diffusion coefficient (D) is constant, equation can be simplified as

$$\frac{\partial C}{\partial t} = D\frac{\partial^2 C}{\partial x^2} \quad (4)$$

This equation can be solved analytically for a semi-infinite medium and the following initial and boundary conditions

C = 0 at x > 0 at time t = 0 (initial condition)

C = Cs at x = 0 and t > 0 (boundary condition)-surface chloride concentration is a constant

Then, the chloride concentrations as a function of x and t can be obtained

$$C(x,t) = Cs\left[1 - erf\left(\frac{x}{2\sqrt{Dt}}\right)\right] \quad (5)$$

Where Cs is the surface chloride concentration and erf is the mathematical error function.

Concrete is a composite, porous material, comprising both solid and liquid phases, in which the diffusion process through the solid is negligible compared to the diffusion through the pores. The rate of the chloride diffusion is therefore not only controlled by the diffusion coefficient through the pore solution but mostly by the physical characteristics and the connectivity of the capillary pore structure. These effects are usually implicitly considered and the diffusion coefficient D is replaced by the effective diffusion coefficient, D_{eff}, which considers the diffusion of chlorides into concrete as a whole. It also considers the effects of chloride binding.

- **Permeation**

Permeation is penetration of a permeate (such as liquid or gas) (e.g. water containing chloride ions), through a porous material under a hydrostatic head. Permeability of concrete characterizes the ease with which a fluid will pass through it, under the action of a pressure differential. It can be described using Darcy's law

$$\frac{\partial q}{\partial t}\frac{1}{A} = k_p\frac{\partial h}{\partial x} \quad (6)$$

Where $\frac{\partial q}{\partial t}$ is the flow rate per unit area, A, k_p is the permeability coefficient and ∂h is the pressure difference across the specimen thickness, x.

Permeability coefficient is affected by the porosity, pore network connectivity and the viscosity

of the permeate. Chloride ions can also penetrate with water into the concrete by penetration.

➢ **Chloride binding in concrete**

As chloride ions penetrate in concrete cover, a portion of them is captured by the cement hydration products. This phenomenon is called chloride binding. It is defined as the interaction between the porous concrete matrix and chloride ions which results in their effective removal from the pore solution. Chloride binding needs to be considered in the service life predictions of concrete structures because 1). Reduction of the free chloride content in the vicinity of the reinforcing steel reduces the probability of corrosion; 2). Removal of chloride ions from the diffusion flux slows down the penetration of chloride; 3). Formation of Friedel's salt results in a less porous structure and slows down the transport of chloride ions[19, 20].

Chloride ions in concrete exist either as free or bound chlorides[21]. In general, it is accepted that only free chloride is relevant for corrosion of the reinforcing steel, although some authors consider that bound chlorides also present a significant corrosion risk. Chlorides can be bound either chemically or physically[22]. Chemical binding of chloride in cementitious materials is a result of reaction between chloride ions and C_3A to form chloroaluminate, namely, Friedel's salt, or the reaction of C_4AF to form a Friedel's salt analogue. Physical binding occurs due to the adsorption onto the amorphous calcium silicate hydrate (C-S-H) gel[23]. Bound chlorides can later be released by sulfate attack or carbonation of the hardened concrete paste[22].

Chloride binding is dependent on many parameters[23, 24]. Studies have confirmed that the higher chloride concentration of external chloride leads to higher chloride content in the pore solution and higher chloride binding[24]. Another important factor is the cement composition. It is considered that tricalcium aluminate (C_3A) and tetracalcium aluminoferrite (C_4AF) content in cement have the biggest impact on the amount of bound chlorides. Tang and Nilsson[25] concluded that the chloride binding capacity of OPC concrete is dependent on the amount of C-S-H gel in concrete and independent of the water-cement ratio and aggregate addition. C-S-H gel dominates the physical binding of chloride[24]. The higher the content of C_3S and C_2S is, the more chloride can be physically bound. Supplementary cementitious materials also affect chloride binding. Use of fly ash or blast furnace slag increases the level of chloride binding, while use of silica fume decreases it[26]. Sulfate resisting Portland cement also has a reduced binding capacity. Among other

parameters that influence the chloride binding are the cation of chloride salt ($CaCl_2$ and $MgCl_2$ result in more bound chlorides than NaCl), temperature (higher temperature decreases the amount of bound chloride), chloride source (more chloride binding is observed when chlorides are added to the mix, than when they penetrate from the outside), sulfate ions (decrease chloride binding), etc.

3.2.2 Critical chloride threshold

In order for steel in concrete to start corroding, a certain amount of chlorides must be exceeded in the steel-concrete interface. The chloride threshold level (or critical chloride concentration) is the concentration of chlorides necessary to break down the protective passive film on the reinforcement steel surface and initiate corrosion. Knowledge of this value is important because it is a vital input parameter in service life design and service life prediction models.

Unfortunately, the chloride threshold level is not a single value valid for all types of concretes, steels and environments, but is impacted by a number of different factors such as concrete cover thickness, temperature, relative humidity, electrical potential of the reinforcement, chemistry of the binder, proportion of total chlorides to that of free chlorides and chloride to hydroxyl ion ratio.

There is no consensus on the value of the critical chloride content. Angst et al[27] reviewed the reported critical chloride content and found a large overall scatter, the published critical chloride content values ranging from 0.04% to 8.34% total chloride by weight of cement. Garica et al[28] found that the critical chloride content had an average value of 0.8% by mass of cement, with a standard deviation of 0.2% for concrete made with Portland cement. ACI committee 222[29] proposed the threshold value is 0.2% by mass of cement content. RILEM[30] considered that a chloride content is in the range 0.3%~0.5% could indicate a low corrosion risk in most cases.

The large span of results might be due to reasons such as

1). Sample preparation, for instance whether the chlorides were added during concrete mixing (admixture), type of chloride salt, binder type, type of steel, etc.;

2). Testing methodology e.g. there is no defined line between potential to concrete and actual progression of steel corrosion;

3). Different exposure conditions.

All these make comparison of threshold values very tricky, and hence the controversy. It would

therefore be appropriate if the total chloride threshold concentration was defined in such a way that it is binder-specific. Moreover, the variability in these values could be decreased if a standardized testing procedure is adopted.

3.3 Chloride ingress in cracked concrete

3.3.1 Cause of cracking

Cracking of concrete is caused by tensile stress once the tensile strength of the concrete is excessed, cracking occurs. Because concrete is relatively weak in tension (i.e. its tensile strength is around 10% of its compressive strength), this happens already at moderate stress levels. This is the reason why concrete is usually reinforced by steel which takes over the tensile stress once the concrete has cracked. Some possible causes of concrete cracking are summarized[31] 1). Plastic settlement cracking; 2). Plastic shrinkage cracks; 3). Thermal contraction cracks; 4). Long term drying shrinkage cracking; 5). Crazing; 6). Cracking due to the corrosion of steel reinforcement; 7). Alkali-silica reaction; 8). Blistering of slabs caused by trapped bleed water; 9). D-cracking due to freeze-thaw damage; 10). Load induced cracking (tensile and bending cracking, shear cracking)

Clearly, there are many possible causes of concrete cracking. Time of cracking is also of importance. Based on the time of crack occurrence, two categories are distinguished cracks developing from distress at either early age (before hardening) or later age (after hardening).

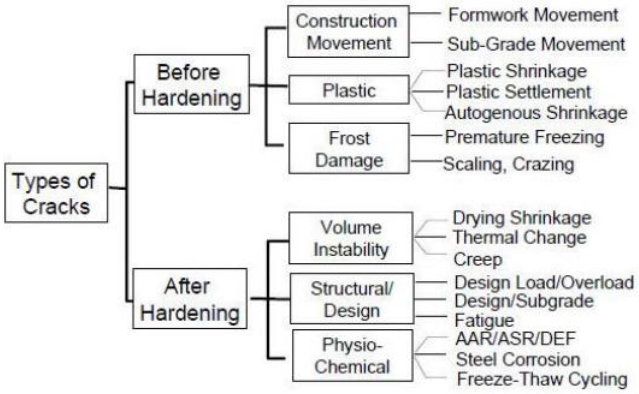

Figure II-5 Type of cracking that may be expected in a concrete structure [32]

Most of the mentioned cracks appeared in concrete can be avoided or minimized through proper construction practices, such as good concrete mixture design, placement, compacting, finishing and curing. However, load induced cracks are inevitable in a reinforced concrete structure. It is therefore important to investigate the effect that cracks have on the durability of reinforced

concrete structures.

3.3.2 Chloride ingress in cracked concrete

As mentioned above, chloride penetration in uncracked concrete is managed by three mechanism. However, chloride ingress in cracked concrete is very different in comparison with in uncracked concrete, because it is a combination of chloride ingress in solid phase of concrete and in cracks. Chloride penetration along cracks can be divided into two phases. In the first phase, convection is the governing mechanism. Chloride penetration is driven by hydraulic pressure. In the second phase, it is controlled by diffusion in cracks, which is driven by concentration gradient. A great number of investigations have confirmed that the characteristics of crack itself, including crack width, crack depth, crack density, external loading and crack self-healing, will significantly impact the chloride penetration in cracked concrete, so a brief review concerning these characteristics is reviewed

3.3.3 Crack width

Crack width is one of the most important characters of cracks. Most of the design codes limit the surface crack width of reinforced concrete exposed to a chloride environment. An overview of different national and international codes is given in Table II-1.

Table II-1 Maximum crack width allowed by different codes[33]

Code	Maximum crack width (mm)
ACI Committee 224 Report	0.15
CEF/FIB Model Code	0.30
BS 8110	0.30
Eurocode	0.30

The chloride penetration across cracked concrete consists of chloride penetration across sound concrete and that along cracks path. Figure II-6 schematically depicts a two-parallel model concerning chloride ingress in cracked concrete[34].

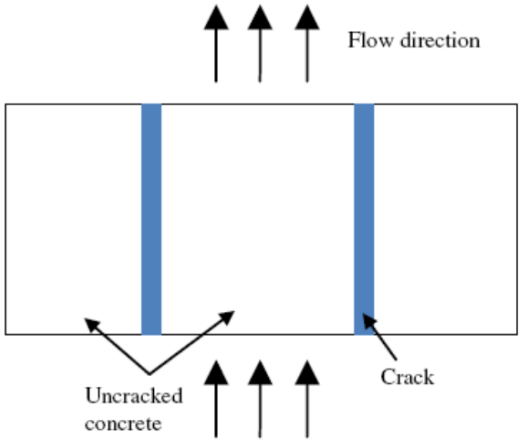

Figure II-6 Two-parallel model for diffusion in cracked concrete

According to the model, an equation quantitatively describing the equivalent diffusion coefficient of cracked concrete was proposed[34]

$$\frac{D_{eq}}{D} = 1 + \frac{4\omega_{cr}\beta_{cr}}{\pi d}\frac{D_{cr}}{D} \tag{7}$$

Where, β_{cr} is a geometry factor of cracks; D_{eq} is the equivalent diffusion coefficient of cracked concrete; D is the diffusion coefficient of sound concrete; D_{cr} is the diffusion coefficient in crack.

From this equation, it is clearly that the equivalent diffusion coefficient of cracked concrete is positively proportional to the crack width. Some published investigations [34-38] have confirmed that chloride diffusion coefficient increased with the increase of crack width, and they also considered that there is a so called threshold crack width, below which the penetration of chloride ions is similar with that of uncracked concrete, whereas, above which the penetration of chloride ions is similar with that of free surface in cracked concrete. Table II-2 gives the relevant research concerning the relationship between effective diffusion coefficient and crack width of concrete.

Table II-2 Threshold crack width of cracked concrete

Authors	**Cracking width (μm)**		**Cracking method**
	Minimum	Maximum	
Sahamaran[35]	100	211	Bending method
Ismail et al[36]	30	200	Expansive core method
Djerbi et al[39]	30	80	Splitting method
Park et al[37]	200		Splitting method
Jang et al[40]	80		Splitting method

Other authors, however, observed no correlation between the crack width and the chloride penetration. In their study on specimens with cast-in cracks, Audenaert et al[41] and Marsavina et al[42] reported no significant influence of the crack width on chloride penetration in parallel-walled cracks. It should be noted, however, that the crack widths examined in these studies were in the range of 200~500 μm, and therefore larger than the "limit" values found in other studies.

According to the mentioned above, it can be considered that crack width plays an important role on chloride penetration in concrete. However, it is quite difficult to find an accurate threshold crack width because the methods and raw materials employed in these studies were diverse.

3.3.4 Crack depth

Crack depth is another important factor on chloride penetration in concrete. If the crack in concrete is not connected to the reinforcement steels, the behavior of chloride penetration to the surface of reinforcement is similar with that of sound concrete because chlorides need to penetrate a part of concrete without any crack.

Marsavinal[41] et al and Audenaert et al[42] used an artificial crack method to investigate the effect of crack depth on the chloride penetration, respectively. A similar result was obtained and it shows that the chloride penetration depth is positively proportional to the crack depth, especially for the longer test durations. The effect of crack depth on the chloride penetration is more pronounced than that of crack width.

3.3.5 Crack density

Crack density is an important parameter to control the chloride penetration in cracked concrete because increase the crack density will provide chloride ions with more pathway to concrete matrix. If these cracks connect to the surface of steel in concrete, increasing crack density means more steel surface would expose to chloride environment. However, the effect of the crack density has received very little attention.

Konin et al[43] studied the effect of micro-cracks on chloride penetration, it was conclude that an increase in the micro-cracking density led to an increase in chloride concentration. Jacobsen et al[44] found that chloride migration rate increased by 2.5, 4.3 and 7.9 times when the crack densities

were 0.46, 0.61 and 0.77 per millimeter compared to the virgin specimen.

3.3.6 Loading condition

The main purpose of the use of reinforced concrete is to carry the external load. Different types of load would alter the width, depth and tortuosity of cracks in concrete. Currently, most of investigations mainly focus on the effect of compression condition and tension condition which are the main source of stress in buildings.

For compression condition, C.C Lim et al[45] found that chloride diffusion coefficient decreased when the uniaxial compression was lower than 70% ultimate compressive strength, because the compressive load closed some microcracks and pores. Furthermore, H.L Wang et al[46] investigated the stress level on the chloride diffusion and indicated that the concentration at a given depth decreased with the increased of the compressive stress, especially for the concrete with high water cement ratio.

In the case of tension condition, Francois and Maso[47] found that chloride diffusion coefficient in the tensile zone of a RC beam was remarkably higher than that in the compressive zone. A similar result was also be obtained by Gowripalan et al[48]. However, chloride concentration at a given depth increased rapidly with the increase of flexural stress, especially for the high water cement ratio[46].

So, it can be concluded that, for tensile stress, it always increases the chloride diffusion coefficient. Connective cracks can form under tensile stress, even though the tensile load is at a relative low level. For the compressive stress, when it is lower than a critical value, no connective cracks form and some pores in concrete are partially closed, chloride diffusion coefficient decreases. On the contrary, when the compressive stress is higher than that critical value, some connective cracks are generated and chloride diffusion coefficient increase.

3.3.7 Self-healing

It has been known that concrete cracks have a certain ability to heal under favorable conditions. This phenomenon is called self-healing. Several mechanisms are thought to govern self-healing[49]

1). Physical cause The main physical cause is swelling of hydrated cement paste near the crack

surface. This is a minor cause contributing to self-closing of cracks;

2). Chemical processes There are three chemical processes which contribute to self-healing. The first one is the hydration of unhydrated cement particles. This might be a significant contribution when crack widths are small (less than 0.1mm) and concrete is young. The second chemical process is the formation of calcium carbonate and the growth of crystals on the crack faces. Calcium ions originating from the concrete pore solution react with carbonate ions in the water and form $CaCO_3$, which precipitates in the crack. This mechanism has been thoroughly examined by Edvardsen[50], and is considered as the most important mechanism leading to self-healing of cracks. The third process occurs in seawater. Due to the presence of $MgSO_4$ in seawater, ettringite and brucite form in the crack[51].

It has been found that self-healing can slow down chloride penetration in cracked concrete/mortar[35, 36, 44, 52-54]. However, no quantified study has been found on the influence of corrosion products precipitation on the permeability of cracked concrete.

4 Effect of cracks on the corrosion of steel in concrete

4.1 Corrosion process in cracked concrete

In uncracked concrete, there is a classical model, proposed by Tuutti[55], in Figure II-7, concerning corrosion process. According to this model, corrosion process would be divided into two stages the initiation stage and the propagation stage. The corrosion initiation phase is a period from construction until the onset of active corrosion. The propagation stage then begins and lasts until the maximum acceptable damage level is obtained. However, this definition is not suitable for cracked concrete.

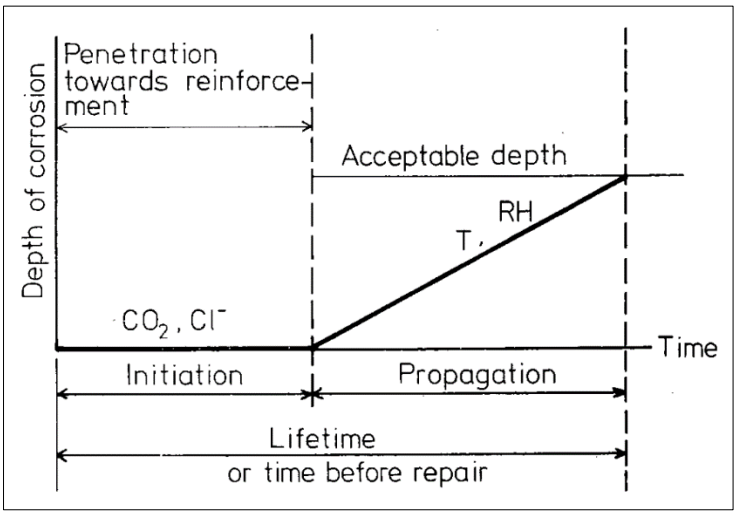

Figure II-7 Schematic sketch of steel corrosion sequence in concrete[55]

François and Arliguie[56] investigated the durability of load reinforced concrete in chloride environment and proposed another model, which is suitable for the corrosion in cracked reinforced concrete. Figure II-8 gave the evolution of the corrosion process for reinforced concrete beam under sustained load.

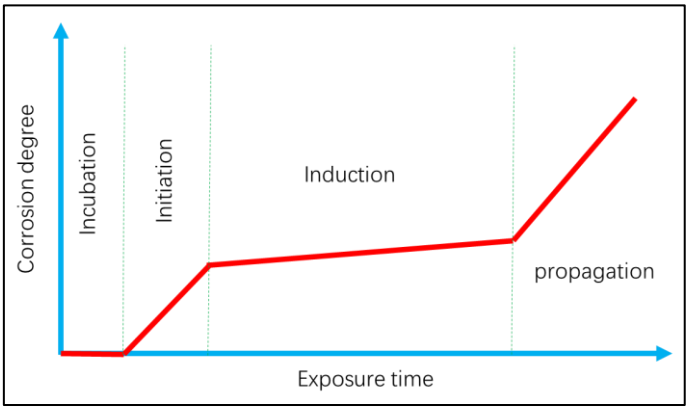

Figure II-8 Evolution of the corrosion process of reinforced concrete[56]

In this model, the corrosion process can be divided into four periods

1). Incubation period. During this period, the cracks of concrete provide easy access, allowing aggressive ions to reach the depth of reinforcement in concrete. The duration of this period is due to the presence of cracks but is not influenced by their width. As a result, once the critical chloride threshold was reached, the passive film on the surface of steel bar located around the cracks was broken down firstly.

2). Initiation period. During this stage, chloride concentration at the depth of reinforcement located between two flexural cracks would not be sufficient to break down the whole passive film. Parts of steel bars without passive layer act as anode, while other parts well protected by concrete,

act as cathode. Since anodic and cathodic areas are separated, steel bars corroded in the form of macro-cell corrosion in this period. Due to the first corrosion products fill the crack tip and limit the access of chloride ions, which causes a repassivation of the steel bar, then, the induction period begins.

3). Induction period. During this period, the corrosion process continues very slowly due to the debonding areas and the bottom of cracks are be sealed by rust products. However, the quantity of these expansive products is not enough to create corrosion-induced cracking. The sealing of cracks slows down strong the development of corrosion. The duration of this period is related to the time taken by chloride ions to penetrate through the porous structure of the concrete cover.

4). Propagation period. When all concrete cover is contaminated by chloride ions, corrosion restarts. Then, the development of rust products induced secondary cracking.

4.2 Corrosion mechanisms of steel in cracked concrete

4.2.1 Electrochemical corrosion systems of steel in medium

According to the fundamental of electrochemistry, two classic corrosion mechanisms are established, namely, micro-cell corrosion (uniform corrosion) and macro-cell corrosion (localized corrosion)[57].

Uniform corrosion can be defined as the electrical coupling of two infinitely close reversible electrodes. It meant that the spatial proximity of the two electrodes allows the ohmic effects due to electrolyte resistance to be overlooked. Where there is no electrical resistance between the anodic and cathodic sites, no potential gradient may exist in the space. Therefore, the equilibrium potential of the coupled system is uniform. Here the uniform character results from the fact that cathodic electrode (O_2/OH^-) is present in dissolved form in the electrolyte (concrete) in contact with the steel. It can thus be assumed that cathodic electrode is present across the entire surface of anodic electrode (Fe/Fe^{2+}).

On the contrary, localized corrosion is defined at the electrical coupling of two spatially separate electrochemical system. These systems may be made up of two reversible electrodes, two distinct corrosion systems (active and passive) or a reversible electrode coupled with a corrosion system. This definition implies that the distance between the two electrodes no longer allows the

ohmic effects due to the electrical resistivity of the electrolyte (concrete) to be overlooked. As the anodic and cathodic sites are distant from one another, they cannot meet a common potential, thus resulting in a significant different between anodic and cathodic potentials, a potentials gradient in the volume and a current, known as galvanic current or macro-cell current.

4.2.2 Corrosion of steel in cracked concrete

In cracked concrete, corrosion starts either in the crack zone or in the area immediately adjacent to the crack. There are two different corrosion mechanisms that are theoretically possible in the region of cracks proposed by Schieβl et al[58]

Mechanism Ⅰ Where both the anodic and cathodic sites are in the zone of the crack. Anodic and cathodic areas are very small and located close to each other, namely, uniformed corrosion. The oxygen required for the cathodic reaction is supplied through the crack.

Mechanism Ⅱ Where the reinforcement in the crack zone acts as an anode, and the passive steel surface between the cracks forms the cathode. In this instance, oxygen penetrates mainly through the uncracked areas of the concrete, that is, localized corrosion. The steel surface involved in this corrosion process is larger than in the first mechanism, hence, higher corrosion rates can be expected.

Ji et al[59] confirmed that micro-cell corrosion must co-exist with macro-cell corrosion of reinforcement in concrete. For micro-cell corrosion, it only took place in the active areas facing the concrete cover, while, macro-cell corrosion occurred between the active areas and the passive areas opposite to the concrete cover or the passive areas protected well by concrete. Zhang et al[60] researched the corrosion behavior of reinforced concrete beams in chloride environment under sustained load and found that macro-cell corrosion mainly took place in the period before propagation stage. While in the propagation period, reinforcement in concrete was corroded mainly in the term of micro-cell corrosion.

4.3 Effect of cracks on the corrosion initiation

A lot of publications demonstrated that cracks accelerated corrosion initiation. Jaffer et al[61] studied the relationship of location between transverse crack and corrosion initiation and found that

corrosion only took place at the intersections between reinforced steel bar and cracks in the concrete. Yu et al[62] investigated the corrosion process in cracked reinforced concrete beams under sustained load. It was found that corrosion mainly initiated at the tips of cracks. Some similar results were also be observed by other researchers[58, 63]. Cracks provide easy pathway for chloride penetration, thus chloride concentration at the surface of steel bars located around the cracks increase rapidly. When the chloride concentration exceeded a threshold value, the passive film on the steel bars broke down and corrosion initiated.

Yu et al[62] and Zhang et al[64] found that the width of flexural cracks does not impact the location where corrosion occurred. It is not difficult to explain the results referred above. The value of crack width is much larger than that of the mean free path of chlorides, in other words, once there is a crack appeared on the surface of concrete, chlorides can access in concrete matrix through this pathway.

4.4 Effect of cracks on the corrosion propagation

Different from the effect of cracks on corrosion initiation, concerning the influence of cracks on corrosion propagation, the literature results are contradictory. In the following section, the effect of cracks width, crack density, crack type and self-healing of crack on the corrosion propagation of steel in concrete will be reviewed.

4.4.1 Crack width

According to the previous published research, the effect of crack width on the corrosion propagation of steel in concrete is in connection with the exposure time. These relevant studies are summarized.

Mohammed et al[65] investigated the effect of crack width on corrosion rate. They found that in the very early age (1-2 weeks), corrosion rate increased with the increase of crack width. After four weeks, however, there was no explicit relationship between crack width and corrosion rate.

Wang et al[40] monitored the corrosion rate of steel bar in concrete beams with cracks of different widths. After initiation, they observed that the corrosion rate in beams with 0.1 mm crack was significantly higher than in beams only with micro-cracks. But in the later stage after *56 weeks*,

corrosion rate in the two situations tended to be almost the same.

Schieβl et al[58] carried out experiments on reinforced specimens with different crack widths. The mass loss of steel in cracked zone due to macro-cell corrosion after *24 weeks and 2 years* was calculated. It was found that corrosion currents increased with growing crack width at *24 weeks*. *After 2 years*, there was no significant relationship between crack width and corrosion rate.

François and Arliguie[66] investigated two reinforced concrete beams with different external load, respectively, in a same chloride environment. They found that, *at 1 year of exposure*, the corrosion degree of reinforced concrete beam with 274 MPa in tensile stress is slightly higher than that of reinforced concrete beam with 176 MPa in tensile stress. However, *at 5 years of exposure*, no obvious difference of corrosion degree between both two reinforced concrete beams.

Beeby et al[67] reported a research program carried out in Technical University Munich, a series of beams were loaded to give cracks width of up to 0.4mm. The beams were exposed to marine environment. They found that, *in the first 2 years,* a considerable influence of crack width on corrosion rate was detectable. However, *after 10 years* the influence of crack width was found to be negligible.

From the above, one possible explanation is that the factor of interfacial conditions are not considered in these studies. At the beginning of corrosion propagation, there is an enough space, formed by top-casting effect[68] or load-induced damage[69], between steel and concrete. During this period, corrosion products, such as rust, firstly fill the space[70]. With the increase of exposure time, these spaces are gradually filled with corrosion products, the penetration of chloride, water and oxygen controlled by the crack width is gradually block by corrosion products. When these spaces are absolutely filled with rust, propagation no longer to be controlled by crack width.

4.4.2 Crack density

Arya et al[71] investigated the effect of crack density on corrosion rate. In this research, corrosion was initiated by spraying the sample with 3% chloride solution or by adding chloride into the concrete. They found that mass loss of reinforcements decreased with the reduction of crack density. It was suggested that limiting the density of cracks would be more effective than controlling surface crack width.

4.4.3 Crack orientation

According to the orientation, cracks can be classified at longitudinal (parallel to the main reinforcements) or transverse (across the main reinforcements). Poursaee et al[72] found that if longitudinal cracks existed, the corrosion behavior was mainly controlled by this crack, even though the surface crack width was only 0.1mm. While, in the case of transverse crack, normally corrosion occurs in the form of macro-cell corrosion, steel in the cracked zone act as anode while the uncracked areas play the role of cathode. transverse cracks have less significant impact on corrosion rate, because corrosion rate is governed by concrete resistance or anodically control but not by crack width.

4.4.4 Crack self-healing

As mentioned above, due to the further hydration of unhydrated cementitious materials, formation of calcite and ettringite, deposition of small particles and expansion of concrete caused by water absorption, self-healing of crack is usually observed in small cracks. Self-healing of cracks reduces the permeability of cracked concrete and decreases corrosion risk of steel.

Mohammed et al[65] found that micro-cell current at the healed cracks is much lower than the unhealed ones. They also found that narrow cracks were healed by ettringite, calcite and brucite when the samples were exposed to the marine environment. Scott et al[73] observed self-healing in some samples when the crack width was smaller than 0.2mm. While the critical value in the investigation of Sahmaran et al[38] was 0.05mm.

Jacobsen et al[44] investigated the effect of self-healing on chloride permeability of concrete. It was found that self-healing resulted in more than 30% reduction of chloride penetration while the improvement in compressive strength of concrete was quite small. Vennesland et al[74] reported that, when the crack width was smaller than 0.4~0.5mm, the crack would be closed by self-healing products before the steel bar was damaged. Gautefall et al[75] proposed that corrosion products of steel may result in blocking of cracks and led to the reduction of corrosion rate.

Otieno et al[53] investigated the relationship between crack width and corrosion rate, they found that corrosion rate for the less than 0.4mm cracked specimens were noticed to decrease before the second reloading. They considered that this can most likely be attributed to crack self-healing

(Figure II-9).

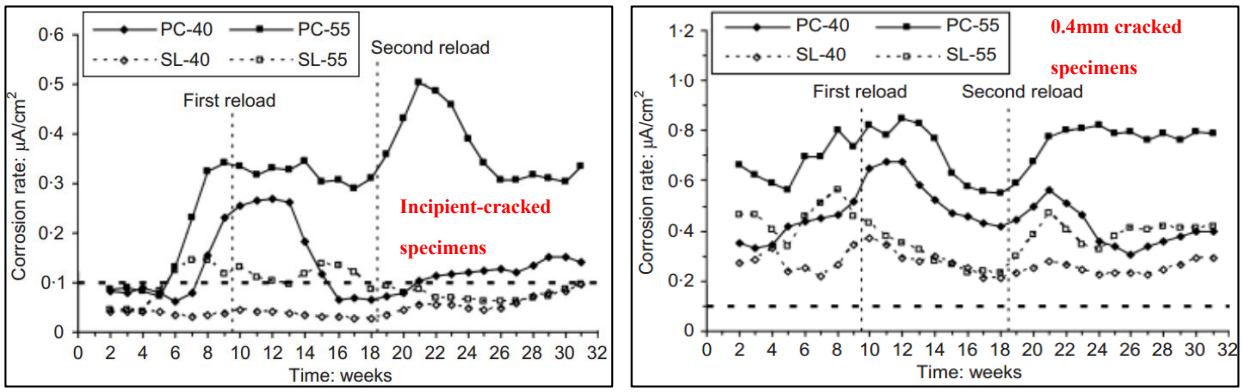

Figure II-9 Corrosion rate of cracked concrete[53]

Many researchers have noticed that the possible impact of self-healing on steel corrosion in concrete, however, its practical quantification is challenging. It is quite difficult to quantify at which degree the self-healing affect corrosion in cracks of different widths.

5 Effect of steel-concrete interfacial conditions on the corrosion of steel in concrete

Reinforced concrete is one of classic materials with multiple interfaces[76]. For reinforced concrete, interfaces mainly consist of aggregate-paste interface and reinforcement-concrete interface, respectively. Over the past, a large amount of investigations reported that the steel-concrete interface conditions influence the structural behavior and durability performance of reinforced concrete, and thus, plays an important role in engineering of reinforced concrete structures[69]. So, in this section, the published investigations concerning the effect of steel-concrete interface on the corrosion behaviors of reinforced concrete will be reviewed. It mainly includes 1). The formation and characteristics of steel-concrete interface; 2). The effect of steel-concrete interfacial conditions on the corrosion behaviors of reinforcement steel in concrete.

5.1 Formation and characteristics of steel-concrete interface

5.1.1 Formation of steel-concrete interface

When reinforcement steel contacts with fresh concrete, firstly, a thin water film generate on the surface of reinforcement steel due to “wall effect”[77], meanwhile, a gradient of content of cement particles between steel surface and bulk concrete is generated. The concentration of cement particles close to the steel surface is about zero and increases with the increase of the distance from

the steel surface to concrete matrix[78]. During compacting of fresh concrete, some airs migrate up to the surface of steel bar in terms of bubble[76] and some bleed water zone are formed at the interface of steel-concrete due to bleeding, segregation and settlement of fresh concrete[70]. With the hardening process of concrete, a passive layer gradually generates on the surface of steel due to high pH value of concrete pore solution. Finally, a specific weak zone between steel and concrete, namely steel-concrete interface, is formed.

5.1.2 Characteristics of steel-concrete interface

Steel-concrete interface consists of steel part and concrete part. In the case of steel part, it mainly contains mill scale, pre-existing rust layer and passive film on the steel surface. However, for the concrete parts, it mainly consists of cement hydration products, air void, crack, water bleed zone, separation and so on. Figure II-10 shows a schematic sketch concerning the steel-concrete interface.

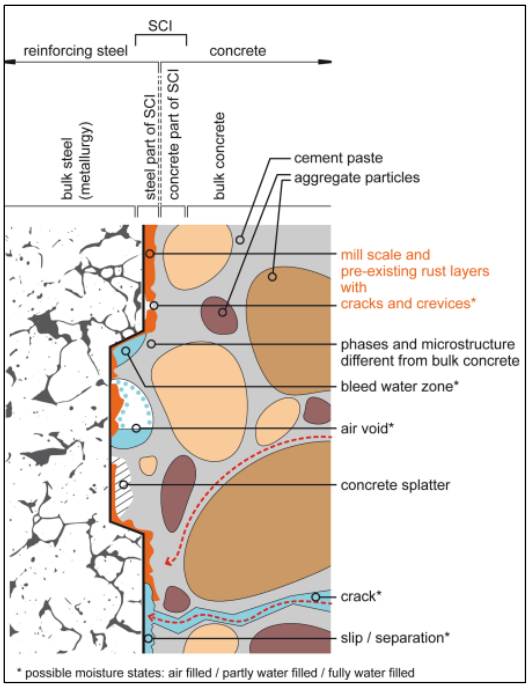

Figure II-10 Schematic illustration of selected characteristics at the steel-concrete interface[69]

The characteristics of the several main components of steel-concrete interface are reviewed, see below

- **Mill scale**

During hot rolling at the steel mill, a so-called mill scale is formed on the reinforcement steel

surface[79]. The mill scale consists of iron oxides mainly containing magnetite, hematite and maghemite. Mill scale is generally brittle and, thus, it is likely to crack under bending of reinforcing steel bars. The thickness of mill scale rang from 2μm to 40μm according to the different manufacturing technique[3].

Because of their larger thickness, the mill scale and the interface between steel and mill scale exhibited voids, crevices and cracks. Some of these voids and crevices were connected to the concrete by cracks, which serve as pathways for concrete pore solution to reach the steel surface, hence allowing ion movement between the pore solution and the crevices (Figure II-11).

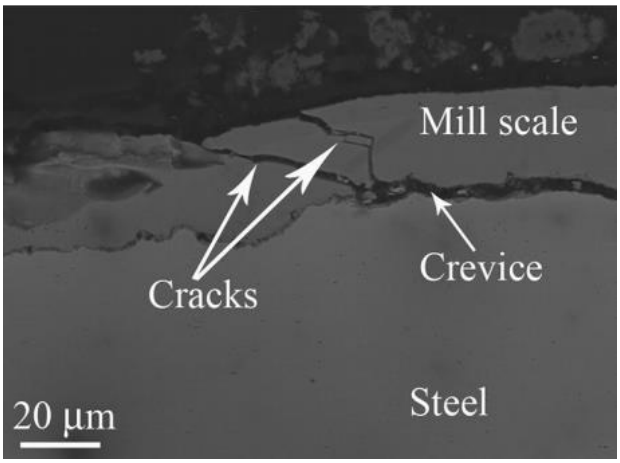

Figure II-11 SEM micrograph of sectioned rebars with mill scale showing cracks and crevices in mill scale [3]

According to observation of the mill scale from 60 years old and 260 years old[80, 81] reinforcement concrete structures, respectively, it is found that mill scale in contact with concrete is relatively stable. However, this layer of oxides offers far less corrosion protection of the underlying steel than a true passive film because there are some cracks and crevices in the mill scale.

- **Pre-existing rust layer**

Once the reinforcement steel leaves the manufacturer, it will experience very different exposure histories, depending on the conditions during transport, handling and storage. When reinforcement steel suffers from outdoor storage, corrosion products may form under atmospheric corrosion on the steel surface. In comparison with mill scale mentioned above, the rust layer formed after the steel manufacturing process will not contain significant amounts of wüstite[69]. Furthermore, significant differences in the electrochemical behavior of these surface were observed, depending on the amount of red/brown rust present[82].

➢ **Passive layer**

The information of a passive film in alkaline environment of different pH value has been widely discussed in solutions by electrochemical techniques. Upon exposure to alkaline solutions, the open circuit potential[83-93] and the polarization resistance of reinforcement steel surface gradually increase[86, 90, 91, 93] with time of exposure, it indicates that a protective iron oxide film asymptotically form on the steel surface.

The quality and stability of passive layer depends on the exposure duration and the chemical composition of alkaline solution. Longer immersion times lead to higher polarization resistance[84, 90, 93]. Some researchers found that when pH > 13, protective properties of the passive layer are clearly observed after about 1 day of immersion, while, at least 3~5 days are required for steel in saturated $Ca(OH)_2$ of which pH value is near 12.5[83, 91, 93-95].

Surface analysis has shown that the passive film formed on steel in alkaline solutions has a bi-layer structure with an inner Fe^{2+}-rich oxy-hydroxide (1~3nm) and outer Fe^{3+}-rich hydroxide film (5~10nm) [90, 96, 97], with the overall thickness typically in the range of 3~15nm[88, 89, 97]. With increasing time of immersion, the outer Fe^{3+} layer of the film increases in thickness, while the inner Fe^{2+} layer remains relatively stable, leading to an observation of increasing ratio Fe^{3+}/Fe^{2+} in the oxide film[88, 90, 91]. Based on Raman spectroscopy[83, 93] it was in concluded that the passive film composition is similar in concrete pore solutions and in sat. $Ca(OH)_2$. However, Ghods et al[2] reported the presence of Ca, K and Na in the passive film from the alkaline solution, suggesting that the pore solution composition may have an influence on the passive film composition and properties.

➢ **Cement hydration products**

As mentioned above, when steel reinforcement contacts with fresh concrete mixtures, a thin water film will form on the surface of rebar due to the so-called “wall effect”[77], then ions from the hydration of cement particles diffuses into this water zone. After hardening of concrete, a layer of cement hydration layer forms at the steel-concrete interface.

Moreau[98] used SEM to characterize the steel-concrete interface and found that segregated portlandite crystals of varying morphology and orientation were a major component of the interfacial regions. Similarly, Al-Khalf and C.L.Page [99] used SEM and EDXA to study the fracture surfaces of steel-mortar. The results indicated that a substantial fraction of the interfacial material

consisted of portlandite crystals of varied morphology.

$Ca(OH)_2$ is an important type of cement hydration products at steel-concrete interface, which restrains the pH drop by the buffering effect against acidification caused by the hydrolysis of iron in pitting corrosion and limits the cathodic reaction by covering the surface of steel available for oxygen. In the case of $Ca(OH)_2$, there is a dispute in relation to the distribution of portlandite crystals, namely, whether there is a continuous rich-lime layer forming on the steel reinforcement surface. Therefore, both two standpoints are reviewed.

A continuous rich-lime layer formed on the surface of steel in concrete

Bentur and Diamond [100]reported that the presence of continuous thin duplex films of portlandite backed by C-S-H in contact with steel fibers. P.J.M.Monteiro et al[101] studied the interfacial conditions of steel-cement paste and indicated that the interfacial film between steel and paste consists of a continuous $Ca(OH)_2$ crystals.

A.K.Suryavanshi et al[102] reported that a thin, dense white deposit layer can be observed on the surface of steel reinforcement after it was taken out from mortar. This layer was analyzed by EDX and was confirmed that it is the portlandite crystal. Therefore, a continuous rich-lime layer formed on the surface of steel in concrete.

A discontinuous lime layer formed on the surface of steel in concrete

Al-Khalf and C.L.Page[99] observed that the portlandite crystals did not form a continuous layer at the steel-mortar interface and were interspersed with C-S-H gel (see Figure II-12).

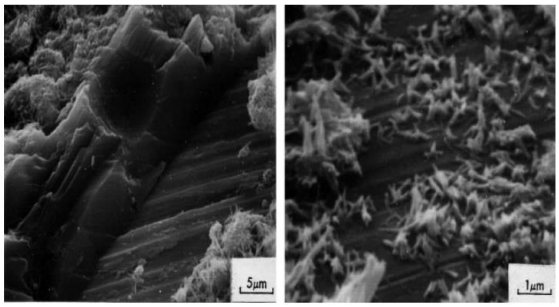

Figure II-12 SEM micrographs illustrating different hydration products at steel-mortar interface[99]

Bentur and Diamond[103] observed steel fibers, surrounded by a discontinuous portlandite layer with pockets of C-S-H gel and occasionally some ettringite. G.K.Glass et al[104] investigated the cement hydration products layer at the steel-concrete interface by BSE and they found that both unhydrated cement grains and C-S-H gel are also located adjacent to the steel, calcium hydroxide

did not form a continuous layer (see Figure II-13).

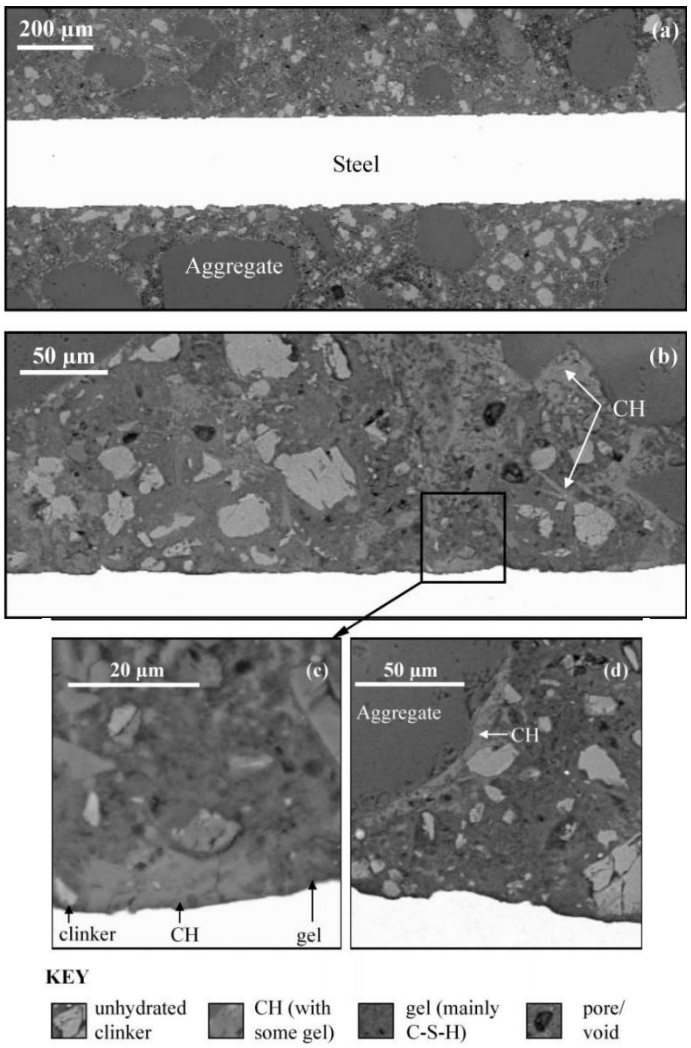

Figure II-13 Backscattered electron images of steel in concrete[104]

A.T.Horne et al[78] researched the interfacial microstructures of steel-paste and aggregate-paste, and indicated that there is a direct correlation between the content of cement hydration products at steel-paste interface and the casting direction of cement paste. If the orientation of steel reinforcement is parallel to the casting direction of paste, the interfacial conditions of steel-paste and aggregate-paste are observed to be very similar (Figure II-14). While, if the steel reinforcement orientates vertically to the casting direction of cement paste, a significant difference of the distribution of cement hydration products between steel and cement paste can be found. The top interfacial conditions of top-casting bar, according to casting direction of cement paste, are similar with the steel orientated perpendicularly as mentioned above. While, in the case of bottom side of top bar, an obvious gap can be observed ranging from 0µm to 40µm in which there is neither

portlandite crystals nor C-S-H gel (Figure II-15).

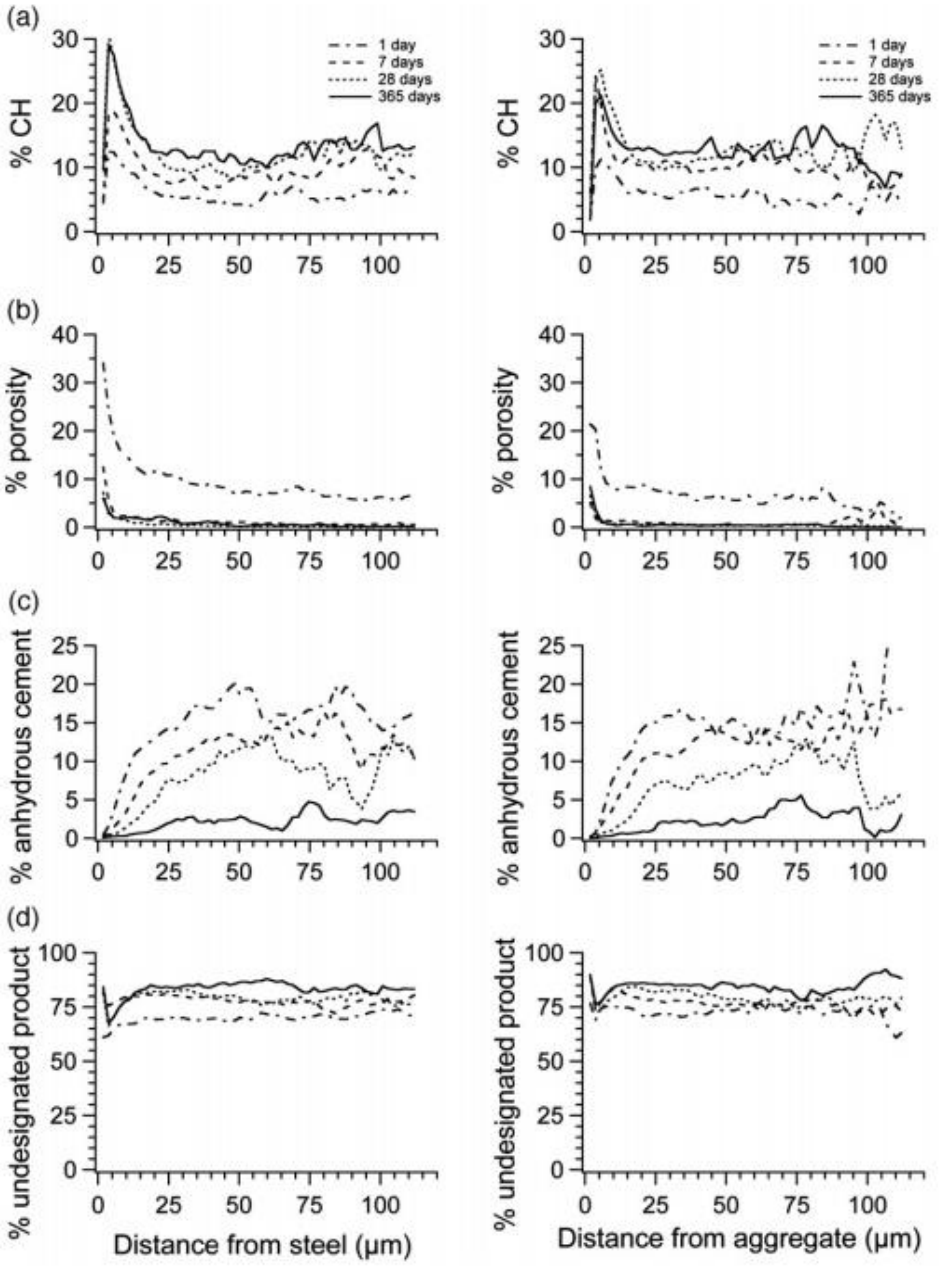

Figure II-14 Microstructural gradients in the interfacial region between cement paste and vertically cast steel(left) and aggregate(right)[78]

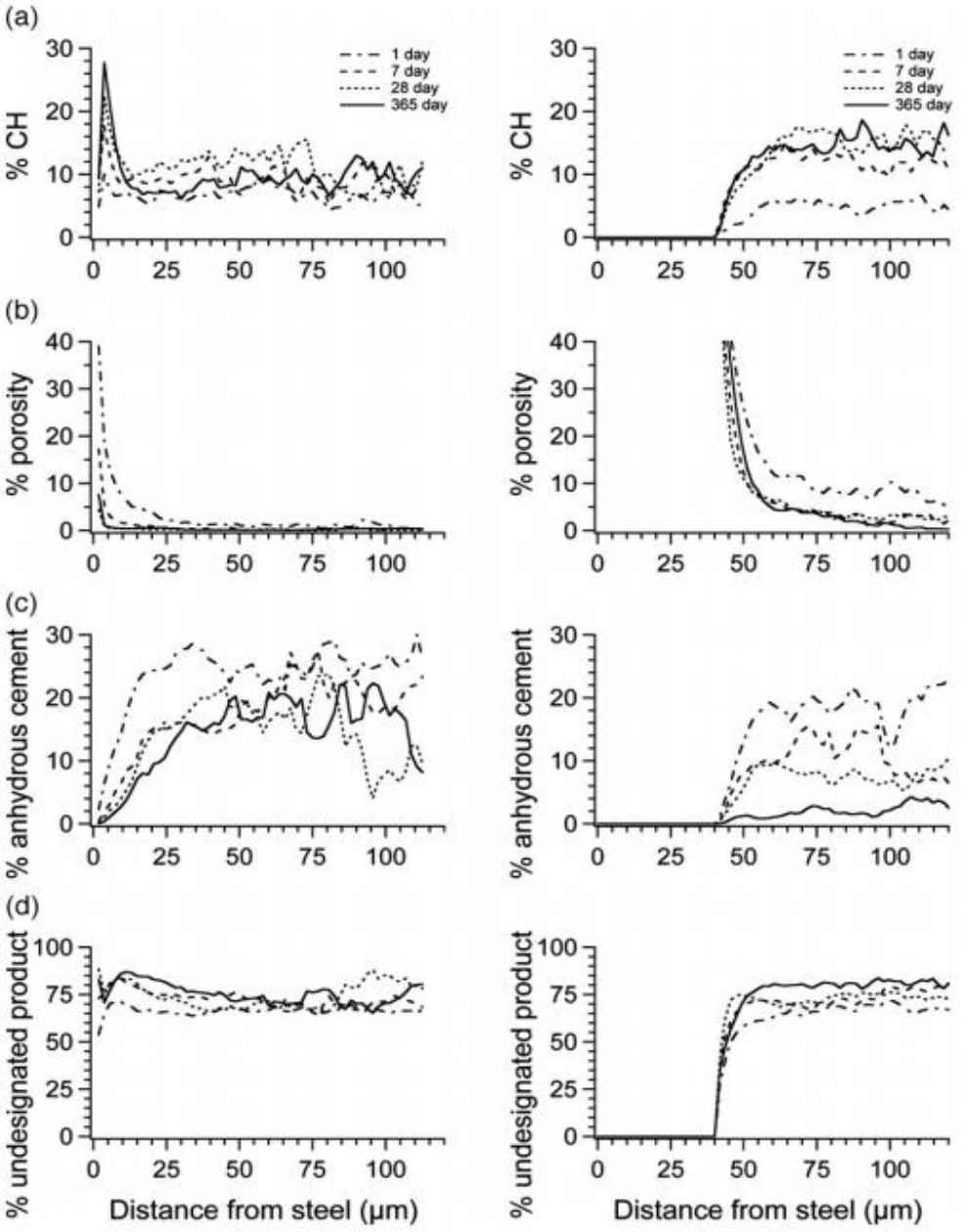

Figure II-15 Microstructural gradients in the interfacial region between cement paste and the topside (left) and underside (right) of horizontally cast steel[78]

Therefore, according to the published investigates mentioned above, although the distribution of portlandite crystal layer is either in continuous or in discontinuous, it is one of the major cement hydration products at the steel-concrete or cement paste interface. The content of cement hydration products at interfacial region, however, is affected by the casting direction of fresh concrete or mortar or cement paste. Apart from $Ca(OH)_2$ layer, the C-S-H gel and ettringite can also be spotted at the interfacial region of steel-concrete.

➢ **Top-casting defects**

Due to bleeding, segregation and settlement of fresh concrete, some top-casting defects formed at the bottom interface of steel-concrete according to the casting direction. Defects at the interface of steel-concrete leads to marked local differences in terms of physical conditions thanks to the fact that the significant change in characteristics of steel in contact with a matrix of cement paste and aggregates compared to steel in contact with a defects (Figure II-16). Due to different formation mechanism, the top-casting defects located at the steel-concrete interface can be divided into two types [69] a). air voids; b). bleed water zone/voids.

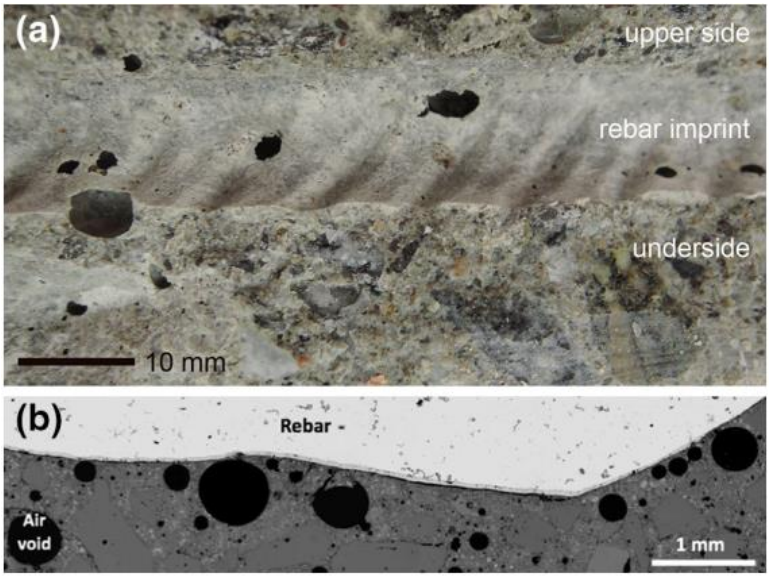

Figure II-16 Interface of steel-concrete [69]

Case of air voids at the interface of steel-concrete

It is well known that air is commonly present in fresh concrete [76]. However, it does not mix with the fresh concrete and is thus present in the form of bubbles. When compacting the fresh concrete, rising air bubbles adhere to the surface of bars or become trapped beneath horizontal surface of surfaces of reinforcement steel. Due to the origin of air voids, they are initially not water-filled.

According to the size of air bubbles, it can be divided into two types, namely, entrained air voids and entrapped air voids. For the entrained air voids, typical diameter of 50 μm, they have normally a near spherical shape[105, 106]. As such, only a minor part of the spherical void is in contact with the steel surface. Therefore, only a very small portion of these air voids can be observed when the steel reinforcement is removed to expose the interface. In the case of entrapped air voids,

they are typically more than 1 mm in diameter. In comparison with entrained air voids, the shape of entrapped air voids can be very irregular because their shape is controlled by the contour of surrounding environment[105].

Case of bleed water zone and voids at the interface of steel-concrete

Some previous studies [68, 70, 107-110] have confirmed that these defects at steel-concrete interface increased in relation to the depth of concrete under the steel. When the depth of concrete under steel is more than 150 mm, some typical top-casting defects can be observed at the underside of steel bar[108]. Mohammed et al [111] also observed that gaps were only found under horizontal bars cast in the top part of reinforced elements and not under those cast in the bottom part. SEM analysis of sections perpendicular to the steel revealed that the bleed-water zone was typically 100~200 μm wide.

Settlement may cause empty voids at the underside of reinforcement steel in concrete, but a thin layer of paste may adhere onto the rebar surface.

Bleed water may also accumulate at the steel-concrete interface to form voids of limited lateral dimensions and may appear similar with entrapped air voids. However, bleed water voids have a more elongated nature or crescent shape and are thereby able to achieve a greater contact area with the rebar surface compared with air voids. Another major difference in comparison with entrapped air voids is that bleed water voids are initially water filled, but can be emptied by chemical shrinkage and upon drying. However, empty bleed water voids may be re-filled with water on re-wetting.

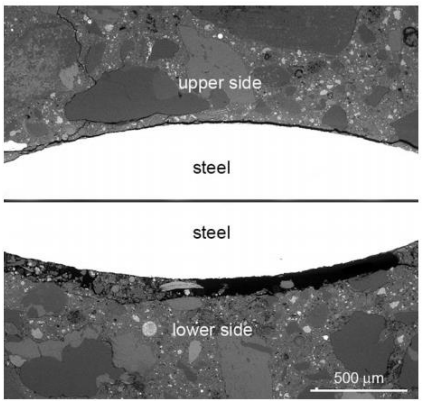

Figure II-17 Bleed water zone under the rebar [112]

- **Crack**

Apart from the factors impacting the interfacial conditions formed by steel and concrete

themselves, load-induced cracks also directly change the interfacial conditions between steel and concrete.

Figure II-18 [69]Shows the damage and cracking at the steel-concrete interface. Once the value of load exceeds the tensile strength of reinforced concrete, a load-induced crack (called primary crack [69]) is formed in concrete, and due to the restraining effect of the reinforcement steel, primary crack is wider at the concrete tensile surface than at the rebar, therefore, generally, the load-induced cracks are in V shape. Upon the formation of primary cracks, due to the transfer of tensile load through the rebar ribs into the concrete and extend with increasing load, internal micro-cracks form around the steel reinforcement rib near the primary crack. Upon further loading, internal cracks grow from their tips and reach the concrete surface to be secondary cracks. Finally, at higher steel stress, longitudinal cracks are initiated near the rebar at the faces of primary cracks and then grow towards the outside of the specimen.

The formation of primary, internal and secondary cracks is accompanied by damage within the steel-concrete interface, i.e. slip and separation. Slip relates to a displacement discontinuity between the reinforcement and the surrounding concrete parallel to the reinforcement, while separation corresponds to a displacement discontinuity between the reinforcement and the surrounding concrete perpendicular to the reinforcement.

The average crack spacing and cracking-induced damage along the steel-concrete interface depends on the steel bar diameter, bond characteristics, concrete strength, concrete cover, the distribution of perpendicular rebars and effective reinforcement ratio. While cracks width of primary, internal and secondary cracks rang between μm and mm, the extent of these cracks can be up to several meters. Similarly, cracking-induced damage at the steel-concrete interface might be several μm and mm in width.

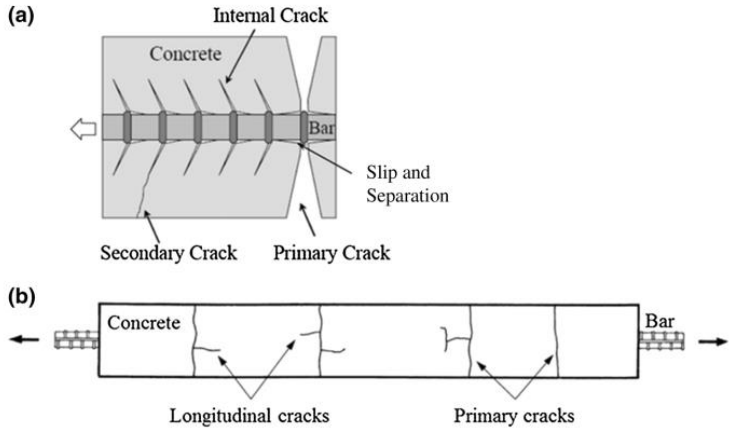

Figure II-18 Schematic illustration of damage and cracking at steel-concrete interface [69]

5.2 Effect of steel-concrete interfacial conditions on the corrosion initiation

As mentioned above, after the chloride concentration exceeded the depassivation threshold of steel bar, corrosion initiation occurs. Critical chloride threshold value represents the chloride concentration in concrete at which the transition from passive steel to active corrosion occurs.

Recently, A large amount of investigations indicated that the steel-concrete interface is the key factor affecting the corrosion initiation of steel in concrete due to the fact that the steel-concrete interfaces formed on the top and bottom sides of steel reinforcement during casting exhibit different characteristics[60, 62, 68-70, 78, 105, 106, 111-165]. In this section, we will review the effect of steel-concrete interfacial conditions on the corrosion initiation of steel in concrete in terms of reinforcing steel type and surface, concrete microstructures and chemistry at the steel-concrete interface, and macroscopic interfacial concrete voids at the steel-concrete interface.

5.2.1 Reinforcing steel type and surface conditions

- **Metallurgy**

Generally, in low carbon steel, there are three major metallographic structures, namely, ferrite, pearlite, and martensite. According to the previous studies[166, 167], pitting corrosion preferentially occurs on ferrite phase and is reported to have corrosion activity in the order of “ferrite > martensite > pearlite”. These indicated that ferrite phase could be more susceptible to chloride-induced pitting corrosion than tempered martensite phase.

Nowadays, quenched and self-tempered (QST) steels with a tempered martensite (TM)

periphery and a ferrite-pearlite (FP) core are widely used in civil engineering across the world[118]. When the manufacture of QST experiences a standard cooling system, a typical cross-section of an ideal and good quality of QST steel rebar can be obtained (see Figure II-19).

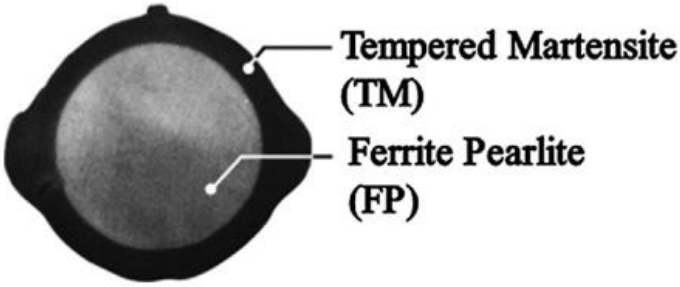

Figure II-19 Cross-sectional phase distribution of a good quality QST steel rebar[122]

However, the standard cooling system may not be necessarily followed and the control parameters in the employed cooling systems might vary across each other-leading to imperfections. Therefore, there is a possibility of improper TM phase formation owing to the poor quality control in the manufacturing lines of QST steel rebar[168, 169]. The defects in the peripheral TM phase in a poor quality QST steel rebar can be broadly classified into discontinuities and eccentricities, as shown in Figure II-20

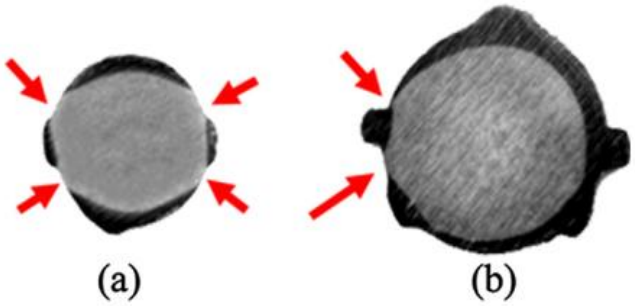

Figure II-20 Poor quality rebars exhibiting (a) discontinuities and (b) eccentric TM phase[122]

An improper martensite-ferrite morphology can act as a cathode-anode combination (galvanic cell). For example, an increase in the martensite volume fraction (from 27% to 48%) increased the cathode-to-anode ratio in dual-phase steels and led to higher corrosion rate[125].

Nandi et al[124] indicated that the average corrosion rate of rebar with inadequate cross-sectional phase distribution was higher than those with adequate cross-sectional phase distribution. Thus, it can be inferred that the inadequate cross-sectional phase distribution could have possibly led to the acceleration of corrosion initiation and the higher corrosion rates.

Trejo and Pillai[126, 170] investigated and compared the critical chloride threshold of different

type of steel rebars in mortar with the method of the accelerated chloride threshold test and indicated that the ferritic-martensitic steels show significantly higher critical chloride threshold than conventional steels.

Angst and Elsener[132] compared reinforcement steels in as-received condition from 9 different countries with respected to their corrosion behavior in chloride-containing saturated $Ca(OH)_2$ solution. They found that the steel microstructure was identified as one of the major influencing parameters, the critical chloride threshold significantly lower for reinforcement steel that underwent thermomechanical strengthening (TM surface layer) compared to cold-work hardened steel (FP microstructure).

Nair and G.Pillai[122] studied the microstructural characteristics of cross-sectional phase distribution of QST steel rebars from different countries and indicated that the average critical chloride threshold for TM coupons was slightly higher than for FP coupons.

In short, although little information on the effect of metallurgy on corrosion initiation of steel in concrete is available, it can be concluded that the microstructure of the rebar surface is likely to play an important role in the corrosion initiation.

- **Rebar geometry**

Apart from the effect of the chemical composition of steel rebar, the geometry of rebars may also influence corrosion initiation by modifying the steel-concrete interface locally, namely due to the presence of ribs on the rebar surface (as shown in Figure II-19), different diameters, or bent parts of the rebars.

Zafar and Sugiyama[119] researched the corrosion behavior of smoothed rebar and deformed rebar in concrete with fly ash. Each concrete specimen had two reinforcements. The layout of specimen used in the work is given in Figure II-21. The corrosion initiation was characterized by the sudden drop of half-cell potential value, and once the corrosion initiated, concrete was broken immediately to observe the visually inspect.

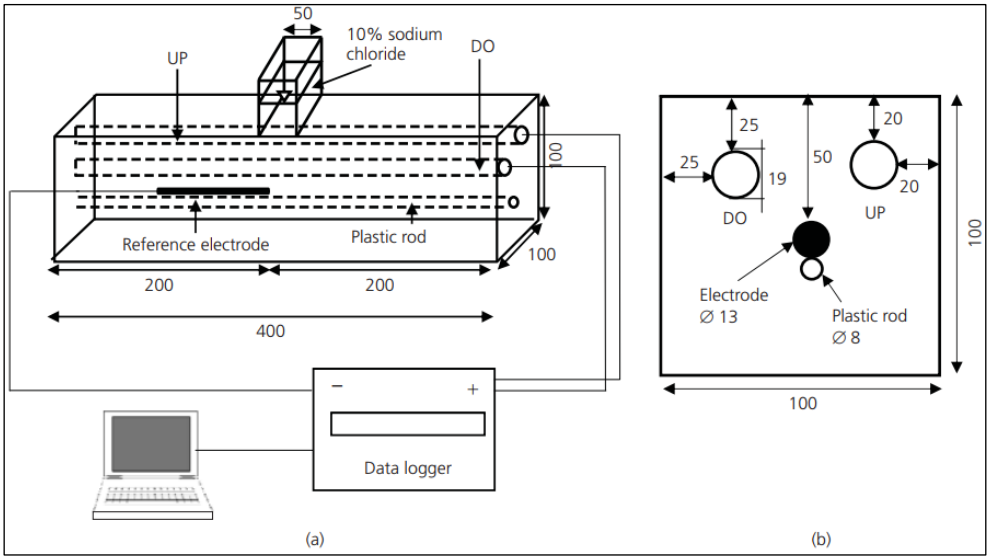

Figure II-21 Layout of specimen[119]

According to their investigations, the corrosion of deformed rebar always initiated at the location of rib, while, for the smooth steel rebar, corrosion mainly occurred at the place of void (Figure II-22).

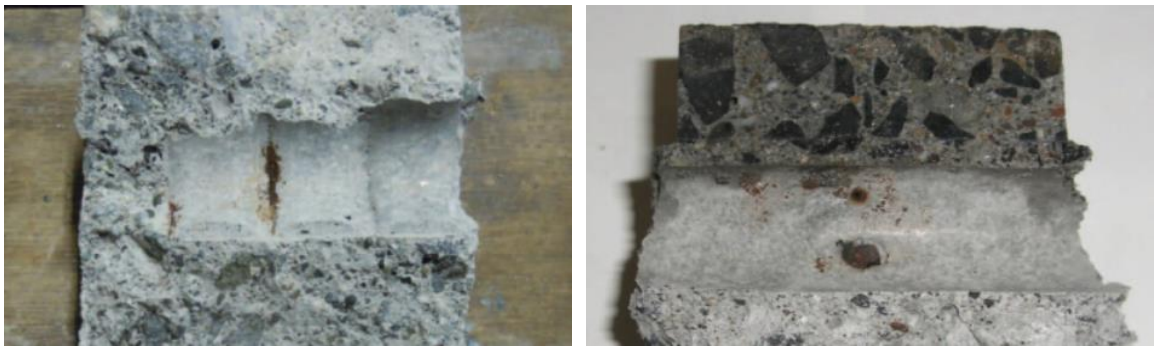

Figure II-22 Location of corrosion initiation[119]

Michel and Angst[171] investigated the local electrochemical properties and the corrosion initiation of reinforcing steel with different surface conditions by the small portable electrochemical sensor. The results are shown in Figure II-23.

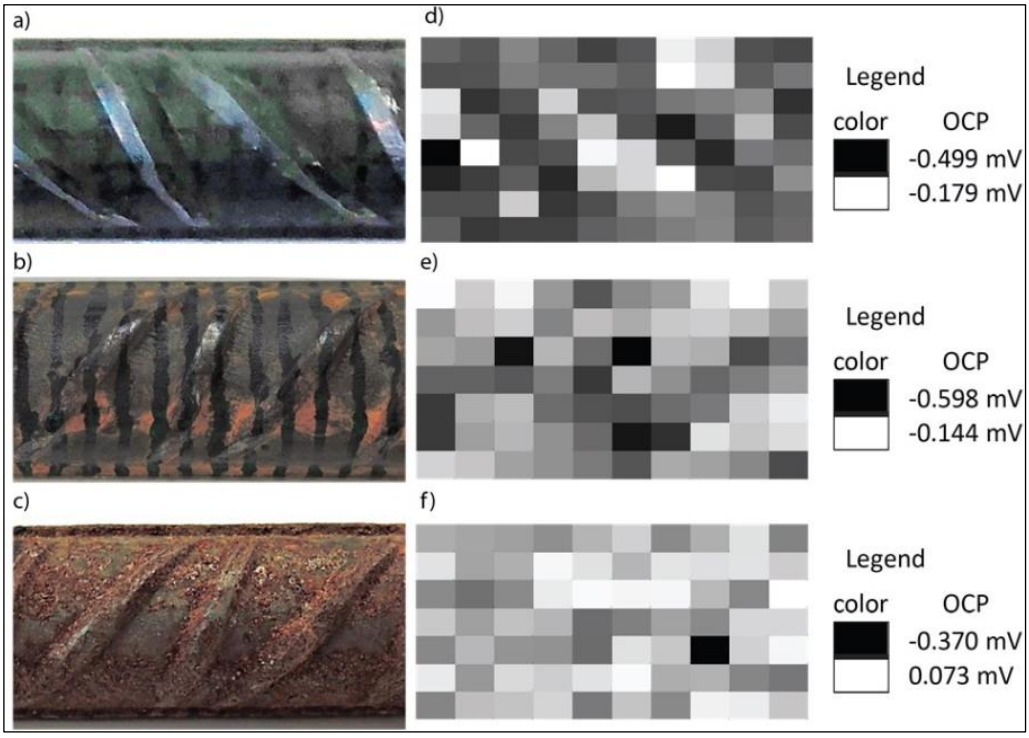

Figure II-23 The distribution of the open circuit potential of steel rebar with different surface condition[171]

It is clearly that the local open circuit potential of steel reinforcement is related to the surface condition of steel rebar. For the steel reinforcement without rust, the negative OCP mainly appeared at the location of rib, while at the no rib zone, the OCP was positive. In the case of steel with absolute rust cover, most of surface was under the condition of positive OCP. For the steel with part rust cover, the OCP was between the steel reinforcement with or without absolute rust cover.

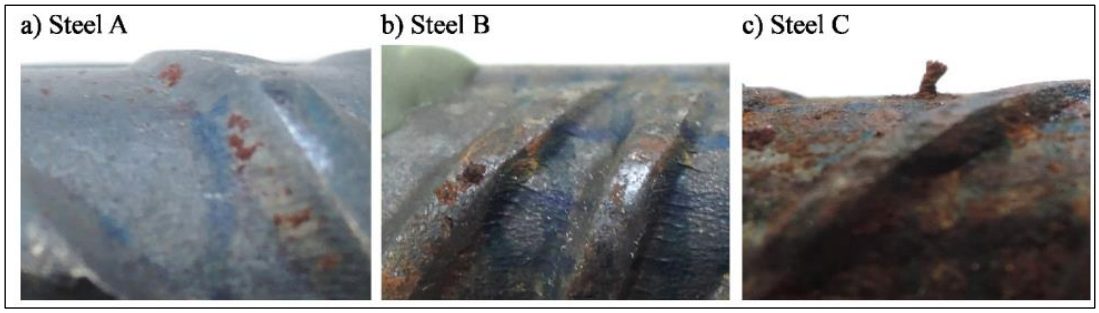

Figure II-24 Location of corrosion initiation of steel bar with different surface condition[171]

The location of corrosion initiation of steel bar is shown in Figure II-24, it can be found that in steel A and steel B, corrosion mainly initiated at the location of rib or near the rib. The authors considered that due to the existence of the rib, the corresponding mill scale and martensitic surface layer were changed and the lattice defects were introduced, which facilitate the corrosion initiation. While, in the case of rusty rebar, due to the presence of uniform rust cover, corrosion does not

preferably initiate on rib.

Kathler et al[139] reported preferential corrosion initiation close to and on ribs for one concrete structure, while this was not observed in two other structures. Sandberg [121]found that corrosion initiated in approx. 70% of the cases in the deformed parts of reinforcing steel bars, particularly on the inside of U-bend rebars. This was attributed to mechanical damage to oxide scales on the rebar during bending.

C.Alonso et al[120] prepared two series of mortar specimens with dimensions of 8×5.5×2 cm to study the impact of the shape of rebar on the corrosion initiation. In the first series, eight specimens with smoothed bars were fabricated, and in the second series, four specimens with ribbed bars were fabricated. The specimen is shown in Figure II-25.

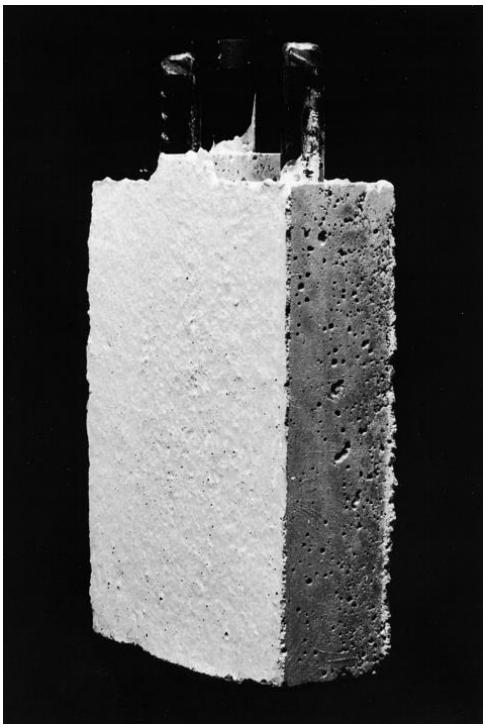

Figure II-25 Aspect of the mortar specimen[120]

The corrosion potential, the electrical resistance and the polarization resistance were recorded periodically during 90 or 200 days and the I_{corr} was calculated through the Stern and Geary equation. And the results of the correlation between I_{corr} and the critical chloride threshold characterized in different mode are shown in Figure II-26.

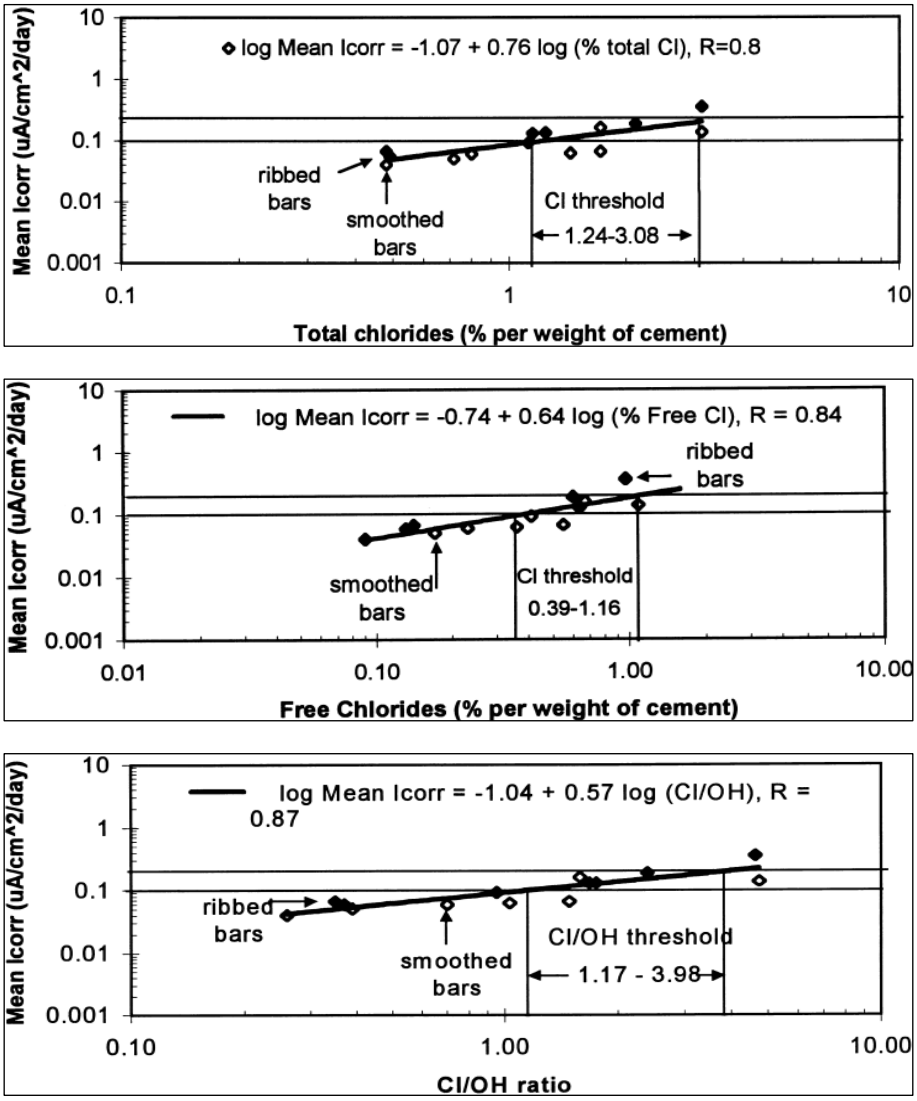

Figure II-26 Relationship between corrosion current and critical chloride threshold (free chloride, total chloride and Cl/OH ratio)[120]

According the results, the shape of steel rebar appeared not to affect the corrosion initiation of steel in mortar and there is obviously linear relationship between critical chloride threshold and the corrosion current (I_{corr}).

In summarizing the literatures, most of the published results consider that the shape of steel reinforcement will impact the corrosion initiation, but it is clear that the current level of documentation does not permit us to quantify the effect of the rebar geometry on corrosion initiation.

- **Mill scale and pre-existing rust layers**

Different researchers[84, 86, 116, 127, 128, 133, 137, 172] reported the influence of steel surface modifications (removing mill scale through sandblasting, polishing or pickling) on the

critical chloride threshold. Some studies were carried out in mortar or concrete[116, 127, 137] and some were performed in alkaline solution[84, 86, 128, 133].

L.T.Mammoliti et al[128] studied the corrosion initiation of steel rebar with different surface conditions (as-received and degreased deformed rebar, ground smooth rebar and a polished cross section of deformed rebar) in alkaline solution with different amount of chloride ions. The specimen is shown in Figure II-27.

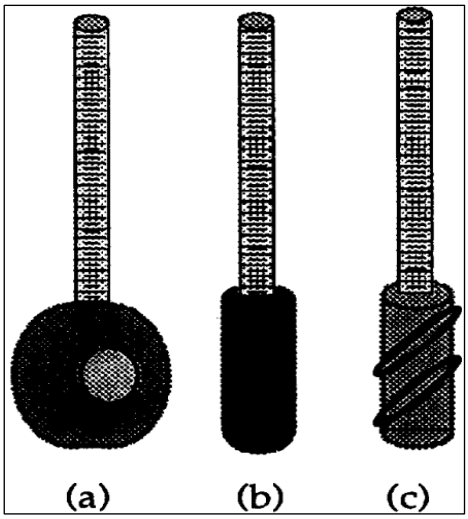

Figure II-27 Schematic representation of samples a) mounted, polished rebar; b) smooth, ground rod and c) degreased, deformed rebar[128]

The results of corrosion current are shown in Figure II-28. It indicated that the corrosion rate of deformed rebar and smooth rebar increased with the increase of chloride concentration, and the deformed rebar had the higher corrosion rate, while the polished rebar kept a relative lower corrosion rate in comparison with the both former. These results revealed that the surface condition of the steel has a major influence on the corrosion initiation and the mill scale can reduce the corrosion initiation phase.

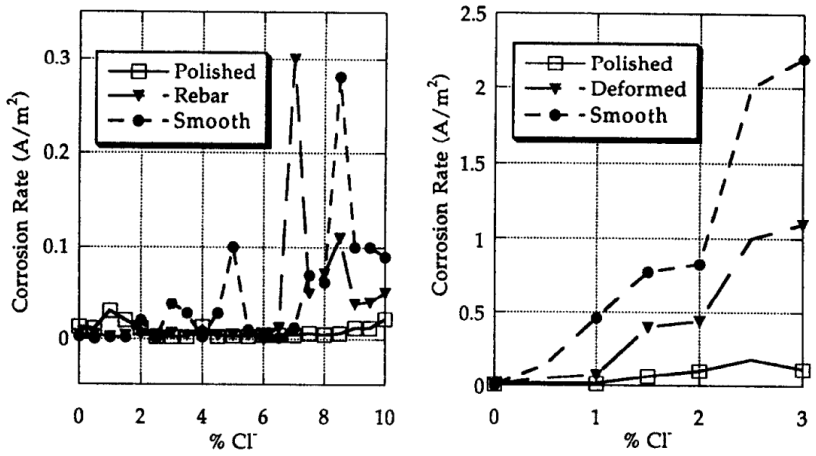

Figure II-28 Corrosion rate of steel rebar[128]

(left figure mean the corrosion current of different specimens in pore solution of pH 13.3; right figure represents the corrosion currents of specimens in filtered $Ca(OH)_2$ solution in which the pH decreased with increasing Cl^-)

G.Pillai and Trejo[137] measured the mill scale from different type of steel rebar (Figure II-29) and compared the critical chloride threshold of different steel bar before or after removing mill scale (Figure II-30).

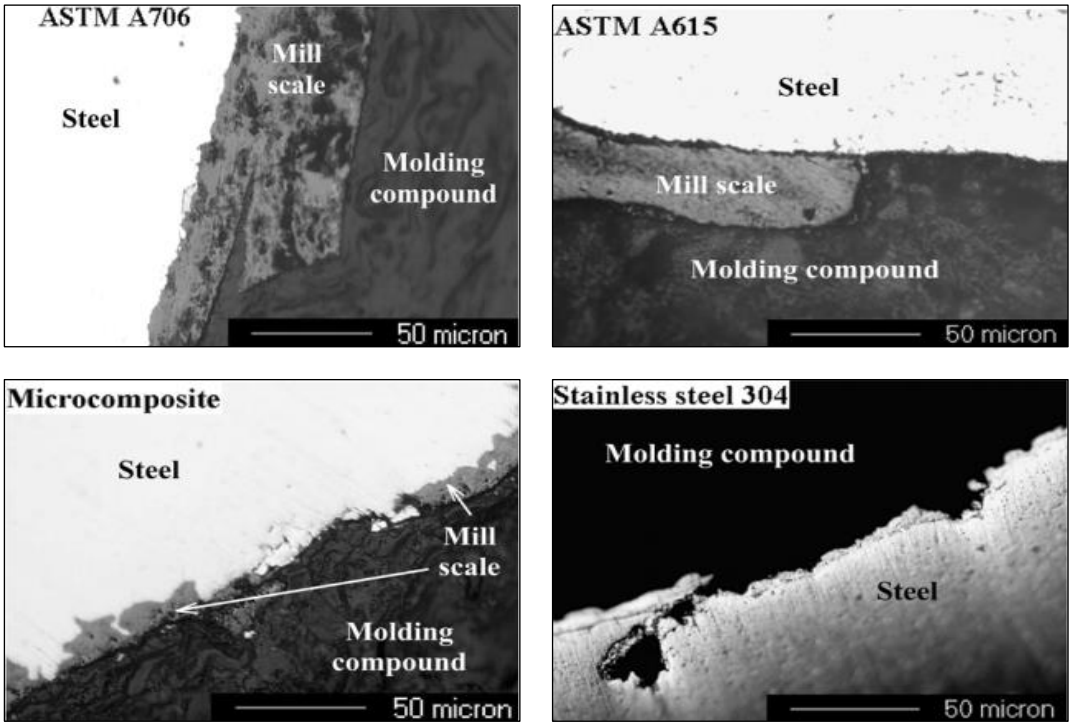

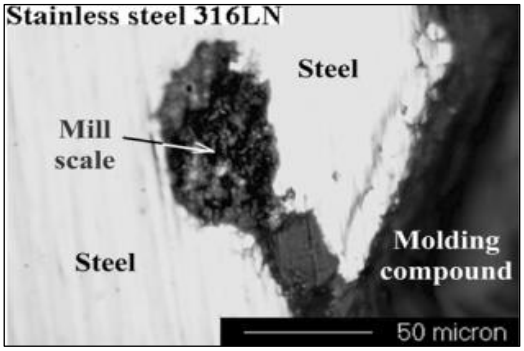

Figure II-29 Typical micrographs of steel reinforcement surface[137]

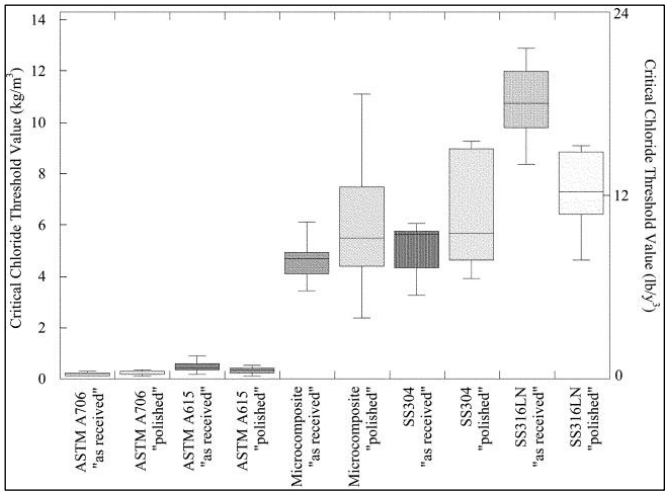

Figure II-30 Critical chloride threshold values for different reinforcement types evaluated in test program[137]

According to their studies, the mill scale on the surface of steel reinforcement is discontinuous and exhibits crevices, which would facilitate the corrosion initiation. Removing the mill scale will positively affect the critical chloride threshold value, but different type of steel reinforcements performed different behavior.

E.Mahallati and M.Saremi[172] reported that the presence of mill scale on steel bars in concrete reduces the electrical resistance and reparability of the passive film, consequently accelerate the corrosion initiation of steel reinforcement in concrete.

Mohammed and Hamada[116] studied the critical chloride threshold value of steel bars and steel-concrete interface in concrete with five surface conditions of steel bars, namely, mill scale (M), polished (P), brown-rusted (BR), black-rusted (BR), and pre-passivated (PP) and indicated that chloride threshold level for the mill scale group was the lowest, mill scale accelerated the corrosion initiation of steel bar in concrete. The similar results can also be found in ref [84, 127]. Therefore, the presence of mill scale appears generally to promote corrosion initiation.

Some investigations[132-134, 165, 173] suggested that the effect of pre-existing rust layers on corrosion initiation may be different from that of mill scale. Mohammed and Hamada[165] as well as Chen et al[133] reported that the critical chloride threshold level increases in the presence of mill scale with additional rust than with mill scale alone. Angst and Elsener[132] compared rebars from different manufacturers and in different pre-rusted condition and reported that the degree of rust did not permit any reliable prediction of the susceptibility to chloride-induced corrosion. The influence of pre-formed rust scales was considered a weaker influencing factor than the manufacturing process or the metal microstructure. Al-Tayyib et al[134] reported that pre-rusting did not promote corrosion initiation of rebars embedded in concrete.

- **Passive film**

The passive layer on the surface of steel reinforcement formed in high pH value environment in concrete is the main barrier against pitting corrosion.

Angst et al[69] summarized the properties of passive layer on steel surface in alkaline environment and indicated that during prolonged exposure of black steel to alkaline solutions or in concrete, the open circuit potential asymptotically increases to more positive values.

S.Jaggi et al[174] studied the ageing of passive film on the oxygen reduction reaction on normal and stainless steel in alkaline solutions and indicated the progressive inhibition of the oxygen reduction with prolong ageing of the passive steel will lead to lower corrosion rates of steel in concrete because the cathode efficiency decrease and to increase in the pitting potential (Figure II-31). The similar results were also reported by Lianfang Li and Alberto A.Sagues[175].

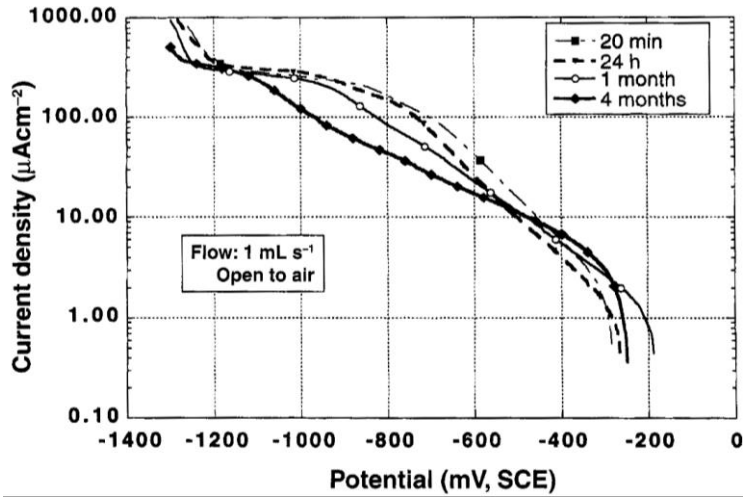

Figure II-31 Influence of the ageing time of the passive film in synthetic pore solution on cathodic polarization curves[174]

According to established theory[176], increasing pitting potential is associated with an increase in critical chloride threshold level. Angst et al[123] summarized the relationship between pre-passivation time and the pitting potential. They reported critical chloride threshold level increases with the increase in the pitting potential of pre-passivated steel.

- **Steel surface preparation**

As mentioned above, the critical chloride threshold level is related to the modified surface of steel rebar[86, 128, 130, 137]. Moreover, literature indicates that the susceptibility of steel rebar to corrosion decreases with the degree of surface preparation.

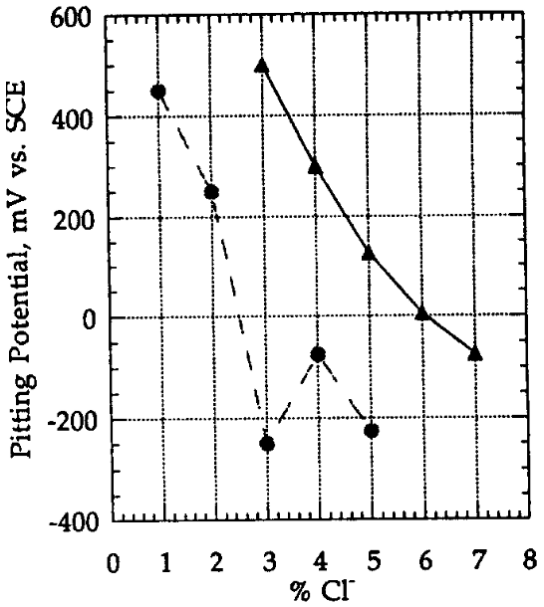

Figure II-32 Pitting potential of specimens as a function of chloride content in buffered $Ca(OH)_2$ solution[128]

(dashed line means the 240 grit, line means the 600 grit)

Mammoliti et al[128] reported that, under a same chloride concentration, with an increase degree of polishing (from grit 240 to grit 600, thereby reducing the surface roughness), pitting potential of carbon steel in $Ca(OH)_2$ solution were shifted to more anodic values (Figure II-32).

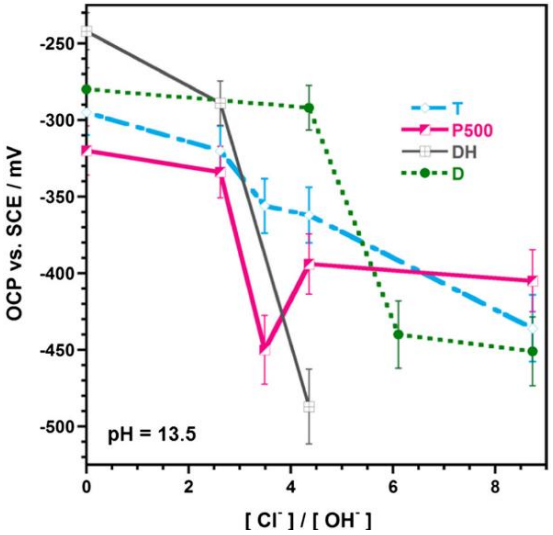

Figure II-33 The evolution of OCP as function of the [Cl-]/[OH-] ratio, measured after 23 h of immersion, for all samples in SCPS1 (pH=13.5)[177]

Figueira et al[177] compared the open circuit potential of steel samples with four different finishes as received (T), diamond-polished (D), polished (P500) and pre-oxidized (DH), corroded in simulated concrete pore solution (Figure II-33) and found that the surface modification significantly affect the corrosion initiation of steel in simulated solution and the diamond-polished sample had the highest critical chloride threshold value.

Consistent with this, comparable relationships between pitting corrosion potential and degree of polishing were reported from studies on stainless steels[135], although the impact was generally less pronounced than in [128, 177]. Therefore, it can be concluded that the steel surface preparation that goes beyond removing oxide scales has a strong effect on corrosion initiation in concrete.

5.2.2 Concrete microstructures at the steel-concrete interface

- **Water to binder ratio**

The water/binder ratio (w/b) is known to play an important role in concrete. Its impacts on mechanical properties and transport, e.g. of chloride ions, are well documented. However, limited published researches concerning the effect of w/b ratio on corrosion initiation are available.

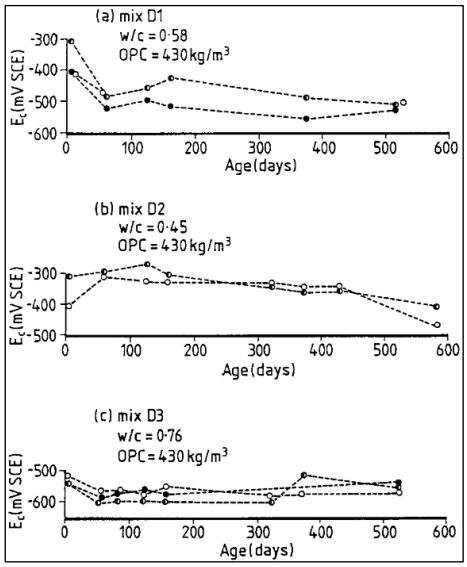

Figure II-34 Corrosion potential versus exposure time[178]

Mangat and Molloy[178] studied the effect of different w/c ratio (from 0.45 to 0.76) on the corrosion potential. All the samples were subjected to a wetting-drying cycle in a marine spray chamber. The results are shown in Figure II-34. In Figure II-34, the groups D1 and D3 achieved relatively negative potential values soon after exposure to chloride environment and maintain these negative values through the test period. The results for D2, however, did not show a reduction in potential occurring in the early period of marine exposure. However, according to the change of corrosion potential, the effect of w/c ratio on the corrosion susceptibility of embedded steel is much less pronounced than the effect of w/b on mechanical and transport properties of concrete. The results are in accordance with these researches reported by Hansson[160] and Breit[179] and Pettersson[159] and Li et al[154].

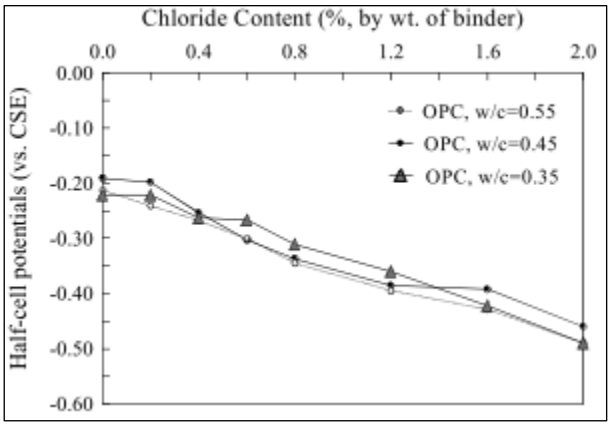

Figure II-35 Variation of half-cell potential with chloride content (effect of water/binder ratio)

Oh et al[155] studied the corrosion behavior of steel bars in concrete. In this research, the

chlorides were admixture into concrete specimens as sodium chloride, of which concentrations vary from zero to two percent by weight of binder (i.e. 0, 0.2, 0.4, 0.6, 0.8, 1.2, 1.6 and 2.0%). The w/c ratio of concrete specimens used in this work varied from 0.35 to 0.55. The relationship between half-cell potential and chloride content impacted by w/c ratio is shown in Figure II-35. According to these results, under the same chloride content, the difference of the half-cell potential of the reinforced concrete with different w/b ratio was slight. It means that the effect of the change of w/c ratio from 0.35 to 0.55 on the susceptibility of corrosion initiation can be negligible.

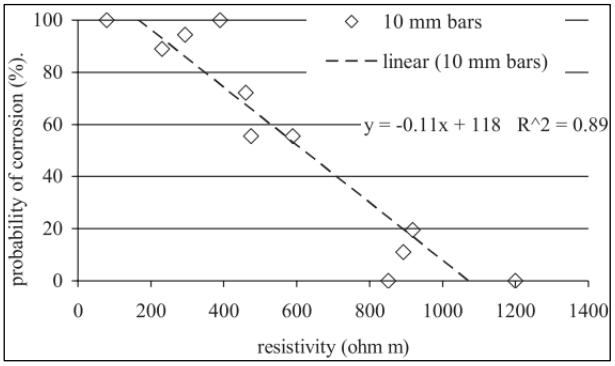

Figure II-36 Probability of corrosion at 24 weeks (after 20 weeks of salt/drying load) as a function of concrete resistivity; w/c 0.40, 0.45, 0.55[180]

Polder[180] exposed concrete (w/b 0.40-0.55) specimens to drying and wetting with chloride solution and detected corrosion initiation with electrochemical measurements. According to the results (Figure II-36), there is a reasonable correlation between concrete resistivity and probability of corrosion. This correlation is caused by the fact that the various mixes had quite different chloride content at 10 mm (bar) depth, between 0.2% and 4% chloride ion by mass of cement. It appears that concrete resistivity has a strong relationship to the penetration of chloride.

Summarizing these studies, both for concrete and mortar, either in natural exposure, under anodic polarization or with mixed-in chloride, the influence of w/b on the susceptibility of steel to corrosion is relatively small. While there is a general agreement that lowering w/b below 0.5 slightly improves the resistance against corrosion initiation, the results for the effect of w/b in the range above 0.5 are contradictory, with an overall negligible influence.

- **Cement type**

Similar to w/b, cement type is also known to be an important parameter in concrete. it should be noted that in this section, we only review the blending of supplementary cementitious materials

with Portland cement. Generally, the common supplementary cementitious materials contain the blast furnace slag, fly ash and silica fume[152]. A number of studies[136, 151, 153, 155-160] reported the critical chloride threshold value when using different supplementary cementitious materials.

Fly ash

Hansson and Sørensen[160] studied the influence of a number of factors on the critical concentration of Cl^- necessary for initiation of corrosion of steel embedded in concrete and reported that fly ash has a negative effect of the corrosion initiation of steel in concrete.

Thomas[157] studied the effect of fly ash content on the critical chloride threshold value of steel reinforcement in concrete in marine environment. And the results can be found in Figure II-37. From the experimental results, the critical chloride threshold value decreases with the increase in the fly ash content. When the content of fly ash was zero, the critical chloride threshold value was approx. 0.7% by mass of cement. However, when added the content of fly ash up to 50%, the critical chloride threshold value reduced to 0.2% by mass of cement. The use of fly ash enhances the susceptibility of corrosion initiation of steel in concrete.

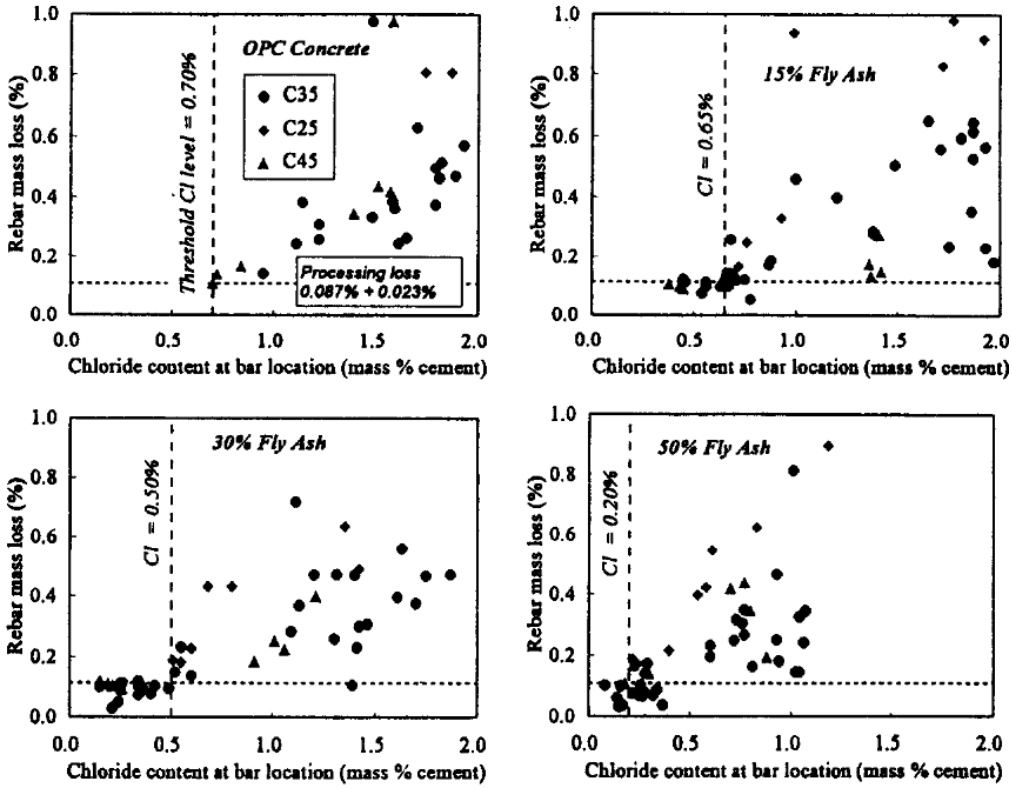

Figure II-37 Effect of fly ash on chloride threshold content[157]

Oh et al[155] reported the effect of fly ash content on the half-cell potential, corrosion area of

steel rebar, total chloride content and free chloride content and the results are shown in Figure II-28 and Table II-3, respectively.

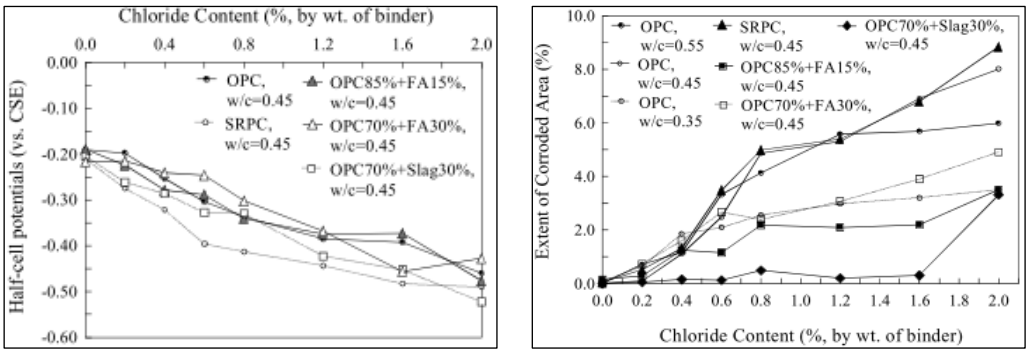

Figure II-38 Variation of half-cell potential with chloride content (left) and Extent of corroded area versus chloride content (right)[155]

According to the results, increasing the dosage of fly ash decreases the half-cell potentials of steel rebar and increases the corrosion area of reinforcement in concrete. And the $[Cl^-]/[OH^-]$, total chloride content and free chloride content decrease with the increase in fly ash content in concrete.

Table II-3 Threshold chloride values obtained from the present study[155]

Types of mixture	Chloride threshold values		
	Total Cl^- (%, by binder weight)	Free Cl^- (%, by binder weight)	$[Cl^-]/[OH^-]$
LI	0.78	0.12	0.16
NI	0.93	0.11	0.26
HI	0.89	0.12	0.19
NV	0.45	0.10	0.27
NIFA15	0.90	0.11	0.19
NIFA30	0.68	0.07	0.21
NISlag30	0.97	0.13	0.23

Ryou and Ann[153] investigated the effect of different type of binders (OPC, fly ash, slag, silica fume) on the corrosion rate and critical chloride threshold of reinforced concrete under internal and external chlorides conditions and the relevant results are shown in Figure II-39.

According to their report, the development of the corrosion rate is greatly influenced by binder type. For corrosion rate, in the state of passivation, for OPC and 10% SF mortars, the corrosion rate was even lower than for 30% pfa and 60% ggbs. In the case of critical chloride threshold, fly ash significantly reduced this value in comparison with other two pozzolanic materials, regardless of internal or external chloride source. These results suggest that fly ash may not provide an enhancement of the corrosion initiation.

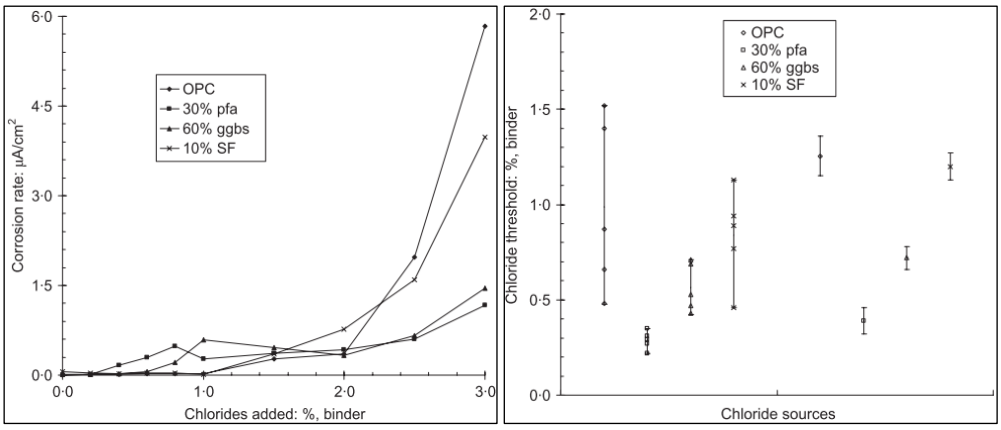

Figure II-39 Development of the corrosion in OPC, 30% pfa, 60% ggbs and 10% SF mortars with chloride in case (left) and Chloride threshold level for corrosion of steel in OPC, 30% pfa, 60% ggbs and 10% SF concrete/mortar depending on chloride sources(internal and external chlorides) (right)[153]

Pillai et al[151] compared the chloride penetration and critical chloride threshold value of concretes with LC3 and fly ash (Figure II-40) and reported that although the fly ash can fine the size of pore in concrete and increase the resistance of concrete against the penetration of chloride ions, however, due to the second hydration process of fly ash with $Ca(OH)_2$ form by the hydration of cement, the buffering capacity of concrete with fly ash was reduced, therefore, diminish the chloride threshold.

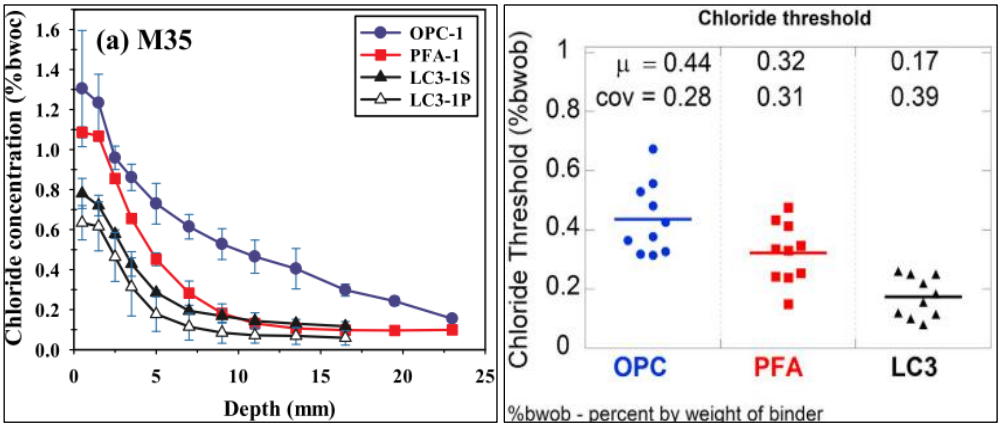

Figure II-40 Chloride profiles in the concrete mixes after 56 days of exposure to chloride solution (left) and Chloride threshold for corrosion initiation of the rebar in OPC, PFA and LC3 mortar(right)[151]

According to the previous reviews, fly ash appears to have a negative effect on the service life of reinforced concrete. Other researchers, however, hold the point that fly ash can delay the corrosion initiation of steel in concrete[156, 158, 159].

Slag

Similar to fly ash, slag is also a common alternative material in concrete industry[152]. Some

investigations[153-156, 158] reported the corrosion initiation of steel in concrete when using the slag.

Schiessl and Breit[156, 158] reported that slag positively affects the corrosion initiation of steel in concrete.

Oh et al[155] reported the effect of slag on the change of half-cell potential, corrosion area and chloride threshold of steel in concrete (in Figure II-38 Variation of half-cell potential with chloride content (left) and Extent of corroded area versus chloride content (right)[155]and Table II-3). In comparison with the control group, the corrosion area of the slag group was lower, however, the half-cell potential and the critical chloride threshold value of slag group were similar with these of control group. Therefore, the effect of slag on the corrosion initiation of steel in concrete reported in this work is negligible. The similar results were also reported by Li et al[154]

Ryou and Ann[153] researched the effect of slag on the corrosion rate and chloride threshold value of steel in concrete and mortar and the results are shown in Figure II-39. From the results, the used of slag can slightly reduce the corrosion rate of steel in mortar, but significantly reduce the level of critical chloride threshold in comparison with the control group. The slag can negatively impact the corrosion initiation of steel in concrete.

Silica fume

Hansson and Sørensen[160] and Pettersson and Krin[159] reported that silica fume can markedly negatively affect the corrosion initiation of steel in concrete, specially, when the used dosage of silica fume was more than 10% by the total mass of binders.

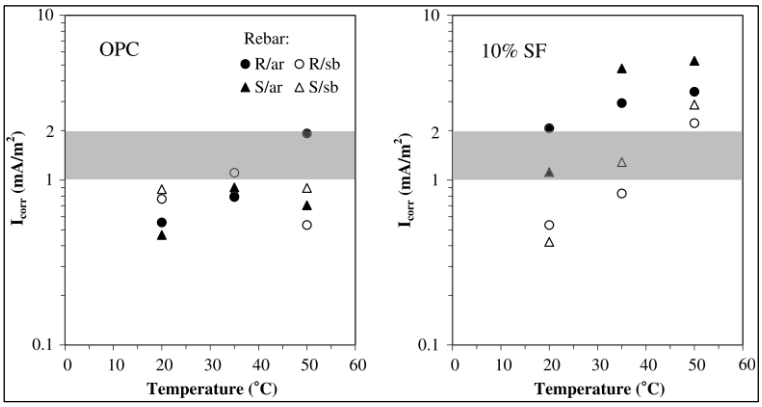

Figure II-41 Corrosion current density in specimens with 2% chlorides by mass of binder[136]

Manera et al[136] studied the effect of silica fume on the corrosion current under different temperature and the correlation between corrosion current and corrosion potential. In their

experiment, cement was partly replaced by silica fume in 10% by mass of binder. The results are shown in Figure II-41 and Figure II-42. In concrete with 2% chloride by mass of binder (Figure II-41), a higher value of corrosion current was measured in concrete with silica fume. The results suggested that a higher susceptibility to pitting corrosion for the bars embedded in concrete with 10% silica fume. In Figure II-42, it can be found that the corrosion probability of rebars embedded in concrete with 10% silica fume is obvious higher than that of OPC under the same chloride concentration. It means that the use of silica fume in concrete would increase the risk of corrosion of steel bar.

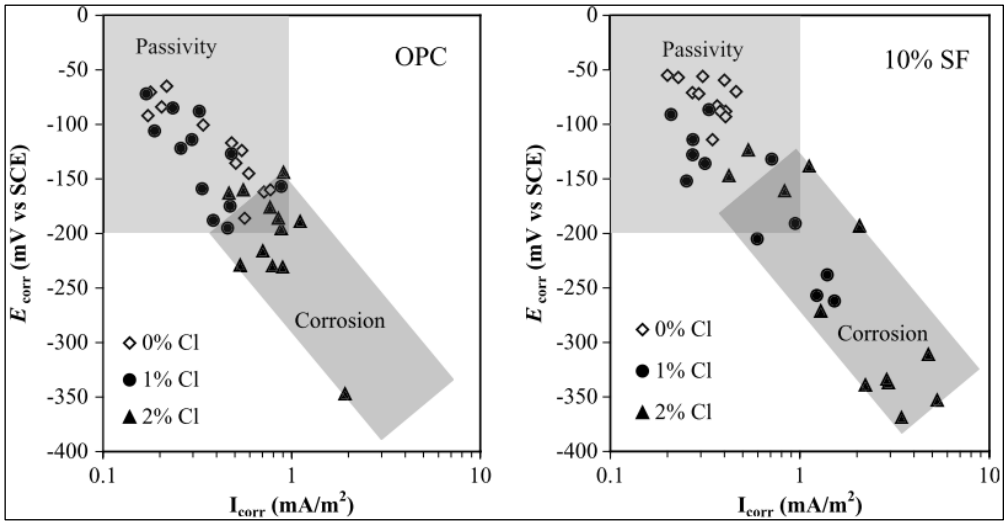

Figure II-42 Relationship between corrosion potential and corrosion current density of rebar[136]

Ryou and Ann[153] reported the effect of silica fume on the corrosion rate and critical chloride threshold of rebar and the results are shown in Figure II-39. From the results, the corrosion rate of steel bar in mortar with 10% silica fume was the highest before corrosion initiation, it means that the silica fume can enhance the risk of corrosion initiation of steel in concrete or mortar. However, the concrete with 10% silica fume had a relative lower critical chloride threshold in comparison with the control group. Thus, the silica fume can negatively affect the corrosion initiation of steel in concrete or mortar.

It is apparent that the literature is ambiguous and even contradictory since for all investigated supplementary cementitious materials both positive and negative effects have been reported. Given the ambiguous nature of reported data on the influence of cement type on critical chloride threshold, it is difficult to conclusively state whether the blending of supplementary cementitious materials with Portland cement has a positive or a negative effect corrosion initiation.

5.2.3 Macroscopic concrete voids at the steel-concrete interface

Due to improper stability of fresh concrete[76], when casting and compacting fresh concrete, some top-casting defects and voids can be formed at the steel-concrete interfacial zone and accelerate the corrosion process of steel in concrete in an aggressive environment[60, 68, 70, 144, 181, 182]. Thus, in this section, the effect of top-casting defects on the corrosion initiation of steel in concrete is reviewed through two parts 1). Interfacial air voids; 2). Bleed water zones.

- **Interfacial air voids**

As mentioned in section 2.5.1, interfacial air voids occur when entrapped or entrained air bubbles in fresh concrete raised up to during compaction and become trapped beneath reinforcing bars.

B.Reddy[146] researched the effect of air voids on the corrosion initiation of smooth steel in different type of concretes (OPC, SRPC, 30% PFA, 65% GGBS). In this work, the air voids were generated by the use of concretes with different workability and the corrosion initiation of steel was characterized by galvanic current and the critical chloride threshold value of smooth steel rebar in concrete was measured immediately when the galvanic current rise suddenly. The results are shown in Figure II-43

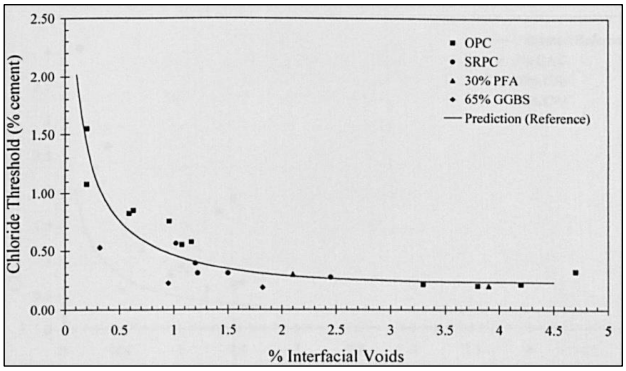

Figure II-43 Effect of cement binders on chloride threshold level[146]

Ann and Buenfeld[142] studied the relationship between critical chloride threshold value and air voids at steel-concrete interface with different type of corrosion inhibitor, and the result is shown in Figure II-44

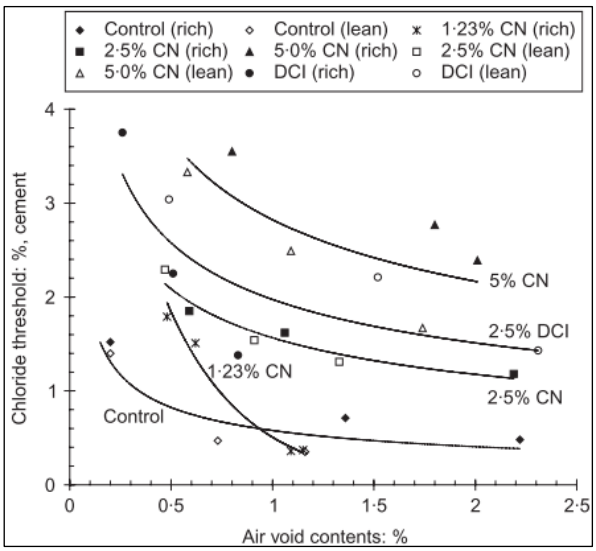

Figure II-44 Chloride threshold level as a function of air void content at the steel-concrete interface, dosage of corrosion inhibitor type and cement content[142]

From Figure II-44, it can be found that the critical chloride threshold value was strongly dependent on the interfacial air void content. A decrease in the air void content at the steel-concrete interface resulted in a significant increase in the critical chloride threshold value for all specimens.

According to the results, critical chloride threshold value reduced with the increase in interfacial air voids, especially, when the percentage of interfacial air voids increased from 0% to 1.5%, the critical chloride threshold value dramatically reduced. After, the number of interfacial air voids appeared not to affect the change of chloride threshold level. However, it should be noted that the presence of air voids at steel-concrete interface increases the risk of corrosion initiation of steel in concrete.

Most of investigations[60, 65, 70, 146, 149] concerning the corrosion behavior of steel in concrete with air voids reported that corrosion mainly initiated at the bottom side of steel according to the casting direction. However, there is a dispute on the location of corrosion initiation of steel in concrete or mortar.

Yonezawa et al[149] studied the effect of filter-induced voids on the corrosion of steel in mortar. The corrosion potential in mortar with or without filter-induced voids was reported in Figure II-45. The results show that the corrosion process of steel in mortar with or without filter-induced voids was very different, filter-induced voids accelerated the corrosion process of steel in mortar.

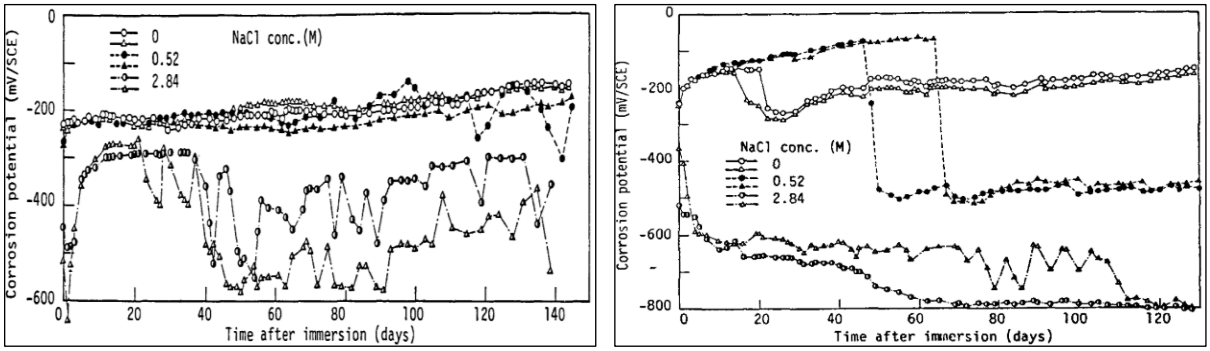

Figure II-45 Corrosion potential of steel electrode in mortar with good adhesion (left) and with a filter paper interposed (right)[149]

Figure II-46 show the surface conditions of steel in mortar with or without filter paper. It is clearly that a dense portlandite crystals layer appeared on the surface of steel in mortar with a good adhesion. However, only some needle-like crystals found on the surface of steel in mortar with filter paper. The former was protected well by mortar, and corrosion mainly initiated at the location with filter paper due to lack of the buffering capacity formed by $Ca(OH)_2$.

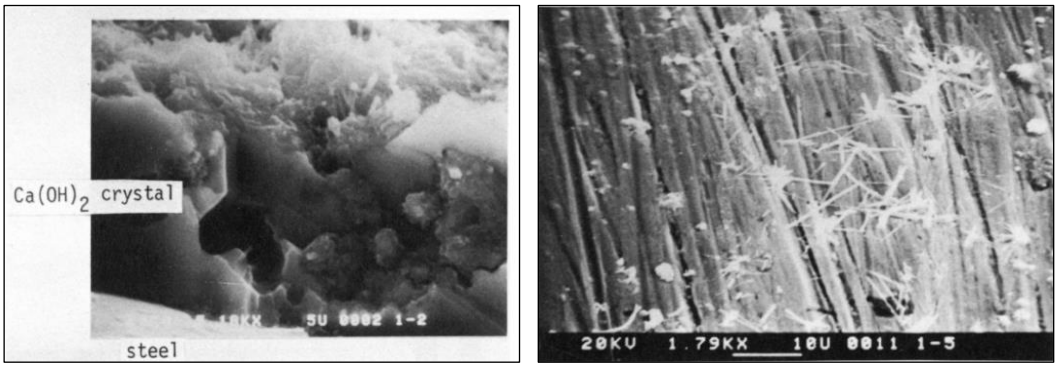

Figure II-46 Steel surface in mortar with good adhesion (left) and with a filter paper interface(right)[149]

B.Reddy[146] investigated the corrosion initiation of smooth steel in concrete with different workability indicated that corrosion mainly initiated at the location of air voids (Figure II-47).

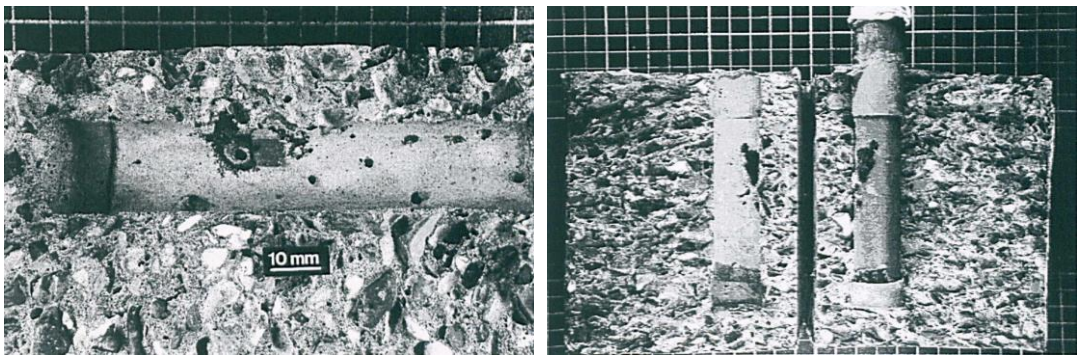

Figure II-47 Corrosion patterns of steel in concrete[146]

Nam et al[143] reported the distribution of air voids at steel-concrete interface and discussed

the effect of air void at steel-interface on the corrosion initiation of ribbed-steel in concrete with two different types of alkalinity. The results are shown in Figure II-48 and Figure II-49

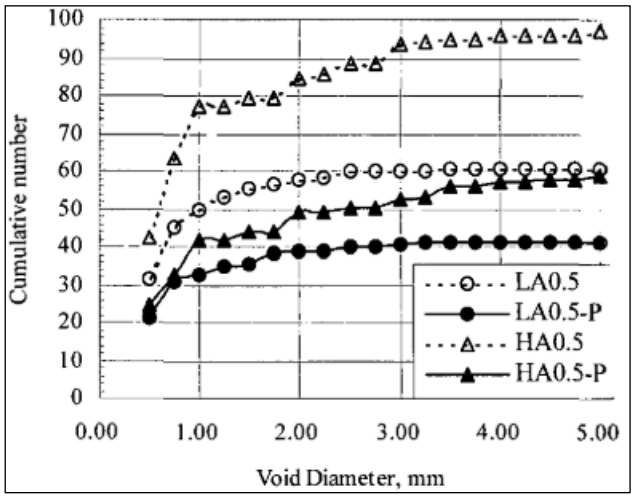

Figure II-48 Average cumulative number of voids along the rebar trace as a function of void diameter[143]

From Figure II-48, the distribution of air voids at steel-concrete interface was affected by the surface condition of steel reinforcement and the alkalinity of concrete. When the as-received rebar in the high alkaline concrete, some air voids can concentrate at the steel-concrete interface. If remove the surface oxide layer (mill scale), the number of air voids at steel-concrete interface can be reduced markedly.

Figure II-49 shows that air voids at the steel-concrete interface facilitated passive film breakdown and onset of localized corrosion and the corrosion tended to initiate at relatively large air voids.

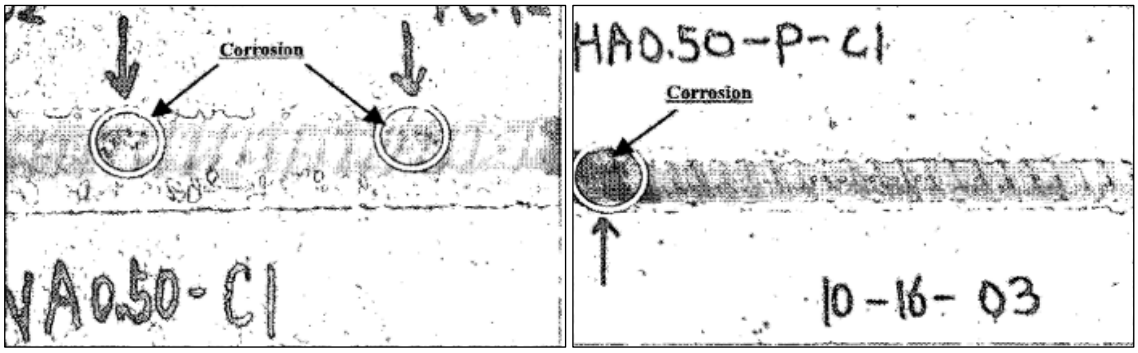

Figure II-49 Photograph of corrosion on the as-received rebar embedded in low alkalinity type specimen (left) and on the polished rebar embedded in high alkalinity specimen (right)[143]

However, there is a number of studies that have reported findings contrary to the above[112, 138-140, 163]. In order to investigate the distribution of rust spots and the effect of different interfacial conditions on the corrosion initiation of steel in concrete, Kathler et al[139] drilled some

reinforced concrete cores containing one centrally located reinforcement steel without any corroding regions from three structures in the Swiss Alps. according to their research, the interfacial defects were divided into four types air void (A), local higher porosity (P), tie wire (W) and no irregularities (N). The critical chloride threshold level of these four zones was measured respectively, and the results are shown in Figure II-50. From the results, although the mean critical chloride threshold value of no irregularities was the lowest compared to other three zones, their scatter for the critical chloride threshold value of no irregularities was the largest. It means that the risk of corrosion initiating at the no irregularities zone was the highest.

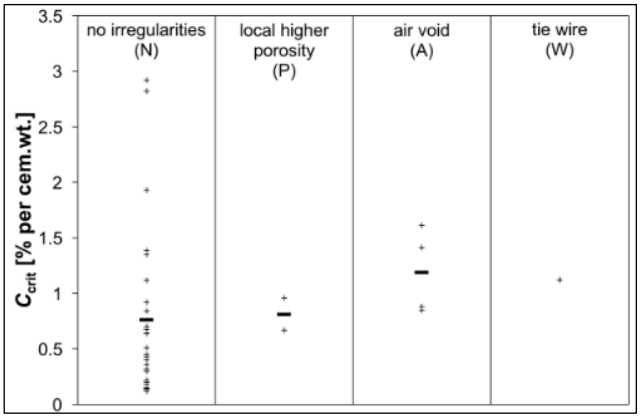

Figure II-50 Critical chloride threshold for different conditions at steel-concrete interface for all structures. Black rectangular mean of critical chloride threshold for all structures[139]

Figure II-51 Examples of irregularities at the steel-concrete interface Locally higher porosity (arrow) and small air voids (left part) as well as coarse air voids (right part). Corrosion initiated in this case at the arrow[139]

According to Figure II-51 and Figure II-52, in one third of the samples where corrosion initiation was not found to correlate with visible irregularities at the steel-concrete interface, there were actually air voids present at the steel-concrete interface (elsewhere). It means that for these samples, corrosion initiated preferentially not at air voids or other defects, but at a location without any visible irregularity. This may be explained by the moisture content of the samples, i.e.

unsaturated. Coarse air voids can only get saturated under prolonged immersion or pressure saturation. In the presence of air in the voids, initiation of corrosion is hardly possible.

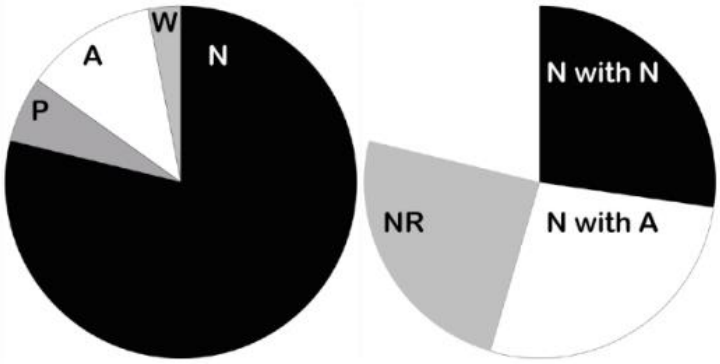

Figure II-52 Left pie chart Occurrence of initiation at different conditions at steel-concrete interface for all structures. Right pie chart The category N (no irregularities at initiation spot) further divided in; (NR not reported)[139]

In conclusion, the impact of interfacial air voids on corrosion initiation in concrete cannot be generalized. The frequently held view that air voids a priori promote corrosion initiation is not always true, based on the reviewed data. The role of interfacial air voids is probably influenced by other conditions, particularly, the moisture conditions in the concrete.

- **Settlement and bleeding zones**

Due to the improper stability or the long setting time of fresh concrete, bleeding, settlement and segregation will occur after casting fresh concrete. As mentioned in section 2.5.1, the size of settlement and bleeding zones increase with the height of concrete below the reinforcing steel[70, 144]. As a result, top-cast horizontal bars exhibit more defects at the underside perimeter than bottom-cast horizontal bars. This effect is well-known by structural engineer as the “top-casting effect”, which not only affects the bond properties between steel reinforcement and concrete, but the durability of reinforced concrete in aggressive environment as well[60].

Bleed water may accumulate under the reinforcement and in the initially empty settlement zone. During hydration the bleed water will be (partly) absorbed into the surrounding paste due to chemical shrinkage causing self-desiccation. Settlement and bleeding zones may thus be empty (air-filled) or partly water-filled. Unless exposed to highly moist environment, it is unlikely that water will be present in large quantities in settlement and bleeding zones in the hardened concrete due to the size of these voids. An exception to this is the case when cracks in the concrete cover provide a link from the settlement and bleeding zones to the exposure environment.

Soylev and François[144] reported the effect of casting height on the settlement and segregation of different types of concretes under the steel reinforcement and the relationship between settlement and segregation of concrete and corrosion behavior of steel reinforcement (Figure II-53 and Figure II-54).

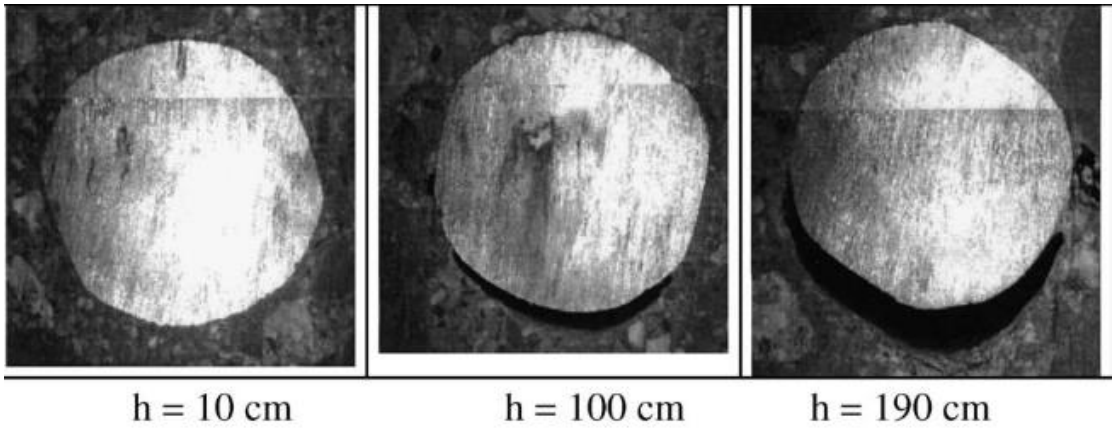

Figure II-53 Three section of C40 at 10, 100 and 190 cm of height, respectively, at video microscope with an enlargement of ×25 magnification[144]

According to these results, the level of bleeding and settlement and the corroded surface of reinforcing steel increased with the increase in concrete depth under steel reinforcement.

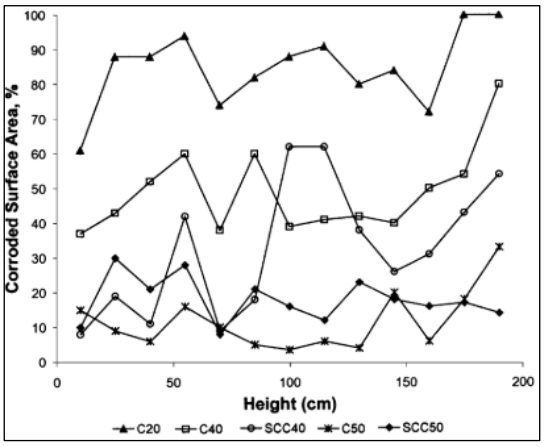

Figure II-54 Variation of the corroded surface area as a percentage of the total surface area of the steel embedded in concrete with concrete depth[144]

Mohammed et al[111] investigated the relationship between chloride concentration of top steel and bottom steel and the macro-cell current density. The reinforced concrete specimen is shown in Figure II-55. The results given in Figure II-56 indicated that corrosion mainly initiated at the bottom side of steel reinforcement although the chloride concentration at the top side of steel rebar was much higher than that of bottom side according to the tendency of spraying direction. They authors had confirmed that there were some gaps under the HTB steel bar and weak interface reduced the

value of critical chloride threshold. The same authors [114]also studied the effect of sea-water on the corrosion initiation of reinforced concrete and indicated the similar results.

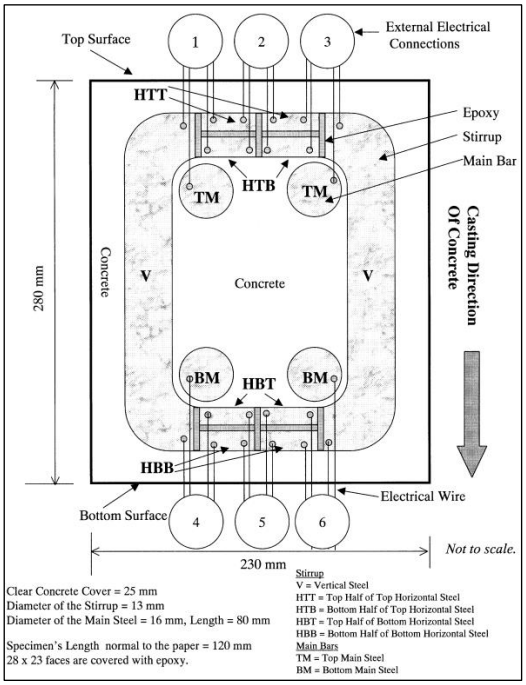

Figure II-55 Layout of specimens[111]

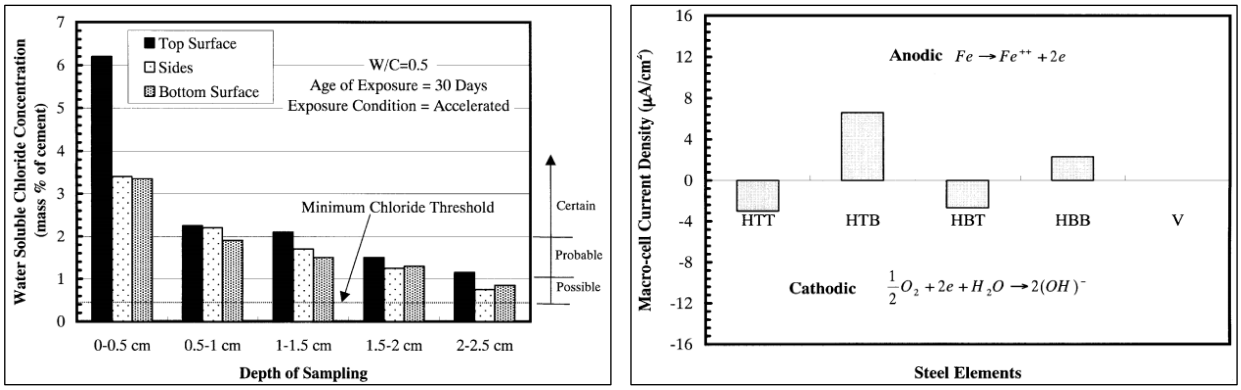

Figure II-56 Chloride profiles and Macro-cell current[111]

Castel et al[68], studied the correlation between corrosion behavior of two reinforced concrete beam corroded for 14 years and 17 years, respectively, in chloride environment and the total chloride concentration at the level of steel reinforcement. The beams were shown in Figure II-57. It should be noted, in Figure II-57, that the compressive surface of B1CL and the tensile surface of A1CL were the top-casting surface, respectively.

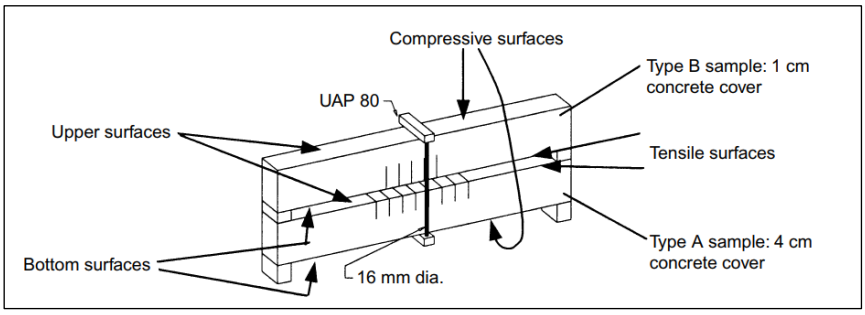

Figure II-57 Loading system in three points flexion[68]

The cracking maps and total chloride concentration at the depth of reinforcement steel of A1CL beam and B1CL beam were shown in Figure II-58 and Figure II-59. It is clearly, all the chloride contents at steel bar have exceeded the maximum usual threshold for corrosion initiation regardless of compressive steel bar or tensile bar. The corrosion initiation, however, mainly initiated on the steel reinforcement with top-casting defects. The results indicated that the critical chloride threshold content is determined not only by total chloride content, but the interfacial conditions of steel-concrete. Indeed, the corrosion behavior of steel in concrete beams strongly depends on the steel-concrete interface conditions.

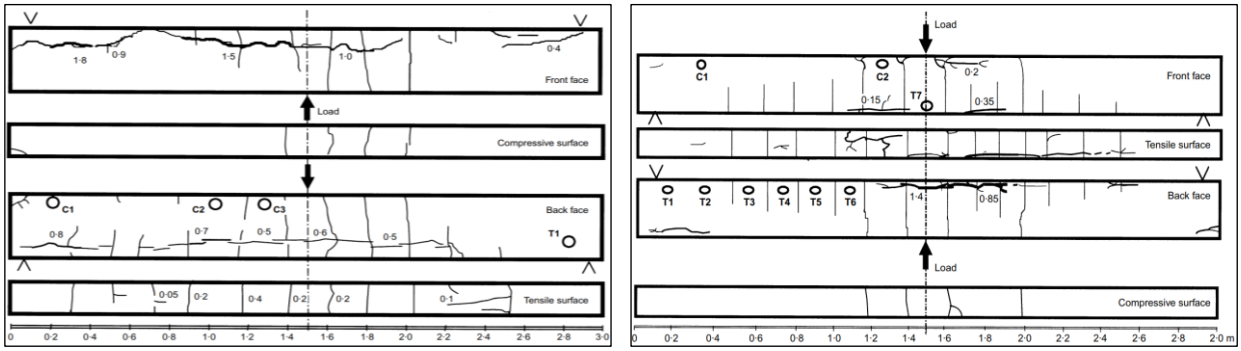

Figure II-58 Cracking maps of A1CL beam (left) and B1CL beam (right)[68]

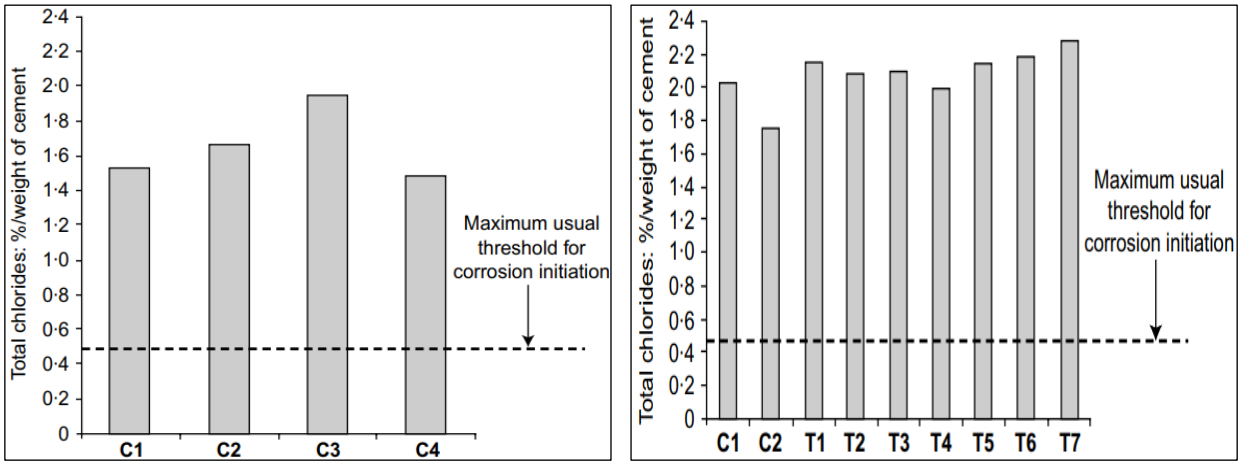

Figure II-59 Total chloride concentration of A1CL beam (left) and B1CL beam (right) at the depth of steel reinforcement[68]

Mohammed et al[115, 183], researched the interfacial microstructures and early corrosion behaviors of reinforced concrete manufactured by alumina cement (AL) and indicated that relatively more corrosion over the steel bars is found even for less chloride ingress and also less oxygen permeability, which is attributed to a porous steel-concrete interface. The details are given in Figure II-60 and

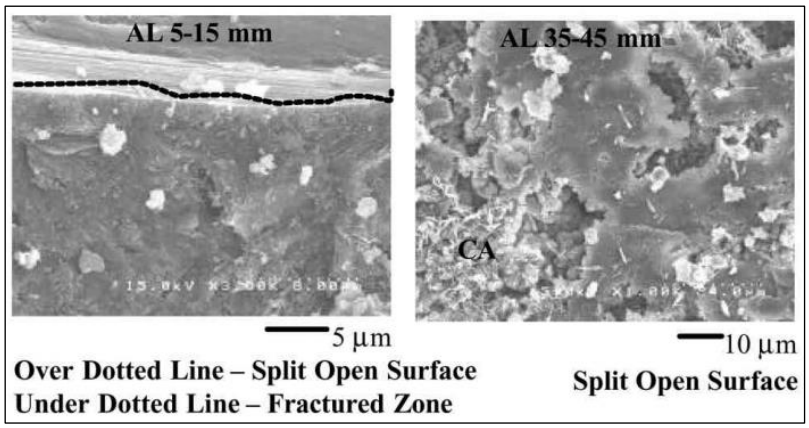

Figure II-60 Interfacial microstructures of AL[183]

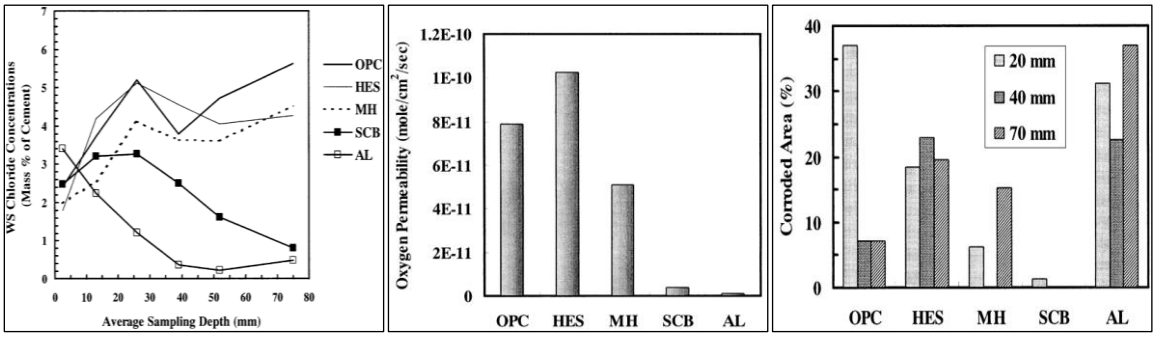

Figure II-61 Chloride profiles, Oxygen permeability and Corrosion area of AL[115]

Vidal et al[117] studied the correlation between total chloride content and corrosion cracking of reinforced concrete beams stored in a chloride environment for 17 years under service loading. The cracking maps of reinforced beam with time are given in Figure II-62and the total chloride content at the steel reinforcement surface was shown in Figure II-63.

The compressive surface of B2CL was the top-casting surface. According to the Figure II-62, it can be found that corrosion initiated at the top-casting area after 6 years, meanwhile, there was no corrosion found on the tensile zone. Until 12 years of storage, several tiny corrosion-induced cracks appeared on the tensile zone, but, simultaneously, corrosion-induced cracks on the compressive zone had connection to form some longer cracks. It means that the corrosion level of compressive bars was higher than that of tensile bars. However, from the results of total chloride content resulted from compressive zone and tensile zone (Figure II-63), chloride concentration of compressive zone was marked lower than that of tensile zone although all the chloride content had exceeded the limitation from ACI and RILEM. This result released that the chloride threshold used by standards was a necessary but not a sufficient parameter to define service life and the steel-concrete interfacial conditions were a determinant parameter.

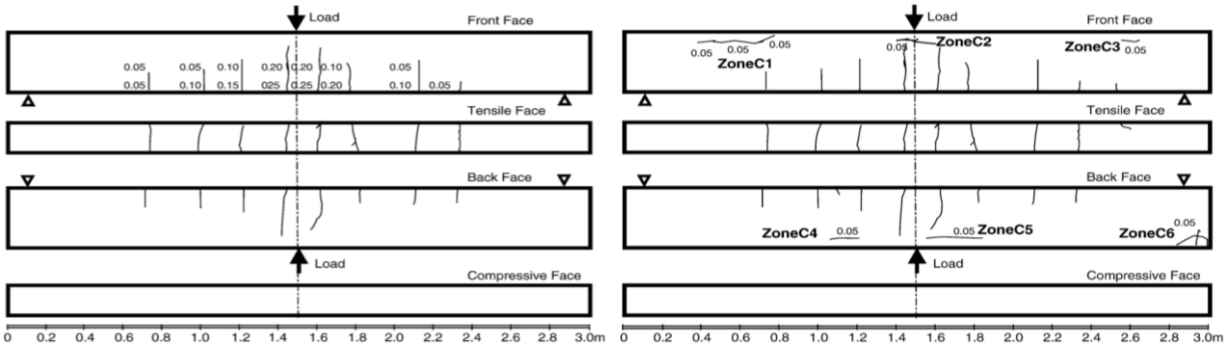

a. Cracking maps of B2CL after 28 days

b. Cracking maps of B2CL after 6 years

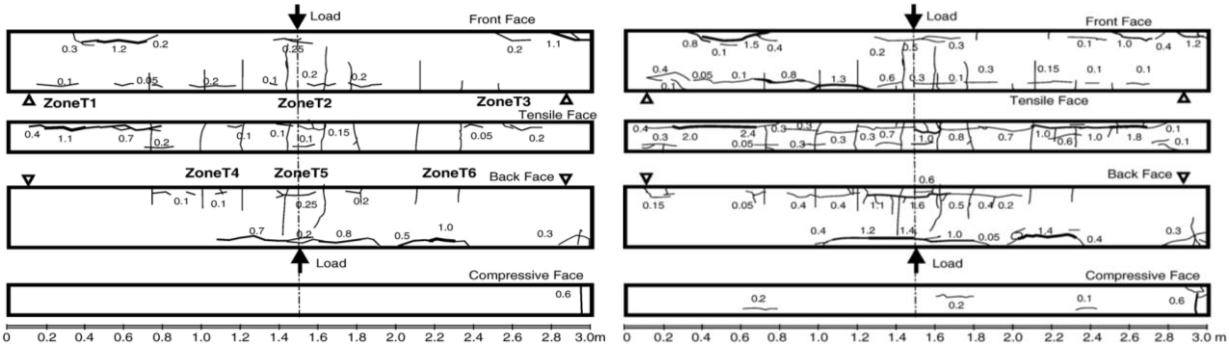

c. Cracking maps of B2CL after 14 years

d. Cracking maps of B2CL after 17 years

Figure II-62 Cracking maps of B2CL beam in different storage[117]

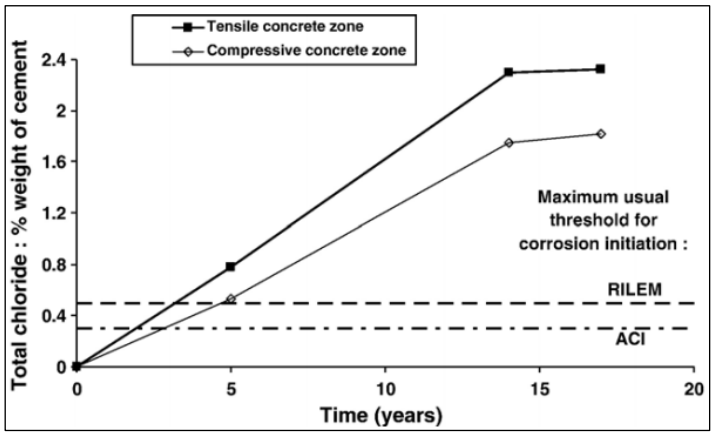

Figure II-63 Total chloride content at the depth of steel reinforcement in compressive and tensile zone of the corroded beams at different stages[117]

Zhang et al[70] studied the chloride-induced corrosion of reinforcement in concrete at different height. The layout of reinforced concrete wall, chloride profiles and polarization resistance change of corroded steel were given in Figure II-64 and Figure II-65, respectively.

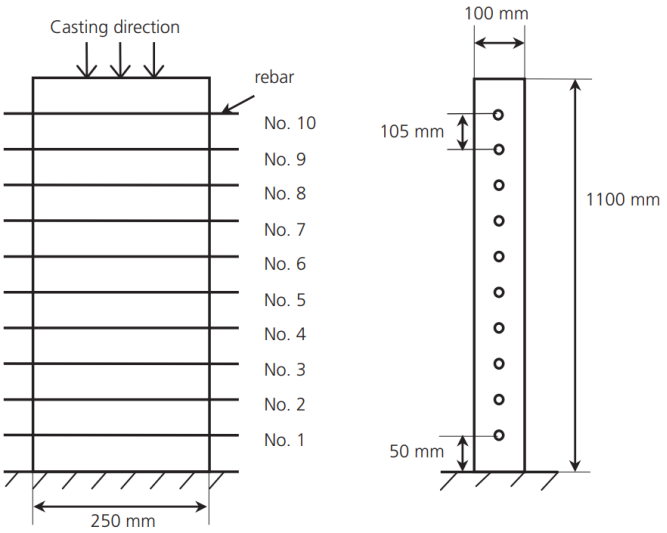

Figure II-64 Layout of E concrete wall[70]

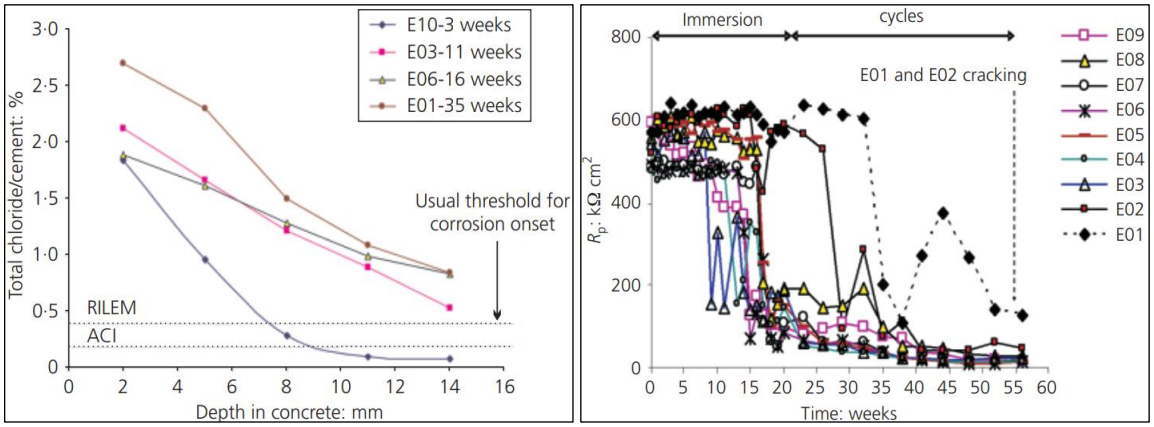

Figure II-65 Total chloride content and Polarization resistance of steel reinforcement[70]

From the results, the Rp of E01 was the highest since the steel-concrete interface was quite perfect. In the case of E03 and E06, although the chloride content at the depth of steel was lower than that of E01, corrosion occurred on E03 and E06, with top-casting defects, at 8th week and 15th week, respectively. Thus, interfacial settlement and bleeding can lead to a reduction in chloride threshold in comparison to specimens without defects. This similar results were also be found by Angst et la[118].

Zhang el al [60]investigated the correlation between total chloride content at the steel surface and the corrosion area of steel reinforcement in concrete in a relative long exposure term (see Figure II-66). They indicated that although higher chlorides appeared at the top surface of steel reinforcement, corrosion, however, mainly took place at the bottom side of compressive bar due to the existence of top-casting defects.

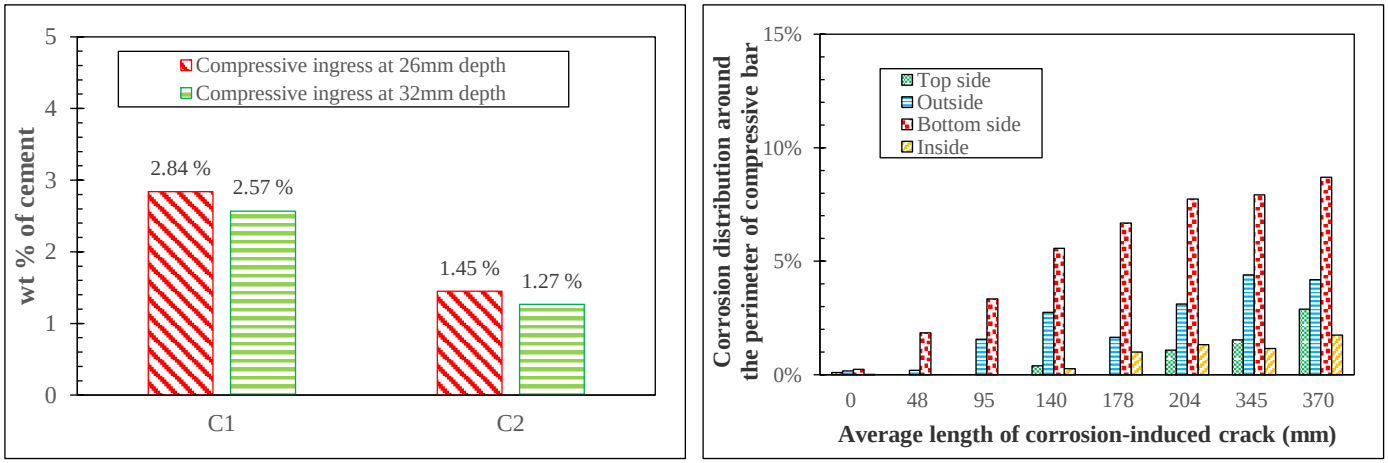

Figure II-66 Total chloride content at the level of compressive bar and the corrosion area around the perimeter of compressive bar[60]

Summary, steel-concrete interfacial settlement and bleeding would markedly reduce the critical chloride threshold of steel in concrete. This is because local steel reinforcement in concrete lacked the buffering capacity formed by cement hydration or even no protection by concrete cover due to the existence of top-casting defects. However, in the case of the decline level of the critical chloride threshold, there is no an accurate value now.

In order to explain the mechanism of the effect of the voids at steel-concrete interface on the corrosion initiation of steel embedded in concrete, Angst et al[123] proposed a proper hypothesis, that are generally valid for the different macroscopic concrete voids, including entrapped and entrained air voids, settlement and bleeding zones, and perhaps cracks slip, and separation as well as other voids. In this hypothesis, the moisture state in voids is the key point. The moisture state and access from exposure environment in different macroscopic interfacial concrete voids are summarized in Table II-4.

Table II-4 Geometry, moisture state and access from exposure environment in different macroscopic interfacial concrete voids (MICVs)[123]

	Entrained air voids	Entrapped air voids	Settlement zones	Bleeding zones	Cracks, slip and separation
Length scale, perpendicular to steel	μm-mm	μm-cm	μm-mm	μm-mm	μm-mm
Length scale, along steel	μm-mm	μm-cm	μm-m	μm-m	μm-cm
Initially water	No	No	No	Yes	Depends on

saturated					exposure
Access to exterior (exposure environment)	No, unless linked to exterior through cracks in the cover	No, unless linked to exterior through cracks in the cover	No, unless linked to exterior through cracks in the cover	No, unless linked to exterior through cracks in the cover	Yes

In this hypothesis, on the combined impact of moisture state and macroscopic interfacial concrete voids on corrosion initiation is illustrated in Figure II-67.

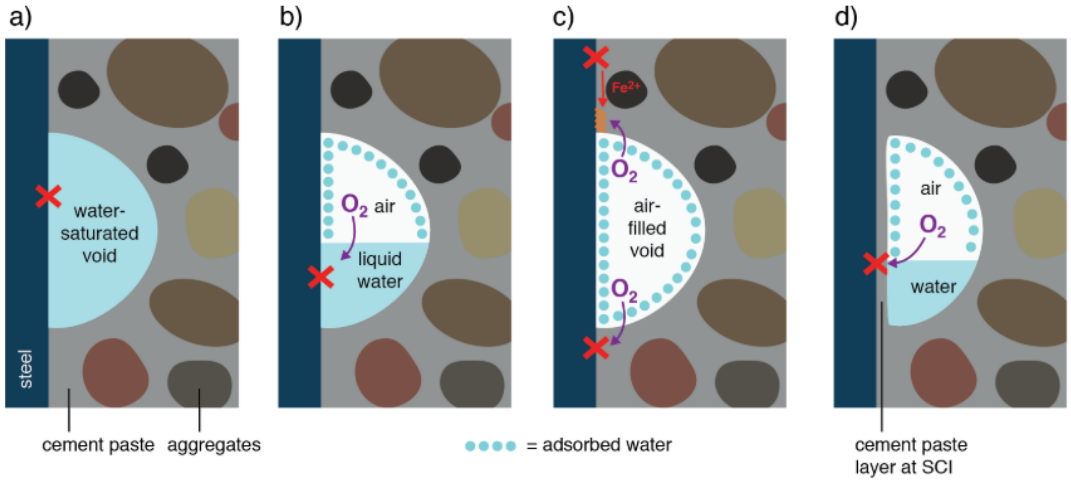

Figure II-67 Schematic sketches illustrating possible roles of macroscopic interfacial concrete voids in corrosion initiation. The red cross indicate the location of corrosion initiation[123]

Firstly, in completely saturated state (a), steel is directly exposed to liquid water (containing chlorides) within the void. In this case, the steel will be more prone to corrosion initiation than steel covered with cement paste. This is because of the absence of calcium hydroxide at the steel surface that locally buffers the pH during stages of early pitting corrosion. During this stage the competitive migration of chloride and hydroxyl ions towards the anodic site is decisive for stablishing stable pit growth. Thus, a locally lower pH buffer capacity significantly impairs the corrosion inhibiting mechanism associated with the presence of a calcium hydroxide rich layer at the steel-concrete interface.

Secondly, in partially saturated state (b), voids containing both liquid electrolyte and air, there is, in addition to the susceptibility to corrosion in the wet areas as mentioned above, an increased availability of oxygen from the air-filled part that potentially aggravates the corrosion initiation process. The mechanism for this may be related to, on the other hand, generally raising the steel potential prior to pitting nucleation and, on the other hand, enhancing the supply of oxygen to sustain

the cathodic activity that is needed to overcome the stage of early pit growth and to achieve stable pitting corrosion. Thus, steel in contact with partially saturated macroscopic interfacial concrete voids may be considered the worst case.

In air-filled state (c), supply of oxygen through diffusional transport across the film of adsorbed water at the steel surface is high. On the contrary, ionic transport within the film of adsorbed water is expected to be severely limited. Thus, it is unlikely to achieve pitting corrosion in the parts of the steel covered with adsorbed water, as this requires the formation of significant galvanic elements, which is impossible due to the strong ohmic control within the adsorbed water film. Electrical resistance measurement reported in [184] indicated that interfacial air voids at non-saturated conditions are indeed electrically inactive. However, for the reasons given in the previous paragraph, air-filled macroscopic interfacial concrete voids may promote corrosion initiation in cement-paste covered steel areas close to the macroscopic interfacial concrete voids, as indicated by the red cross in (c).

(d) shows the case where a cement paste layer is present at the steel surface adjacent to the macroscopic interfacial concrete voids. Here, the susceptibility to corrosion is expected to be lower that in the case of (b), mainly due to the pH buffering and barrier effect of the cement paste layer. Depending on the thickness of this cementitious layer as well as the reservoir of calcium hydroxide available, corrosion may still preferentially start here, particularly in unsaturated condition due to the combination of increased supply of oxygen and high ionic conductivity enabling the formation of galvanic elements to stabilize early pit growth.

Summarizing the different cases illustrated in Figure II-67, corrosion may be expected to initiate in the macroscopic interfacial concrete voids or next to it, depending on the saturation state.

5.3 Effect of steel-concrete interface on the corrosion propagation

Compared to the effect of interfacial defects of steel-concrete on the corrosion initiation of steel in concrete or mortar, the relevant researches on the impact of interfacial defects on the corrosion propagation of steel in concrete are limited. In the past decades, on this topic, the researches mainly focused on the effect of top-casting defects on the corrosion propagation of steel in concrete[52, 60, 62, 70, 108, 181, 185]. Therefore, these investigations are review in this section.

François and Arliguie[185] investigated the development of corrosion-induced cracks of reinforced concrete beams. In this research, four reinforced concrete beams, labeled A1, A2, B1 and B2, stored in a chloride environment (in terms of salt fog with 35g/L NaCl) for 12 years, were measured and the results of B1 beam are shown in Figure II-68. They indicated that corrosion-induced cracks firstly appeared at the zone of top-casting reinforcement steels after 7 years in salt fog. And after 11 years in salt fog, several tiny corrosion-induced cracks were found at the area of bottom-casting steel rebars, however, at the same time, some longer and wider corrosion-induced cracks appeared at the zone of top-casting reinforcement. It means that top-casting defects can accelerate the corrosion propagation of steel in concrete in chloride environment. The same results were also reported by Castel et al[68], Vidal et al[117], Zhang et al[186] and Yu et al[62].

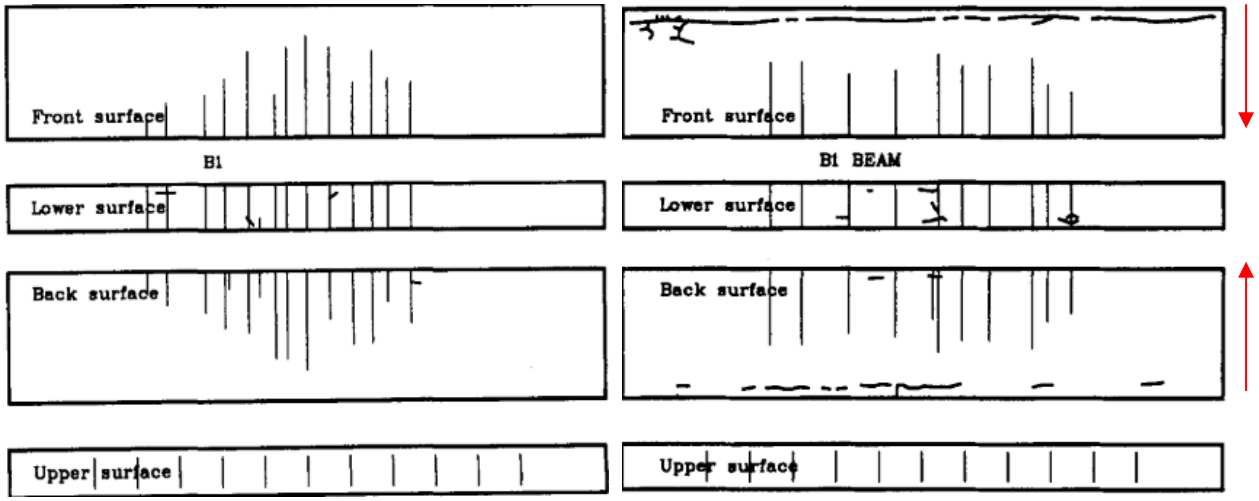

(a) Cracking maps after 6 years in salt fog (b) Cracking maps after 7 years in salt fog

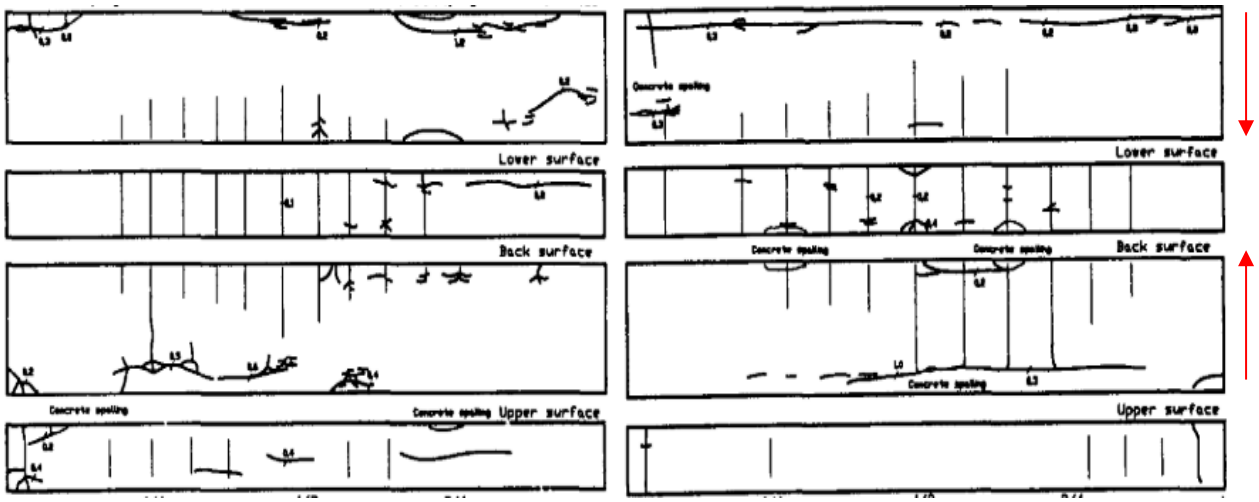

(c) Cracking maps after 11 years in salt fog (d) Cracking maps after 12 years in salt fog

Figure II-68 Cracking maps in salt fog (B1)[185]

Yu et al[181] studied the influence of steel-concrete interface defects on the development of

chloride-induced corrosion in reinforced concrete beams under sustained loading. In this investigation, four reinforced concrete beams in 3 m long, stored in a salt fog environment, were studied. They indicated that corrosion-induced cracks always developed much more quickly along the top-cast steel bars due to the existence of top-casting-induced defects, which were favorable to both initiation and propagation of corrosion.

Zhang et al[60] researched the relationship between average width and length of corrosion-induced cracks and corrosion area of steel reinforcement with top-cast defects. In their research, top-cast defects markedly accelerated the corrosion of steel rebar when the average width and length of corrosion-induced cracks were less than 184μm and 88μm, respectively. Once these values were exceeded, the function of top-cast defects on the corrosion rate of steel rebar gradually reduced, and at last, the top-cast defects appeared to no longer affect the corrosion process of steel bars.

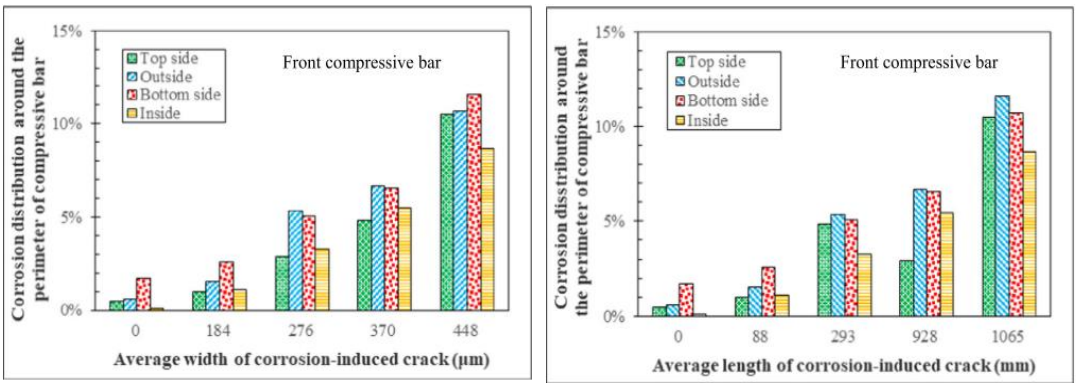

Figure II-69 Relationship between average width (left) and length (right) of corrosion-induced cracks and corrosion distribution around the perimeter of reinforcement steel[60]

In conclusion, although some published investigations indicated that the top-casting defects accelerated the corrosion initiation of steel in concrete. The impact of top-casting defects on the corrosion propagation of reinforcing steel in concrete, however, received a limited attention up to now.

6 Corrosion of stirrups in reinforced concrete

As mentioned in the introduction, the plain concrete is a typical quasi-brittle material, for the tensile strength of which is markedly relatively lower in comparison with its compressive strength. Thus, reinforcing steels are used to reinforce concrete in all most concrete constructions.

Generally, reinforcing steels are induced in concrete by the way of steel frame (Figure II-70),

and the role of stirrups is to fix the main steel rebars during manufacturing and install steel frame and to carry the shear stress during the service life of reinforced concrete buildings. Therefore, stirrup can be regarded as an important part in reinforced concrete constructions.

Figure II-70 Steel frame

6.1 Interfacial conditions of stirrup-concrete

Generally, a common stirrup can be divided into three parts according to the casting direction of fresh concrete: horizontal legs, vertical legs and corners of stirrups. For the horizontal legs of stirrup, it is defined that the orientation of the legs of stirrup perpendiculars to the casting direction of fresh concrete. However, the vertical legs mean the legs of stirrup parallels to the casting direction of fresh concrete. An illustration schematic of common stirrup is shown in Figure II-71.

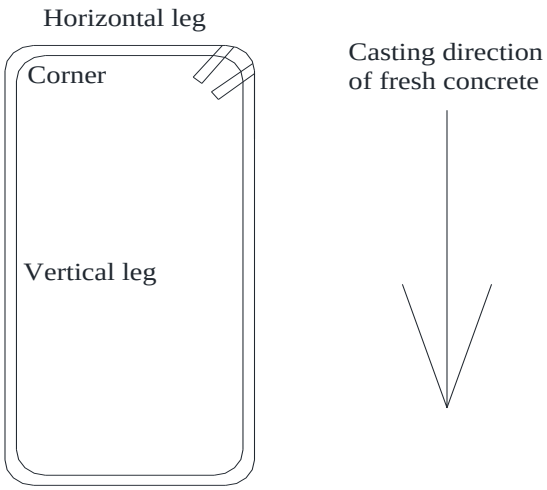

Figure II-71 Illustration schematic of common stirrup

For the horizontal legs of stirrups in concrete, as they commonly locates in the same plane of main reinforcing steels, therefore, it can be considered that these legs of stirrup possess the same

porous, loose interfacial conditions in concrete compared to the main steel rebars[60, 187, 188].

For the vertical legs of stirrups, Horne et al[78] (Figure II-14) confirmed that interfacial conditions between vertical legs of stirrup and concrete was perfect, no defects surrounded steel rebar.

For the corners of stirrups, there now are hardly any literatures concerning them in terms of interfacial condition between corners of stirrup and concrete. However, it can be considered that there is an intersection point between main steel rebars and corners of stirrup. Alhozaimy et al[189] reported that the concrete closer to an intersection point tends to be much more porous than the concrete far from the rebars.

Summary, for the interfacial condition of stirrup-concrete, defects mainly located in the interface of bottom side of horizontal leg of stirrup-concrete and the corner of stirrup-concrete. However, the interface between top side of horizontal leg and vertical leg of stirrup was perfect.

6.2 Corrosion behavior of stirrup in reinforced concrete

Mohammed et al[111] analyzed the macro-cell current of different parts of stirrup (Figure II-55) and reported that pitting corrosion mainly took place at the bottom side of horizontal leg of stirrup according to the casting direction, this can be attributed to presence of top-casting defects. However, the vertical leg and top side of horizontal legs of stirrup were subjected to general corrosion, for there was no defects around them (Figure II-72).

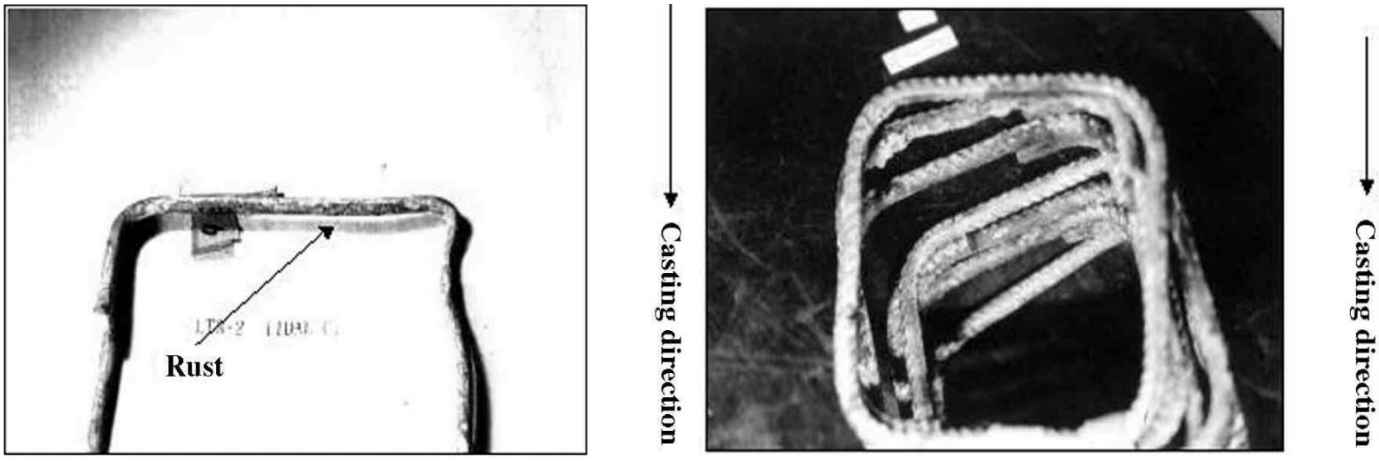

Figure II-72 Corrosion of stirrup[111]

Yu et al[62] studied the corrosion of reinforced concrete beams and indicated that some severe pitting corrosion mainly occurred at the top horizontal legs corresponding to the tensile surface,

especially when the stirrups were located at the mid span of reinforced concrete beam. A few pitting corrosions, however, took place at the top half vertical legs, While, there were hardly any pitting corrosion spotted at the bottom horizontal legs of stirrups (Figure II-73).

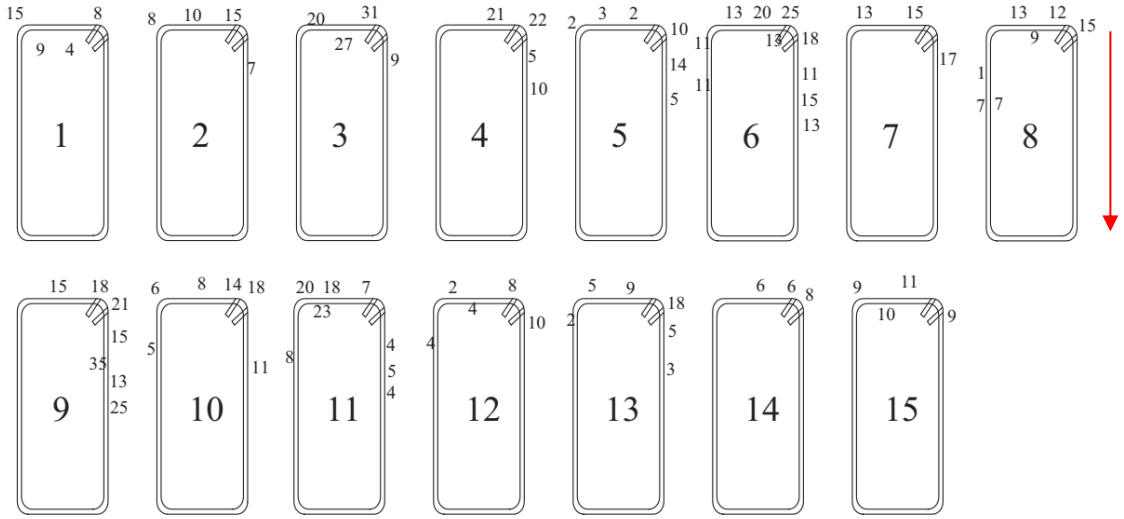

Figure II-73 Stirrup diameter loss (%)[62]

Alhozaimy et al[189] counted the total intrusion volume of different point on the steel rebar and investigated the corrosion of the intersection between rebars and found that a higher corrosion rate took place at the location of the intersection of two bars because of the presence of porous concrete (Table II-5).

Table II-5 MIP results for concrete specimens at the intersection and mid points[189]

Specimen ID	Location	Total intrusion volume (ml/g)
1	Mid point	0.082
2	Mid point	0.061
3	Mid point	0.057
4	Mid point	0.076
Average value	Four Mid points	0.069
5	Intersection	0.088
6	Intersection	0.094
7	Intersection	0.063
8	Intersection	0.079
Average value	Four intersection points	0.081

According to the published results, it can be found that the corrosion of stirrup was related to the interfacial condition between stirrup and concrete and corrosion mainly appeared on the horizontal legs and the corner of stirrups. However, the vertical leg of stirrup only suffered from faint corrosion.

6.3 Correlation between stirrups and main steel rebars in terms of corrosion

It is well known that stirrups electrically connect main reinforcing steels in steel frame when it suffered from corrosion. However, the correlation between stirrups and main reinforcing steels in terms of corrosion is now under argument.

6.3.1 Stirrups protect main steel rebar against corrosion

Du et al[190] analyzed the corrosion of stirrups in reinforced concrete elements and reported that activation-passivation galvanic corrosion took place between stirrups and main steel rebars when outside of stirrup were corroded firstly, and the outside of stirrup acted as anode and the inside of stirrup and main rebars played as cathode. After stirrups and main steel rebars contacted aggressive agents absolutely, different metal contacting corrosion occurred, stirrups acted as anode and main steel acted as cathode. The main steel rebars were protected by stirrups regardless of activation-passivation galvanic corrosion or different metal contacting corrosion. The similar results can also be found in ref[191, 192].

Tong[193] revealed that stirrups protected the main steel rebars in terms of corrosion and the corrosion of main reinforcing steels reduced with the increase in the diameter of stirrup.

6.3.2 Stirrups accelerate main steel rebar corrosion

Otsuki et al[194] investigated the relationship between stirrups and main steel rebars and found that the main steels connected with the stirrup show significant macrocell corrosion compared to the main steel not connected with the stirrup. Stirrups help to form significant macrocell corrosion of main steel by connecting the andic area with the cathodic areas. The similar results can also be found in ref[195]. However, François et al[196] consider that these conclusions obtained are not necessarily to long-term corrosion processes.

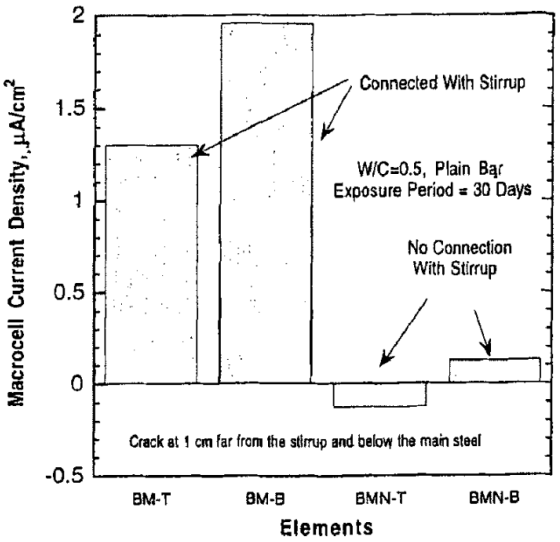

Figure II-74 Macrocell current density of main steels (with and without connection with stirrup)[194]

7 Reference

[1] P. Ghods, O.B. Isgor, F. Bensebaa, D. Kingston, Angle-resolved XPS study of carbon steel passivity and chloride-induced depassivation in simulated concrete pore solution, Corrosion Science, 58 (2012) 159-167.

[2] P. Ghods, O. Isgor, G. Carpenter, J. Li, G. McRae, G. Gu, Nano-scale study of passive films and chloride-induced depassivation of carbon steel rebar in simulated concrete pore solutions using FIB/TEM, Cement and Concrete Research, 47 (2013) 55-68.

[3] P. Ghods, O. Isgor, G. McRae, J. Li, G. Gu, Microscopic investigation of mill scale and its proposed effect on the variability of chloride-induced depassivation of carbon steel rebar, Corrosion Science, 53 (2011) 946-954.

[4] J.R. Mackechnie, Predictions of reinforced concrete durability in the marine environment, University of Cape Town, 1995.

[5] H. Böhni, Corrosion in reinforced concrete structures, Elsevier2005.

[6] J. Shi, W. Sun, Recent research on steel corrosion in concrete, Journal of the Chinese Ceramic Society, 9 (2010).

[7] M.B. Otieno, The development of empirical chloride-induced corrosion rate prediction models for cracked and uncracked steel reinforced concrete structures in the marine tidal zone, University of Cape Town, 2014.

[8] Z.-T. CHANG, Corrosion rate of steel reinforcement in concrete in seawater and influence of concrete crack width, The University of New South Wales Sydney, Australia, 2007.

[9] K.Z. Kahhaleh, J.O. Jirsa, E. Vaca-Cortés, H.G. Wheat, R. Carrasquillo, Corrosion Performance of Epoxy-Coated Reinforcement: Macrocell Tests, University of Texas at Austin. Center for Transportation Research, 1998.

[10] T.D. Marcotte, Characterization of chloride-induced corrosion products that form in steel-reinforced cementitious materials, (2001).

[11] P. Schieβl, M. Raupach, Influence of concrete composition and microclimate on the critical Chloride content in concrete, Corrosion of Reinforcement in Concrete, Page, Treadaway and Bamforth, Editors, Elsevier Applied Science, London, (1990) 49-54.
[12] E. Poulsen, L. Mejlbro, Diffusion of chloride in concrete: theory and application, CRC Press2014.
[13] L. Bertolini, B. Elsener, P. Pedeferri, E. Redaelli, R. Polder, Corrosion of steel in concrete: prevention, diagnosis, repair. 2013, John Wiley & Sons, 2004.
[14] A. Küter, M.R. Geiker, J.F. Olesen, H. Stang, C. Dauberschmidt, M. Raupach, Chloride ingress in concrete cracks under cyclic loading, 3rd International Conference on Construction Materials: Performance, Innovations and Structural Implications, The University of British Columbia, 2005.
[15] L. Tang, L.-O. Nilsson, P.M. Basheer, Resistance of concrete to chloride ingress: Testing and modelling, CRC Press2011.
[16] D.P. Bentz, E.J. Garboczi, Y. Lu, N. Martys, A.R. Sakulich, W.J. Weiss, Modeling of the influence of transverse cracking on chloride penetration into concrete, Cement and Concrete Composites, 38 (2013) 65-74.
[17] P.W. Atkins, J. De Paula, J. Keeler, Atkins' physical chemistry, Oxford university press2018.
[18] A. Fick, V. On liquid diffusion, The London, Edinburgh, and Dublin Philosophical Magazine and Journal of Science, 10 (1855) 30-39.
[19] T.U. Mohammed, T. Yamaji, H. Hamada, Chloride diffusion, microstructure, and mineralogy of concrete after 15 years of exposure in tidal environment, ACI Materials Journal, 99 (2002) 256-263.
[20] A. Guerrero, S. Goni, V. Allegro, Durability of class C fly ash belite cement in simulated sodium chloride radioactive liquid waste: Influence of temperature, Journal of hazardous materials, 162 (2009) 1099-1102.
[21] G. Glass, N. Buenfeld, The influence of chloride binding on the chloride induced corrosion risk in reinforced concrete, Corrosion Science, 42 (2000) 329-344.
[22] A. Neville, Chloride attack of reinforced concrete: an overview, Materials and structures, 28 (1995) 63.
[23] H. Justnes, A review of chloride binding in cementitious systems, NORDIC CONCRETE RESEARCH-PUBLICATIONS-, 21 (1998) 48-63.
[24] Q. Yuan, C. Shi, G. De Schutter, K. Audenaert, D. Deng, Chloride binding of cement-based materials subjected to external chloride environment–a review, Construction and building materials, 23 (2009) 1-13.
[25] T. Luping, L.-O. Nilsson, Chloride binding capacity and binding isotherms of OPC pastes and mortars, Cement and concrete research, 23 (1993) 247-253.
[26] C. Arya, N. Buenfeld, J. Newman, Factors influencing chloride-binding in concrete, Cement and Concrete research, 20 (1990) 291-300.
[27] U. Angst, B. Elsener, C.K. Larsen, Ø. Vennesland, Critical chloride content in reinforced concrete—a review, Cement and concrete research, 39 (2009) 1122-1138.
[28] V. Garcia, R. François, M. Carcasses, P. Gegout, Potential measurement to determine the chloride threshold concentration that initiates corrosion of reinforcing steel bar in slag concretes, Materials and structures, 47 (2014) 1483-1499.
[29] B.B. Hope, C.K. Nmai, Protection of Metals in Concrete Against Corrosion, American Concrete Institute (ACI) 222R-01, (2001).

[30] R.D. Recommendation, Draft recommendation for repair strategies for concrete structures damaged by reinforcement corrosion, Materials and Structures, 27 (1994) 415-436.
[31] W. Party, Non-structural cracks in concrete, Report of a Concrete Society Working Party (The Concrete Society, London, 1986) pp, (1992) 1-38.
[32] B. Šavija, Experimental and numerical investigation of chloride ingress in cracked concrete, TU Delft, (2014).
[33] S.M. Adiyastuti, Influence of cracks on chloride induced corrosion in reinforced concrete flexural members, University of New South Wales2005.
[34] S.Y. Jang, B.S. Kim, B.H. Oh, Effect of crack width on chloride diffusion coefficients of concrete by steady-state migration tests, Cement and Concrete Research, 41 (2011) 9-19.
[35] M. Sahmaran, Effect of flexure induced transverse crack and self-healing on chloride diffusivity of reinforced mortar, Journal of Materials Science, 42 (2007) 9131-9136.
[36] M. Ismail, A. Toumi, R. Francois, R. Gagne, Effect of crack opening on the local diffusion of chloride in cracked mortar samples, Cement and concrete research, 38 (2008) 1106-1111.
[37] S.-S. Park, S.-J. Kwon, S.H. Jung, Analysis technique for chloride penetration in cracked concrete using equivalent diffusion and permeation, Construction and Building Materials, 29 (2012) 183-192.
[38] M. Mahmaran, Yaman, Influence of transverse crack width on reinforcement corrosion initiation and propagation in mortar beams, Canadian Journal of Civil Engineering, 35 (2008) 236-245.
[39] A. Djerbi, Bonnet, A. Khelidj, V. Baroghel-Bouny, Influence of traversing crack on chloride diffusion into concrete, Cement and Concrete Research, 38 (2008) 877-883.
[40] J. Wang, S.V. Nanukuttan, P. Basheer, Y. Bai, Influence of micro and macro cracks due to sustained loading on chloride-induced corrosion of reinforced concrete beams, (2014).
[41] K. Audenaert, L. Marsavina, G. De Schutter, Influence of cracks on the service life of concrete structures in a marine environment, Key Engineering Materials, Trans Tech Publ, 2009, pp. 153-160.
[42] L. Marsavina, K. Audenaert, G. De Schutter, N. Faur, D. Marsavina, Experimental and numerical determination of the chloride penetration in cracked concrete, Construction and Building Materials, 23 (2009) 264-274.
[43] A. Konin, R. Francois, G. Arliguie, Penetration of chlorides in relation to the microcracking state into reinforced ordinary and high strength concrete, Materials and structures, 31 (1998) 310-316.
[44] S. Jacobsen, J. Marchand, L. Boisvert, Effect of cracking and healing on chloride transport in OPC concrete, Cement and Concrete Research, 26 (1996) 869-881.
[45] C. Lim, N. Gowripalan, V. Sirivivatnanon, Microcracking and chloride ion diffusion of concrete under sustained uniaxial compression, Special Publication, 221 (2004) 893-910.
[46] H. Wang, C. Lu, W. Jin, Y. Bai, Effect of external loads on chloride transport in concrete, Journal of materials in civil engineering, 23 (2011) 1043-1049.
[47] R. Francois, J. Maso, Effect of damage in reinforced concrete on carbonation or chloride penetration, Cement and Concrete Research, 18 (1988) 961-970.
[48] N. Gowripalan, V. Sirivivatnanon, C. Lim, Chloride diffusivity of concrete cracked in flexure, Cement and Concrete research, 30 (2000) 725-730.

[49] M. De Rooij, K. Van Tittelboom, N. De Belie, E. Schlangen, Self-healing phenomena in cement-Based materials: state-of-the-art report of RILEM technical committee 221-SHC: self-Healing phenomena in cement-Based materials, Springer2013.
[50] C. Edvardsen, Water permeability and autogenous healing of cracks in concrete, Materials Journal, 96 (1999) 448-454.
[51] T.U. Mohammed, N. Otsuki, H. Hamada, Corrosion of steel bars in cracked concrete under marine environment, Journal of materials in civil engineering, 15 (2003) 460-469.
[52] R. François, A. Castel, T. Vidal, N.-A. Vu, Long term corrosion behavior of reinforced concrete structures in chloride environnement, Journal de Physique IV (Proceedings), EDP sciences, 2006, pp. 285-293.
[53] M. Otieno, M. Alexander, H.-D. Beushausen, Corrosion in cracked and uncracked concrete-influence of crack width, concrete quality and crack reopening, Magazine of Concrete Research, 62 (2010) 393-404.
[54] I.S. Yoon, E. Schlangen, Long/short term experimental study on chloride penetration in cracked concrete, Key Engineering Materials, Trans Tech Publ, 2010, pp. 765-768.
[55] K.S. Tuutti, Corrosion of steel in concrete, (1982).
[56] R. Francois, G. Arliguie, Durability of loaded reinforced concrete in chloride environment, Special Publication, 145 (1994) 573-596.
[57] R. François, S. Laurens, F. Deby, Corrosion and Its Consequences for Reinforced Concrete Structures, Elsevier2018.
[58] P. Schieβl, M. Raupach, Laboratory studies and calculations on the influence of crack width on chloride-induced corrosion of steel in concrete, Materials Journal, 94 (1997) 56-61.
[59] Y.-s. Ji, W. Zhao, M. Zhou, H.-r. Ma, P. Zeng, Corrosion current distribution of macrocell and microcell of steel bar in concrete exposed to chloride environments, Construction and Building Materials, 47 (2013) 104-110.
[60] W. Zhang, L. Yu, R. François, Influence of top-casting-induced defects on the corrosion of the compressive reinforcement of naturally corroded beams under sustained loading, Construction and Building Materials, 229 (2019) 116912.
[61] S. Jaffer, C. Hansson, The influence of cracks on chloride-induced corrosion of steel in ordinary Portland cement and high performance concretes subjected to different loading conditions, Corrosion science, 50 (2008) 3343-3355.
[62] L. Yu, R. François, V.H. Dang, V. L'Hostis, R. Gagné, Development of chloride-induced corrosion in pre-cracked RC beams under sustained loading: Effect of load-induced cracks, concrete cover, and exposure conditions, Cement and Concrete Research, 67 (2015) 246-258.
[63] R. Francois, G. Arliguie, Reinforced concrete: correlation between cracking and corrosion, Special Publication, 126 (1991) 1221-1238.
[64] R. Zhang, A. Castel, R. François, The corrosion pattern of reinforcement and its influence on serviceability of reinforced concrete members in chloride environment, Cement and Concrete Research, 39 (2009) 1077-1086.
[65] T.U. Mohammed, N. Otsuki, M. Hisada, T. Shibata, Effect of Crack Width and Bar Types on Corrosionof Steel in Concrete, Journal of Materials in Civil Engineering, 13 (2001) 194-201.
[66] R. François, G. Arliguie, Effect of microcracking and cracking on the development of corrosion in reinforced concrete members, Magazine of Concrete Research, 51 (1999) 143-150.

[67] A. Beeby, Cracking, cover and corrosion of reinforcement, Transactions and Journal of British Ceramic Society, 81 (1982) 63-66.
[68] A. Castel, T. Vidal, R. François, G. Arliguie, Influence of steel-concrete interface quality on reinforcement corrosion induced by chlorides, Magazine of Concrete Research, 55 (2003) 151-159.
[69] U.M. Angst, M.R. Geiker, A. Michel, C. Gehlen, H. Wong, O.B. Isgor, B. Elsener, C.M. Hansson, R. François, K. Hornbostel, The steel-concrete interface, Materials and Structures, 50 (2017) 143.
[70] R. Zhang, A. Castel, R. François, Influence of steel-concrete interface defects owing to the top-bar effect on the chloride-induced corrosion of reinforcement, Magazine of Concrete Research, 63 (2011) 773-781.
[71] C. Arya, F. Ofori-Darko, Influence of crack frequency on reinforcement corrosion in concrete, Cement and Concrete Research, 26 (1996) 345-353.
[72] A. Poursaee, C.M. Hansson, The influence of longitudinal cracks on the corrosion protection afforded reinforcing steel in high performance concrete, Cement and Concrete Research, 38 (2008) 1098-1105.
[73] A. Scott, M. Alexander, The influence of binder type, cracking and cover on corrosion rates of steel in chloride-contaminated concrete, Magazine of Concrete Research, 59 (2007) 495-505.
[74] O. Vennesland, O. Gjoro, Effect of cracks in submerged concrete sea structures on steel corrosion, Materials Performance, 20 (1981) 49-51.
[75] O. Gautefall, O. Vennesland, Effects of cracks on the corrosion of embedded steel in silica-concrete compared to ordinary concrete, Nordic Concrete Research, 2 (1983) 17-28.
[76] P.K. Mehta, P.J. Monteiro, Concrete Microstructure, Properties and Materials, 2017.
[77] 姬永生, 司维, 宋萌, 袁迎曙, 颜於滕, 混凝土中钢筋锈蚀层发展和细观结构分析, 建筑结构学报, (2009) 303-308.
[78] A. Horne, I. Richardson, R. Brydson, Quantitative analysis of the microstructure of interfaces in steel reinforced concrete, Cement and Concrete Research, 37 (2007) 1613-1623.
[79] R.S. Raman, Characterisation of ‘rolled-in’,‘fragmented’and ‘red’scale formation during secondary processing of steels, Engineering Failure Analysis, 13 (2006) 1044-1050.
[80] A. Demoulin, C. Trigance, D. Neff, E. Foy, P. Dillmann, V. L’Hostis, The evolution of the corrosion of iron in hydraulic binders analysed from 46-and 260-year-old buildings, Corrosion Science, 52 (2010) 3168-3179.
[81] M.T. Walsh, A.A. Sagüés, Steel corrosion in submerged concrete structures—Part 1: field observations and corrosion distribution modeling, Corrosion, 72 (2016) 518-533.
[82] M. Stefanoni, U. Angst, B. Elsener, Local electrochemistry of reinforcement steel–distribution of open circuit and pitting potentials on steels with different surface condition, Corrosion Science, 98 (2015) 610-618.
[83] A. Poursaee, C. Hansson, Reinforcing steel passivation in mortar and pore solution, Cement and Concrete Research, 37 (2007) 1127-1133.
[84] P. Ghods, O. Isgor, G. McRae, G. Gu, Electrochemical investigation of chloride-induced depassivation of black steel rebar under simulated service conditions, Corrosion Science, 52 (2010) 1649-1659.
[85] S.A. El Haleem, S.A. El Wanees, E.A. El Aal, A. Diab, Environmental factors affecting the corrosion behavior of reinforcing steel II. Role of some anions in the initiation and inhibition of pitting corrosion of steel in Ca (OH) 2 solutions, Corrosion science, 52 (2010) 292-302.

[86] L. Li, A. Sagues, Chloride corrosion threshold of reinforcing steel in alkaline solutions—open-circuit immersion tests, Corrosion, 57 (2001) 19-28.
[87] J. Flis, H. Pickering, K. Osseo-Asare, Interpretation of impedance data for reinforcing steel in alkaline solution containing chlorides and acetates, Electrochimica Acta, 43 (1998) 1921-1929.
[88] A. Rossi, G. Puddu, B. Elsener, The surface of iron and Fe10Cr in alkaline media, Corrosion of reinforcement in concrete—mechanisms, monitoring, inhibitors and rehabilitation techniques, EFC Publication, (2007).
[89] Y.-M. Chen, M.E. Orazem, Impedance analysis of ASTM A416 tendon steel corrosion in alkaline simulated pore solutions, Corrosion Science, 104 (2016) 26-35.
[90] M. Sánchez, J. Gregori, C. Alonso, J. García-Jareño, H. Takenouti, F. Vicente, Electrochemical impedance spectroscopy for studying passive layers on steel rebars immersed in alkaline solutions simulating concrete pores, Electrochimica Acta, 52 (2007) 7634-7641.
[91] E. Volpi, A. Olietti, M. Stefanoni, S.P. Trasatti, Electrochemical characterization of mild steel in alkaline solutions simulating concrete environment, Journal of Electroanalytical Chemistry, 736 (2015) 38-46.
[92] J. Williamson, O.B. Isgor, The effect of simulated concrete pore solution composition and chlorides on the electronic properties of passive films on carbon steel rebar, Corrosion Science, 106 (2016) 82-95.
[93] A. Poursaee, Corrosion of steel bars in saturated Ca (OH) 2 and concrete pore solution, Concrete research letters, 1 (2010) 90-97.
[94] P. Ghods, O. Isgor, G. McRae, T. Miller, The effect of concrete pore solution composition on the quality of passive oxide films on black steel reinforcement, Cement and Concrete Composites, 31 (2009) 2-11.
[95] C. Hansson, A. Poursaee, A. Laurent, Macrocell and microcell corrosion of steel in ordinary Portland cement and high performance concretes, Cement and Concrete Research, 36 (2006) 2098-2102.
[96] S. Haupt, H. Strehblow, Corrosion, layer formation, and oxide reduction of passive iron in alkaline solution: a combined electrochemical and surface analytical study, Langmuir, 3 (1987) 873-885.
[97] P. Ghods, O. Isgor, J. Brown, F. Bensebaa, D. Kingston, XPS depth profiling study on the passive oxide film of carbon steel in saturated calcium hydroxide solution and the effect of chloride on the film properties, Applied Surface Science, 257 (2011) 4669-4677.
[98] M. Moreau, Contribution a l'etude d'adherence entre les constitiants hydrates du cement portland artificiel et l'armature enrobee REVUE DES MATERIAUX DE CONSTRUCTION ET DE TRAVAUX PUBLICS-CIMENTS BETONS, (1973).
[99] M. Al Khalaf, C. Page, Steel/mortar interfaces: microstructural features and mode of failure, Cement and Concrete Research, 9 (1979) 197-207.
[100] A. Bentur, S. Diamond, S. Mindess, The microstructure of the steel fibre-cement interface, Journal of Materials Science, 20 (1985) 3610-3620.
[101] P. Monteiro, O.E. Gjorv, P.K. Mehta, Microstructure of the steel-cement paste interface in the presence of chloride, Cement and Concrete Research, 15 (1985) 781-784.
[102] A. Suryavanshi, J. Scantlebury, S. Lyon, Corrosion of reinforcement steel embedded in high water-cement ratio concrete contaminated with chloride, Cement and Concrete Composites, 20 (1998) 263-281.

[103] A. Bentur, S. Diamond, S. Mindess, Cracking processes in steel fiber reinforced cement paste, Cement and Concrete Research, 15 (1985) 331-342.
[104] G. Glass, R. Yang, T. Dickhaus, N. Buenfeld, Backscattered electron imaging of the steel–concrete interface, Corrosion Science, 43 (2001) 605-610.
[105] R.C. Mielenz, V.E. Wolkodoff, J.E. Backstrom, H.L. Flack, Orgin, Evolution, and Effects of the Air Void System in Concrete. Part 1-Etrained Air in Unhardend Concrete, Journal Proceedings, 1958, pp. 95-121.
[106] M.R.A. SON, Degradation of concrete in cold weather conditions, Durability of Concrete and Cement Composites, (2007) 282.
[107] T.A. Söylev, R. Francois, Effects of bar-placement conditions on steel-concrete bond, Materials and structures, 39 (2006) 211-220.
[108] T.A. Soylev, R. François, Corrosion of reinforcement in relation to presence of defects at the interface between steel and concrete, Journal of materials in civil engineering, 17 (2005) 447-455.
[109] T.A. Soylev, R. François, Quality of steel-concrete interface and corrosion of reinforcing steel, Cement and Concrete Research, 33 (2003) 1407-1415.
[110] F. Chen, C.-Q. Li, H. Baji, B. Ma, Quantification of steel-concrete interface in reinforced concrete using Backscattered Electron imaging technique, Construction and Building Materials, 179 (2018) 420-429.
[111] T.U. Mohammed, N. Otsuki, H. Hamada, T. Yamaji, Chloride-induced corrosion of steel bars in concrete with presence of gap at steel-concrete interface, Materials Journal, 99 (2002) 149-156.
[112] U. Angst, Chloride induced reinforcement corrosion in concrete: Concept of critical chloride content–methods and mechanisms, (2011).
[113] K.Y. Ann, H.-W. Song, Chloride threshold level for corrosion of steel in concrete, Corrosion science, 49 (2007) 4113-4133.
[114] T.U. Mohammed, H. Hamada, T. Yamaji, Performance of seawater-mixed concrete in the tidal environment, Cement and concrete research, 34 (2004) 593-601.
[115] T.U. Mohammed, H. Hamada, T. Yamaji, Concrete after 30 years of exposure—Part II: chloride ingress and corrosion of steel bars, Materials Journal, 101 (2004) 13-18.
[116] T.U. Mohammed, H. Hamada, Corrosion of steel bars in concrete with various steel surface conditions, ACI Materials Journal, 103 (2006) 233.
[117] T. Vidal, A. Castel, R. François, Corrosion process and structural performance of a 17 year old reinforced concrete beam stored in chloride environment, Cement and Concrete Research, 37 (2007) 1551-1561.
[118] U.M. Angst, B. Elsener, C.K. Larsen, Ø. Vennesland, Chloride induced reinforcement corrosion: Electrochemical monitoring of initiation stage and chloride threshold values, Corrosion Science, 53 (2011) 1451-1464.
[119] I. Zafar, T. Sugiyama, Laboratory investigation to study the corrosion initiation of rebars in fly ash concrete, Magazine of Concrete Research, 66 (2014) 1051-1064.
[120] C. Alonso, C. Andrade, M. Castellote, P. Castro, Chloride threshold values to depassivate reinforcing bars embedded in a standardized OPC mortar, Cement and Concrete research, 30 (2000) 1047-1055.
[121] P. Sandberg, The Effect of Defects at the Steel-Concrete Interface, Exposure Regime, and Cement Type on Pitting Corrosion in Concrete, Lund University, Division of Building Materials, TVBM-3081, (1998).

[122] S.A. Nair, R.G. Pillai, Microstructural and corrosion characteristics of Quenched and Self-Tempered (QST) steel reinforcing bars, Construction and Building Materials, 231 (2020) 117109.
[123] U.M. Angst, M.R. Geiker, M.C. Alonso, R. Polder, O.B. Isgor, B. Elsener, H. Wong, A. Michel, K. Hornbostel, C. Gehlen, The effect of the steel–concrete interface on chloride-induced corrosion initiation in concrete: a critical review by RILEM TC 262-SCI, Materials and Structures, 52 (2019) 88.
[124] S. Nandi, N. Tewary, J. Saha, S. Ghosh, Microstructure, mechanical properties and corrosion performance of a few TMT rebars, Corrosion Engineering, Science and Technology, 51 (2016) 476-488.
[125] P. Sarkar, P. Kumar, M.K. Manna, P. Chakraborti, Microstructural influence on the electrochemical corrosion behaviour of dual-phase steels in 3.5% NaCl solution, Materials Letters, 59 (2005) 2488-2491.
[126] D. Trejo, R.G. Pillai, Accelerated chloride threshold testing: part I-ASTM A 615 and A 706 reinforcement, Materials Journal, 100 (2003) 519-527.
[127] D. Boubitsas, L. Tang, The influence of reinforcement steel surface condition on initiation of chloride induced corrosion, Materials and Structures, 48 (2015) 2641-2658.
[128] L. Mammoliti, L. Brown, C. Hansson, B. Hope, The influence of surface finish of reinforcing steel and pH of the test solution on the chloride threshold concentration for corrosion initiation in synthetic pore solutions, Cement and Concrete research, 26 (1996) 545-550.
[129] M. Qasem, Y. Yi, S. Al Hanaei, P. Cho, Electrochemical behavior of reinforcing steel for nuclear reactor containment buildings, IOSR J. Mech. Civil Eng., 13 (2016) 80-90.
[130] M.F. Hurley, J.R. Scully, Threshold chloride concentrations of selected corrosion-resistant rebar materials compared to carbon steel, Corrosion, 62 (2006) 892-904.
[131] B. Baroux, Further insights on the pitting corrosion of stainless steels, Corrosion mechanisms in theory and practice, (1995) 265-309.
[132] U. Angst, B. Elsener, Forecasting chloride-induced reinforcement corrosion in concrete–effect of realistic reinforcement steel surface conditions, 4th International Conference on Concrete Repair, Rehabilitation and Retrofitting (ICCRRR-4), Taylor & Francis Group, 2015, pp. 177-184.
[133] S. Chen, B. Cao, K. Ma, Effects of pH-value and chloride ion concentration on passivation behavior of steel rebar in different surface conditions, CORROSION AND PROTECTION, 35 (2014) 808-812.
[134] A. Al-Tayyib, M.S. Khan, I. Allam, A. Al-Mana, Corrosion behavior of pre-rusted rebars after placement in concrete, Cement and Concrete Research, 20 (1990) 955-960.
[135] V. Alar, G. Baršić, B. Runje, Ž. Alar, The influence of the surface finishing on the electrochemical behaviour of austenitic and superaustenitic steels, Materialwissenschaft und Werkstofftechnik, 43 (2012) 725-732.
[136] M. Manera, Ø. Vennesland, L. Bertolini, Chloride threshold for rebar corrosion in concrete with addition of silica fume, Corrosion Science, 50 (2008) 554-560.
[137] R.G. Pillai, D. Trejo, Surface condition effects on critical chloride threshold of steel reinforcement, ACI Materials Journal, 102 (2005) 103.
[138] M. Kosalla, M. Raupach, Chloride-Induced Depassivation of Steel in Concrete—Influence of Electrochemical Potential and Anodic Polarization Level, Service Life and Durability of Reinforced Concrete Structures, (2019) 107.

[139] C.B. Käthler, U.M. Angst, B. Elsener, Towards understanding corrosion initiation in concrete–influence of local concrete properties in the steel-concrete interfacial zone, MATEC Web of Conferences, EDP Sciences, 2018, pp. 04002.
[140] U.M. Angst, B. Elsener, The size effect in corrosion greatly influences the predicted life span of concrete infrastructures, Science advances, 3 (2017) e1700751.
[141] U. Angst, M. Wagner, B. Elsener, A. Leemann, P. van Nygaard, Schlussbericht ASTRA AGB 2012/010: Methode zur Bestimmung des kritischen Chloridgehalts an bestehenden Stahlbetonbauwerken, (2016).
[142] K. Ann, N. Buenfeld, The effect of calcium nitrite on the chloride-induced corrosion of steel in concrete, Magazine of Concrete Research, 59 (2007) 689-697.
[143] J.-G. Nam, W.H. Hartt, K. Kim, Effects of Air Void at the Steel-Concrete Interface on the Corrosion Initiation of Reinforcing Steel in Concrete under Chloride Exposure, Journal of the Korea Concrete Institute, 17 (2005) 829-834.
[144] T.A. Soylev, R. François, Quality of steel–concrete interface and corrosion of reinforcing steel, Cement and Concrete Research, 33 (2003) 1407-1415.
[145] G. Glass, B. Reddy, The influence of the steel concrete interface on the risk of chloride induced corrosion initiation, COST, 2002, pp. 227-232.
[146] B. Reddy, Influence of the steel-concrete interface on the chloride threshold level, University of London, 2001.
[147] G. Glass, B. Reddy, N. Buenfeld, R. Viles, Process for the protection of reinforcement in reinforced concrete, International Patent Publication No. WO, 1 (2001) A1.
[148] M.L. Allan, Probability of corrosion induced cracking in reinforced concrete, Cement and Concrete Research, 25 (1995) 1179-1190.
[149] T. Yonezawa, V. Ashworth, R. Procter, Pore solution composition and chloride effects on the corrosion of steel in concrete, Corrosion, 44 (1988) 489-499.
[150] G. Monfore, G.J. Verbeck, Corrosion of prestressed wire in concrete, Journal Proceedings, 1960, pp. 491-516.
[151] R.G. Pillai, R. Gettu, M. Santhanam, S. Rengaraju, Y. Dhandapani, S. Rathnarajan, A.S. Basavaraj, Service life and life cycle assessment of reinforced concrete systems with limestone calcined clay cement (LC3), Cement and Concrete Research, 118 (2019) 111-119.
[152] A.A. Ramezanianpour, Cement replacement materials, Springer, Berlin. doi, 10 (2014) 978-973.
[153] J. Ryou, K. Ann, Variation in the chloride threshold level for steel corrosion in concrete arising from different chloride sources, Magazine of Concrete Research, 60 (2008) 177-187.
[154] Y. Li, Y. Zhu, X. Zhu, Y. Ge, S. Laura, Chloride ion critical content in reinforced concrete, Journal of Wuhan University of Technology-Mater. Sci. Ed., 22 (2007) 737-740.
[155] B.H. Oh, S.Y. Jang, Experimental investigation on the threshold chloride concentration for corrosion initiation in reinforced concrete structures, (2005).
[156] W. Breit, Kritischer korrosionsauslösender Chloridgehalt–Untersuchungen an Mörtelelektroden in chloridhaltigen alkalischen Lösungen, Materials and Corrosion, 54 (2003) 430-439.
[157] M. Thomas, Chloride thresholds in marine concrete, Cement and concrete research, 26 (1996) 513-519.

[158] P. Schiessl, W. Breit, Local repair measures at concrete structures damaged by reinforcement corrosion-aspects of durability, SPECIAL PUBLICATION-ROYAL SOCIETY OF CHEMISTRY, 183 (1996) 525-534.
[159] K. Pettersson, Corrosion threshold value and corrosion rate in reinforced concrete, CBI REPORT 2: 92, (1992).
[160] C.M. Hansson, B. Sørensen, The threshold concentration of chloride in concrete for the initiation of reinforcement corrosion, Corrosion rates of steel in concrete, ASTM International1990.
[161] J. Shi, J. Ming, Influence of defects at the steel-mortar interface on the corrosion behavior of steel, Construction and Building Materials, 136 (2017) 118-125.
[162] U.M. Angst, C. Boschmann, M. Wagner, B. Elsener, Experimental protocol to determine the chloride threshold value for corrosion in samples taken from reinforced concrete structures, JoVE (Journal of Visualized Experiments), (2017) e56229.
[163] M. Kosalla, M. Raupach, Potential differences between passive reinforcement segments in concrete components in dependency of binder type, aeration conditions and quality of the steel/concrete‐interface, Materials and Corrosion, 67 (2016) 639-651.
[164] J. Harnisch, M. Raupach, Untersuchungen zum kritischen korrosionsauslösenden Chloridgehalt unter Berücksichtigung der Kontaktzone zwischen Stahl und Beton, Beton‐und Stahlbetonbau, 106 (2011) 299-307.
[165] T.U. Mohammed, H. Hamada, Corrosion of horizontal bars in concrete and method to delay early corrosion, Materials Journal, 103 (2006) 303-311.
[166] B. Lu, W. Li, J. Luo, S. Chiovelli, Pitting susceptibility of induction-quenched pipeline with microstructural heterogeneity, Journal of Materials Science, 47 (2012) 6823-6834.
[167] L.R. Bhagavathi, G. Chaudhari, S. Nath, Mechanical and corrosion behavior of plain low carbon dual-phase steels, Materials & Design, 32 (2011) 433-440.
[168] R. Markan, Steel Reinforcement for India, Relevance of Quenching & Tempering Technology, Steelworld, (2005) 4.
[169] J. Noville, TEMPCORE®, the most convenient process to produce low cost high strength rebars from 8 to 75 mm, Proceedings of the METEC and 2nd European Steel Technology and Application Days (ESTAD) Conference, Düsseldorf, Germany, 2015, pp. 15-19.
[170] D. Trejo, R.G. Pillai, Accelerated chloride threshold testing—Part II: Corrosion-resistant reinforcement, Materials Journal, 101 (2004) 57-64.
[171] L. Michel, U. Angst, Towards understanding corrosion initiation in concrete–Influence of local electrochemical properties of reinforcing steel, MATEC Web of Conferences, EDP Sciences, 2018, pp. 04001.
[172] E. Mahallati, M. Saremi, An assessment on the mill scale effects on the electrochemical characteristics of steel bars in concrete under DC-polarization, Cement and Concrete Research, 36 (2006) 1324-1329.
[173] F. YANG, Corrosion protection of steel embedded in new sustainable cementitious materials, Italy, 2018.
[174] S. Jaggi, B. Elsener, H. Bohni, Oxygen reduction on mild steel and stainless steel in alkaline solutions, European Federation of Corrosion Publications(UK), 31 (2000) 3-12.
[175] L. Li, A.A. Sagues, Metallurgical effects on chloride ion corrosion threshold of steel in concrete, University of South Florida, 2001.

[176] L. Bertolini, B. Elsener, P. Pedeferri, E. Redaelli, R. Polder, Corrosion of steel in concrete, Wiley Online Library2013.
[177] R.B. Figueira, A. Sadovski, A.P. Melo, E.V. Pereira, Chloride threshold value to initiate reinforcement corrosion in simulated concrete pore solutions: The influence of surface finishing and pH, Construction and Building Materials, 141 (2017) 183-200.
[178] P. Mangat, B. Molloy, Factors influencing chloride-induced corrosion of reinforcement in concrete, Materials and Structures, 25 (1992) 404-411.
[179] W. Breit, Critical corrosion inducing chloride content–State of the art and new investigation results, Betontechnische Berichte 1998-2000, (2001) 631-637.
[180] R.B. Polder, Critical chloride content for reinforced concrete and its relationship to concrete resistivity, Materials and corrosion, 60 (2009) 623-630.
[181] L. Yu, R. François, R. Gagné, Influence of steel-concrete interface defects induced by top-casting on development of chloride-induced corrosion in RC beams under sustained loading, Materials and Structures, 49 (2016) 5169-5181.
[182] R.M. Ghantous, S. Poyet, V. L'Hostis, N.-C. Tran, R. François, Effect of crack openings on carbonation-induced corrosion, Cement and Concrete Research, 95 (2017) 257-269.
[183] T.U. Mohammed, H. Hamada, T. Yamaji, Concrete After 30 Years of Exposure--Part I: Mineralogy, Microstructures, and Interfaces, ACI Materials Journal-American Concrete Institute, 101 (2004) 3-12.
[184] K. Hornbostel, U. Angst, B. Elsener, C. Larsen, M. Geiker, On the limitations of predicting the ohmic resistance in a macro-cell in mortar from bulk resistivity measurements, Cement and Concrete Research, 76 (2015) 147-158.
[185] R. François, G. Arliguie, Influence of service cracking on reinforcement steel corrosion, Journal of Materials in Civil Engineering, 10 (1998) 14-20.
[186] R. Zhang, A. Castel, R. François, Concrete cover cracking with reinforcement corrosion of RC beam during chloride-induced corrosion process, Cement and Concrete Research, 40 (2010) 415-425.
[187] W. Zhang, R. François, L. Yu, Influence of load-induced cracks coupled or not with top-casting-induced defects on the corrosion of the longitudinal tensile reinforcement of naturally corroded beams exposed to chloride environment under sustained loading, Cement and Concrete Research, 129 (2020) 105972.
[188] S.K. Goudar, B. Das, S. Arya, Microstructural Study of Steel-Concrete Interface and Its Influence on Bond Strength of Reinforced Concrete, Advances in Civil Engineering Materials, 8 (2019) 171-189.
[189] A. Alhozaimy, R.R. Hussain, R. Al-Zaid, A. Al Negheimish, Investigation of severe corrosion observed at intersection points of steel rebar mesh in reinforced concrete construction, Construction and Building Materials, 37 (2012) 67-81.
[190] M. Du, D. Niu, D. Zhang, Q. Li, Brief analysis of the factors affecting stirrup corrosion, SiChuang building science, 37 (2011) 96-98.
[191] O. Geng, Reinforcement corrosion and degradation rate of concrete members China railway publishing house2010.
[192] M. Wang, Research on galvanic corrosion mechanics of stirrups in concrete structure, Guangxi University 2008.

[193] L. Tong, Research on the damage of concrete and the influence for the longitudinal reinforcement corrosion by stirrup corrosion Structural Engineering, Xi'an University of Architecture and Technology, 2013.
[194] T.U. Mohammed, N. Otsuki, M. Hisada, Corrosion of steel bars with respect to orientation in concrete, ACI Materials Journal, 96 (1999) 154-159.
[195] T. MOHAMMED, A Study on Corrosion of Plain and Deformed Steel Bars with Respect to Bar Orientation and Cracks in Concrete, Doctoral Thesis, Department of Civil Engineering, Tokyo Institute of Technology, (1997).
[196] R. Francois, A. Castel, Influences of bending crack and water-cement ratio on chloride-induced corrosion of main reinforcing bars and stirrups. Discussion and Closure, ACI Materials Journal, 98 (2001).

III. Experimental program

1 Introduction

The research in this thesis concerns three experimental programs, which were started in 2010, 2013 and 2017, respectively. In the following sections, some details of the two experimental programs are presented.

2 Experimental program started in 2010

In order to study the effect of exposure conditions on the corrosion process, a set of reinforced concrete beams were cast in 2010 by Dang.

2.1 Specimens

Twelve reinforced concrete beams were cast in this program, six beam of type As and six beams of type Bs. All the beams have a dimension of 3000×280×150 mm.

2.2 Configurations

The casting direction of all the beams was the same as the exposure condition. For As beam, tensile bars were cast on bottom. For type B beams, compressive bars were cast on top (Figure III-1).

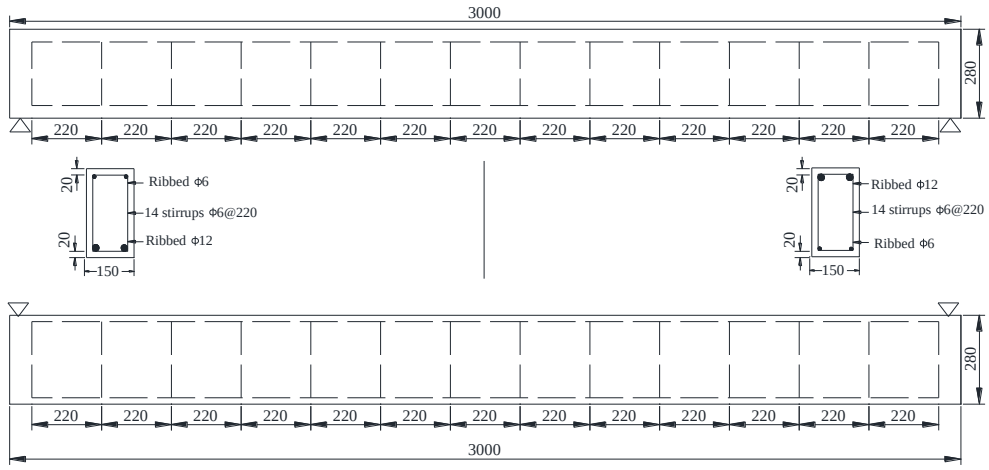

Figure III-1 Dimension of beam cast in 2010 (mm)

2.3 Materials

Table III-1 and Table III-2 provide the chemical composition of cement and concrete composition, respectively. The water/cement ratio was finely adjusted to obtain a slump of 70 mm.

According to the compression tests on the cylindrical specimens, the average compressive strength of the concrete was 45 MPa. The elastic modulus was 32GPa. The tensile strength was 4.7 MPa, which was tested by splitting test on the cylindrical specimens. The porosity was about 15.2%.

Table III-1 Cement composition

	SiO_2	Al_2O_3	Fe_2O_3	CaO	MgO	SO_3	Na_2O
Weight	21.4	6.0	2.3	63.0	1.4	3.0	0.5

Table III-2 Concrete proportioning

Mix composition		
Rolled gravel (silica+limestone)	5-15 mm	1109 kg/m^3
Sand	0-5 mm	745 kg/m^3
Portland cement OPC (high performance)		364 kg/m^3
Water		182 kg/m^3

2.4 Loading system

A three-point system was applied to the beams according to coupling a beam of As and a beam of Bs together. The loading system consisted of two steel brackets, two threaded rods and four nuts as presented in Figure III-2. Loading was applied by tightening the nuts on the threaded rods indicated in Figure III-2. There were two strain gauges on each threaded rod, which were used to calculated the applied load.

Two levels of the load were applied: the moment at the mid-span of the beams was 13.5 kN •m which corresponded to the maximum load versus durability in an aggressive environment for the beams in As and the maximum load versus resistance for the beams in Bs according to the former French code (B.A.E.L., 1983, French regulations for reinforced concrete structures). The load was marked as level 1 and the beams under level 1 were named A1 and B1 respectively; the moment at the mid-span was 21.2 kN •m which corresponded to the maximum load versus resistance for the beam in As and 80% of the failure load and equal to twice the design service load in aggressive environment. The beams loaded in level 2 were named A2 and B2 respectively.

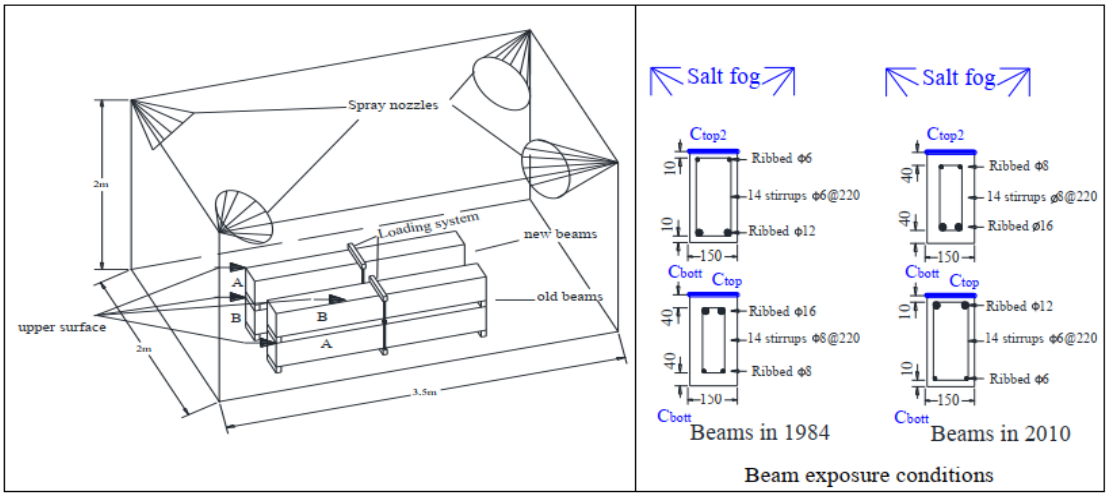

Figure III-2 Location of the beams cast in 1984 and 2010

2.5 Exposure environment

After being loaded together, the beams were exposed in a chloride environment (Figure III-2). From 2010 to 2019, the exposure condition is always wetting and drying cycles. Each cycle contains two days of wetting followed by two weeks of drying. During the wetting period, a salt fog (35 g/L of NaCl, equivalent to the salt concentration of seawater) was generated by four spray nozzles located at each upper corner of the chloride chamber. The door of the chloride chamber is opened during the drying period, the temperature is the same as the natural outdoor environment of southwest France, with monthly average temperatures ranging from 5.1℃ to 21.3℃.

3 Experimental program started in 2013

In order to study the impact of top-casting defects on corrosion process, four reinforced concrete beams with the same concrete cover depth were cast in 2013 by Linwen Yu. These beams were named type C beams.

3.1 Specimens

In order to simulate the reinforced concrete elements applied in the construction industry, the dimension of all the beams in this program was 3000×280×150 mm.

3.2 Configurations

Each beam was reinforced with two 12 mm bars deformed in tension with a cover of 26 mm

and two 6 mm bars deformed in compression also with a cover of 26 mm. The stirrups had a diameter of 6 mm and the space between two stirrups was 220 mm (

Figure III-3).

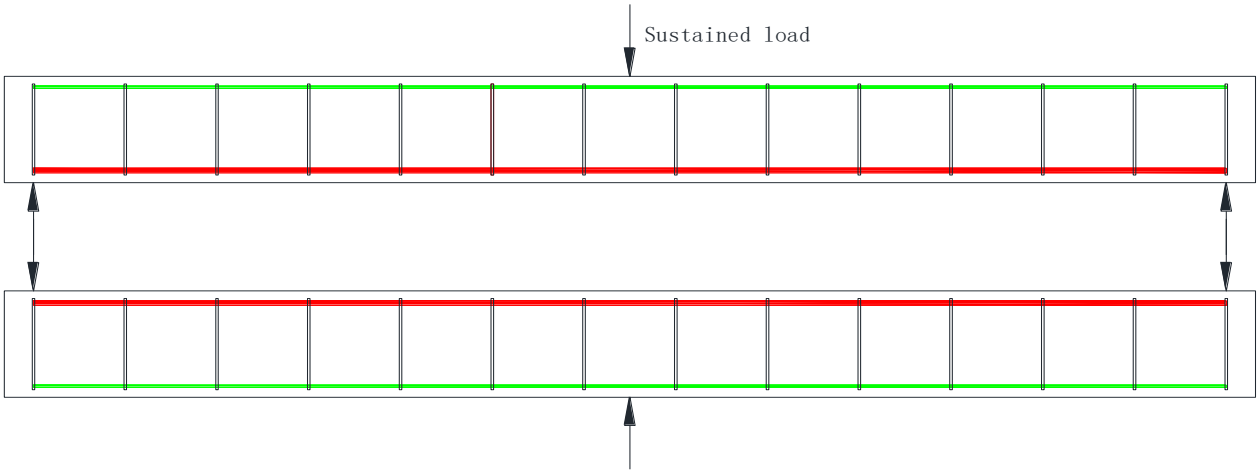

Figure III-3 Dimension type of C beams cast in 2013 (all dimension in mm)

3.3 Materials

Table III-3 and Table III-4 provide the chemical composition of cement and concrete composition, respectively. The water/cement ratio was finely adjusted to obtain a slump of 70 mm.

According to the compression tests on the cylindrical specimens, the average compressive strength of the concrete was 45 MPa. The elastic modulus was 32GPa. The tensile strength was 4.7 MPa, which was tested by splitting test on the cylindrical specimens. The porosity was about 15.2%.

Table III-3 Cement composition

	SiO_2	Al_2O_3	Fe_2O_3	CaO	MgO	SO_3	Na_2O
Weight	21.4	6.0	2.3	63.0	1.4	3.0	0.5

Table III-4 Concrete proportioning

Mix composition		
Rolled gravel (silica+limestone)	5-15 mm	1109 kg/m^3
Sand	0-5 mm	745 kg/m^3
Portland cement OPC (high performance)		364 kg/m^3
Water		182 kg/m^3

3.4 Casting directions

The four beams were divided into two groups beam C1 and beam C2 were in Group 1 while

beam C3 and beam C4 were in Group 2. The casting direction is presented in Figure III-4. Compressive bars were cast on top in Group 1 while tensile bars were cast on top in Group 2.

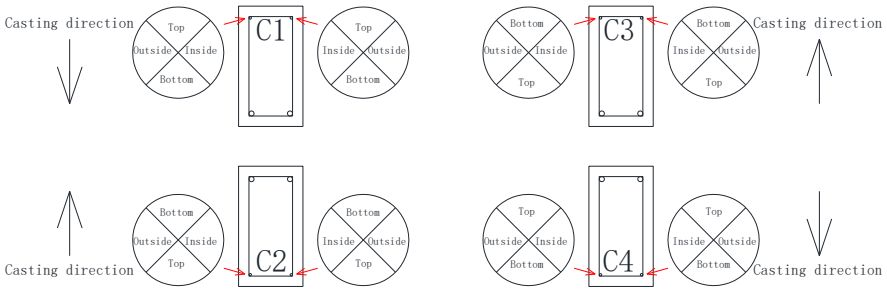

Figure III-4 Casting direction and location of the beams

3.5 Loading system

The bending moment applied on Group 1 was M_{ser1}=21.2 kN•m (corresponding to a point load of 30 kN) and that on Group 2 was M_{ser2}=14.1 kN•m (corresponding to a point load of 20 kN). M_{ser1} corresponds to about 80% of the failure load and was chosen to obtain crack width largely higher that is required by EuroCode 2. Ms_{er2} corresponds to about 50% of the failure load and matches the Ultimate Limit State design in a non-aggressive environment according to EuroCode 2.

3.6 Exposure environment

After being loaded together, the beams were exposed in a chloride environment (Figure III-5). From 2013 to 2017, the exposure condition is always wetting and drying cycles. Each cycle contains two days of wetting followed by two weeks of drying. During the wetting period, a salt fog (35 g/L of NaCl, equivalent to the salt concentration of seawater) was generated by four spray nozzles located at each upper corner of the chloride chamber. The door of the chloride chamber is opened during the drying period, the temperature is the same as the natural outdoor environment of southwest France, with monthly average temperatures ranging from 5.1℃ to 21.3℃.

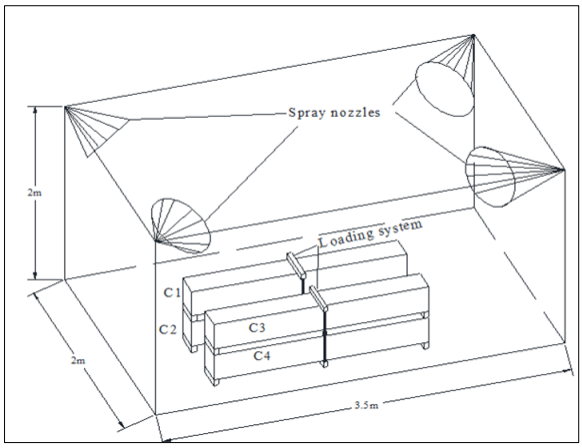

Figure III-5 Loading system and exposure conditions

4 Experimental program started in 2017

In order to study the impact of top-casting defects on corrosion initiation of reinforced concrete, six reinforced concrete blocks with the same concrete cover depth were cast in 2017. These beams were named type G blocks.

4.1 Specimens

The dimension of all the concrete blocks in this program was 280×210×150 mm.

4.2 Configuration

For all six reinforced concrete blocks, the layout of steel frames consists of five main bars with 12 mm in diameter, four of main bars were fixed at the corner of stirrups which had a diameter of 6 mm and one placed at the center acting as a reference bar for galvanic current testing. The end of main bars solders a wire to measure the galvanic current between reference bars and main bars.

The six concrete blocks were divided into two groups, G1-1, G1-2 and G1-3 were in the group of G1, while G2-1, G2-2 and G2-3 were in the group of G2. For the whole G1 and G2 reinforced concretes, each corner of stirrups was covered by insulating material to exclude the effect of stirrups on the corrosion of main bars. For G1-1, G1-2 and G1-3, an artificial crack with 1 mm in width and 27 mm in depth was set by a substantial plastic sheet at the location of midcourt line of the top surface of each concrete specimen. However, no artificial crack was made at the same location of G2-1, G2-2 and G2-3. The configuration is provided in Figure III-6.

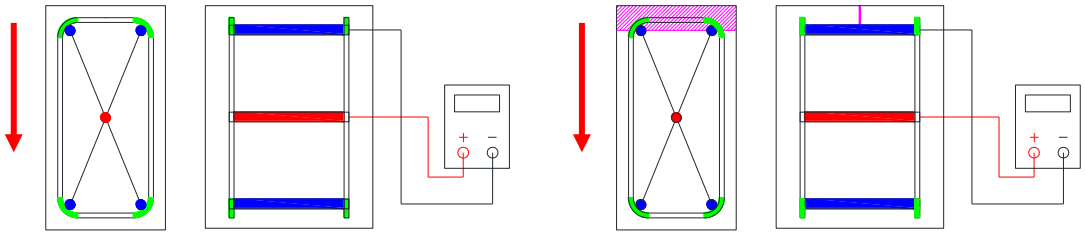

Figure III-6 Configuration of G1 and G2

(The green zone means the insulating material; the blue bars correspond to the four deformed bars fixed at the corner of stirrup; the red bar denotes the reference bar; the amaranth zone represents the area of artificial crack; the red arrow meant the casting direction)

4.3 Materials

The compositions of cement and concrete were also the same as that used in the C beams. It is presented in Table III-3 and Table III-4, respectively. The water/cement ratio was finely adjusted to obtain a slump of 70 mm. The average compressive strength of G1 and G2(tested on 110×220 mm cylindrical specimens) was 45 MPa at 28 days and the elastic modulus was 32 GPa and the tensile strength was 4.7 MPa.

4.4 Casting direction

The casting direction was described in Figure III-6. It should be noted that, before casting, all the steel frames of G1 and G2 were set in a same long mold and the casting work was conducted once at for all.

4.5 Exposure environment

The exposure environment in this program is completely the same as that in the program started in 2013. However, it should be noted that a new system of wetting-drying cycle was conducted. For the new system, each cycle contains two days of wetting followed by five days of drying.

IV. Corrosion behavior of reinforcing steel in concrete with top-casting-induced defects and cracks under chloride environment

1 Introduction

This chapter mainly discusses the corrosion behavior of steel in concrete in different corrosion period under chloride environment. It is well known that the corrosion process of steel in concrete can be divided into two periods corrosion initiation and corrosion propagation. According to the published results, it can be found that the cracks and top-casting defects strongly impact the corrosion behavior of steel in concrete.

Generally, cracking is an inherent characteristic of concrete elements. As mentioned above in chapter 2, cracking of concrete occurs due to shrinkage, creep, freeze/thaw cycles, external loads and so on. Now, a large amount of published results has confirmed that cracking accelerates the corrosion initiation, for cracking provides aggressive agents, such as chloride, CO_2 and water, with some easy paths to penetrate to the level of steel. Whether the corrosion propagation period is affected by cracks, however, is still under debate. Some researchers consider that cracks accelerate chloride-induced corrosion by increasing the concrete penetrability, and that corrosion rate also increases with increased crack width. Others hold the view that cracks have no impact on long-term corrosion propagation, the corrosion rate gradually diminished with the increase of exposure time.

Similar to the cracking, the interfacial defects of steel-concrete are also inevitable in reinforced concrete structures. Normally, the interfacial defects of steel-concrete, including air voids and bleed water voids formed due to the bleeding, segregation and settlement of fresh concrete under the horizontal steel bars, have a higher porosity and looser structure. These defects, which increase with increasing depth of concrete under the horizontal bars, not only alter the microenvironment around the steel bars, but facilitate the migration of the aggressive agents along the reinforcing steel as well.

In the past decade, some investigations found that the interfacial defects of steel-concrete are the key factor to control the corrosion initiation of steel in concrete. However, the issue concerning the initial point of pitting corrosion is still under debate. The interface of steel-concrete consists of reinforcing steel and concrete. From the concrete part, some published research considered that the location of corrosion initiation was related to the location interfacial voids. Others reported that the corrosion initiation is correlation with the interfacial saturated of steel-concrete. From the steel part, some investigations indicated that the rebar geometry is the key factor to impact the steel corrosion initiation. While others consider that microstructure of steel surface mainly control to the occurrence

of corrosion initiation. Moreover, the effect of top-casting defects in steel-concrete interface on the corrosion propagation of steel in concrete is still not clear. Apart from the corrosion of main reinforcing steels, the corrosion behavior of stirrups is also an important issue. Recently, most of published literatures focus on the shear capacity of stirrups used in reinforced concrete structures, however, it is received little research attention in terms of the corrosion of stirrups. According to the fundamental of different metal contacting corrosion, stirrups, act as the anode, are sacrificed to protect the main steel rebars. However, other researchers consider that stirrups do not protect the main steels, but accelerate its corrosion process. Stirrup is an important part in the reinforced concrete buildings; therefore, it is necessary to understand the corrosion behavior of stirrups used in reinforced concrete elements.

In practice, it is inevitable that cracks and top-casting-induced defects should be present simultaneously in reinforced concrete. Thus, based on the fact, three objectives of this thesis are proposed in the section 4 of chapter Ⅰ.

For the first objective, the corrosion behavior of steel in concrete with top-casting defects and transverse crack in corrosion initiation, is present in section 2. In the experimental program, two groups of reinforced concrete blocks, labelled Group A and Group B were prepared. Three samples were cast for each group. In the case of Group B, an artificial crack with a width of 1 mm and a depth of 27 mm was made in the middle location of the top surface in each sample. There was no artificial crack in the samples of Group A. The size of these concrete blocks is 210×150×280 mm. The concrete cover depths of the stirrups and the main bars were 16 mm and 21 mm, respectively. Insulating thermoplastic pipes were coated on the stirrups contacting the four main bars so as to prevent electrical connections among the main bars. Another deformed steel bar was fixed in the center of the steel framework with fishing line regarded as a metallic coupon.to measure the corrosion current between each main bar and the central bar All the samples stored in a cyclic chloride environment to accelerate the corrosion rate.

In this work, the microstructures of the steel-concrete interface, the cement hydration products at the steel-concrete interface, chloride penetration along the interface, the chloride profiles, the galvanic corrosion current, and the distribution of pitting corrosion on steel rebar were studied and compared. The effect of top-casting defects and/or artificial crack on the corrosion behavior of steel

in concrete was discussed. The relationship between corrosion initiation and steel geometry and location of voids was analyzed and compared. More details about the experiment and the results are presented in section 2 of this chapter.

In the case of the second objective, the impact of top-casting defects and/or load-induced cracks on the corrosion development and corrosion behavior of corroded reinforced concrete in corrosion propagation, it was answered in Section 3 and Section 4, respectively. In the experimental program, four 3000×280×150 mm reinforced concrete beams were cast. The concrete cover depth is 20 mm and the height of the beams is 280 mm. Some top-casting defects are expected to form under the top bars. In order to investigate the effect of top-casting defects on corrosion development, the four beams were cast in different directions with respect to their exposure directions. They were corroded in a chloride environment under sustained loading. Cracking maps were recorded at different stages during the corrosion process. Chloride profiles, loss of cross-section and corrosion maps of different main bars were measured after the ending of exposure.

In this experiment, as tensile zone and compressive zone of these four beams are subject different corrosion conditions due to the different loading and exposure conditions, they are discussed in separate groups, respectively.

In the case of tensile zone, the effect of service crack on the corrosion of tensile bars, the effect of top-casting defects on the evolution of corrosion-induced cracking in tensile zone and the cross-sectional loss of tensile bar, and the corrosion propagation around the perimeter of the tensile bars were discussed. More details about the experiment and results of tensile bar are presented in section 3 of this chapter.

For the compressive zone, the effect of top-casting defects on the corrosion-induced cracking and cross-sectional loss of compressive bars, the effect of casting direction and exposure condition on chloride ingress and the relationship between pitting corrosion and corrosion-induced cracks were discussed. More details about the experiment and results of tensile bar are presented in section 4 of this chapter.

For the third object, the corrosion behavior of stirrups in reinforced concrete beams exposed for 9 years, it was answered in Section 5. In the experimental program, two 3000×280×150 mm reinforced concrete beams were cast in 2010. The concrete cover depth is 40 mm and the height of

the beams is 280 mm. They were corroded in a chloride environment under sustained loading. Cracking maps were recorded at different stages during the corrosion process. Loss of cross-section and corrosion maps of stirrups were measured after the ending of exposure.

In this section, the corrosion behavior of horizontal legs and vertical legs of stirrups were analyzed and compared, the relationship between stirrups and main reinforcing steels were discussed.

The macroscopic experimental part of these studies mentioned above, including the preparation of samples, the chloride profiles, the corrosion current, and the loss of cross-section of steel bars and stirrups were prepared and measured in Laboratoire Matériaux et Durabilité des Constructions in France. While the microscopic experimental part, e.g. BSE and Nanoindentation test, and the chloride penetration test were achieved in Chongqing University in China. The three investigations were described in four papers. The section 5 is paper in preparation. The section 2, section 3 and section 4 are three articles published in journal Cement and Concrete Research and Constructions and Building Materials, respectively.

2 Influence of artificial cracks and interfacial defects on the corrosion behavior of steel in concrete during corrosion initiation under a chloride environment

2.1 Abstract

In this study, the effect of both artificial cracks and defects of the steel-concrete interface on the initiation and propagation of steel reinforcement corrosion in concrete under a chloride environment is investigated. This work was based on two groups of reinforced concrete blocks, with or without artificial cracks. The microstructures of the steel-concrete interface, the cement hydration products at the steel-concrete interface, chloride penetration along the interface, the chloride profiles, the galvanic corrosion current, and the distribution of pitting corrosion on steel rebar were studied and compared. Experimental results show that the location of initial corrosion is related to top-casting defects but not to the location of air bubbles. Pitting corrosion mainly initiated at the rib foot of the bottom side of the deformed steel rebar with top-casting defects. Steel in concrete with an artificial crack exhibited a fast initiation period immediately followed by a propagation period. The presence of both artificial crack and top-bar effect thus led to faster deterioration than in un-cracked structures.

Key words Corrosion; Chloride; Top-casting defects; Crack; Interface; Reinforced concrete

2.2 Introduction

The deterioration of reinforced concrete structures caused by chloride-induced corrosion is a major threat to their service life. Severe chloride-induced corrosion of steel in concrete results in a loss of cross-section of the steel reinforcement and cracking or even spalling of the concrete cover [1]. Generally, the corrosion process of steel in concrete is divided into two phases [2] an initiation phase and a propagation phase. Some factors, such as cement type, water to binder ratio, load-induced cracks, the steel-concrete interface, and the surface conditions of the steel reinforcement, affect the corrosion initiation of steel in concrete [3].

Cracking, an inherent characteristic of concrete elements, which occurs due to shrinkage, creep, freeze/thaw cycles, external loads, and so on [4], is considered as one of the most common types of damage in reinforced concrete structures. Previous studies have confirmed that cracks accelerate the

initiation of corrosion by creating preferential pathways for aggressive agents (CO_2, chlorides and water) to reach the surface of the steel bars[5-10]. Whether the corrosion propagation period is affected by cracks, however, is still under debate. Some researchers [11-14] consider that cracks accelerate chloride-induced corrosion by increasing the concrete penetrability, and that corrosion rate also increases with increased crack width. Others [6, 15-17] hold the view that cracks have no impact on long-term corrosion propagation. François and Arliguie [16-18] investigated the corrosion behaviors of reinforced concrete in a chloride environment in the long term and found that, after corrosion initiation, the corrosion rate clearly decreased with time. Ghantous et al. [19] studied the effect of crack openings on carbonation-induced corrosion of steel in mortar. Similarly, they found that, after the initiation phase, the corrosion rate decreased with time and the free corrosion potential increased independently of the crack opening. Zhang et al[20] studied the corrosion behavior of reinforced concrete beam with load-induced cracks and reported that the corrosion of steel was not related to the cracks in corrosion propagation. Shi et al.[21] compared the chloride-induced corrosion behavior of steel in large concrete samples with or without sustained flexural loading. They reported that, in the first 15 days, steel reinforcements in loaded concrete exhibited a higher corrosion rate than those in unloaded concrete. However, a similar corrosion rate was found after 60 days of accelerate corrosion. One possible interpretation of the above results is that corrosion products sealed the cracks and prevented penetration of the aggressive species [21, 22]. Michel et al. [23] found no clear relationship between the corrosion rate of steel bars and the surface width of concrete cracks. They considered that steel corrosion behavior was related to the quality of the steel-concrete interface while the surface crack width could not describe the steel-concrete interface quality reliably.

Generally, the steel-concrete interface mainly consists of mill scale, passive layer, pre-existing rust layer, interfacial defects and cement hydration products [24]. When the height of concrete under horizontal steel bars is greater than 15 cm [25-27], some top-casting-induced defects form at the bottom side of the rebar as a result of floating air bubbles and bleeding, segregation and settlement of fresh concrete [28, 29]. A top-casting-induced defect is mainly characterized as a more porous zone containing larger crystals of portlandite and ettringite [30-33]. It results in remarkably different micro-environments between the top and the bottom part of the steel-concrete interface. Therefore,

top-casting-induced defects not only facilitate the transportation of aggressive species but also accelerate the corrosion of reinforcing steel in concrete [34, 35].

As far as corrosion initiation of steel in concrete or mortar is concerned, most of the published research [3, 6, 16, 25-28, 35-41] has confirmed that corrosion preferentially initiates on the side of the steel reinforcement facing the top-casting defects. However, the issue concerning the initial point of pitting corrosion is still under debate. Some researchers [40, 42] consider that corrosion starts preferentially in the voids at the steel-concrete interface. Zafar and Sugiyama [43] reported that the initial point of corrosion was related to the steel geometry. The corrosion of deformed rebar always began at the location of ribs, while, for smooth steel rebar, corrosion mainly occurred at the position of voids. Angst et al. [3, 41, 44] considered that the corrosion location was related to the local saturated condition of interfacial voids but did not always occur near the voids. Paul et al[45, 46] reported that pitting corrosion initiated at the location of bending cracks.

In practice, it is inevitable that cracks and top-casting-induced defects should be present simultaneously in reinforced concrete. The objective of this investigation is to study the corrosion behavior of steel reinforcements in concrete samples with top-casting-induced defects and artificial cracks that are simultaneously exposed to a chloride environment. Firstly, the interfacial characteristics of steel-concrete are analyzed. Secondly, the penetration of chloride ions into the steel-concrete interface is investigated. Finally, the corrosion rate and the corrosion distribution of steel in concrete are determined.

2.3 Experimental program

2.3.1 Reinforced concrete specimens

Two groups of reinforced concrete blocks, labeled Group A and Group B, were prepared. All the A and B reinforced concrete blocks had dimensions of 210×150×280 mm.

As presented in Figure IV-1, each concrete block contained a steel framework consisting of two stirrups with a diameter of 6 mm and four main deformed bars with 12 mm in diameter and 160 mm in length. The concrete cover depths of the stirrups and the main bars were 16 mm and 21 mm, respectively. Insulating thermoplastic pipes (yellow zones in Figure 1) were coated on the stirrups contacting the four main bars so as to prevent electrical connections among the main bars. Another

deformed steel bar (the red bar in Figure 1), 160 mm in length, was fixed in the center of the steel framework with fishing line. The central bar (metallic coupon) had a concrete cover depth of about 69 mm with respect to the lateral surfaces. It could be considered to be in a passive state at all times due to the high concrete cover depth. So, the current between each main bar and the central bar could be used to define the corrosion rate of the main bars. Electrical wires were soldered onto the four main bars and the central bar so as to measure the corrosion current.

Three samples were cast for each group. In the case of Group B, an artificial crack with a width of 1 mm and a depth of 27 mm was made. It should be noted that some published investigation[6, 16, 20, 47] reported that the crack width more than 0.5mm does not affect the corrosion propagation, therefore, a width of 1mm was selected for the artificial crack. For the setting of artificial crack, a shim was fixed at the middle location of the steel framework before casting concrete and was removed after initial setting of concrete. There was no artificial crack in the samples of Group A.

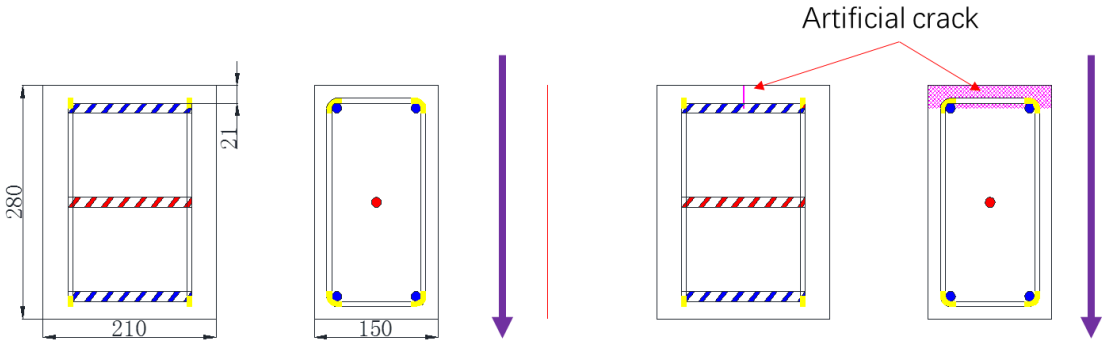

(a) Reinforced concrete block of group A (b) Reinforced concrete block of group B

Figure IV-1 Layout of reinforced concrete blocks A and B

(*The blue bars indicate the main deformed rebars; the red bar corresponds to the metallic coupon; the yellow zone at each corner of the stirrups represents the insulating thermoplastic pipes; the purple arrows indicate the casting direction*)

2.3.2 Materials

Cement (CEM Ⅰ, Grade 52.5 R) with a density of 3.15 g/cm^3 and Blaine specific surface area of 415 m^2/kg, manufactured by the Lafarge Cement Group, was used to prepare the concrete in this study. The chemical composition is given in Table IV-1.

Table IV-1 Cement chemical composition (%)

	SiO_2	Al_2O_3	Fe_2O_3	CaO	MgO	SO_3	Na_2O
Weight	21.4	6.0	2.3	63.0	1.4	3.0	0.5

The concrete mixture proportions are given in Table IV-2, which maintains the consistent of

concrete properties with author's previous research[6, 20, 35, 37]. The slump of the concrete was 70 mm. Its average compressive strength at 28 days (tested on 110×220 mm cylindrical specimens) was 45 MPa. The elastic modulus was 32 GPa and the tensile strength, tested by splitting test on the cylindrical specimens, was 4.7 MPa. The porosity was about 15.2%.

Table IV-2 Concrete mix proportions

Rolled gravel (silica+limestone)	5-15 mm	746.1 kg/m^3
Sand	0-5 mm	895.3 kg/m^3
Portland cement OPC (high performance)		436 kg/m^3
Water		218 kg/m^3

2.3.3 Casting and curing of reinforced concrete beams

In order to maintain consistency with the concrete properties used in previous research[20, 35, 37],when these reinforced concrete blocks were cast, the fresh concrete was placed in the formwork in two layers, each approximately half of the height of the mold. An internal vibrator was used to compact the concrete.

The casting direction of reinforced concrete blocks A and B is shown in Figure IV-1. After casting, all the reinforced concrete blocks were covered with a plastic sheet in order to avoid any shrinkage cracking. The specimens were demolded after 24 h and then cured in a standard curing room with a temperature of (20±2) °C and relative humidity of higher than 95%.

2.3.4 Exposure conditions

After 28 days of curing, all the reinforced concrete blocks were immediately exposed to an aggressive chloride environment. The top-cast surface of the blocks was the upper exposure surface. The aggressive environment was a salt fog (35 g/L of NaCl corresponding to the chloride concentration of sea water), which was generated by four spray nozzles located one at each upper corner of a sealed chamber, the details of which can be found in [6]. The exposure environment condition was wetting/drying cycles with two days of spraying followed by five days of drying. The drying temperature was the ambient temperature of southwest France, with a monthly average ranging from 5.1 °C to 21.3 °C, and the monthly average value of relative humidity varied from 50% to 84%.

2.3.5 Measurement of galvanic corrosion current

In this work, a measurement from ASTM G71 was introduced[48]. The galvanic corrosion current, which was generated by the corrosion potential decrease between top-casting bar and the coupon due to corrosion took place on the top-casting bar, was measured weekly, on the first day of the drying period, by a multimeter with an accuracy of 0.01 μA.

For the galvanic current measurements, the metallic coupon was connected to the positive pole of the multimeter, while the main bar was connected to the negative pole. If corrosion took place on the main steel bar, a galvanic current could be measured due to the potential decrease of the main bar.

2.3.6 Chloride measurement

In case of the chloride profiles, according to the results of galvanic corrosion current, after 28 wetting-drying cycles, concrete cores 25 mm in diameter and 47 mm in depth were taken from the casting surface to prepare powder samples for chloride concentration testing. In order to exclude the effect of artificial cracks on the chloride penetration, the concrete core was located mid way between the artificial crack and one end of the concrete block (Figure IV-2). Chloride ions were extracted with nitric acid at 80 °C and the chloride contents were determined by potentiometric titration with $AgNO_3$. The chloride profiles were plotted to a depth of 47 mm. In this study, the total chloride content per unit weight of cement was calculated from the content measured per weight of concrete, using the cement proportion in the concrete mix.

For the chloride contents in steel-concrete interface, the measurement was carried out by EDS test in SEM. The chloride content in interface was quantified by the way of [Cl]/[Ca] ratio proposed by. Richardson et al[49]. In order to ensure the accuracy of chloride content, in the same zone observed by SEM, for A-1 sample, 87 and 83 small measured areas were selected randomly in bottom interface and top interface, respectively, and for B-1, 88 and 80 small areas were measured, respectively. The detail information for the treatment of samples was described in section 2.7.

2.3.7 Microstructure of the steel-concrete interface

After the concrete cores for chloride profile testing had been taken, one prism containing a top-

cast bar was obtained from the front side of samples A-1 and B-1 (Figure IV-2). Each prism was cut along the back dashed line (in vertical view figure) and was divided into three parts. For part 1, they were split along the length of steel rebar (blue dashed line in front view figure) to obtain the top and bottom interface of top-casting bar to characterized the distribution of air bubbles in steel-concrete interface. The reinforced concrete samples of part 2 were transversely cut and used to observe the distribution of top-casting defects surrounding the perimeter of steel by the backscattered electron (BSE) imaging test. For part 3, they were split along the blue dashed line to obtain the top and bottom interface of top-cast bar for the scanning electron microscope (SEM) and energy dispersive spectrometer (EDS) measurements to observe the morphology of cement hydration products and chemical elements in the steel-concrete interface, respectively.

For samples of part 2 and part 3, firstly, samples were cut to size and dried to constant weight in a vacuum oven at 60 °C. In the case of the BSE test, these samples were placed in a cylindrical mold filled with epoxy resin in a vacuum environment then ground and polished with 500, 1000 and 3000 grade silicon carbide paper and diamond pastes with a polishing machine. For the SEM and EDS tests, samples were sprayed by gold and then fixed on the stage by conductive tape. All the samples were store in a vacuum oven to standby application. A scanning electron microscope manufactured by Tescan in the Czech Republic and nanoindentation apparatus manufactured by Micro Materials Ltd. in the United Kingdom were employed to analyze the microstructure and defect distribution of the steel-concrete interface.

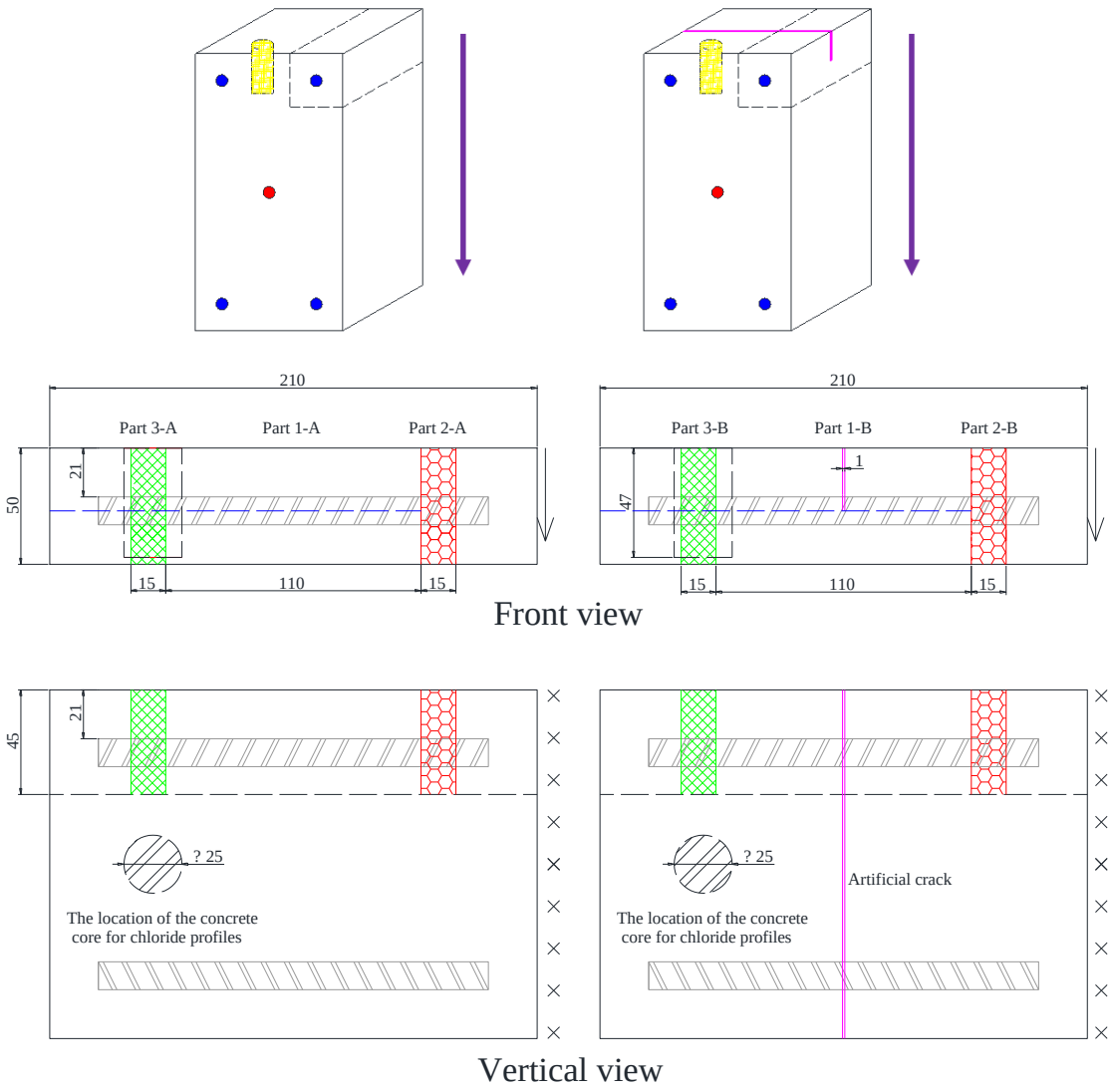

Figure IV-2 Illustration of the position of samples for different tests

(*The black dashed lines in concrete blocks indicate the direction of sawing; the arrows and the crosses near the concrete block mean the casting direction*)

2.4 Results and Discussion

2.4.1 Characterization of the steel-concrete interface

In this section, the steel-concrete interfacial conditions of A-1 and B-1 are discussed and compared in terms of air bubble distribution, microstructure and cement hydration products. In the case of microstructure, the transverse fracture surface of the steel-concrete interface was analyzed by BSE and nanoindentation. The products of cement hydration at the interface between steel and concrete were measured by SEM and EDS.

➢ **Distribution of air bubbles at the steel-concrete interface**

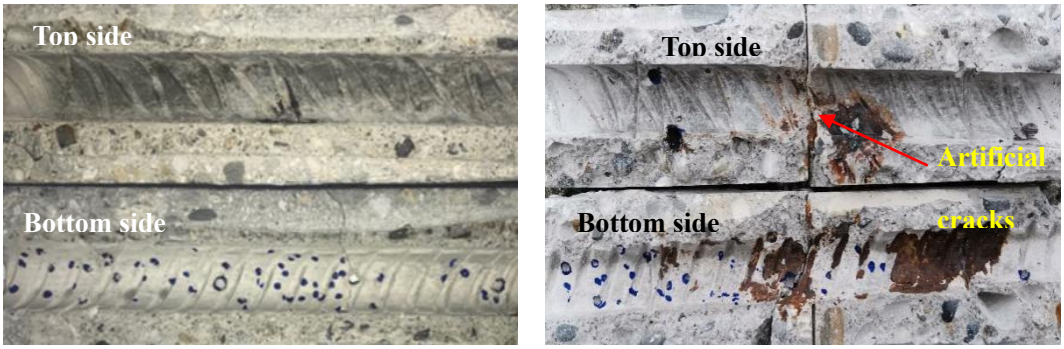

(a) A-1 (b) B-1

Figure IV-3. Steel-concrete interface along top steel reinforcement

The distribution of air bubbles in the steel-concrete interface of A-1 and B-1 is shown in Figure IV-3. It is obvious that there were some air bubbles located at the bottom interface. However, the top interface was quite perfect. This result is in accordance with previous investigation [50].

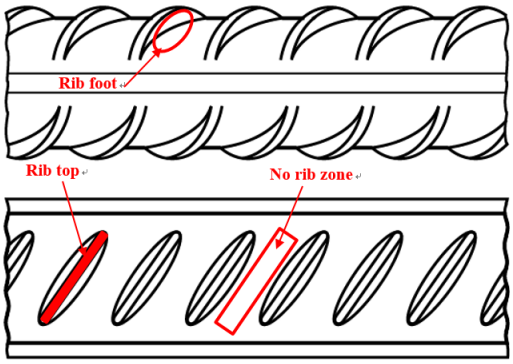

Figure IV-4 Schematic illustration of the deformed steel rebar

The surface of the deformed rebar was divided into three parts, rib foot, rib top and no-rib zone (Figure IV-4). The number of air voids in the three zones was counted and the ratio of the number of the air bubbles in a given zone to the number of air bubbles at the bottom steel-concrete interface was calculated (Figure IV-5). From Figure IV-3 and Figure IV-5, it is clear that most of the air voids were located at the rib foot. About one quarter of the air voids appeared on the no-rib zone, while no more than 10% were found at the rib top.

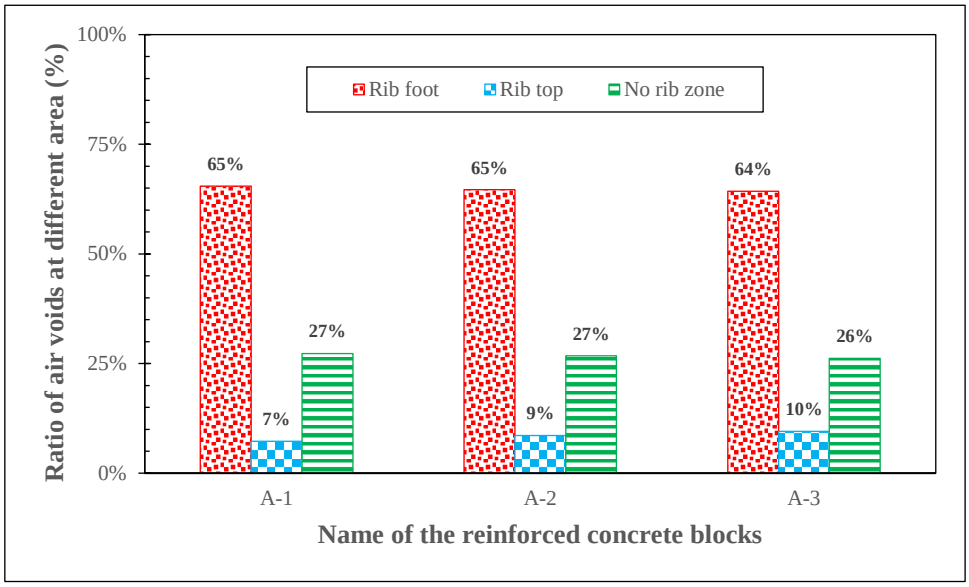

Figure IV-5. Distribution of air voids in various areas of the steel-concrete interface

The defects in the steel-concrete interface consisted of air voids and bleed water zones or voids [24]. In the case of the formation of air voids under the reinforcing steel, when the fresh concrete was compacted, air bubbles migrated up to the bottom surface of the ribbed-steel reinforcement simultaneously. When rising air voids were in contact with the rib top area, most of the air bubbles could not adhere to this small, hard surface, so they continued to migrate along the contour of the rib and accumulated at the location of the rib foot. So, the air bubbles in the rib foot zone had two origins some came from the rib top and others came directly from the fresh concrete. For the no-rib zone, rising air voids could migrate up to this area directly, and then blend to form a large air void at the surface of the no-rib zone of the steel rebar. Therefore, the air bubble ratio was lowest at the rib top and highest at the rib foot, the ratio in the no-rib zone being between those at rib foot and rib top.

Apart from the distribution of air bubbles, the color of the top interface was deeper than that of the bottom interface. A similar result was also reported by Angst et al. [44]. Due to the top-cast effect, a loose and porous layer of cement hydration products formed under the steel reinforcement. However, the layer of cement hydration products at the top steel-concrete interface was denser [33, 38, 51] and this difference in microstructure between the top and bottom interfaces was reflected by the color.

➢ **Density of the steel-concrete interface around the perimeter of the steel bar**

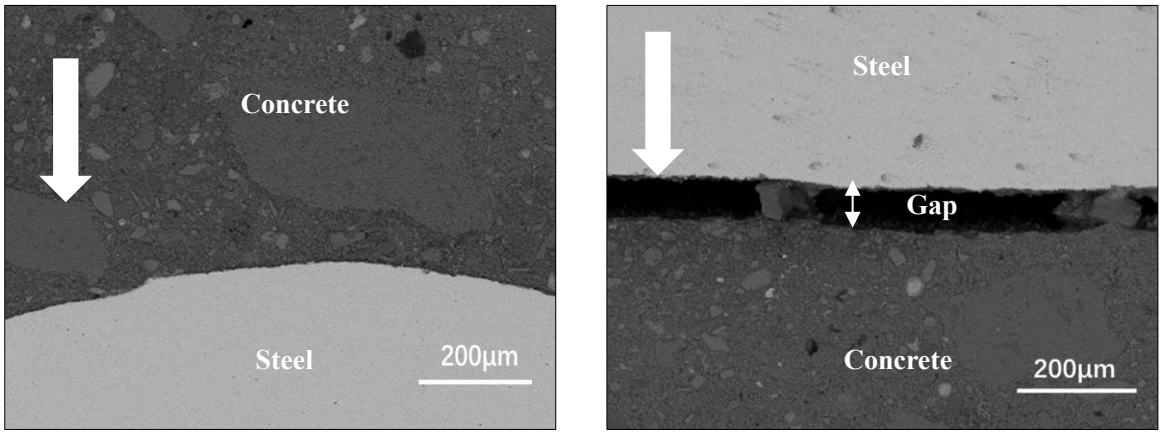

Figure IV-6. BSE and nanoindentation of top-cast bar of A-1

(White arrows correspond to the casting direction)

The density of the steel-concrete interface around the perimeter of the steel was characterized by BSE and nanoindentation. The results are presented in Figure IV-6. From the results of BSE, it can be observed that the steel-concrete interface at the top of the steel bar was relatively dense, and there were no obvious macro defects. However, an obvious gap can be observed in the steel-concrete interface at the bottom of the steel bar. These results are in accordance with [26, 33]. The gaps under the steel bar formed mainly due to water bleeding and settlement of the fresh concrete.

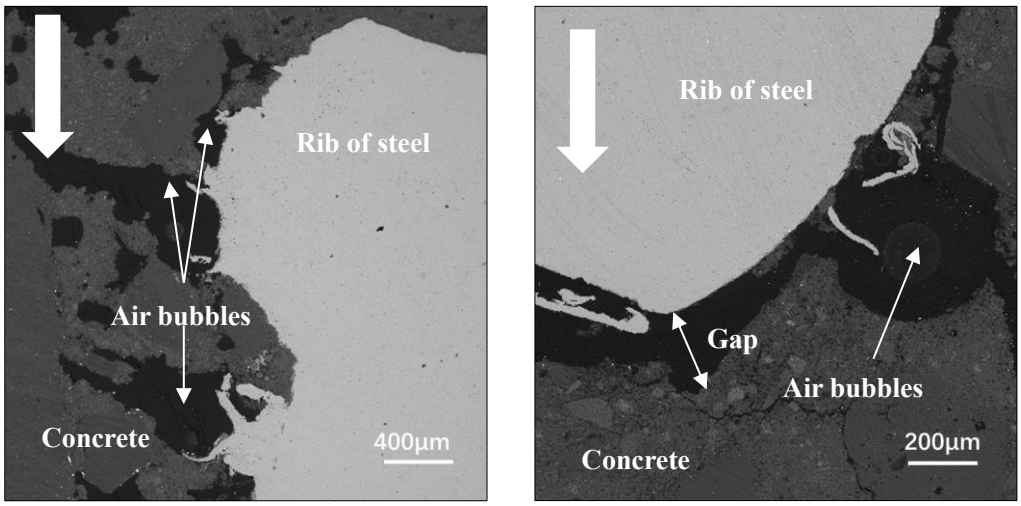

Figure IV-7 BES of rib of A-1

Moreover, air bubbles appeared at the locations of the top and bottom rib zones of the steel-concrete interface (in Figure IV-7). One possible explanation is that air bubbles and bleeding water adhered easily at the location of rib zone because of the special shape.

In summary, bleeding water voids always appeared at the bottom part of the steel-concrete

interface. Combining the results of Figure IV-3 and Figure IV-5 shows that most of the air bubbles were concentrated at the rib foot in the bottom part of the steel-concrete interface, although some of them probably appeared in the top part of the steel-concrete interface.

➢ **Distribution of hydration products in the steel-concrete interface**

Figure IV-8 and Figure IV-9 present the cement hydration products at rib foot, rib top and in the no rib zone as observed by SEM. Figure IV-10 shown the results of the element analysis of the cement hydration products in the steel-concrete interface by EDS. It should be noted that the observation of SEM and the measurement of EDS were carried out at the same location.

In the case of the top interface of A-1, no obvious crystals can be found, but some large particles can be spotted at the rib foot and rib top. Figure IV-10 (a)shows these big particles to be $Ca(OH)_2$, with some ettringites and C-S-H gel in the top steel-concrete interface. This result is in accordance with [33, 52]. However, the $Ca(OH)_2$ did not form typical plate-like crystals [53], as the concrete cover of the top interface was too dense to provide enough space for crystals to grow. The hydration products at rib foot and rib top were looser and more porous than on the no-rib zone and, according to the previous analysis, due to the existence of ribs on the steel reinforcement, the microstructures of the rib zone were more complex than in the no-rib zone, so a weak steel-concrete interface would be formed at that location in spite of the fact that the rib was situated at the top according to the casting direction.

In the case of the bottom interface of A-1, some plate-like and needle-like crystals could be observed on the bottom interface. According to the results shown in Figure IV-10 (b), the plate-like crystals were $Ca(OH)_2$ and the needle-like ones were ettringites. Due to bleeding, and segregation and settlement of fresh concrete, some bleeding water zones formed at the bottom side of the steel and provided sufficient conditions for the growth of crystals. Similarly to the top interface, the microstructures of the rib foot and rib top were more loose and porous than that of the no-rib zone. However, the whole bottom interface was looser and more porous than the top interface.

According to these results, for a reinforcing steel at a given height, the quality of the steel-concrete interface was influenced by the casting direction as well as the shape of the steel reinforcement. The top-cast effect does not impact the type of cement hydration products around the steel rebar, but it affects their structures.

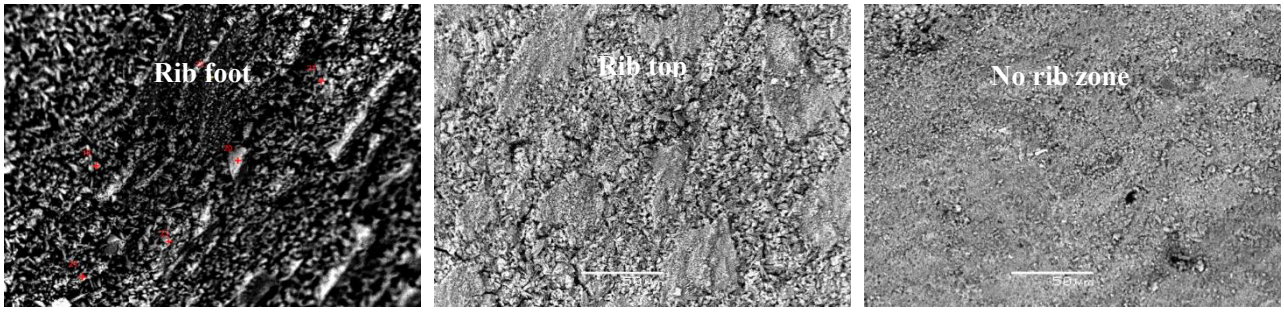

Figure IV-8 SEM results of top interface of A-1

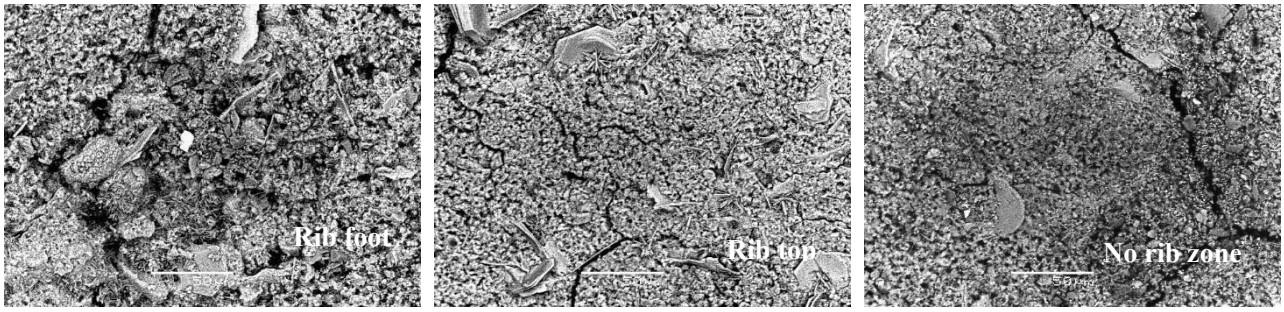

Figure IV-9 SEM results of bottom interface of A-1

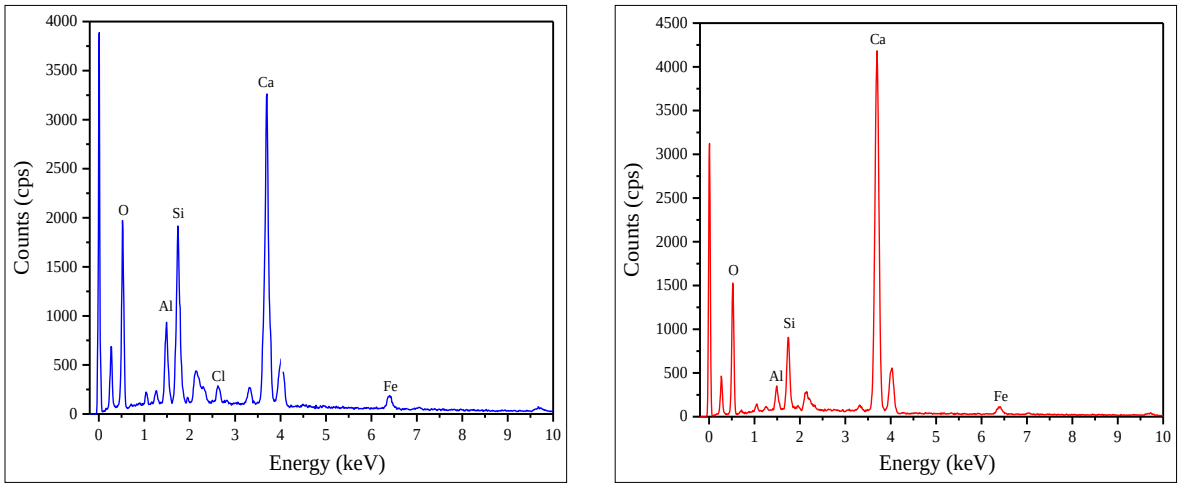

(a) Top interface of A-1 (b) Bottom interface of A-1

Figure IV-10 EDS results for interface of A-1

2.4.2 Penetration of chloride ions into the steel-concrete interface

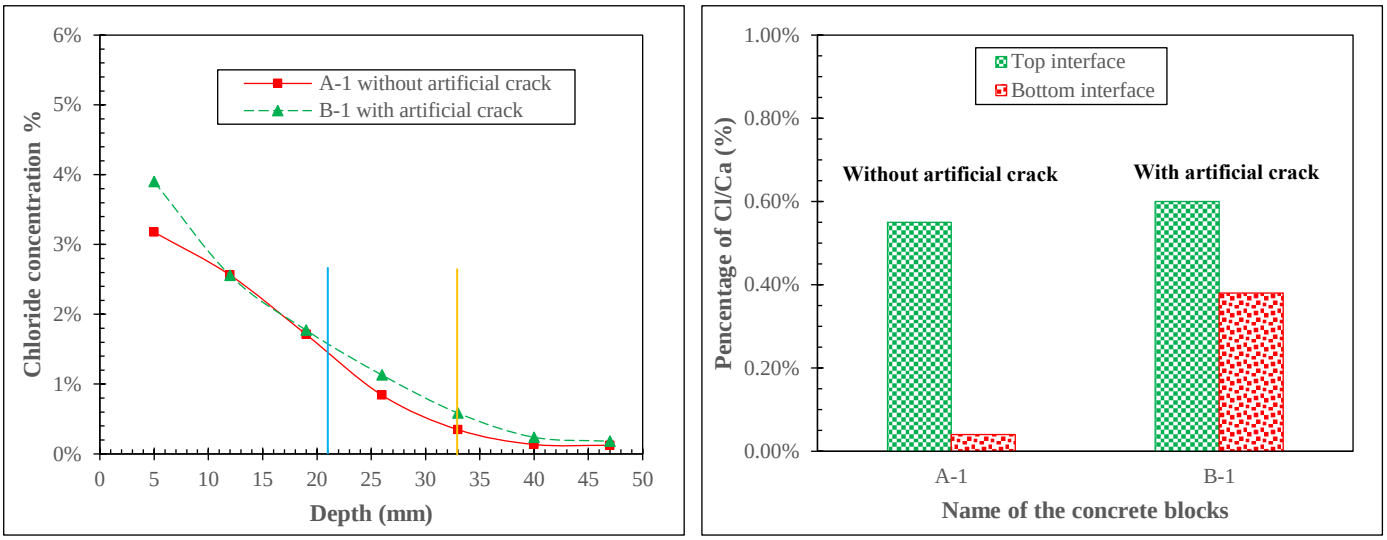

(a) Chloride profiles in sound concrete (b) Chloride content at the steel-concrete interface

Figure IV-11. Chloride profiles in sound concrete and chloride elements at steel-concrete interface

(The blue and yellow lines indicate the depth of the top surface and the bottom surface, respectively, of steel rebars)

The chloride profiles in sound concrete and the chloride content evaluated by EDS at the steel-concrete interface are shown in Figure IV-11. It should be noted that all the information of chloride represented the total chloride regardless of the chloride profiles or chloride content evaluated by EDS test.

The chloride profiles in sound concrete (Figure IV-11 (a)) show that the chloride concentration of sample A-1 is approximately the same as that of sample B-1 at the same depth. This is easy to understand that all the samples were the same regardless of cracked concrete or uncracked concrete, therefore, at a given depth, the chloride content was similar.

In order to further investigate the chloride penetration in the steel-concrete interface, after SEM observation, on the same surface, some small areas were selected to analyze the chloride content by EDS test. Comparing the chloride concentration in the top and bottom parts of the steel-concrete interface (Figure IV-11 (b)), we find that the chloride content in the top part of the steel-concrete interface was higher than that in the bottom part. This can be ascribed to the distance from concrete surface to the top part of steel-concrete interface is thinner compared to that from concrete surface to the bottom part of steel-concrete interface. Therefore, during a relative short exposure period, the top part can receive more chloride ions than that of bottom part. For the sample with the artificial

crack, the chloride concentration in the top part of the steel-concrete interface was slightly higher than that in the sample without an artificial crack. However, the chloride concentration in the bottom part was significantly higher when the sample had an artificial crack than when it did not. This can be attributed to the fast penetration rate of chloride in the artificial crack and in the bottom part of the steel-concrete interface.

In the case of uncracked concrete, the motion of chloride ions is mainly controlled by the quality of the concrete cover [54], so the chloride content was lower in the bottom than in the top interface. However, in the case of cracked concrete, the chloride ions present had followed two different paths some had penetrated through the concrete cover, similarly to the situation in the uncracked concrete, while the other chlorides had followed the artificial crack. Due to higher density of the top steel-concrete interface relative to the bottom interface and the presence of top-casting defects [38], the transport of chloride ions resulting from the artificial crack mainly occurred in the bottom interface. A schematic illustration concerning the transport of chloride ions is shown in Figure IV-12.

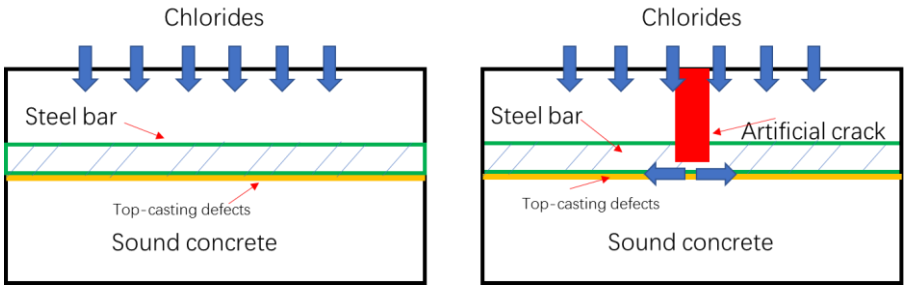

Figure IV-12. Schematic illustration of chloride penetration in uncracked concrete and cracked concrete

2.4.3 Effect of interfacial damage and artificial crack on the corrosion initiation process in steel

➢ **Case of no artificial crack**

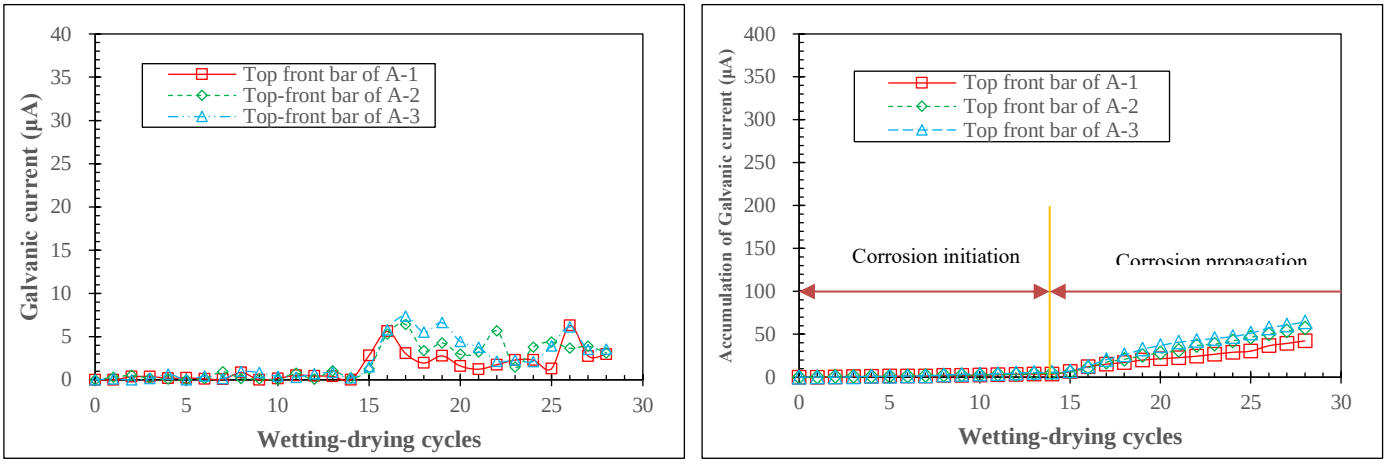

(a) Galvanic current (b) Accumulation of galvanic current

Figure IV-13. Galvanic corrosion current in the top bars of A blocks

Figure IV-13 presents the galvanic corrosion current and its cumulative value for the top-cast bar of three samples in Group A. It is clear that the results are consistent with the model proposed by Tuutti [2]. The period from 0 to 14 wetting-drying cycles corresponded to the corrosion initiation period and corrosion propagation took place after the 14th wetting-drying cycle. After 28 cycles, the steel rebar of sample A-1 was extracted from the concrete to check which areas were actually corroded.

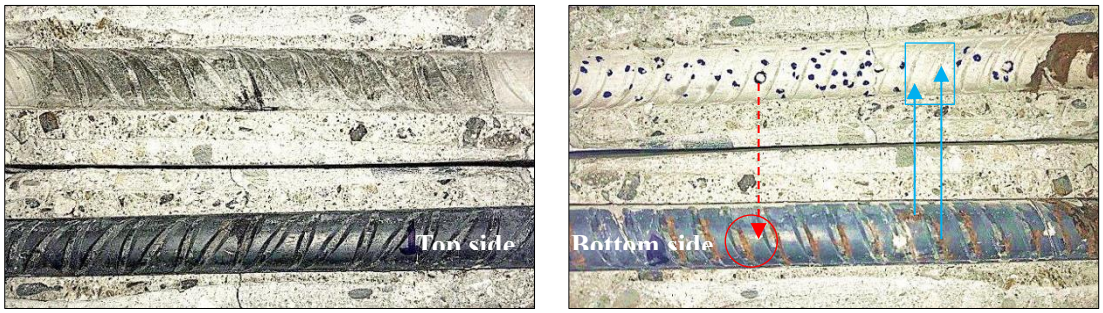

Figure IV-14. Corrosion pattern of top bar of A-1

The corrosion pattern of the top bar of A-1 is shown in Figure IV-14. It is clear that rust stains were always found on the bottom part of the steel according to the casting direction. Furthermore, the rust stains mainly appeared at the rib foot zone of the bottom interface. Although, the locations of rust cannot be regarded as the places of pitting corrosion[45, 46]. However, after recording the stains rust of the surface, the steel rebars were brushed and checked that the locations of the rust on the steel surface represent the places of small pitting corrosion, which always initiated in the bottom

interface of steel-concrete,, as reported in many publications [25, 28, 37, 55, 56]. Furthermore, the rust stains mainly appeared at the rib foot zone of the bottom interface. Some investigations [40, 57] have revealed corrosion starting in the air voids at the steel-concrete interface but, according to our results, corrosion initiation was not related to the location of air voids, e.g. corrosion took place at the rib foot without air voids (see the blue frame), or no corrosion occurred in the no-rib zone with air bubbles (see the red circle).

After brushing the surface of the steel rebars of block A-1, corrosion maps were drawn and are shown in Figure IV-15. It should be noted that, in order to study the distribution of pitting corrosion around the perimeter of the steel reinforcement, the steel rebar was divided into four areas, namely, top surface, bottom surface, inside surface and outside surface according to the casting direction and concrete cover. It can be observed that pitting corrosion only appeared at the bottom surface and was mainly distributed in the vicinity of the rebar rib foot.

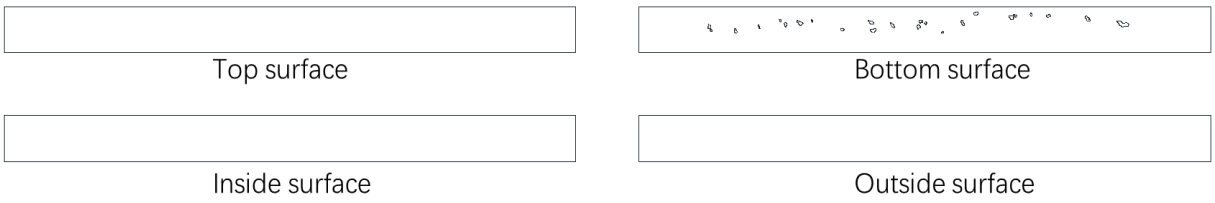

Figure IV-15. Corrosion maps of top steel rebar of A-1

In order to investigate the pitting corrosion further, the 160 mm long steel rebar was divided into 320 segments along its length. Then, the ratio of the total pitting corrosion area to the total bottom area of each segment was calculated according to Figure 17.The results are presented in Figure IV-16.

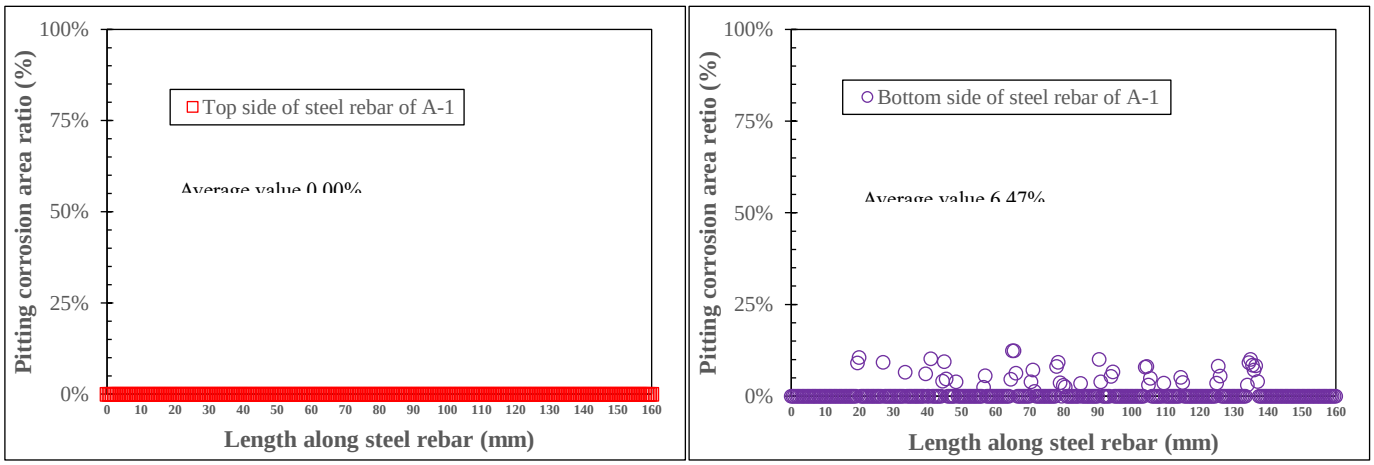

(a) Top surface of steel rebar of A-1

(b) Bottom surface of steel rebar of A-1

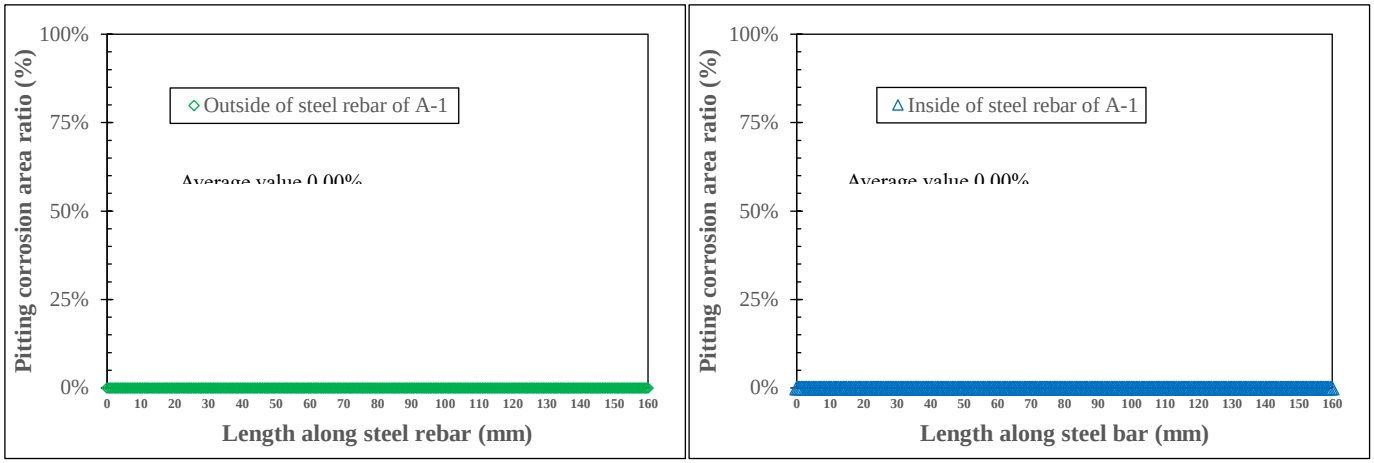

(c) Outside surface of steel rebar of A-1 (d) Inside surface of steel rebar of A-1

Figure IV-16. Pitting corrosion area ratio along the steel rebar of A-1

According to the chloride profiles presented in Figure IV-11, the chloride concentration in the top interface was much higher than that of the bottom interface. However, Figure IV-16 shows that pitting corrosion only took place at the rib foot zone of the bottom surface of the steel rebar and the average pitting corrosion area accounted for 6.4% of the total bottom interface. This means that the presence of the rib zone of a steel rebar is a critical factor for chloride corrosion initiation in steel reinforcement.

To sum up, the corrosion initiation is not correlated with the distribution of air bubbles, but is strongly correlated with “rib foot”. The rib foot is characterized by a special shape compared to other zones and top-casting-induced defects mainly concentrate at this place, leading to corrosion initiation (Figure IV-5). Apart from the top-casting-induced defects, metallographic defects, formed due to poor quality control in the steel rebar manufacturing line, are commonly generated at the location of the rib foot, which gives rise to the formation of a cathode-anode combination (galvanic cell). This is one possible reason why corrosion firstly takes place at the rib foot [58-60]. When chlorides penetrated the concrete, they reached the top steel-concrete interface first and then a proportion of the chlorides could penetrate along the perimeter of the steel rebar to accumulate at the bottom interface. Due to the presence of metallographic defects and top-casting defects at the rib foot location, which reduced the local chloride threshold [61], corrosion started at the rib foot of the bottom side of the steel rebar firstly.

➢ **Case of samples with artificial cracks**

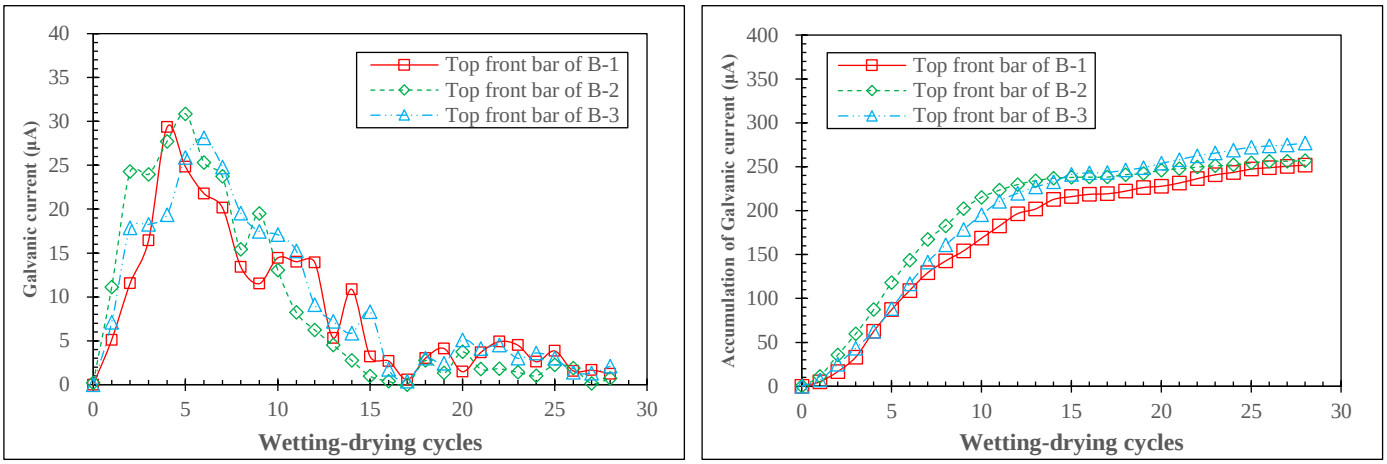

(a) Galvanic current (b) Accumulation of galvanic current

Figure IV-17. Galvanic corrosion current of the top bar of B blocks

The galvanic corrosion current and its cumulative results for the top front bar of three samples in Group B are shown in Figure IV-17. The cumulative curve of galvanic current is consistent with the corrosion model of cracked reinforced concrete proposed by François et al. [62].

From 0 to 13 wetting-drying cycles, due to the presence of the artificial crack, the top front steel bars in all B blocks exhibited a higher corrosion rate than the top front bars in all A blocks. However, after the 15th cycle, a similar corrosion rate was identified for top front steel rebars in both A blocks and B blocks.

According to the 4-phase model proposed by François et al.[62], it is clear from Figure IV-17 that the incubation period is too short to be observed. This is because the chloride ions penetrating via the artificial crack contact the top side of the steel rebar located at the crack, resulting in immediate initiation of corrosion on the top side. This result is consistent with that of Figure IV-20.

The initiation period at the crack location occurs during about the 12th-13th wetting-drying cycles and is then followed by the propagation phase. The induction phase defined in François et al.'s model [62] is reduced to zero due to the presence of top-casting defects[20].

It should be noted that the first corrosion-induced cracks of B-1 appeared after 16 wetting-drying cycles (Figure IV-18).

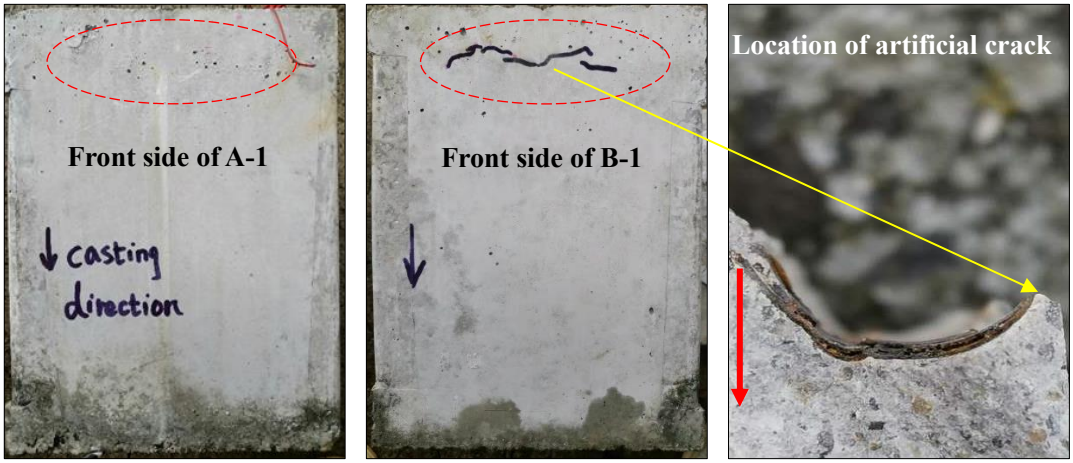

(a) Front side of A-1 (b) Front side of B-1 (c) Cross-section of B-1 at artificial crack

Figure IV-18. Cracking patterns of the front side of A-1 and B-1 and Cross-section of B-1 at the location of the artificial crack

Figure IV-18 shows the distribution of corrosion-induced cracks in B-1. Corrosion-induced cracks firstly appeared near the artificial crack, this result was in accordance with Paul et al[45, 46].. The distribution of corrosion products at the bottom interface of B-1 (Figure IV-3 and Figure IV-18) suggests that rust firstly deposited at the bottom interface in the vicinity of the artificial crack, which was gradually sealed as the corrosion process developed. Therefore, the corrosion rate gradually decreased. When the stress formed by the corrosion products exceeded the tensile strength of the concrete cover, corrosion-induced cracks appeared.

Figure IV-19. Corrosion pattern of top bar of B-1

After 28 cycles, the top steel rebars were extracted from the concrete blocks to check the real state of corrosion, and the results are shown in Figure IV-19. The rust was mainly distributed on the bottom interface and, on the top interface, small pieces of corrosion products appeared in the vicinity of the artificial crack. However, the location of rust does not represent the location of pitting corrosion.

After cleaning the steel surface, the distribution of pitting corrosion on the different sides of

steel rebar of B-1 is depicted in Figure IV-20. It can be observed that, on the top surface and on the inside surface, several corrosion pits can be found around the location of the artificial crack. On the bottom surface of the steel rebar, many sites of pitting corrosion can be observed, even far from the artificial crack.

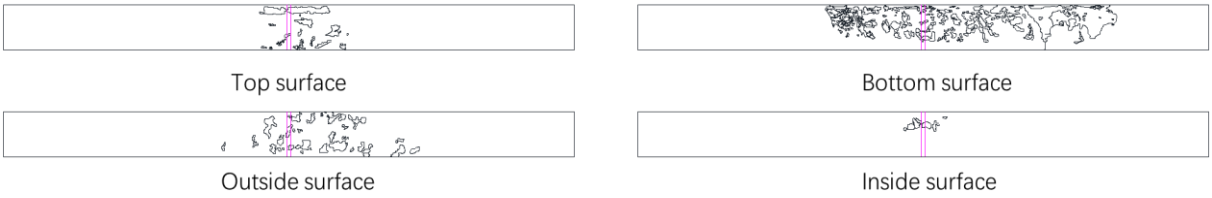

Figure IV-20. Corrosion maps of top steel rebar of B-1

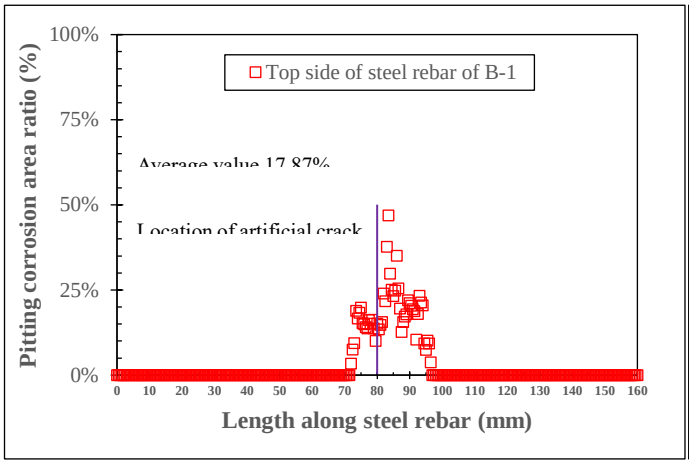

(a) Top surface of steel rebar of B-1

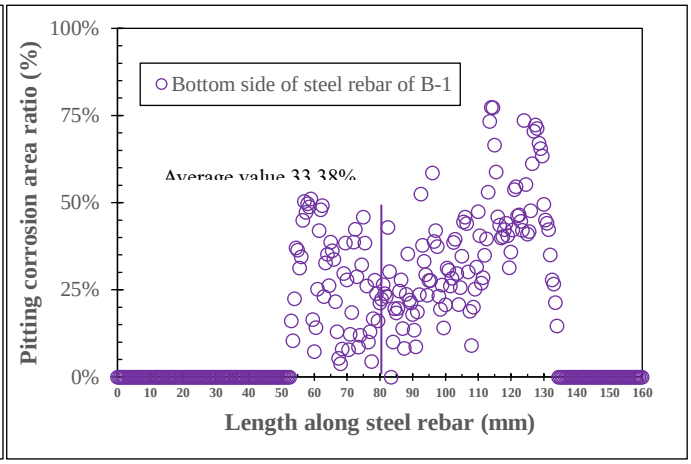

(b) Bottom surface of steel rebar of B-1

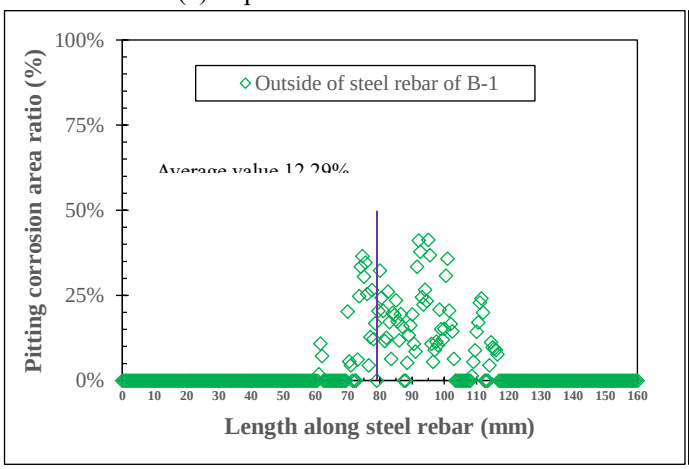

(c) Outside surface of steel rebar of B-1

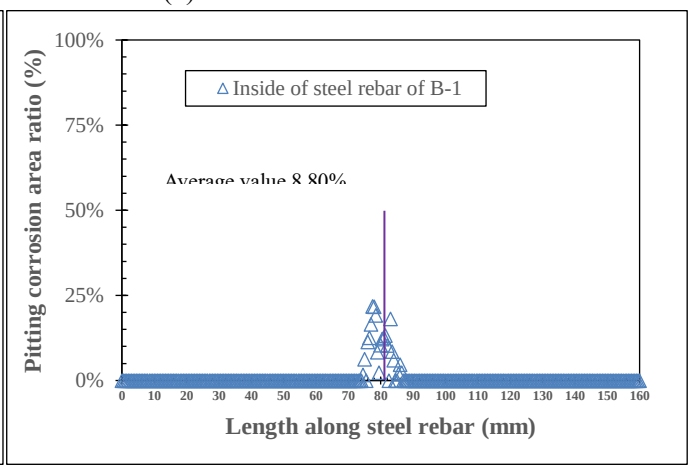

(d) Inside surface of steel rebar of B-1

Figure IV-21. Pitting corrosion distribution along the steel rebar of B-1

The ratio of the pitting corrosion area to the total area of each side of the segment is shown in Figure IV-21.

In the case of the top surface, the pitting corrosion mainly gathered around the artificial crack and the worst was found within the width of the crack. This was because the opening of artificial crack was wide, 1 mm, and thus allowed chloride solution to come into contact with the steel surface.

For the bottom surface, pitting corrosion mainly occurred at locations that were far from the artificial crack. According to the previous analysis, chloride ions penetrate from the artificial crack and migrate along the bottom steel-concrete interface. Due the existence of top-casting-induced defects, which reduced the local chloride threshold of steel rebar [3, 24, 33, 52, 61, 63-66], pitting corrosion was initiated at the weak point of the bar.

In the case of the outside surface, apart from the artificial crack, chloride ions could penetrate from the outer lateral face of the concrete cover and, thus, the corrosion field was wider than that of top side.

For the inside surface, the chloride ions could not travel to the steel surface easily, so a smaller number of pitting corrosion sites appeared near the artificial crack.

2.4.4 Discussion

In cases with both an artificial crack and top-casting-induced defects, corrosion initiation was immediate and was followed by the propagation phase, which led to the appearance of the first corrosion-induced cracks within 17 cycles (about 4 months of exposure). This could be a criterion to define the end of service life.

Without artificial cracks, corrosion started only when chlorides reached the rebars through the concrete cover. Because of the thin cover of 21 mm, the chloride ingress period before initiation lasted for only 17 cycles (about 4 months) due to top-surface exposure, ponding and wetting-drying effects.

It should be noted that apart from group A and group B present here, some other reinforced concrete blocks with the same steel frame, cement, concrete and exposure conditions are still being monitored for long-term research. From the results of these monitored samples, which are in accordance with this paper, in the absence of artificial cracks, they exhibited corrosion-induced cracks only after 45 wetting-drying cycles (about 1 year). The conclusion that could be done is that the presence of artificial crack coupled with top cast defect leads to a high reduction of the time for the appearance of corrosion-induced cracks. So, for the specific study here, in cases where top-casting-induced defects are present, the service life of samples without artificial cracks appears to be at least 2.5 times longer than that of samples with artificial cracks.

From the corrosion model for cracked reinforced concrete, without top-casting-induced defects, proposed by François et al[17], there is an induction between corrosion initiation and corrosion propagation. According to the results of accumulative galvanic current, however, it can be found that no obvious induction appeared between corrosion initiation and propagation in the presence of artificial crack and top-casting-induced defects. From author's previous research[20], for the RC beams with load-induced cracks and top-casting-induced defects, the propagation stage follows the initiation stage directly, and then the induction period length is zero. It was ascribed to the presence of the top-casting-induced defects which favor the creation of large amounts of corrosion products along the interface and thus a pressure high enough to crack the concrete. Therefore, it could be expected that once the presence of top-casting defects, there was no transition between corrosion initiation and propagation regardless of artificial crack concrete blocks or load-induced cracks RC beams.

2.5 Conclusion

This work focused on artificial cracks and the effect of top-casting defects on corrosion initiation in reinforced concrete. The microstructures of the steel-concrete interface, chloride penetration at this interface, and the corrosion process of top-cast bars in concrete with or without an artificial crack were studied and compared. The following conclusions can be drawn

1. Although a higher concentration of chloride ions was found at the top side of the steel rebar than at the bottom side, corrosion always initiated at the bottom side of reinforcing steel due to the presence of top-casting defects, regardless of the presence or absence of an artificial crack.

2. Corrosion initiation had no correlation with the distribution of air bubbles, but showed high correlation with the "rib foot" of the steel rebar, as corrosion mainly initiated at the rib foot location.

3. In presence of both artificial cracks and top-casting defects, chlorides ingressed along the bottom part of the steel concrete interface and initiated corrosion at different locations along the rebar. This marked extension of pitting corrosion induced large amounts of corrosion products, which led to the formation of corrosion-induced cracks. As a result, corrosion initiation was followed by corrosion propagation. Top-casting defects associated with direct access for chlorides from the outside, e.g. via an artificial crack or load-induced cracks, is the worst scenario for

corrosion and needs special attention from designers to avoid premature deterioration of reinforced concrete structures.

4. In absence of an artificial crack but in presence of top-casting defects, chlorides ingress through the concrete cover to reach the rebar. Despite the fact that the top side of steel bars is closer to the outside surface of concrete and thus is exposed to chloride ingress firstly, the corrosion initiates at the bottom side of rebars.

5. With a cover of 21 mm and the presence of top-casting defects, the service life, based on the criterion of appearance of corrosion-induced cracks, is 2.5 longer in the absence of an artificial crack than in its presence. It is expected, and is one perspective of the work, that this difference in service life will increase with larger thickness of the concrete cover.

2.6 References

[1] L. Bertolini, B. Elsener, P. Pedeferri, E. Redaelli, R. Polder, Corrosion of steel in concrete: prevention, diagnosis, repair. 2013, John Wiley & Sons, 2004.

[2] K.S. Tuutti, Corrosion of steel in concrete, (1982).

[3] U.M. Angst, M.R. Geiker, M.C. Alonso, R. Polder, O.B. Isgor, B. Elsener, H. Wong, A. Michel, K. Hornbostel, C. Gehlen, The effect of the steel–concrete interface on chloride-induced corrosion initiation in concrete: a critical review by RILEM TC 262-SCI, Materials and Structures, 52 (2019) 88.

[4] M. Soutsos, Concrete durability: a practical guide to the design of durable concrete structures, Thomas Telford London2010.

[5] R. Francois, I. Khan, N.A. Vu, H. Mercado, A. Castel, Study of the impact of localised cracks on the corrosion mechanism, European Journal of Environmental and Civil Engineering, 16 (2012) 392-401.

[6] L. Yu, R. François, V.H. Dang, V. L'Hostis, R. Gagné, Development of chloride-induced corrosion in pre-cracked RC beams under sustained loading: Effect of load-induced cracks, concrete cover, and exposure conditions, Cement and Concrete Research, 67 (2015) 246-258.

[7] S. Jaffer, C. Hansson, The influence of cracks on chloride-induced corrosion of steel in ordinary Portland cement and high performance concretes subjected to different loading conditions, Corrosion science, 50 (2008) 3343-3355.

[8] R. Francois, G. Arliguie, Reinforced concrete: correlation between cracking and corrosion, Special Publication, 126 (1991) 1221-1238.

[9] P. Schieβl, M. Raupach, Laboratory studies and calculations on the influence of crack width on chloride-induced corrosion of steel in concrete, Materials Journal, 94 (1997) 56-61.

[10] A. Scott, M. Alexander, The influence of binder type, cracking and cover on corrosion rates of steel in chloride-contaminated concrete, Magazine of Concrete Research, 59 (2007) 495-505.

[11] M. Otieno, M. Alexander, H.-D. Beushausen, Corrosion in cracked and uncracked concrete-influence of crack width, concrete quality and crack reopening, Magazine of Concrete Research, 62 (2010) 393-404.
[12] M.B. Otieno, The development of empirical chloride-induced corrosion rate prediction models for cracked and uncracked steel reinforced concrete structures in the marine tidal zone, University of Cape Town, 2014.
[13] M. Otieno, H. Beushausen, M. Alexander, Towards incorporating the influence of cover cracking on steel corrosion in RC design codes: the concept of performance-based crack width limits, Materials and Structures, 45 (2012).
[14] Z.-T. CHANG, Corrosion rate of steel reinforcement in concrete in seawater and influence of concrete crack width, The University of New South Wales Sydney, Australia, 2007.
[15] C. Fu, N. Jin, H. Ye, X. Jin, W. Dai, Corrosion characteristics of a 4-year naturally corroded reinforced concrete beam with load-induced transverse cracks, Corrosion Science, 117 (2017) 11-23.
[16] R. François, G. Arliguie, Influence of service cracking on reinforcement steel corrosion, Journal of Materials in Civil Engineering, 10 (1998) 14-20.
[17] R. François, G. Arliguie, Effect of microcracking and cracking on the development of corrosion in reinforced concrete members, Magazine of Concrete Research, 51 (1999) 143-150.
[18] R. Francois, G. Arliguie, Durability of loaded reinforced concrete in chloride environment, Special Publication, 145 (1994) 573-596.
[19] R.M. Ghantous, S. Poyet, V. L'Hostis, N.-C. Tran, R. François, Effect of crack openings on carbonation-induced corrosion, Cement and Concrete Research, 95 (2017) 257-269.
[20] W. Zhang, R. François, L. Yu, Influence of load-induced cracks coupled or not with top-casting-induced defects on the corrosion of the longitudinal tensile reinforcement of naturally corroded beams exposed to chloride environment under sustained loading, Cement and Concrete Research, 129 (2020) 105972.
[21] J. Shi, W. Sun, Recent research on steel corrosion in concrete, Journal of the Chinese Ceramic Society, 9 (2010).
[22] G. Fang, W. Ding, Y. Liu, J. Zhang, F. Xing, B. Dong, Identification of corrosion products and 3D distribution in reinforced concrete using X-ray micro computed tomography, Construction and Building Materials, 207 (2019) 304-315.
[23] A. Michel, A.O.S. Solgaard, B.J. Pease, M.R. Geiker, H. Stang, J.F. Olesen, Experimental investigation of the relation between damage at the concrete-steel interface and initiation of reinforcement corrosion in plain and fibre reinforced concrete, Corrosion Science, 77 (2013) 308-321.
[24] U.M. Angst, M.R. Geiker, A. Michel, C. Gehlen, H. Wong, O.B. Isgor, B. Elsener, C.M. Hansson, R. François, K. Hornbostel, The steel-concrete interface, Materials and Structures, 50 (2017) 143.
[25] R. Zhang, A. Castel, R. François, Influence of steel-concrete interface defects owing to the top-bar effect on the chloride-induced corrosion of reinforcement, Magazine of Concrete Research, 63 (2011) 773-781.
[26] T.A. Soylev, R. François, Quality of steel-concrete interface and corrosion of reinforcing steel, Cement and Concrete Research, 33 (2003) 1407-1415.

[27] T.A. Soylev, R. François, Corrosion of reinforcement in relation to presence of defects at the interface between steel and concrete, Journal of materials in civil engineering, 17 (2005) 447-455.
[28] A. Castel, T. Vidal, R. François, G. Arliguie, Influence of steel-concrete interface quality on reinforcement corrosion induced by chlorides, Magazine of Concrete Research, 55 (2003) 151-159.
[29] T.U. Mohammed, H. Hamada, Corrosion of horizontal bars in concrete and method to delay early corrosion, Materials Journal, 103 (2006) 303-311.
[30] M. Moreau, Contribution a l'etude d'adherence entre les constitiants hydrates du cement portland artificiel et l'armature enrobee REVUE DES MATERIAUX DE CONSTRUCTION ET DE TRAVAUX PUBLICS-CIMENTS BETONS, (1973).
[31] B.S. Hamad, M.S. Itani, Bond strength of reinforcement in high performance concrete: role of silica fume, casting position, and superplasticizer dosage, Materials Journal, 95 (1998) 499-511.
[32] O.E. Gjorv, P.J. Monteiro, P.K. Mehta, Effect of condensed silica fume on the steel-concrete bond, Materials Journal, 87 (1990) 573-580.
[33] A. Horne, I. Richardson, R. Brydson, Quantitative analysis of the microstructure of interfaces in steel reinforced concrete, Cement and Concrete Research, 37 (2007) 1613-1623.
[34] A. Suryavanshi, J. Scantlebury, S. Lyon, Corrosion of reinforcement steel embedded in high water-cement ratio concrete contaminated with chloride, Cement and Concrete Composites, 20 (1998) 263-281.
[35] L. Yu, R. François, R. Gagné, Influence of steel-concrete interface defects induced by top-casting on development of chloride-induced corrosion in RC beams under sustained loading, Materials and Structures, 49 (2016) 5169-5181.
[36] N. Silva, Chloride induced corrosion of reinforcement steel in concrete-Threshold values and ion distributions at the concrete-steel interface, Chalmers University of Technology2013.
[37] W. Zhang, L. Yu, R. François, Influence of top-casting-induced defects on the corrosion of the compressive reinforcement of naturally corroded beams under sustained loading, Construction and Building Materials, 229 (2019) 116912.
[38] F. Chen, C.-Q. Li, H. Baji, B. Ma, Effect of design parameters on microstructure of steel-concrete interface in reinforced concrete, Cement and Concrete Research, 119 (2019) 1-10.
[39] F. Chen, C.-Q. Li, H. Baji, B. Ma, Quantification of steel-concrete interface in reinforced concrete using Backscattered Electron imaging technique, Construction and Building Materials, 179 (2018) 420-429.
[40] J. Ryou, K. Ann, Variation in the chloride threshold level for steel corrosion in concrete arising from different chloride sources, Magazine of Concrete Research, 60 (2008) 177-187.
[41] S. Arya, B. Das, S.K. Goudar, Microstructural Study of Steel-Concrete Interface and Its Influence on Bond Strength of Reinforced Concrete, Advances in Civil Engineering Materials, 8 (2019) 171-189.
[42] W.H. Hartt, J. Nam, Effect of cement alkalinity on chloride threshold and time-to-corrosion of reinforcing steel in concrete, Corrosion, 64 (2008) 671-680.
[43] I. Zafar, T. Sugiyama, Laboratory investigation to study the corrosion initiation of rebars in fly ash concrete, Magazine of Concrete Research, 66 (2014) 1051-1064.
[44] U.M. Angst, B. Elsener, C.K. Larsen, Ø. Vennesland, Chloride induced reinforcement corrosion: Electrochemical monitoring of initiation stage and chloride threshold values, Corrosion Science, 53 (2011) 1451-1464.

[45] S.C. Paul, G.P.A.G. Van Zijl, Corrosion deterioration of steel in cracked SHCC, International Journal of Concrete Structures and Materials, 11 (2017) 557-572.
[46] S.C. Paul, G.P. van Zijl, Crack formation and chloride induced corrosion in reinforced strain hardening cement-based composite (R/SHCC), Journal of Advanced Concrete Technology, 12 (2014) 340-351.
[47] C. Boschmann Kathler, U.M. Angst, M. Wagner, C.K. Larsen, B. Elsener, Effect of cracks on chloride-induced corrosion of steel in concrete-a review: Etatsprogrammet Varige konstruksjoner 2012-2015, ETH Zurich, 2017.
[48] A. G71-81, Standard Guide for Conducting and Evaluating Galvanic Corrosion Tests in Electrolytes, (2003).
[49] A. Girão, I. Richardson, C. Porteneuve, R. Brydson, Composition, morphology and nanostructure of C–S–H in white Portland cement pastes hydrated at 55 C, Cement and Concrete Research, 37 (2007) 1571-1582.
[50] N. Otsuki, M. Hisada, N.B. Diola, T. Uddin, Experimental study on interfacial transition zones in reinforced concrete, Doboku Gakkai Ronbunshu, 1998 (1998) 155-167.
[51] U. Angst, Chloride induced reinforcement corrosion in concrete: Concept of critical chloride content–methods and mechanisms, (2011).
[52] C. Page, Mechanism of corrosion protection in reinforced concrete marine structures, Nature, 258 (1975) 514.
[53] H.F. Taylor, Cement chemistry, Thomas Telford1997.
[54] L. Tang, L.-O. Nilsson, P.M. Basheer, Resistance of concrete to chloride ingress: Testing and modelling, CRC Press2011.
[55] J. Shi, J. Ming, Influence of defects at the steel-mortar interface on the corrosion behavior of steel, Construction and Building Materials, 136 (2017) 118-125.
[56] T.U. Mohammed, N. Otsuki, H. Hamada, T. Yamaji, Chloride-induced corrosion of steel bars in concrete with presence of gap at steel-concrete interface, Materials Journal, 99 (2002) 149-156.
[57] J.-G. Nam, W.H. Hartt, K. Kim, Effects of Air Void at the Steel-Concrete Interface on the Corrosion Initiation of Reinforcing Steel in Concrete under Chloride Exposure, Journal of the Korea Concrete Institute, 17 (2005) 829-834.
[58] S. Nandi, N. Tewary, J. Saha, S. Ghosh, Microstructure, mechanical properties and corrosion performance of a few TMT rebars, Corrosion Engineering, Science and Technology, 51 (2016) 476-488.
[59] S.A. Nair, R.G. Pillai, Microstructural and corrosion characteristics of Quenched and Self-Tempered (QST) steel reinforcing bars, Construction and Building Materials, 231 (2020) 117109.
[60] L. Michel, U. Angst, Towards understanding corrosion initiation in concrete–Influence of local electrochemical properties of reinforcing steel, MATEC Web of Conferences, EDP Sciences, 2018, pp. 04001.
[61] B. Reddy, Influence of the steel-concrete interface on the chloride threshold level, University of London, 2001.
[62] R. François, S. Laurens, F. Deby, 2 - Scale and Structural Effects on the Corrosion of Reinforced-Concrete Reinforcements, Corrosion and its Consequences for Reinforced Concrete Structures, Elsevier2018, pp. 43-62.
[63] P. Lambert, C. Page, P. Vassie, Investigations of reinforcement corrosion. 2. Electrochemical monitoring of steel in chloride-contaminated concrete, Materials and Structures, 24 (1991) 351-358.

[64] C. Page, K. Treadaway, Aspects of the electrochemistry of steel in concrete, Nature, 297 (1982) 109.
[65] R. Zhang, A. Castel, R. François, Concrete cover cracking with reinforcement corrosion of RC beam during chloride-induced corrosion process, Cement and Concrete Research, 40 (2010) 415-425.
[66] U.M. Angst, M.R. Geiker, M.C. Alonso, R. Polder, O.B. Isgor, B. Elsener, H. Wong, A. Michel, K. Hornbostel, C. Gehlen, The effect of the steel-concrete interface on chloride-induced corrosion initiation in concrete: a critical review by RILEM TC 262-SCI, Materials and Structures, 52 (2019) 88.

3 Influence of load-induced cracks coupled or not with top-casting-induced defects on the corrosion of the longitudinal tensile reinforcement of naturally corroded beams exposed to chloride environment under sustained loading

3.1 Abstract

This paper discusses the effect of both load-induced cracks and top-casting-induced defects on the corrosion characteristics of the tensile bars in reinforced concrete beams under sustained loading and exposure to a chloride environment. Four reinforced concrete beams exposed to climate accelerated natural corrosion were used in the present work. The cracking maps, chloride profiles and cross-sectional loss of four beams were studied and compared with each other. Experimental results show that the presence of load-induced cracks is not the sole cause of early propagation of corrosion. As a result, top-casting-induced defects are the most significantly impacting factor accelerating the deterioration of reinforced concrete. With top-casting-induced defects, corrosion starts at service cracks and then develops preferentially at the bottom surface of the tensile bar. Without top-casting-induced defects, corrosion starts at service cracks but does not develop along the tensile bar. It is only when the chloride content at the depth of reinforcement reaches a critical value that corrosion develops along the tensile bar – preferentially at the outside surface of the rebar because of its probable higher chloride content.

Key words chloride; top-casting-induced defects; steel/concrete interface; corrosion propagation; service cracks

3.2 Introduction

Corrosion of the steel reinforcement is probably the most serious threat to reinforced concrete structures in modern times. The deterioration of reinforcements embedded in reinforced concrete structures leads to several coupled effects[1] longitudinal cracking of concrete cover due to expansive corrosion products; steel cross-section reduction and the degradation of the steel-concrete bond. As a result of these effects, the service life and the load-bearing capacity of reinforced concrete structures are considerably reduced.

Cracking, an inherent characteristic of concrete members, can occur due to shrinkage, creep,

freeze/thaw cycles, external loads, and so on. Studies [2-5] confirm that cracks accelerate the initiation of corrosion by creating preferential pathways for aggressive agents (liquid, gaseous and ionic). François et al. [6] state that, in the presence of service cracks, reinforcement corrosion is always initiated at the crack tip within a few weeks, whether in the presence of chlorides or carbonation. However, the question of whether the corrosion propagation period is affected by crack width is still under debate. Some researchers consider[3, 7-9] that cracks accelerate chloride-induced corrosion by increasing concrete penetrability and that the corrosion rate also increases with increased crack width in propagation stage. However, other investigations revealed[10-14] that cracks do not enhance the corrosion process or the enhancing effect diminished with time.

Several researchers [4, 8, 15-19] consider that the corrosion rate of reinforcement increases with increasing service crack width and the European construction standards, EuroCode 2 [20] fix crack width limitations for durability, in addition to cover depth requirements. In contrast, other studies have found that there is no relationship between the width of a service crack and the corrosion process [2, 21-23], while defects at the steel/concrete interface is the decisive factor for deterioration of reinforced concrete in an aggressive environment [24-36]. Both controversy effect of cracks width and the fact that predicted and observed crack widths can vary significantly lead to the absence of crack width limitations for durability from the current version of American Construction Standard ACI 318-14 [37].

Defects located at the bottom side of a horizontal bar, according to the casting direction, may occur due to bleeding, segregation and settlement of fresh concrete [33, 38] when the steel bars are positioned at depths greater than 15 cm [24, 34, 35]. They accelerate corrosion initiation and propagation in the re-bar [30, 38]. There is a large difference of cement hydration products and concrete structure at the bottom side of a reinforcement bar according to whether defects are present or not[39]. When the corrosion of reinforcement steel in concrete occurred, the side of the steel bar exposed to defects acts as an anode, while the other sides, protected by dense concrete, act as the cathode [24, 38]. So corrosion is always initiated at the side of the steel bar exposed to defects [31]. However, there are few reports on the effect of defects on the corrosion characteristics of tensile bars in corrosion propagation [25].

A tensile reinforcement bar is an integral part of a reinforced concrete element used in the

construction industry, and much research has been devoted to it [2, 21-25, 28, 30, 32, 34, 40-48]. The study reported in this paper investigates the impact of load-induced cracks associated or not with top-casting-induced defects on the corrosion characteristics of the tensile zone of concrete beams in the relatively short term (less than 4 years).

3.3 Experimental program

3.3.1 Reinforced Concrete Specimens

Four concrete beams were prepared in 2013. These beams were named C beams. All the beams were cast with the dimension of 3000×280×150 mm. The layout of reinforced concrete beams and the location of sustained load are shown in Figure IV-22. The red lines in the figure mean the tensile bars, while the green lines correspond to compressive bars. 14 stirrups were used between both types of deformed steel bars in Figure IV-22. The black arrows mean the direction of load applied.

Figure IV-23 shows the cross-section of C beams. The thickness of concrete cover around stirrups is 20mm. The diameter of compressive bar, tensile bar and stirrup used here is 6mm, 12mm and 6mm, respectively.

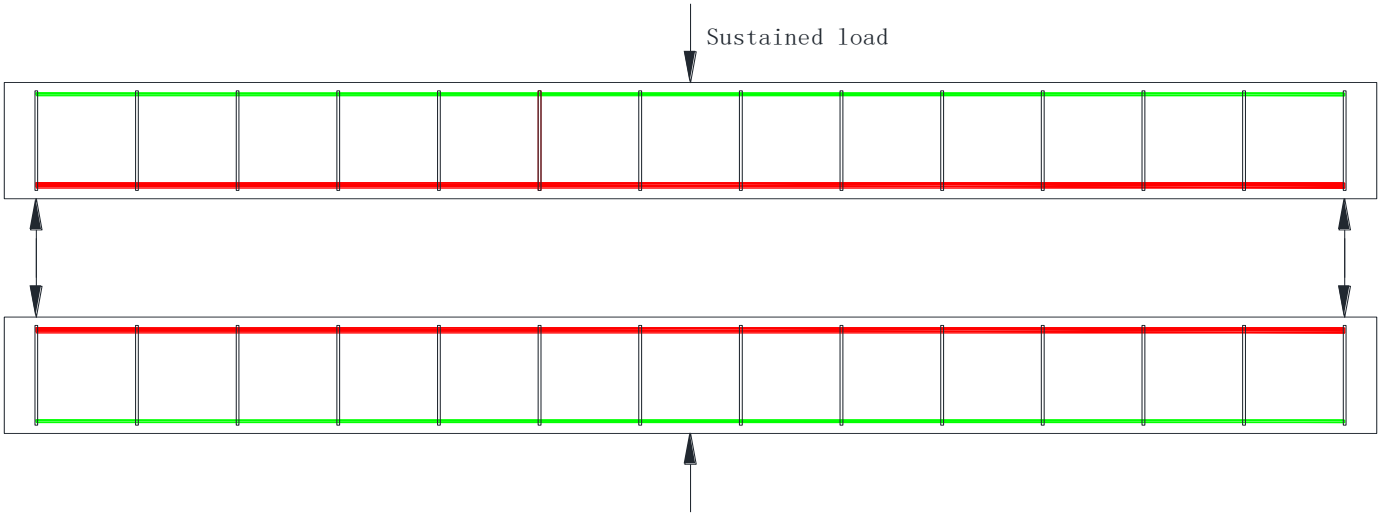

Figure IV-22 Layout of the reinforced concrete beams

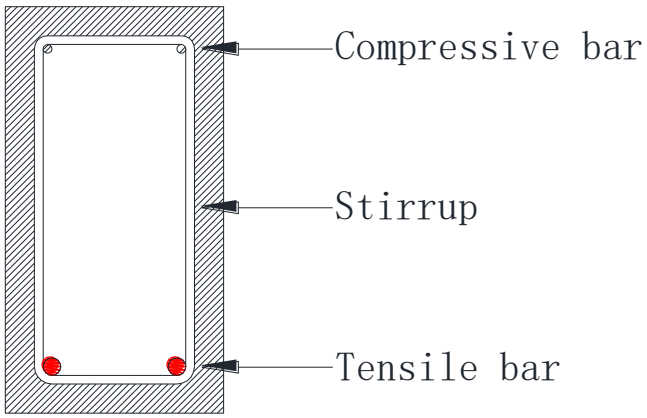

Figure IV-23 Cross-section of C beams

3.3.2 Materials

Cement (CEM Ⅰ, Grade 52.5 R) manufactured by Lafarge Cement Group Co. Ltd, with 3.15 g/cm^3 in density and 415 m^2/kg in Blaine specific surface area, was used to prepare the concrete used in this study, its chemical compositions area given in Table IV-3.

Table IV-3 Cement compositions

	SiO_2	Al_2O_3	Fe_2O_3	CaO	MgO	SO_3	Na_2O
Weight	21.4	6.0	2.3	63.0	1.4	3.0	0.5

The concrete mixture proportion is given in Table IV-4. The slump of concrete was 70 mm. The average compressive strength of the concrete at 28 days (tested on 110×220mm cylindrical specimens) was 45 MPa. The elastic modulus was 32 GPa. The tensile strength was 4.7 MPa, which was tested by splitting test on the cylindrical specimens. The porosity was about 15.2%.

Table IV-4 Concrete proportion

Mix composition		
Rolled gravel (silica+limestone)	5-15 mm	1109 kg/m^3
Sand	0-5 mm	745 kg/m^3
Portland cement OPC (high performance)		364 kg/m^3
Water		182 kg/m^3

3.3.3 Casting and curing of reinforced concrete beams

When casting these beams, the fresh concrete was placed in the framework in two layers, each approximately half of the height of the mould. An internal vibrator was used to compact concrete.

The casting direction of these beams was given in Figure IV-24, the black arrow near the cross-section of each beam means the casting direction. The red zones under the compressive bars or tensile bars according to the casting direction mean the water bleeding zones.

In the case of C1 beam, the tensile bars were the bottom casting bars according to the casting direction and the tensioned surface was the bottom surface due to sustained load. For C2 beam, the tensile bars were the bottom casting bars according to the casting direction while the tensioned surface due to the sustained load was the top surface. It is expected that no top-casting defects appear at the interface of tensile bar-concrete according to the casting direction.

In the case of C3 beam, the tensile bars were the top casting bars according to the casting direction while the tensioned surface was the bottom surface due to the sustained load. For C4 beam, the tensile bars were the casting bars according to the casting direction and the tensioned surface was the top surface according to the sustained load. It is expected that some top-casting defects appearing at the interface of tensile bars-concrete according to the top-casting effect.

After casting, all the four beams were covered with a plastic sheet in order to avoid any shrinkage cracking, then, after demoulding, they were cured in laboratory at ambient temperature for 28 days.

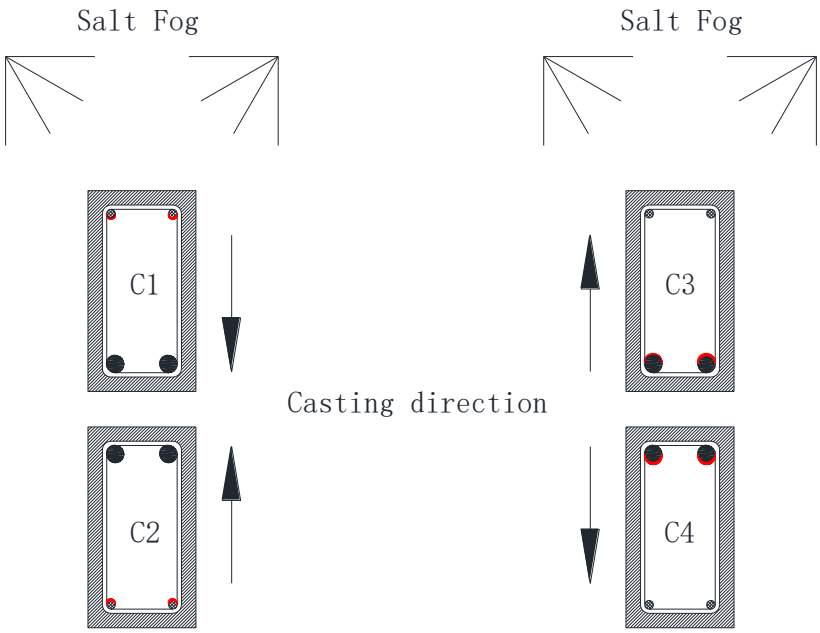

Figure IV-24 Location of the beams exposed in chloride chamber

3.3.4 Loading and exposure conditions

After curing of 28 days, a three-point loading system was used. The details in relation to the loading mode of the four beams are shown in Figure IV-25. In the case of loading system, there were two strain gauges on each threaded rod, which were used to adjust the applied load. The loading device is located at mid-span, as a result, the tensile zone of the two beams load together are located are the inner-side.

Two loading values were used Mser1= 21.2 kN•m (beams labelled C1 or C2), and Mser2 = 14.1 kN•m (beams labelled C3 and C4). Mser1 corresponds to about 80% of the failure load and is about two times the Serviceability Limit State (SLS) design to be exposed to chloride environment according the former French standard. Mser2 corresponds to about 50% of the failure load and matches the Ultimate Limit State (ULS) design in a non-aggressive environment according to former French standard[49]. In the loading device, beam C1 was above beam C2, and beam C3 above beam C4.

As a result, there are two main differences between C1-C2 and C3-C4 beams the casting direction and the loading level. Nevertheless, previous studies on two others set of RC beams[10, 11] have shown that the loading level, above the SLS limit state do not affect the corrosion process in both short and long terms.

After the load was applied, some transverse cracks can be observed on the beams, their patterns were described in ref[25] and their width on the tensile surface ranged from 65 to 830µm.

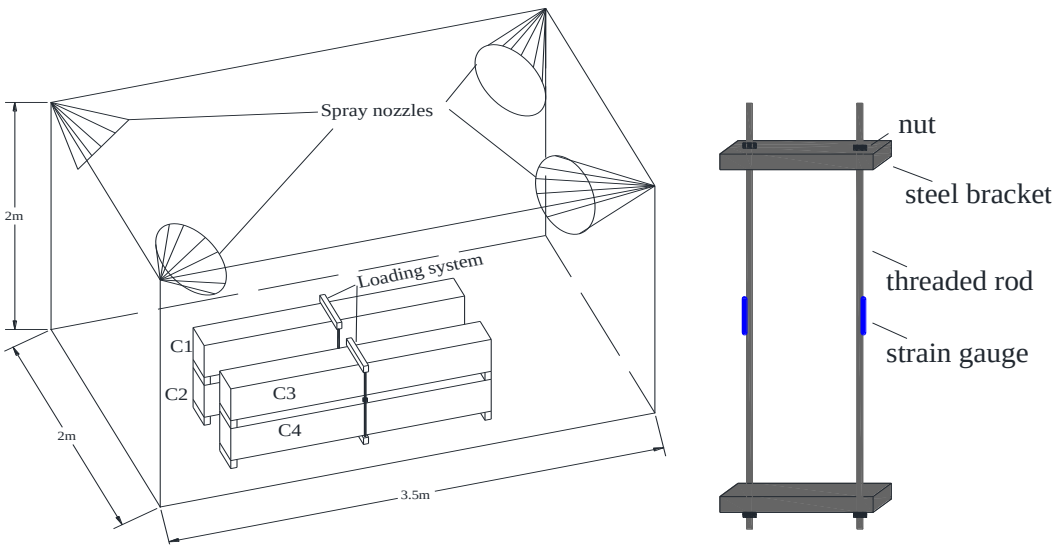

Figure IV-25 Loading system and exposure conditions

After loading, the beams were exposed to an aggressive chloride environment immediately. The aggressive environment was a salt fog (35 g/L of NaCl corresponding to the chloride concentration of sea water). All the four beams were subjected to wetting/drying cycle with two days wetting and five days drying. The temperature was the ambient temperature of southwest France, with monthly average ranging from 5.1℃ to 21.3℃ and the relative humidity of monthly average value varies from 50% to 84%.

3.3.5 Cracking maps

Prior to aggressive chloride chamber, the location and widths of load-induced cracks were recorded after loading at 28 days. And then, during exposure in the chloride environment, visual inspections were carried out periodically to check if they showed any cracks induced by corrosion. Corrosion-induced cracking of the four beams was mapped and the crack widths were measured by a video microscope having an accuracy of 0.01mm and a magnification ranging from 25 times to 175 times.

3.3.6 Top-casting-induced defects

At the end of the experimental work, some parts of C beams were observed with back scattered electron imaging (BSE) in order to characterize the presence of water-bleeding induced defect at the bottom side of re-bars. A core extracted from C3 beam was also extracted and observed by X-Ray Tomography to confirm the effect of water-bleeding defect on corrosion development. A zone in beam C3 without corrosion-induced cracks was chosen on front side tensile bar close to the support, the locations of these zones in blue block were given in Figure IV-29.

3.3.7 Chloride profiles

After the corrosion-induced cracking maps of the Group 1 and Group 2 beams had been recorded at 38 months and 48 months, respectively, some concrete powder samples were extracted from these beams for chloride concentration testing. The locations of collected samples are indicated with green circles in Figure IV-27 to Figure IV-30, the number of each green circle was given around it. Each sample of concrete powder from the tensile surface and the lateral sides of the four corroded beams was collected by dry drilling. Chloride ions were extracted with nitric acid at 80℃ and the

chloride contents were determined by potentiometric titration with $AgNO_3$. The chloride profiles were plotted to a depth of 37.5 mm in beams C1 and C2 while, for beams C3 and C4, the collection depth of concrete powder was up to 35 mm from the concrete surface. In this study, the total chloride content per unit weight of cement was determined, which was calculated from the content measured per weight of concrete, using the cement proportion in the concrete mixture.

3.3.8 Corrosion distribution along and around the tensile bar

The corroded tensile bars were extracted and cleaned chemically by immersion in Clark's solution (ISO 8407). Each corroded tensile bar was divided into 4 parts that were labeled outside-lateral surface, outside-tensile surface, inside-lateral surface, and inside-tensile surface according to their location in the beam (Figure IV-26).

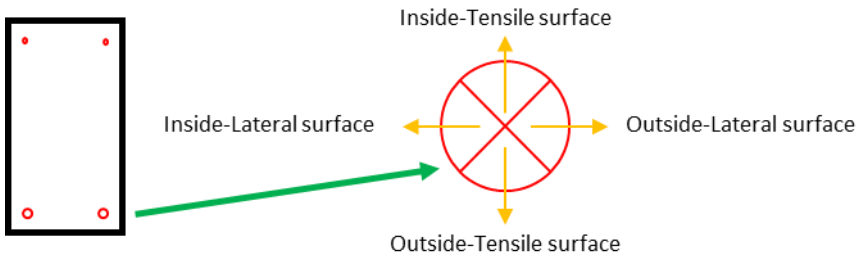

Figure IV-26 Separation in four parts around the perimeter of tensile bars according to the location of concrete

A quantitative description of the location of corrosion pits around the perimeter of tensile bars was noted according to the four zones defined in Figure IV-26. Then, the weight loss of the steel bars was used to calculate the loss of cross-section. The bars were cut into short pieces of different lengths according to the corrosion pattern (pitting or general corrosion) and corrosion details. The length of each section depended on the corrosion condition along the bar and was measured with vernier calipers with an accuracy of 0.02 mm. Each short section was weighed on a balance with an accuracy of 0.01g. The loss of cross-section was then calculated with Equation 1. The original mass of the short sections was calculated with Equation 2.

$$\Delta As = \frac{Mo-M}{Mo} \times As \qquad \text{Equation 1}$$

$$Mo = \rho \times As \times L \qquad \text{Equation 2}$$

where ρ (g/cm^3) is the density of the steel bar, considered to be 7.85 g/cm^3;

L (mm) is the length of each short section;

Δ As (mm^2) is the average loss of cross-section of the corroded bars over the short section length;

As (mm^2) is the nominal cross-section of the steel bars;

M (g) is the residual mass of the short sections of corroded bars;

Mo (g) is the nominal mass of the steel bars.

3.4 Experiment Results

3.4.1 Maps of corrosion-induced cracks according to time

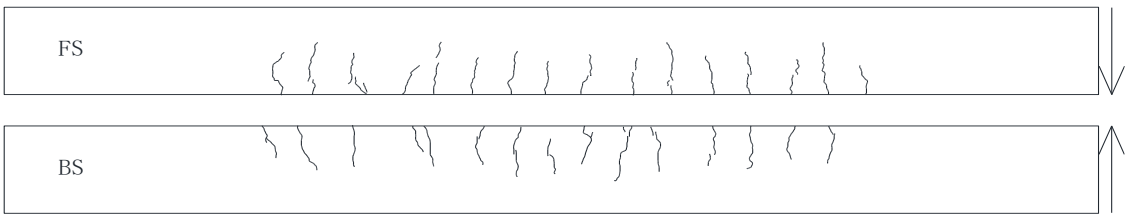

Figure IV 29.1 Cracking situation on C1 beam at 28 days

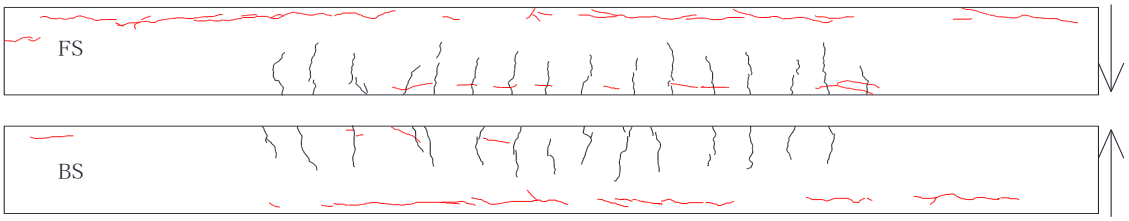

Figure IV 29.2 Cracking situation on C1 beam at 29 months

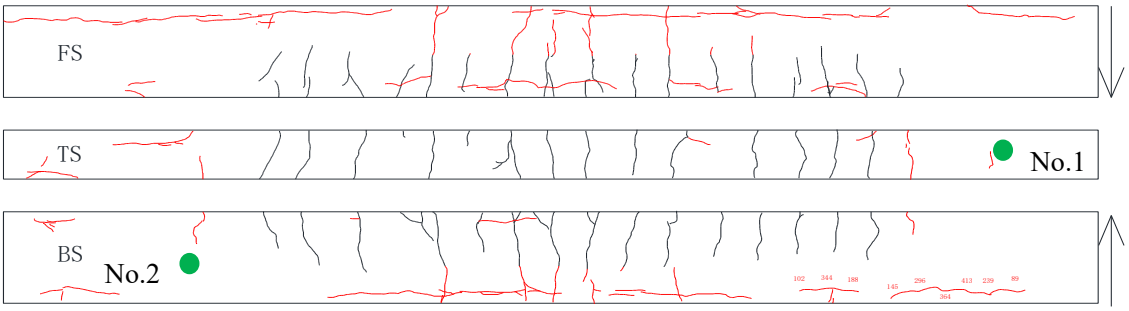

Figure IV 29.3 Cracking situation on C1 beam at 38 months

Figure IV-27 Cracking situation on C1 beam

(The red lines in Figures 6~9 represent corrosion-induced cracks, while the black lines correspond to load-induced cracks. The black arrows on the right side represent the casting direction of concrete; the blue block means the location of the sample used for BSE or X-Ray Tomography.)

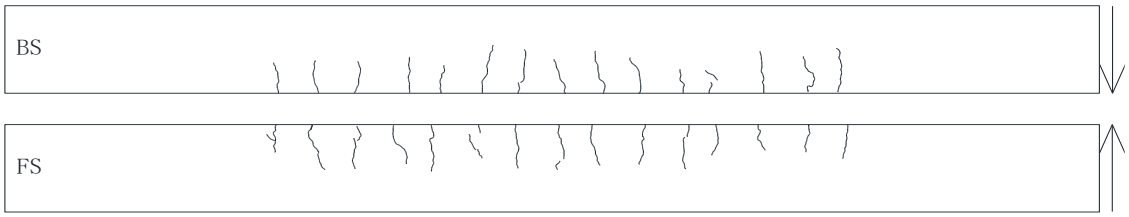

Figure IV 30.1 Cracking situation on C2 beam at 28 days

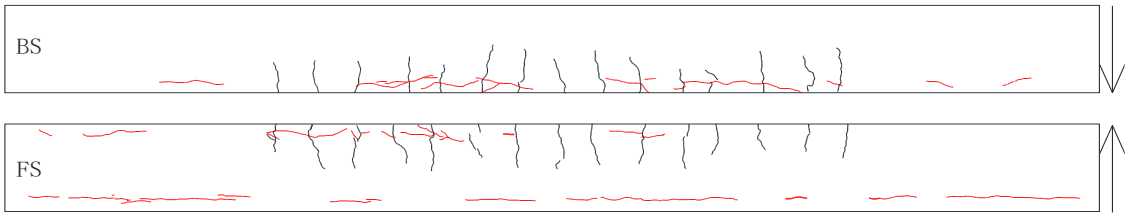

Figure IV 30.2 Cracking situation on C2 beam at 29 months

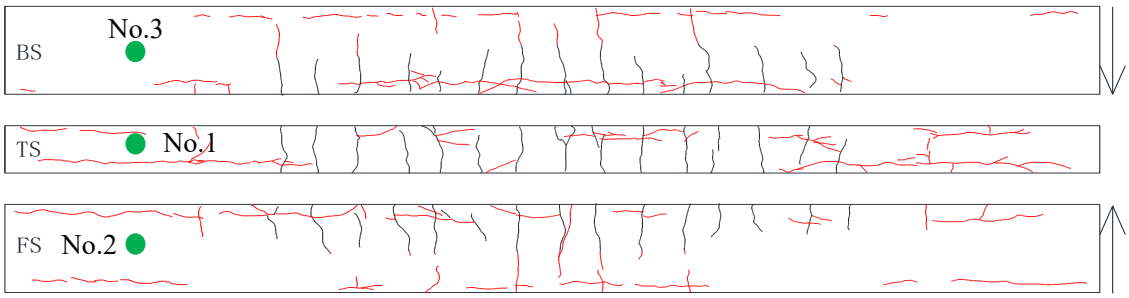

Figure IV 30.3 Cracking situation on C2 beam at 38 months

Figure IV-28 Cracking situation on C2 beam

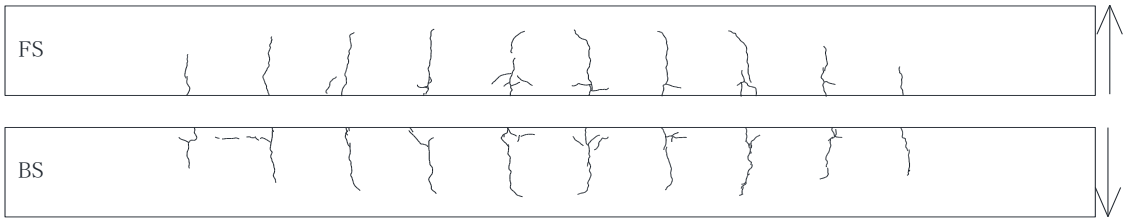

Figure IV 31.1 Cracking situation on C3 beam at 28 days

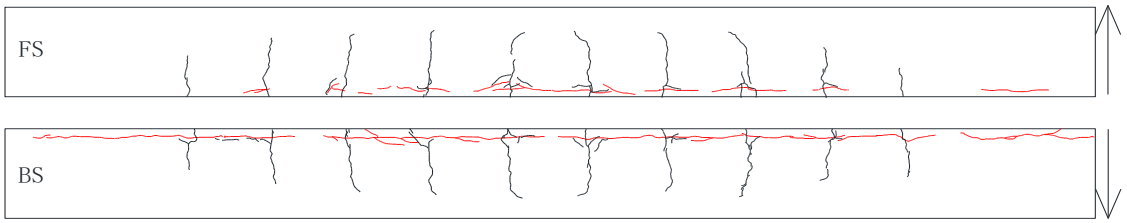

Figure IV 31.2 Cracking situation on C3 beam at 29 months

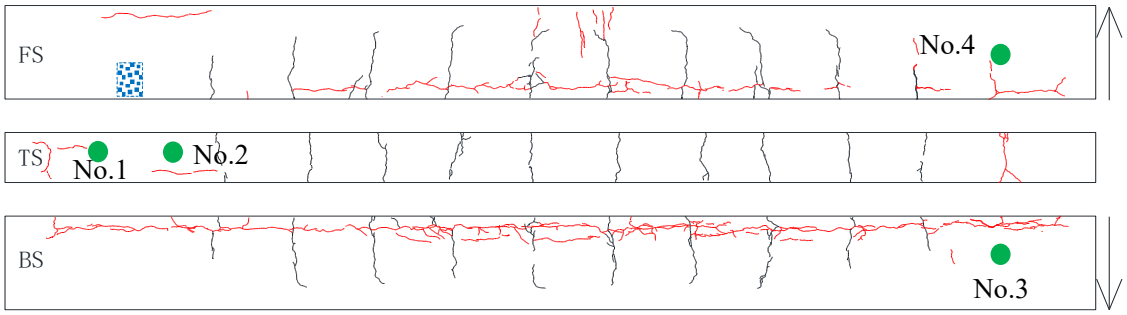

Figure IV 31.3 Cracking situation on C3 beam at 48 months

Figure IV-29 Cracking situation on C3 beam

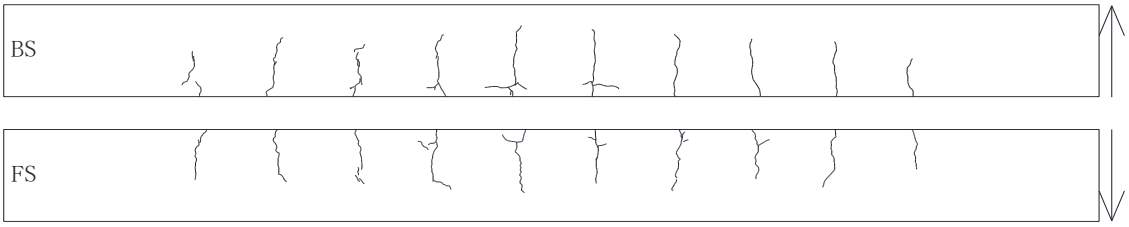

Figure IV 32.1 Cracking situation on C4 beam at 28 days

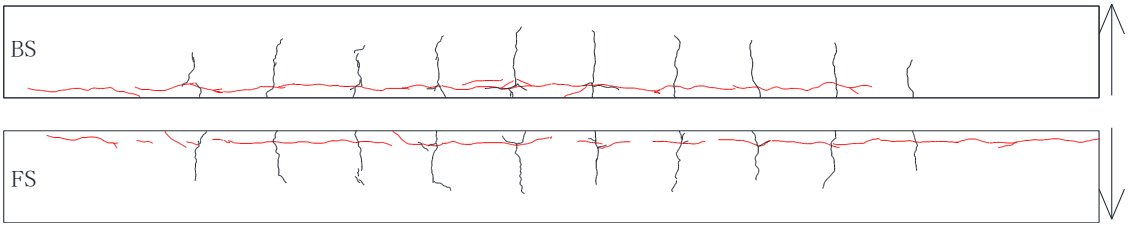

Figure IV 32.2 Cracking situation on C4 beam at 29 months

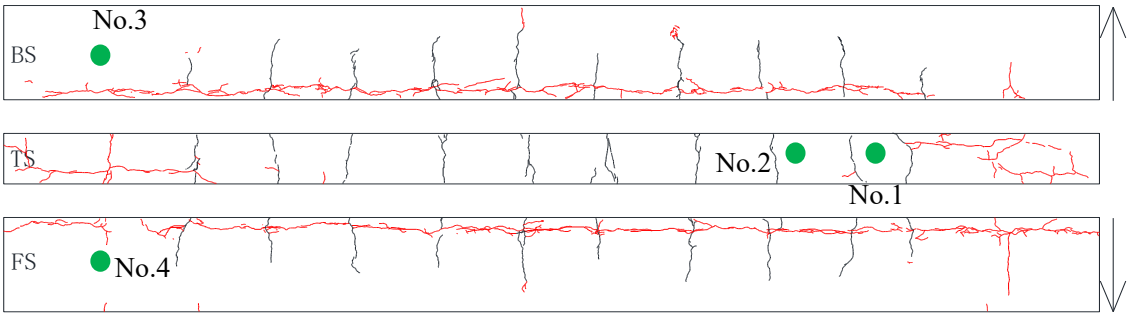

Figure IV 32.3 Cracking situation on C4 beam at 48 months

Figure IV-30 Cracking situation on C4 beam

The cracking states of tensile surface and lateral faces of the C beams are shown on the cracking maps of Figure IV-27. Before the beams were subjected to the aggressive environment, the distribution of load-induced cracks formed by the three-point-bending system on C beams was recorded. The cracking maps are presented in Figures IV-29.1, IV 30.1, IV 31.1 and IV 32.1, respectively for beams C1 to C4.

For beam C1, no corrosion-induced cracks had appeared on tensile parts at 24 months of

exposure [25]. At 29 months, a few tiny discontinuous corrosion-induced cracks were visible in the vicinity of the tensile zones. More corrosion-induced cracks were found in the same area at 38 months of exposure (Figure IV-27).

For beam C2, no corrosion-induced cracks were visible on tensile parts after 24 months of exposure [25]. At 29 months and 38 months, cracking in the tensile zones was similar to that observed on beam C1 (Figure IV-28).

For beam C3, after 8 months of exposure to the chloride environment, some corrosion-induced cracks were visible on the surfaces of tensile zones and they became continuous and wider at 24 months [25]. After 29 months of exposure, the cracking patterns were not significantly different from those at 24 months. After 48 months of exposure, some new corrosion-induced cracks had appeared on the tensile zones (Figure IV-29).

For beam C4, in Figure IV-30, as for beam C3, after 8 months of exposure to the chloride environment, some corrosion-induced cracks were visible on the surfaces of tensile zones and became continuous and wider at 24 months [25]. After 29 months and 48 months of exposure, the results concerning the corrosion-induced cracks on the tensile zones was similar to those obtained with beam C3.

3.4.2 Characterization of top-cast defects at the steel-concrete interface

Observations by BSE were performed on TOP bars and BOTTOM bars of C beams according to casting direction to characterize the water-bleeding defects on bottom side of top-cast bars (call top-casting-induced defects). Figure IV-31.1 and Figure IV-31.2 show that bottom side of top-cast bars exhibit a gap between steel and concrete which size varies from 0.1 mm to 0.35 mm along the bar. On the contrary, Figure 10.3 shows that the bottom side of bottom-cast rebars is perfectly linked to concrete and that no visible defect is present.

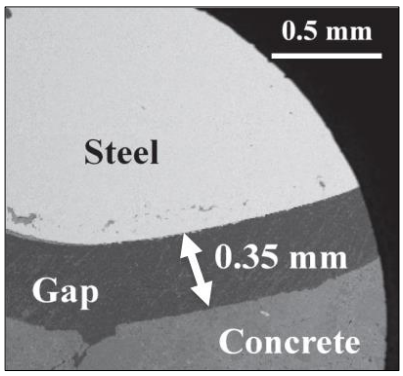

IV 33.1 Bottom side of top bar

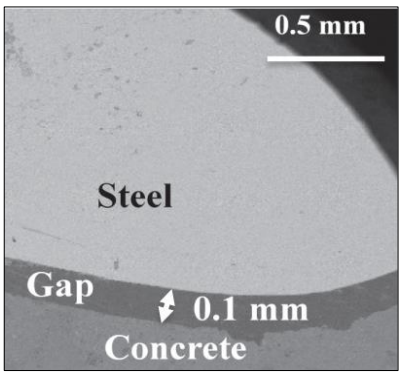

IV 33.2 Bottom side of top bar

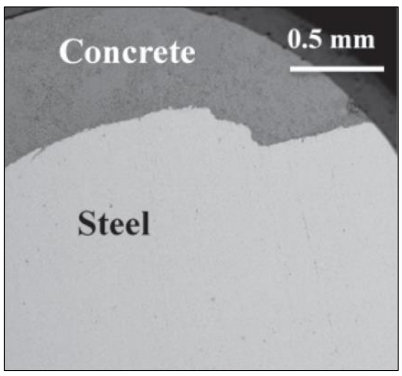

IV 33.3 Bottom side of bottom bar

Figure IV-31 Comparison between bottom side of top-cast bars and bottom-cast bar of C beam

Steel-concrete interface was also observed on top side of both top-casting and bottom-casting rebars. Figure IV-32 show a typical view of the top-side interface which appears to be exempted of any visible defects.

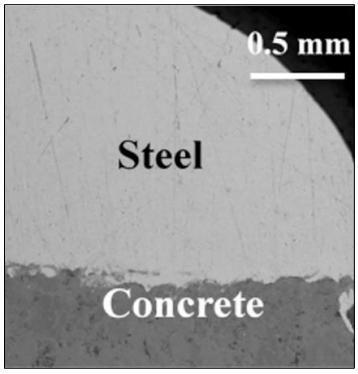

Figure IV-32 Typical view of steel-concrete interface on top side of top-casting bar without any visible defects, same result is obtained on bottom bar

Some cores were also extracted from C3 beam in zones far from load-induced cracks, close to support and then observed by X-ray Computed Tomography (CT). Figure IV-33shows that corrosion products have formed on the bottom side of the top-cast bar in the water-bleeding void which is visible all along the interface. On the contrary no corrosion is visible on the top side of the bar.

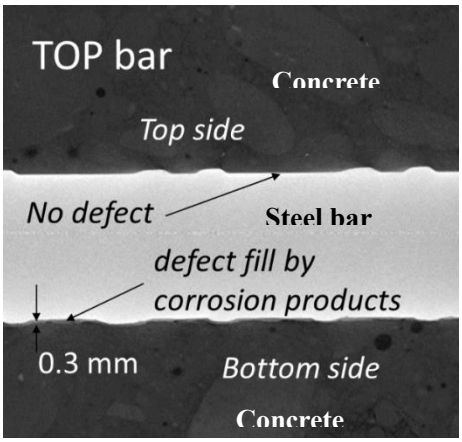

Figure IV-33 X-Ray CT image of top-casting bar of C3 beam water-bleeding defects filled by corrosion products are clearly visible all along the steel-concrete interface

3.4.3 Penetration of chloride ions

C1 and C2 beams were tested before C3 and C4 beams because of the appearance of corrosion-induced cracks in front of their compressive reinforcements at 24 months, which was not the case for C3 and C4. Analysing C1 and C2 beams in first allows to check the effect of bleeding defects on the corrosion of compressive reinforcements. As a result, penetration profiles of chloride ions do not correspond to the same term for beams C1 and C2 and C3 and C4.

The penetration of chloride ions at different depths from the tensile and lateral surfaces of the reinforced concrete are described in Figure IV-34 and Figure IV-35, respectively. From Figure IV-34 and Figure IV-35, it can be noted that the chloride ion concentration was significantly higher than usual chloride threshold initiating corrosion. The two figures also indicated that chloride content in concrete was higher when the tensile surface corresponded to the top-exposed surface to salt fog, which could be explained by chloride accumulation at the top surface and gravity effect combined with convection from the top surface[30].

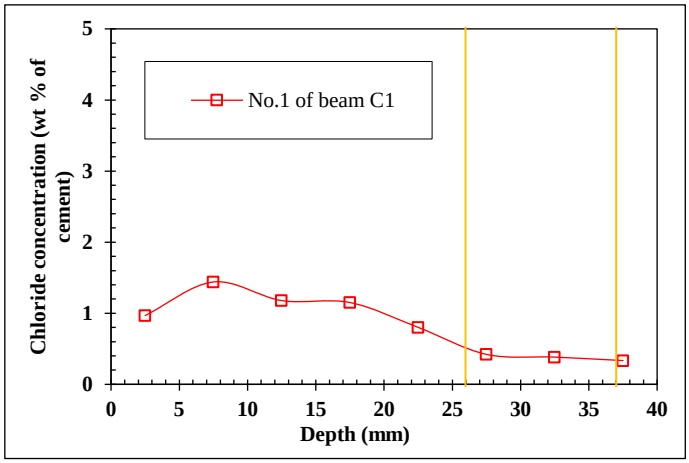

Figure IV-34.1Tensile surface of beam C1

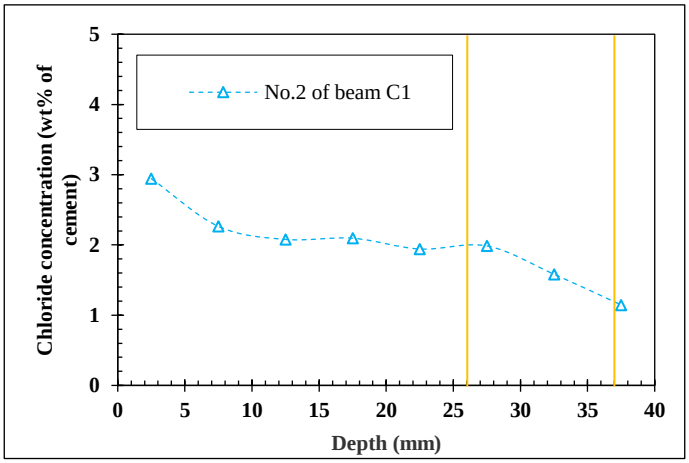

Figure IV-34.2 Lateral surface of beam C1

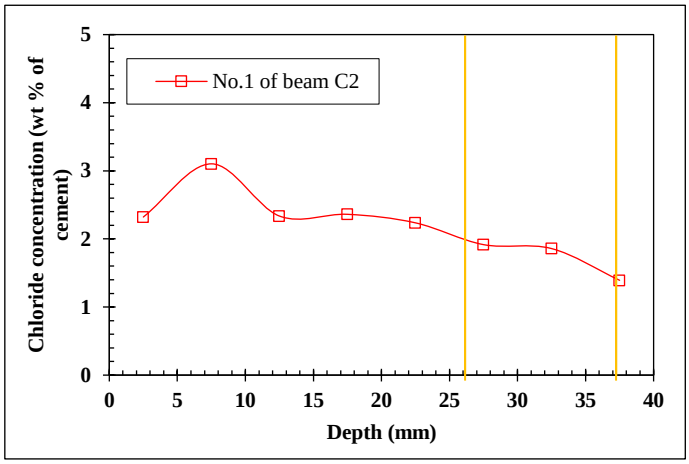

Figure IV-34.3Tensile surface of beam C2

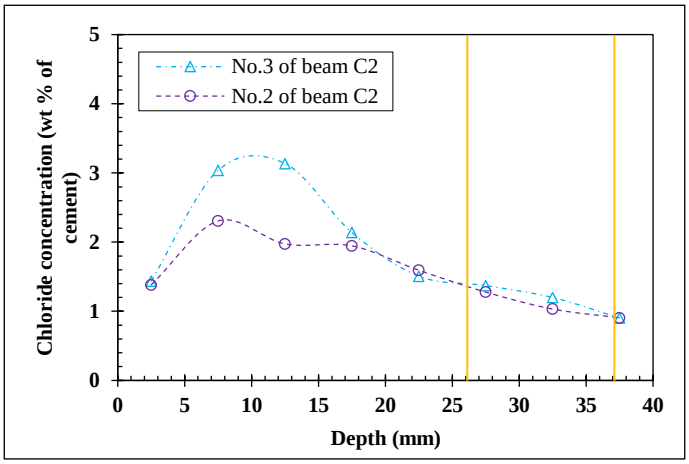

Figure IV-34.4 Lateral surface of beam C2

Figure IV-34 Chloride profiles on the beam C1 and beam C2 after 38 months of exposure

(The yellow lines show the location of tensile bar and the distance between them represents its diameter.)

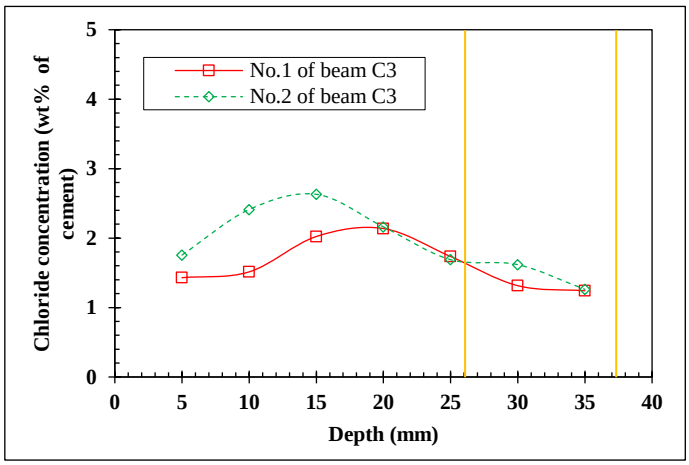

Figure IV-35.1 Tensile surface of beam C3

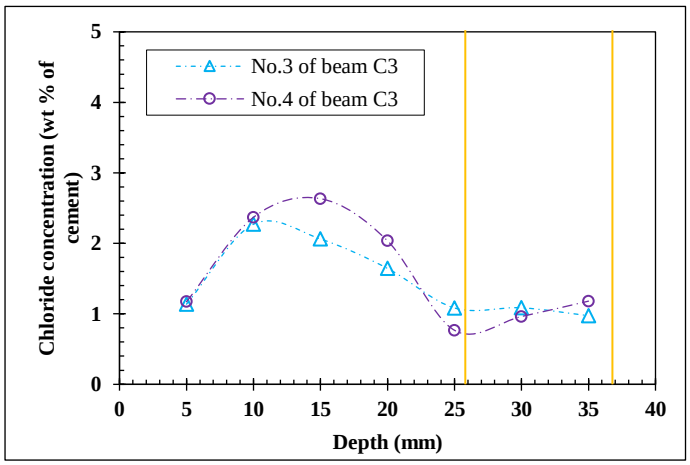

Figure IV-35.2 Lateral surfaces of beam C3

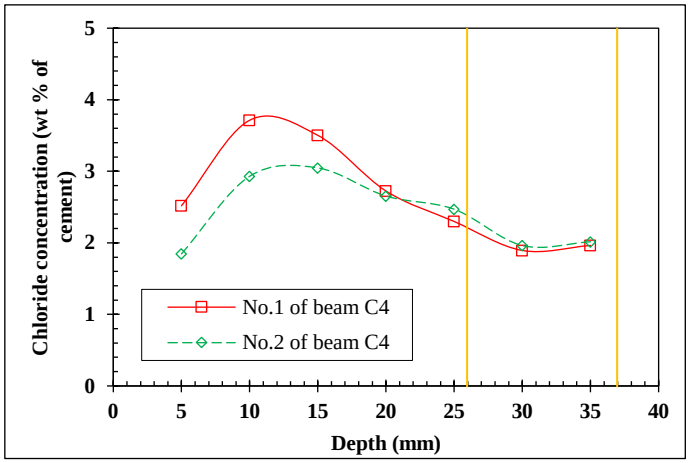

Figure IV-35.3 Tensile surface of beam C4

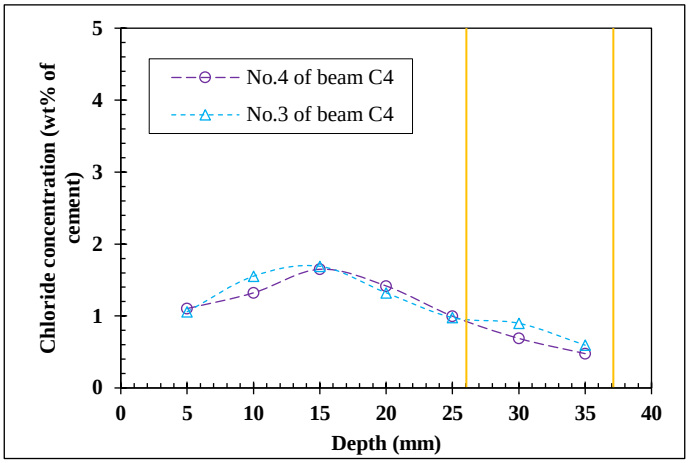

Figure IV-35.4 Lateral surfaces of beam C4

Figure IV-35 Chloride profiles on beam C3 and bean C4 after 48 months of exposure

(The yellow lines show the location of tensile bar and the distance between them represents its diameter.)

The chloride profiles appear to be quite flat, because the chloride penetration is more like a convection process than a diffusion process. This is quite logical since the exposure corresponded to wetting (2 days) drying (5 days) cycles. Moreover, despite the quite short term, there is a convection zone about 10-15 mm long starting from the outer surface where the chloride content is weaker, which confirms the strong convection effect.

Chloride profiles for beams C1 and C2 were recorded 10 months before the profiles on beams C3 and C4 and it appears (see Figure IV-34 and Figure IV-35) that the difference is small, which means that, due to convection, the amount of chlorides close to the rebars was significant in a short duration.

3.4.4 Cross-sectional loss of tensile bars

The cross-sectional losses of tensile bars embedded in the four C beams are described in Figure IV-36. Because measurement of the loss of cross-section is a destructive test, it corresponded to the end of the experiment durations 38 months pour beams C1 and C2, and 48 months for beams C3 and C4.

For beams C1 and C2, tensile bars were bottom-cast bars and the average corrosion degree was quite similar (less than 5%). Nevertheless, C1 exhibited deeper pits than C2. This phenomenon could be linked to the coupled effect of corrosion-induced cracks and moisture conditions which are different at bottom tensile surface (beam C1) and top tensile surface (beam C2) large moisture conditions decreasing the macro-cell effect. A similar phenomenon was spotted by Zhu et al. for

bottom tensile exposure [40].

For beams C3 and C4, tensile bars corresponded to top-cast bars and the average corrosion degree was also quite similar to, but significantly higher than, in C1 and C2 (more than 10%). C3 exhibited deeper pits than C4, which could, again, be linked to the exposure conditions. More chlorides entered via the tensile surface for C4, which was the exposed top tensile surface (Figure 14). Similar experimental results for top tensile exposure have been recorded by Dang and François and Yu et al. [30, 44, 46, 47].

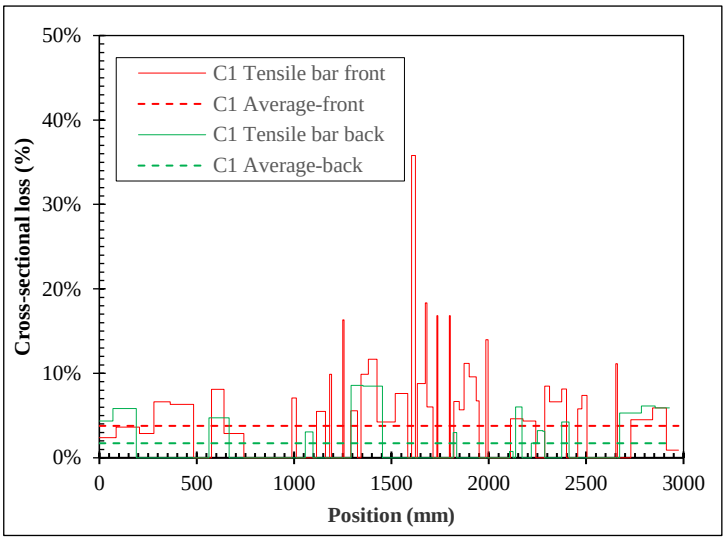

Figure IV-36.1 C1 at 38 months

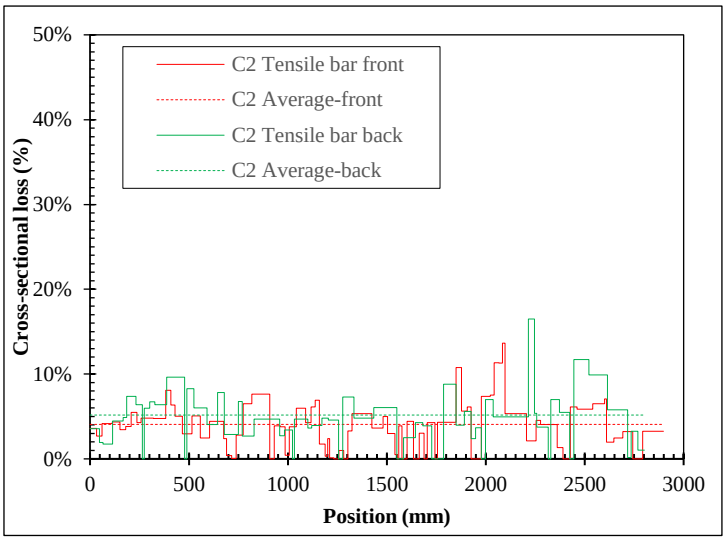

Figure IV-36.2 C2 at 38 months

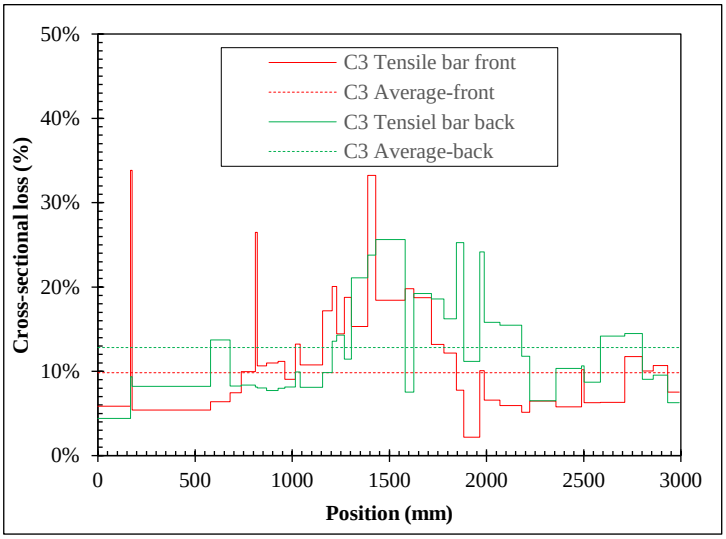

Figure IV-36.3 C3 at 48 months

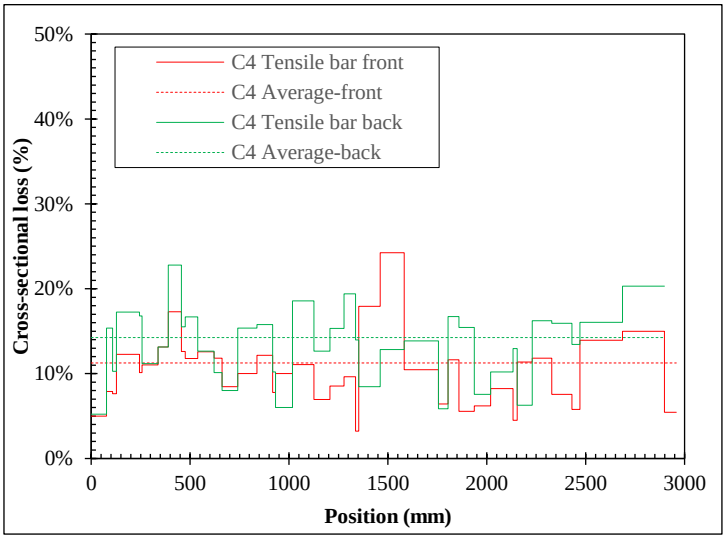

Figure IV-36.4 C4 at 48 months

Figure IV-36 Cross-sectional loss of tensile bars embedded in C beams

3.5 Discussion

It is generally reported that the effect of load-induced cracks on corrosion diminishes with time, becoming negligible in the long term[50]. It is therefore interesting to discuss the effect of load-induced cracks on corrosion development in this study, considering the relatively short duration of the experiments (less than 4 years.)

3.5.1 Effect of service cracks (and their widths) on the corrosion of tensile bars

Figure IV-37 and Figure IV-38 present the superposition of the cracking maps and the corrosion maps for the tensile bars of C beams from the bottom, top and outside directions.

From the location of corrosion zones and the location of load-induced cracks, it is clear that there is no correlation between them and that the corrosion zones appear randomly distributed along the bars. This result is in accordance with previously reported results [42].

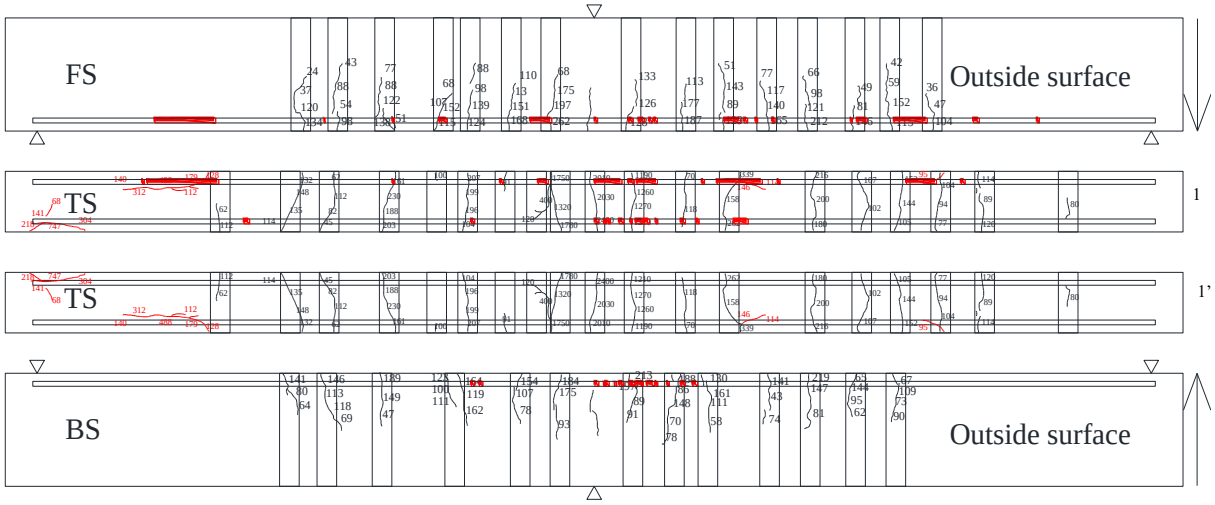

Beam C1

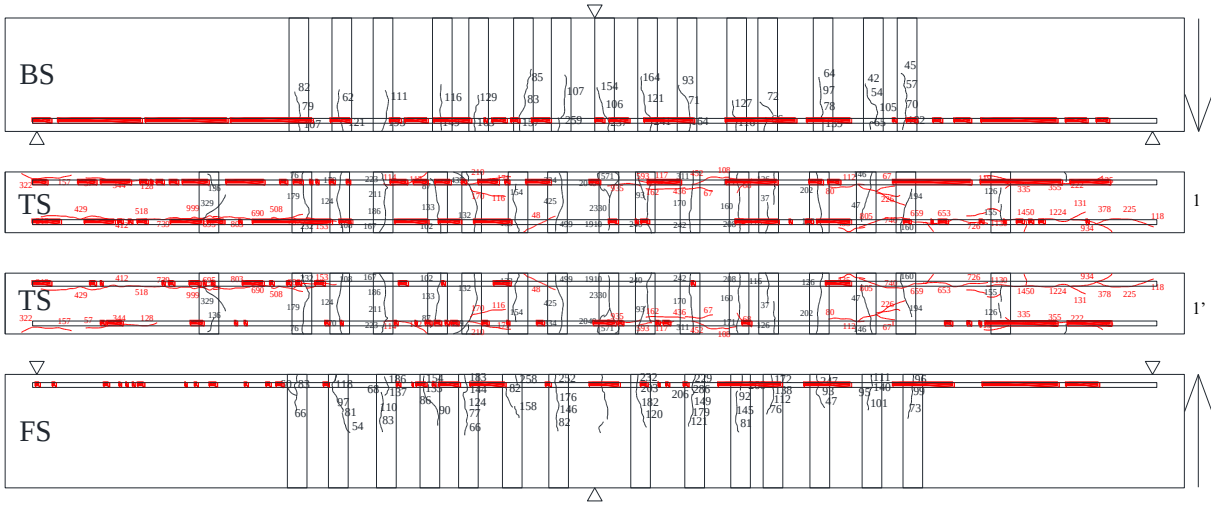

Beam C2

Figure IV-37 Corrosion maps of beam C1 and C2

(The red zones mean the corrosion area of reinforcement steel; Arrows on the right side mean the casting direction; 1 and 2 represent the bottom surface of front and back tensile bars respectively, 1' and 2' mean the top surface of front and back tensile bars respectively.)

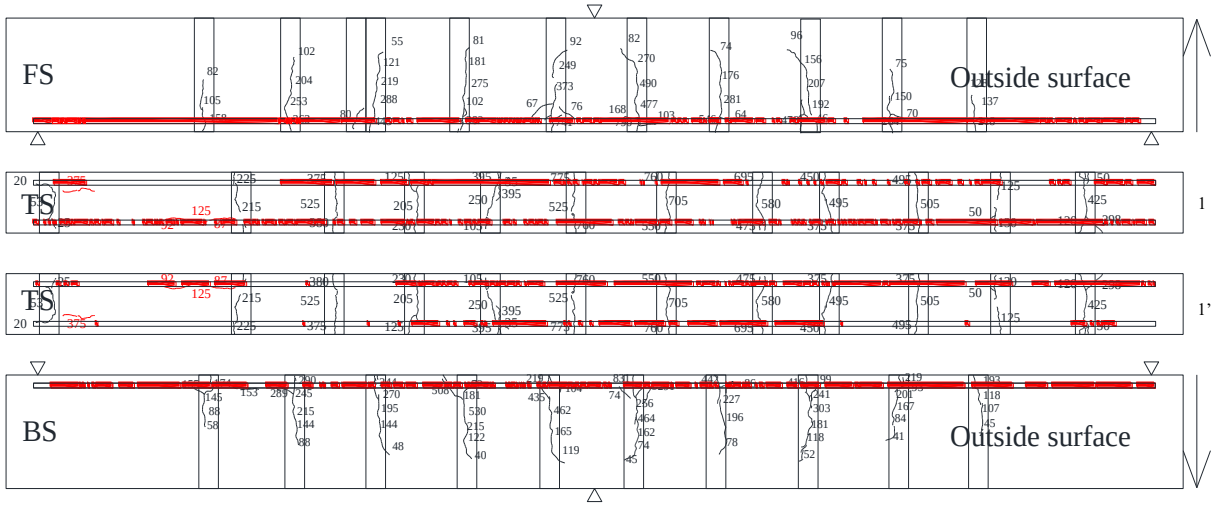

Beam C3

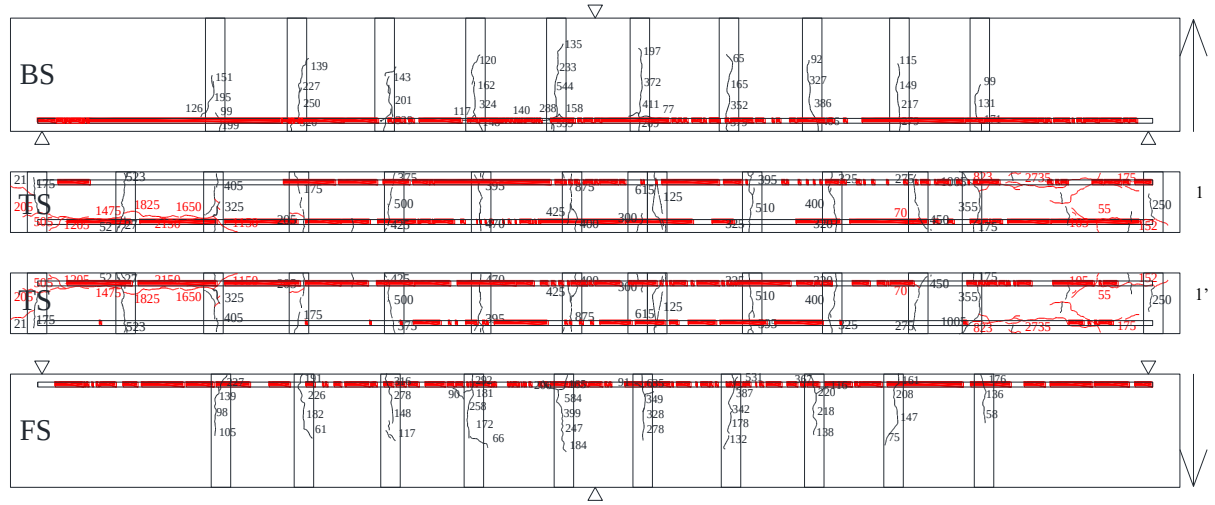

Beam C4

Figure IV-38 Corrosion maps of beam C3 and C4

(The red zones mean the corrosion area of reinforcement steel; Arrows on the right side mean the casting direction; 1 and 2 represent the outside-tensile surface of front and back tensile bars respectively, 1' and 2' mean the inside-tensile surface of front and back tensile bars respectively.)

To further investigate the effect of service crack width on the corrosion development of reinforcement bars, the relationship between this width and the loss of cross-section of tensile bars embedded in C beams was investigated.

Concerning the effect of load-induced crack widths on the degree of corrosion, an interval 50 mm wide was defined around each service crack (see the black vertical lines around the service cracks in Figure IV-37 and Figure IV-38) and represented the length of damage of the steel/concrete interface resulting from load-induced cracks [51]. As a result, all the corrosion pits found in the interval of 50 mm were considered to be due to the presence of the load-induced crack. The results are illustrated in Figure IV-39. On the other hand, a corrosion pit found outside the interval of 50 mm is considered to be no correlated with the crack and then correspond to 0 mm width service crack.

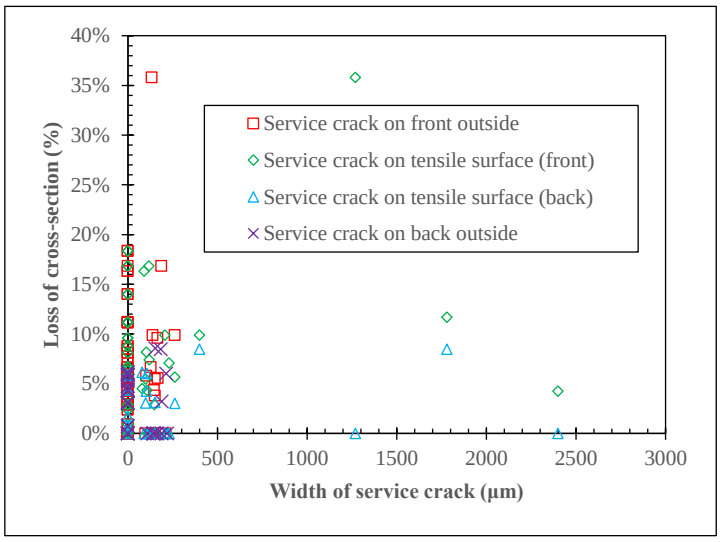

Figure IV-39.1 C1 beam

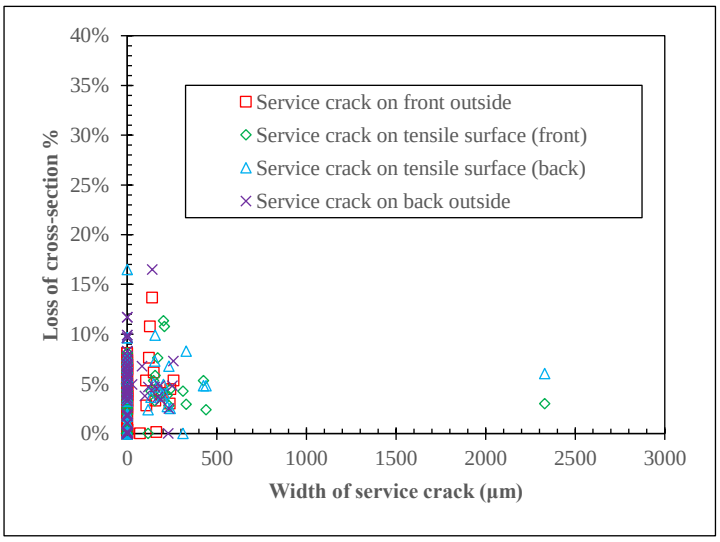

Figure IV-39.2 C2 beam

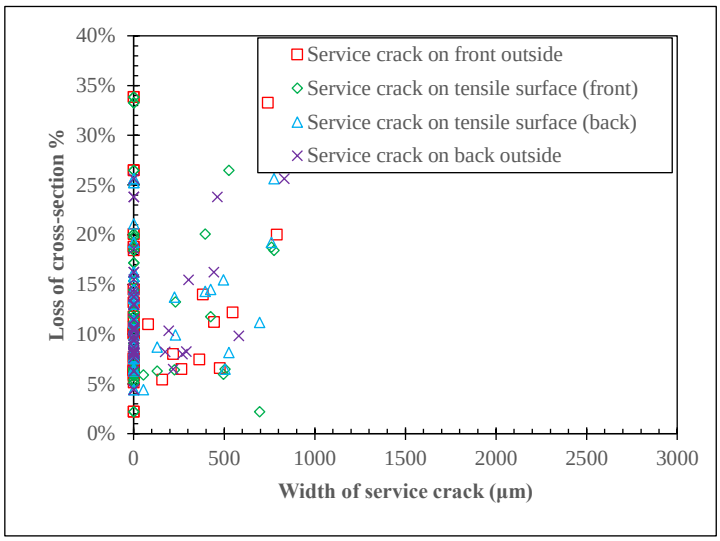

Figure IV-39.3 C3 beam

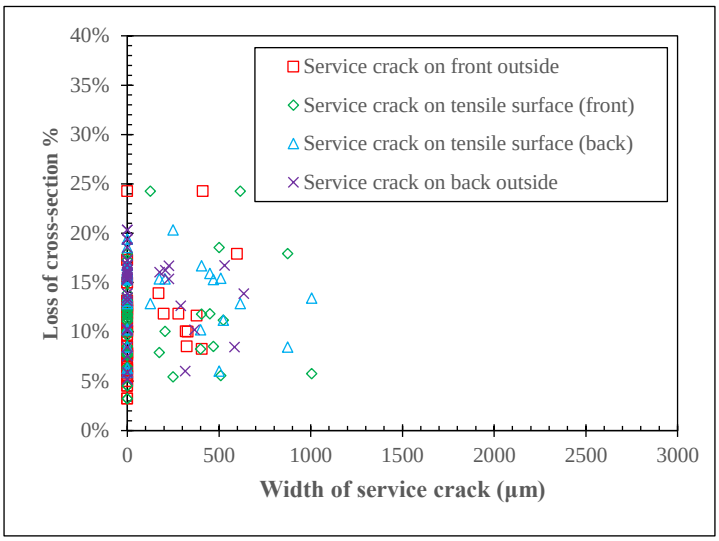

Figure IV-39.4 C4 beam

Figure IV-39 Relationship between service cracking width and loss of cross-section of tensile bar

Figure IV-39 shows no correlation between the width of service cracks and the loss of cross-section of tensile bars. Moreover, zones far from service cracks and zones without service cracks (close to the supports) show the same loss of cross section as zones in front of service cracks.

The locations of pits do not correspond to the locations of the cracks, even if we consider a 50 mm length of rebar around the cracks. For C1 and C2 without casting-induced-defects, it would be expected that corrosion develops firstly close to load-induced cracks but it was not the case as corrosion-induced cracks appear only after more than 24 months of exposure at a time where chlorides ingress through the cover was sufficient to initiate corrosion, which explains the presence of corrosion damage all along the bars.

Moreover, for C1 and C2 beams, there are some minor service cracks not associated with initiation of corrosion this result could be explained by a kind of cathodic protection induces by the macro-cell corrosion at major cracks as it was also observed by Susuki et al[52].

For C3 and C4 with the presence of top-casting-induced defects, it seems that these defects allow chlorides to penetrate along the tensile bars and corrosion to develop at the weakest points of the steel/concrete interface all along the tensile bars. The fact that both corrosion-induced cracks appear after only 8 months of exposure and average degrees of corrosion are significantly higher for C3 and C4 in comparison with C1 and C2 tends to confirm this assumption.

Similar conclusions were also proposed by François and Arliguie[2], Zhang et al.[24] and Dang and François[47] but some arguments considering the long duration of the experiments were

developed to explain the possibility that only the long-term corrosion is not correlated with service cracks. The results presented in this experiment correspond to a relatively short term and confirm that the widths of service cracks have no effects on corrosion development and, moreover, that even the presence of load-induced cracks does not influence corrosion development in the absence of top-cast defects at the SCI. Of course, this result could be modified by the loading conditions in this experiment, sustained loading could favor the healing of cracks by corrosion products, which would not be the case for cyclic loading, for which the dynamics need further investigations.

It could be considered that service cracks provided direct access of chlorides to rebars, leading to the development of corrosion at the weakest points of the steel/concrete interface and not necessarily at crack locations [50]. However, from the results put forward in this section, it appears that corrosion is related to the penetration of chlorides through cracks only in the case of top-casting-induced defects. Without top-casting-induced defects, corrosion is related to the penetration of chlorides through the concrete cover even in the presence of load-induced cracks.

3.5.2 Effect of top-casting-induced defects on the evolution of corrosion-induced cracking in tensile zone

In this section, the effect of top-casting-induced defects on the corrosion development of tensile bars will be discussed. The evolution of the length of corrosion-induced cracks is considered as a nondestructive parameter to monitor corrosion development.

- **Case of absence of top-casting-induced defects around the tensile bars beams C1 and C2**

For beam C1 without top-casting-induced defects around the tensile bars, there were no corrosion-induced cracks after 24 months of exposure and, in the case of beam C2, only tiny corrosion-induced cracks had appeared at 24 months of exposure (Figure IV-40). Because service cracks led to a shortening of the initiation stage, the absence of corrosion-induced cracks on C1 beams after 24 months of exposure is the sign that corrosion did not propagate after earlier initiation at load-induced cracks.

This period before 24 months corresponds to the “induction period” defined in [53, 54]. Load-induced cracks on the tensile surface of beam C1 and C2, providing direct access for chlorides, initiated corrosion but did not lead to propagation, thanks to the healing of cracks by the first

corrosion products.

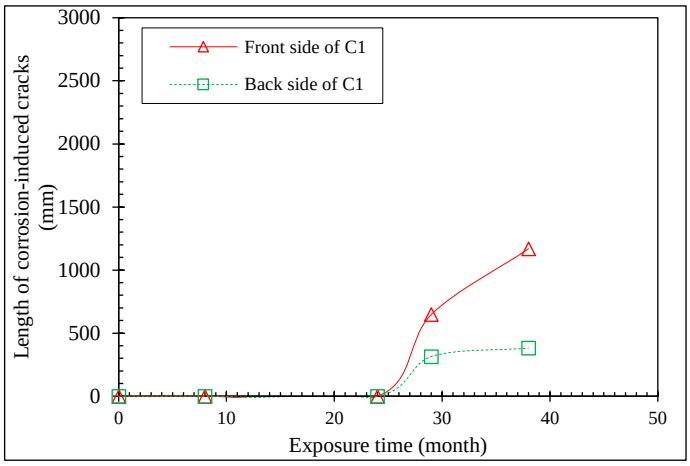

Figure IV-40.1 Beam of C1

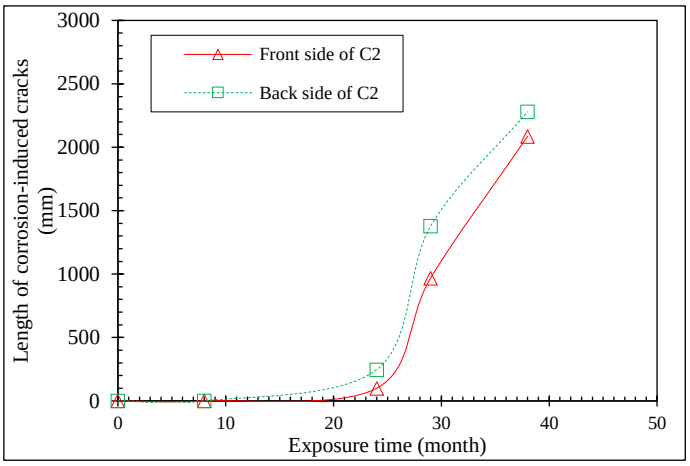

Figure IV-40.2 Beam of C2

Figure IV-40 Evolution of the length of corrosion-induced cracks versus time for C1 and C2 beams

Consequently, the first corrosion-induced cracks are only visible for both C1 and C2 beams at 29 months of exposure but appear at the same time close to a support (i.e. far from load-induced cracks) and close to some load-induced cracks.

This confirms that, without top-casting-induced defects, load-induced cracks or load-induced damage have no effect on the corrosion propagation.

➢ **Case of presence of top-casting-induced defects around the tensile bars beams C3 and C4**

For beams C3 and C4, with top-casting-induced defects at the steel/concrete interface, the corrosion had started to propagate before 8 months of exposure (Figure IV-41), leading to the appearance of corrosion-induced cracks. This result suggests a possible ingress of chloride along the interface, favored by the top-casting-induced defects, and then the development of many corrosion pits all along the steel bars.

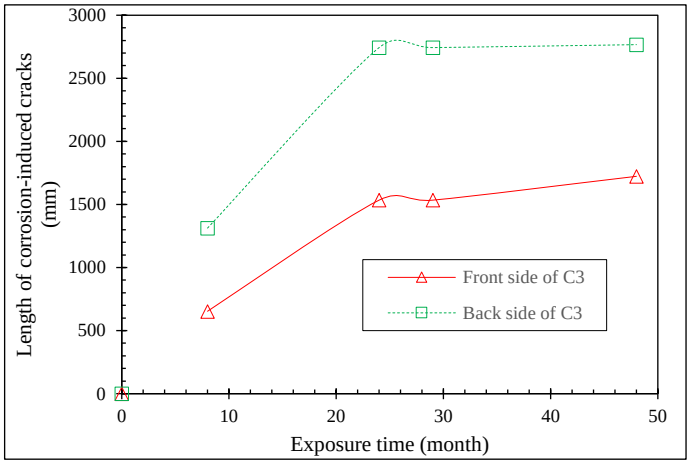

Figure IV-41.1 Beam of C3

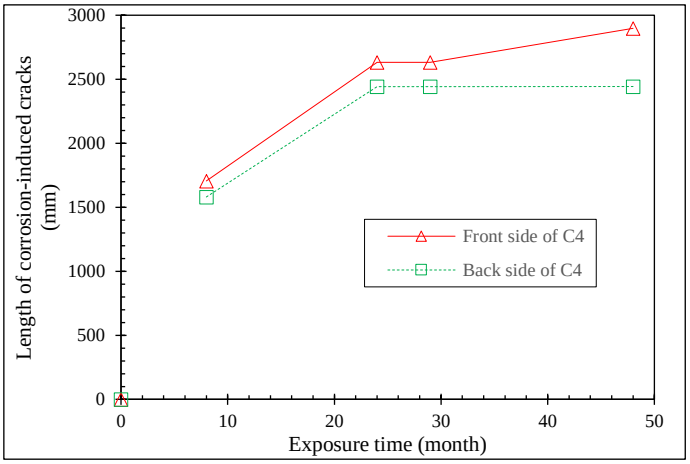

Figure IV-41.2 Beam of C4

Figure IV-41 Evolution of length of corrosion-induced cracks versus time for C3 and C4 beams

Consequently, the first corrosion induced cracks are visible for both C3 and C4 beams at only 8 months of exposure, close to load-induced cracks but also all along the beams.

This shows that, with top-casting-induced defects, there is an effect of load-induced cracks which is linked, not to the intensity of the load or the size of the cracks, but to the fact that cracks facilitate chloride access to the re-bars[2, 3, 5, 7]. As a result, chlorides can then spread all along the rebars because of defects, developing corrosion at the weakest points of the SCI and then leading to fast propagation of corrosion that is not correlated with the location and size of cracks.

3.5.3 Effect of top-casting-induced defects on both average and maximum cross-sectional loss of tensile bar

At the end of the experiments 38 months for C1 and C2 beams and 48 months for C3 and C4 beams, both the average and maximum degrees of corrosion were measured.

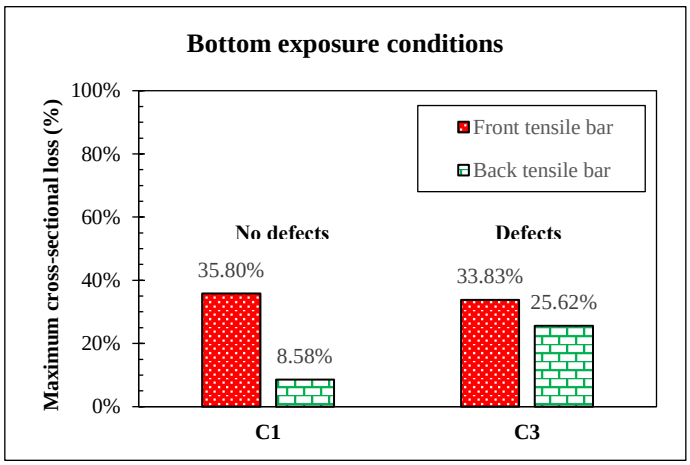

Figure IV-42.1 Maximum cross-sectional loss

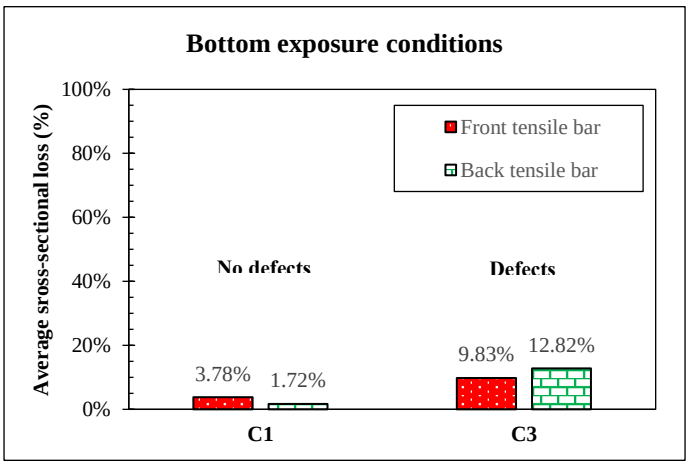

Figure IV-42.2 Average cross-sectional loss

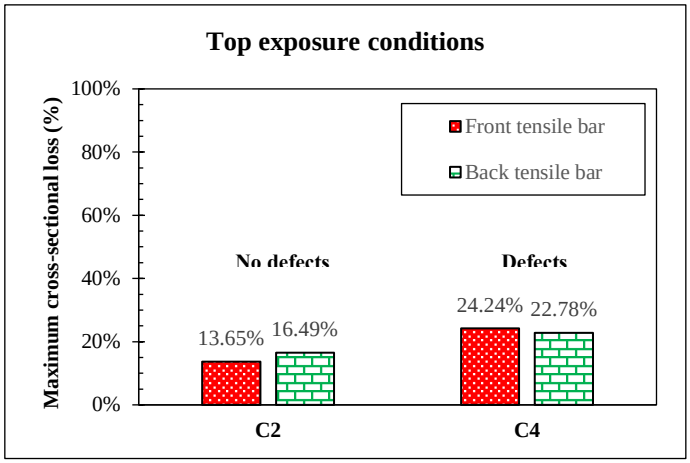

Figure IV-42.3 Maximum cross-sectional loss

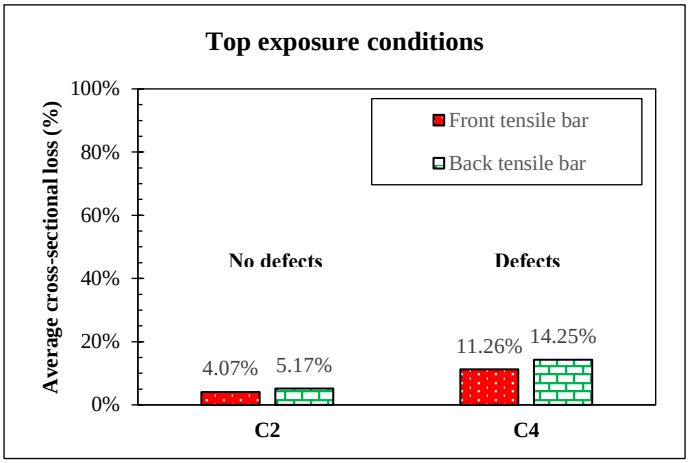

Figure IV-42.4 Average cross-sectional loss

Figure IV-42 Effect of defects on the loss of cross section of tensile bar

Figure IV-42 presents the loss of cross section of tensile bars for the four beams, in both average value and maximum value. Each picture shows a comparison of tensile bars with or without top-casting-induced defects. The main result is that average corrosion is significantly higher in the case of top-casting-induced defects than without them. Maximum loss of cross-section is also higher when top-casting-induced defects are present but the difference is not as significant as for the average value. This confirms that top-casting-induced defects allow a greater length of tensile bars to be affected by the corrosion process.

3.5.4 Corrosion propagation around the perimeter of the tensile bars

The presence of top-casting-induced defects on C3 and C4 beams lead to a difference of corrosion distribution along the perimeter of rebars. Figure IV-43 shows the location of top-cast defects on C3 and C4 beams, while there were no defects below the tensile bars of C1 and C2 beams due to their bottom casting.

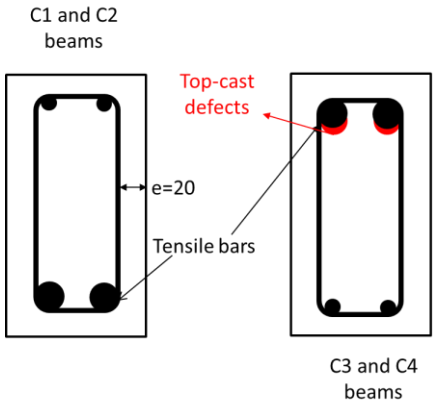

Figure IV-43 Location of top-casting-induced defects on C3 and C4 beams

The extent of the pitting corrosion area is separated into 4 segments around the perimeter of each re-bar according to the nomenclature of Figure IV-26. In presence of top-casting-induced defects, corrosion is present all along the perimeter while it is not the case in absence of top-cast defects

Indeed, Figure IV-44 presents the extent of pitting corrosion area on each tensile bar of the C1 and C2 beams in absence of top-casting-induced defects. It is obvious from Figure IV-44 that corrosion is more developed on the parts of the bar perimeter that are closer to the external surfaces of the beams corresponding to the source of chloride ingress. Chlorides reach the re-bars firstly from the outside facing parts and then induce corrosion, which means that they do not move easily around the perimeter.

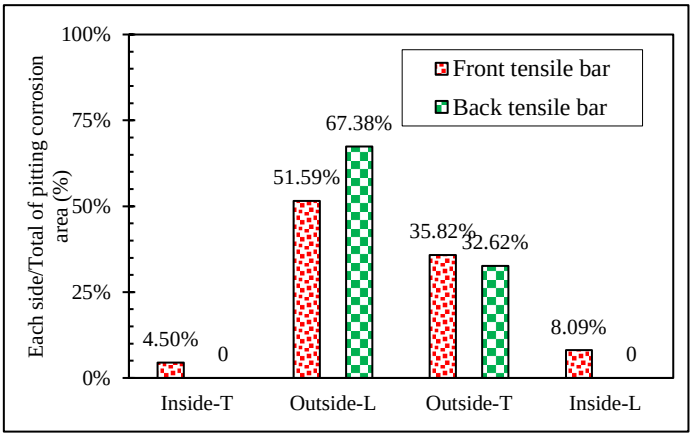

Figure IV-44.1 Beam C1

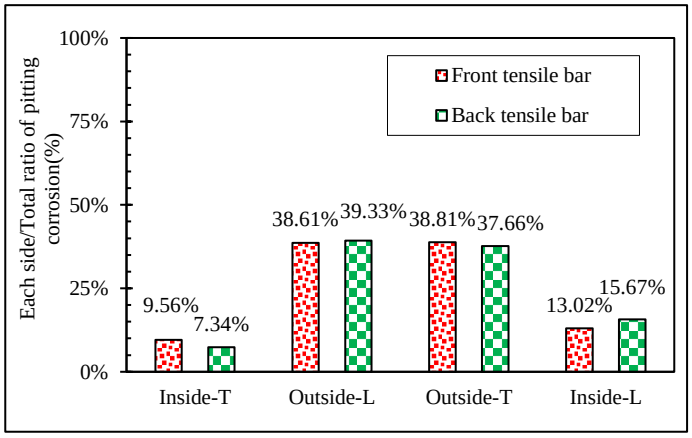

Figure IV-44.2 Beam C2

Figure IV-44 Corrosion distribution around the perimeter in absence of top casting defects

Figure IV-45 shows the distribution of corrosion around the perimeter of tensile bars in the presence of top-casting-induced defects. It corresponds to beams C3 and C4, where the tensile

bars are top-casting-induced bars. It is obvious from Figure IV-45 that corrosion has developed almost uniformly around the perimeter of the rebars. For beams C3 and C4, the top-casting-induced defects are located on the inside-T zone defined in Figure IV-26.

Because of the top-casting-induced defects, chlorides coming from load-induced cracks have propagated along the rebars, leading to the appearance of corrosion induced cracks in the short term. The corrosion induced cracks lead to a de-confinement of the concrete around the rebars and thus favor a quasi-uniform distribution of pitting around the perimeter.

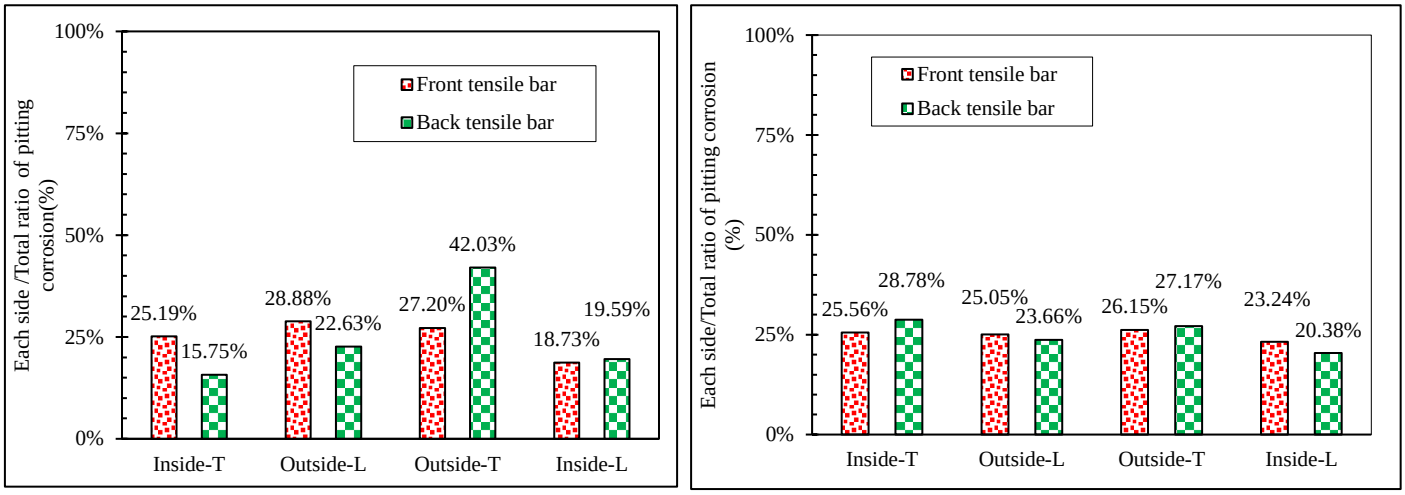

Figure IV-45.1 Beam C3 Figure IV-45.2 Beam C4

Figure IV-45 Corrosion distribution around the perimeter in presence of top casting defects

3.5.5 Phenomenological model of corrosion process of tensile bar

The classical model regarding the corrosion process in uncracked concrete was proposed by Tuutti [55]. In this model, it is considered that the corrosion process can be divided into two stages the initiation stage and the propagation stage. François et al. [6] proposed another model, in four phases, which is suitable for corrosion in cracked concrete (Figure IV-46).

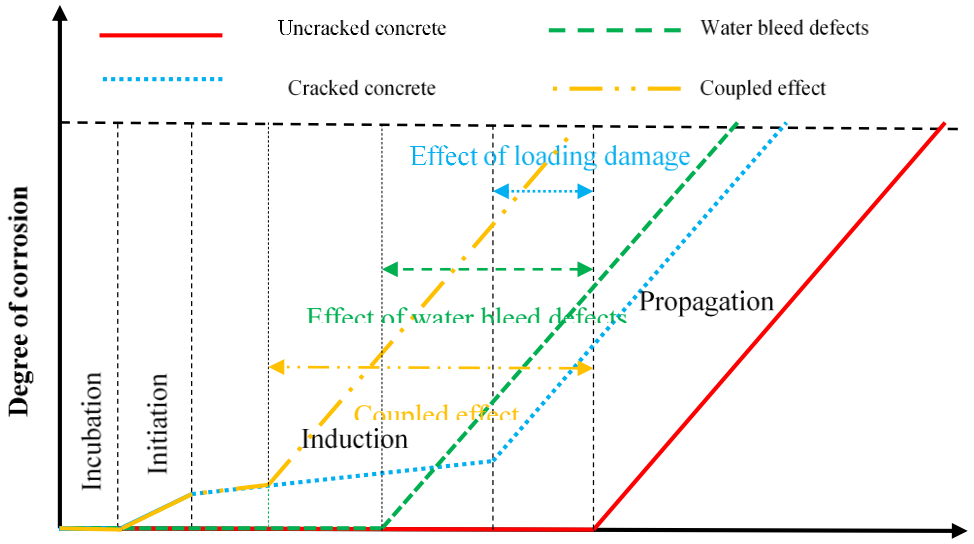

Figure IV-46 Phenomenological models for corrosion process in concrete and for cracked structure [6, 56]

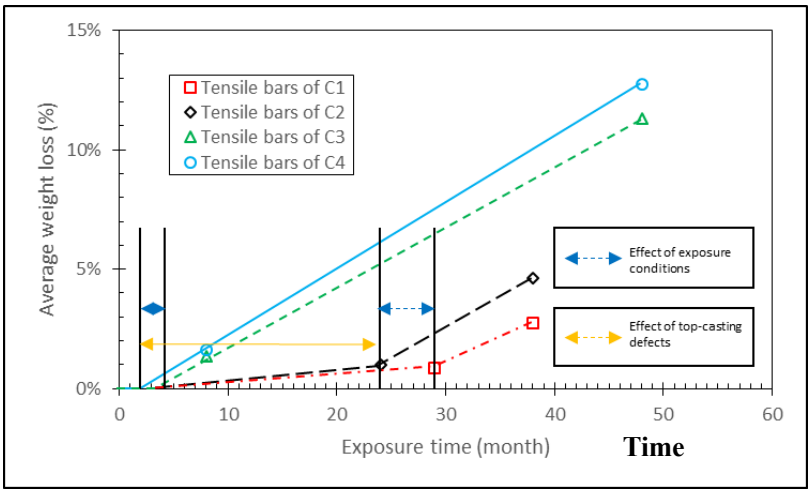

Figure IV-47 Corrosion process of C beams in cracked zone

The corrosion process of tensile bars of the four C beams is presented in Figure IV-47 according to the average weight loss of tensile bars.

Average weight loss at 8, 24 and 28 months was calculated by using the opening of the corrosion-induced crack width according to the method proposed by Vidal et al. [57].

In the presence of top-casting-induced defects (beams C3 and C4), the propagation stage follows the initiation stage directly; the induction period is zero.

In the absence of top-casting-induced defects (beams C1 and C2), the initiation at the crack location is followed by an induction period corresponding to the time needed for chloride ingress through the concrete cover in non-cracked zones. When sufficient chlorides reach the re-bars, the

propagation stage begins. There is an effect of the exposure conditions for chloride ingress a top-exposed tensile surface leads to higher chloride ingress than a bottom exposed tensile surface.

3.6 Conclusion

Four beams with the same concrete and same cover depth but different casting directions and exposure conditions were investigated. The work focused on the study of the corrosion of tensile bars in presence of load-induced cracks due to the sustained loading conditions. For 2 beams (C3 and C4) the load-induced cracks were coupled with the presence of top-casting-induced defects.

The cracking maps, chloride profiles of concrete, cross-sectional loss of tensile bars, and corrosion distribution around and along the tensile bars of the four beams were studied and compared with each other. The following conclusions were drawn

There is no correlation between the opening of load-induced cracks and corrosion development or the loss of cross-section due to corrosion for relatively short-term experiments. These results confirm those obtained for long-term exposure by Beeby[58] and François and Arliguie[10].

Despite the chloride ingress to rebars facilitate by load-induced cracks, no initiation of corrosion at some crack locations could be found in the case of no top-casting-induced defects along the tensile bars. This phenomenon was also observed by Susuki et al[52], and could be explained by the macro-cell corrosion development at major cracks which avoid the corrosion development at minor cracks.

Without top-casting-induced defects, there is no correlation between the existence of load-induced cracks and corrosion propagation. Corrosion is initiated at cracks but does not propagate, because the cracks heal as already mentioned in previous articles [10, 58-62].

With top-casting-induced defects, corrosion is initiated at cracks and propagates because of the ingress of chlorides all along the bars due to defects. This result could explain much of the controversy concerning cracks reported in the literature as many of the studies were performed on top casting bars [7, 9, 52, 56].

In a cracked concrete structure, the initiation stage is mainly controlled by load-induced cracks [50], the induction stage before propagation is controlled by top-casting-induced defects and exposure conditions, where top-casting-induced defects are the main effect factor.

3.7 References

[1] L. Bertolini, B. Elsener, P. Pedeferri, E. Redaelli, R.B. Polder, Corrosion of steel in concrete: prevention, diagnosis, repair, John Wiley & Sons2013.
[2] R. François, G. Arliguie, Influence of service cracking on reinforcement steel corrosion, Journal of Materials in Civil Engineering, 10 (1998) 14-20.
[3] C. Arya, F. Ofori-Darko, Influence of crack frequency on reinforcement corrosion in concrete, Cement and Concrete Research, 26 (1996) 345-353.
[4] M. Otieno, M. Alexander, H.-D. Beushausen, Corrosion in cracked and uncracked concrete,influence of crack width, concrete quality and crack reopening, Magazine of Concrete Research, 62 (2010) 393-404.
[5] R. Francois, J. Maso, Effect of damage in reinforced concrete on carbonation or chloride penetration, Cement and Concrete Research, 18 (1988) 961-970.
[6] R. François, S. Laurens, F. Deby, 2 - Scale and Structural Effects on the Corrosion of Reinforced-Concrete Reinforcements, Corrosion and its Consequences for Reinforced Concrete Structures, Elsevier2018, pp. 43-62.
[7] M. Otieno, M. Alexander, H.-D. Beushausen, Corrosion in cracked and uncracked concrete-influence of crack width, concrete quality and crack reopening, Magazine of Concrete Research, 62 (2010) 393-404.
[8] M. Makita, Y. Mori, K. Katawaki, Marine corrosion behavior of reinforced concrete exposed at tokyo bay, Special Publication, 65 (1980) 271-290.
[9] A. Scott, M. Alexander, The influence of binder type, cracking and cover on corrosion rates of steel in chloride-contaminated concrete, Magazine of Concrete Research, 59 (2007) 495-505.
[10] R. François, G. Arliguie, Effect of microcracking and cracking on the development of corrosion in reinforced concrete members, Magazine of Concrete Research, 51 (1999) 143-150.
[11] R. Francois, G. Arliguie, Reinforced concrete: correlation between cracking and corrosion, Special Publication, 126 (1991) 1221-1238.
[12] T.U. Mohammed, T. Yamaji, T. Aoyama, H. Hamada, Corrosion of steel bars in cracked concrete made with ordinary Portland, slag and fly ash cements, Special Publication, 199 (2001) 699-718.
[13] T.U. Mohammed, N. Otsuki, M. Hisada, T. Shibata, Effect of Crack Width and Bar Types on Corrosionof Steel in Concrete, Journal of Materials in Civil Engineering, 13 (2001) 194-201.
[14] R. Francois, I. Khan, N.A. Vu, H. Mercado, A. Castel, Study of the impact of localised cracks on the corrosion mechanism, European Journal of Environmental and Civil Engineering, 16 (2012) 392-401.
[15] Y. Ji, Y. Hu, L. Zhang, Z. Bao, Laboratory studies on influence of transverse cracking on chloride-induced corrosion rate in concrete, Cement and Concrete Composites, 69 (2016) 28-37.
[16] M. Mahmaran, Yaman, Influence of transverse crack width on reinforcement corrosion initiation and propagation in mortar beams, Canadian Journal of Civil Engineering, 35 (2008) 236-245.
[17] L. Chun-Qing, R.E. Melchers, Z. Jian-Jun, Analytical model for corrosion-induced crack width in reinforced concrete structures, ACI Structural Journal, 103 (2006) 479.
[18] J. Ryu, N. Otsuki, Application of electrochemical techniques for the control of cracks and steel corrosion in concrete, Journal of applied electrochemistry, 32 (2002) 635-639.

[19] W. Danilecki, An investigation into the effect of crack width on the corrosion of reinforcement in reinforced concrete, (1969).
[20] E. Committee, Eurocode2: Design of concrete structures-Part 1-2: General rules-Structural fire design, ENV 1992-1-2, 1995.
[21] R.M. Ghantous, S. Poyet, V. L'Hostis, N.-C. Tran, R. François, Effect of crack openings on carbonation-induced corrosion, Cement and Concrete Research, 95 (2017) 257-269.
[22] C. Fu, N. Jin, H. Ye, X. Jin, W. Dai, Corrosion characteristics of a 4-year naturally corroded reinforced concrete beam with load-induced transverse cracks, Corrosion Science, 117 (2017) 11-23.
[23] R. Zhang, A. Castel, R. François, The corrosion pattern of reinforcement and its influence on serviceability of reinforced concrete members in chloride environment, Cement and Concrete Research, 39 (2009) 1077-1086.
[24] R. Zhang, A. Castel, R. François, Influence of steel-concrete interface defects owing to the top-bar effect on the chloride-induced corrosion of reinforcement, Magazine of Concrete Research, 63 (2011) 773-781.
[25] L. Yu, R. François, R. Gagné, Influence of steel-concrete interface defects induced by top-casting on development of chloride-induced corrosion in RC beams under sustained loading, Materials and Structures, 49 (2016) 5169-5181.
[26] T.U. Mohammed, N. Otsuki, H. Hamada, T. Yamaji, Chloride-induced corrosion of steel bars in concrete with presence of gap at steel-concrete interface, Materials Journal, 99 (2002) 149-156.
[27] J. Ryou, K. Ann, Variation in the chloride threshold level for steel corrosion in concrete arising from different chloride sources, Magazine of Concrete Research, 60 (2008) 177-187.
[28] U.M. Angst, M.R. Geiker, A. Michel, C. Gehlen, H. Wong, O.B. Isgor, B. Elsener, C.M. Hansson, R. François, K. Hornbostel, The steel-concrete interface, Materials and Structures, 50 (2017) 143.
[29] T. Vidal, A. Castel, R. François, Corrosion process and structural performance of a 17 year old reinforced concrete beam stored in chloride environment, Cement and Concrete Research, 37 (2007) 1551-1561.
[30] L. Yu, R. François, V.H. Dang, V. L'Hostis, R. Gagné, Development of chloride-induced corrosion in pre-cracked RC beams under sustained loading: Effect of load-induced cracks, concrete cover, and exposure conditions, Cement and Concrete Research, 67 (2015) 246-258.
[31] A. Michel, A.O.S. Solgaard, B.J. Pease, M.R. Geiker, H. Stang, J.F. Olesen, Experimental investigation of the relation between damage at the concrete-steel interface and initiation of reinforcement corrosion in plain and fibre reinforced concrete, Corrosion Science, 77 (2013) 308-321.
[32] R. Zhang, A. Castel, R. François, Concrete cover cracking with reinforcement corrosion of RC beam during chloride-induced corrosion process, Cement and Concrete Research, 40 (2010) 415-425.
[33] A. Castel, T. Vidal, R. François, G. Arliguie, Influence of steel-concrete interface quality on reinforcement corrosion induced by chlorides, Magazine of Concrete Research, 55 (2003) 151-159.
[34] T.A. Soylev, R. François, Quality of steel-concrete interface and corrosion of reinforcing steel, Cement and Concrete Research, 33 (2003) 1407-1415.
[35] T.A. Soylev, R. François, Corrosion of reinforcement in relation to presence of defects at the interface between steel and concrete, Journal of materials in civil engineering, 17 (2005) 447-455.

[36] W. Zhang, L. Yu, R. François, Influence of top-casting-induced defects on the corrosion of the compressive reinforcement of naturally corroded beams under sustained loading, Construction and Building Materials, 229 (2019) 116912.
[37] A.C. Institute, ACI 318-14: Building Code Requirements for Structural Concrete and Commentary, Farmington Hills, 2008.
[38] T.U. Mohammed, H. Hamada, Corrosion of horizontal bars in concrete and method to delay early corrosion, Materials Journal, 103 (2006) 303-311.
[39] A. Horne, I. Richardson, R. Brydson, Quantitative analysis of the microstructure of interfaces in steel reinforced concrete, Cement and Concrete Research, 37 (2007) 1613-1623.
[40] W. Zhu, R. François, Y. Liu, Propagation of corrosion and corrosion patterns of bars embedded in RC beams stored in chloride environment for various periods, Construction and Building Materials, 145 (2017) 147-156.
[41] L. Yu, R. François, V.H. Dang, V. L'Hostis, R. Gagné, Structural performance of RC beams damaged by natural corrosion under sustained loading in a chloride environment, Engineering Structures, 96 (2015) 30-40.
[42] L. Yu, R. François, V.H. Dang, V. L'Hostis, R. Gagné, Distribution of corrosion and pitting factor of steel in corroded RC beams, Construction and Building Materials, 95 (2015) 384-392.
[43] I. Khan, R. François, A. Castel, Prediction of reinforcement corrosion using corrosion induced cracks width in corroded reinforced concrete beams, Cement and concrete research, 56 (2014) 84-96.
[44] V.H. Dang, R. François, Prediction of ductility factor of corroded reinforced concrete beams exposed to long term aging in chloride environment, Cement and Concrete Composites, 53 (2014) 136-147.
[45] W. Zhu, R. François, D. Coronelli, D. Cleland, Effect of corrosion of reinforcement on the mechanical behaviour of highly corroded RC beams, Engineering Structures, 56 (2013) 544-554.
[46] R. François, I. Khan, V.H. Dang, Impact of corrosion on mechanical properties of steel embedded in 27-year-old corroded reinforced concrete beams, Materials and structures, 46 (2013) 899-910.
[47] V.H. Dang, R. Francois, Influence of long-term corrosion in chloride environment on mechanical behaviour of RC beam, Engineering Structures, 48 (2013) 558-568.
[48] A. Castel, T. Vidal, K. Viriyametanont, R. François, Effect of reinforcing bar orientation and location on bond with self-consolidating concrete, ACI Structural Journal, 103 (2006) 559.
[49] B.A.E.L French regulations for reinforced concrete structures 1983.
[50] C. Boschmann Kathler, U.M. Angst, M. Wagner, C.K. Larsen, B. Elsener, Effect of cracks on chloride-induced corrosion of steel in concrete-a review: Etatsprogrammet Varige konstruksjoner 2012-2015, ETH Zurich, 2017.
[51] R.M. Ghantous, R. François, S. Poyet, V. L'hostis, F. Bernachy-Barbe, D. Meinel, L. Portier, N.-C. Tran, Relation between crack opening and extent of the damage induced at the steel/mortar interface, Construction and Building Materials, 193 (2018) 97-104.
[52] K. Suzuki, Y. Ohno, S. Praparntanatorn, H. Tamura, Mechanism of steel corrosion in cracked concrete, Corrosion of reinforcement in concrete, (1990) 19-28.
[53] R. François, G. Arliguie, G. Escadeillas, O. Francy, Optimisation des structures en béton armé vis-à-vis de la corrosion, Revue française de génie civil, 2 (1998) 949-968.

[54] R. François, G. Arliguie, durabilité du béton armé soumis à l'action des chlorures, Annales de l'Institut Technique du Batiment et des Travaux Publics, 1994.
[55] K.S. Tuutti, Corrosion of steel in concrete, (1982).
[56] K. Pettersson, O. Jorgenson, P. FidjestolI, The effect of cracks on reinforcement corrosion in high-performance concrete in a marine environment, Special Publication, 163 (1996) 185-200.
[57] T. Vidal, A. Castel, R. Francois, Analyzing crack width to predict corrosion in reinforced concrete, Cement and concrete research, 34 (2004) 165-174.
[58] A. Beeby, Corrosion of reinforcing steel in concrete and its relation to cracking, Structural Engineer, 56 (1978).
[59] C. Arya, L.A. Wood, The relevance of cracking in concrete to corrosion of reinforcement, Concrete Society1995.
[60] A. Bentur, S. Diamond, N. Berke, Steel Corrosion in concrete. E & FN Spon, Chapman & Hall) London, UK, 1997.
[61] R. François, A. Castel, T. Vidal, N.-A. Vu, Long term corrosion behavior of reinforced concrete structures in chloride environnement, Journal de Physique IV (Proceedings), EDP sciences, 2006, pp. 285-293.
[62] P. Schieβl, M. Raupach, Laboratory studies and calculations on the influence of crack width on chloride-induced corrosion of steel in concrete, Materials Journal, 94 (1997) 56-61.

4 Influence of top-casting-induced defects on the corrosion of the compressive reinforcement of naturally corroded beams under sustained loading

4.1 Abstract

This paper discusses the effect of top-casting-induced defects on the corrosion development of compressive bars in reinforced concrete beams exposed to a chloride environment, under sustained loading. Four reinforced concrete beams, exposed to artificial climate of accelerated natural corrosion for 38 months and 48 months, respectively, were tested. The cracking maps, chloride profiles, cross-sectional loss, and corrosion distribution around the perimeter and along the re-bars of four beams were studied and compared with each other. Experimental results show that top-casting-induced defects encouraged corrosion to develop first at the bottom surface of compressive bars and their presence strongly accelerated the corrosion process. Without top-casting-induced defects, the corrosion was more prominent on the outside part of re-bars facing the concrete surface exposed to chloride ingress. After the appearance of corrosion-induced cracks, corrosion gradually developed all around the perimeter of re-bars, with the result that top-casting-induced defects no longer affected the corrosion process.

Key words corrosion; chloride; top-casting defects; steel-concrete interface; reinforced concrete

4.2 Introduction

Many factors affect the deterioration of reinforced concrete and chloride-induced corrosion of steel is one of the most serious causes of steel corrosion, especially in structures in contact with sea water or de-icing salts [1]. A large number of studies have been carried out on the factors affecting chloride-induced corrosion [2-15].The corrosion process leads to several coupled effects[2] longitudinal cracking of the concrete cover due to expansive corrosion products, steel cross-section reduction, and the degradation of the steel-concrete bond. As a result of these effects, the service life and the load-bearing capacity of reinforced concrete elements are considerably reduced.

Vidal et al. [16] observed that the steel-concrete interface condition was a determinant parameter in corrosion initiation, having an impact comparable to that of the chloride threshold.

Mohammed et al. [9] observed that defects in the steel-concrete interface were only found under horizontal bars cast in the top part of reinforced elements and not under those cast in the bottom part. Zhang et al. and Soylev and François [17-19] found that defects of the reinforcement-concrete interface at the bottom part of the steel increased in relation to the depth of concrete under the steel and that, when this depth was not greater than 15 cm, the steel-concrete interface was perfect.

Kenny and Katz [20] observed that the porosity at the bottom of the reinforcement bar was notably higher than at the top when the bar was cast horizontally. Horne et al. [21] observed that there was more porosity and less $Ca(OH)_2$ under horizontal bars than above. The micro-environment at the bottom of steel cast horizontally was significantly different from that at the top side.

Soylev and François [19] divided defects of the steel-concrete interface into two types macro-defects and micro-defects. Macro-defects were gross defects that prevented there being contact between steel and concrete and therefore prevented the formation of the specific protection provided by the interfacial layer. Ryou and Ann [11] observed that corrosion initiated in the voids at the steel-concrete interface, regardless of whether the chlorides were of external or internal origin. Hartt and Nam [22] found that corrosion initiated preferentially at air voids of diameter larger than 2.5 mm. Yu et al. [23] found that corrosion-induced cracks always developed much more quickly along top-cast steel bars, owing to the existence of top-casting-induced defects, and they were favorable to both the initiation and the propagation of corrosion.

Zhang et al. [17]observed that before the appearance of corrosion-induced cracks, corrosion mainly occurred at the bottom part of top-casting bar according to the casting direction due to the fact that defects at the steel-concrete interface under a horizontal bar promoted anodic behavior, while a sound steel-concrete interface allowed re-bars to act as cathodes. Dang and Francois[24] studied the corrosion behavior of 27-year-old corroded beam and found that generalized corrosion can be observed around the perimeter of steel bars after the appearance of corrosion-induced cracks. It meant that corrosion process of top-casting bar gradually changes from localized corrosion to generalized corrosion with the development of corrosion-induced cracks.

Since tensile and compressive zones are subject to different corrosion conditions due to the different loading and exposure conditions, they ought to be discussed in separate groups. This study presents only the impact of top-casting-induced defects on the corrosion characteristic of the

compressive zone in the relatively long term. In the work presented here, four beams of sizes typically used in the construction industry were investigated. They were corroded in a chloride environment under sustained loading, and corrosion-induced cracking maps, chloride profiles, distribution of pitting and loss of cross-section of steel bars were recorded at 38 and 48 months. The effects of defects in the steel-concrete interface under horizontal compressive bars on the chloride-induced corrosion characteristics are discussed in this paper.

4.3 Experimental program

4.3.1 Raw materials and properties

Cement (CEM I, Grade 52.5) manufactured by Lafarge Cement Group Co., Ltd, with 3.15 g/cm^3 in density and 415 m^2/kg in Blaine specific surface area, was used to prepare the concrete used in this study, its chemical compositions are given in Table IV-5.

Table IV-5 Cement composition

	SiO_2	Al_2O_3	Fe_2O_3	CaO	MgO	SO_3	Na_2O
Weight **%**	21.4	6.0	2.3	63.0	1.4	3.0	0.5

The concrete mixture proportion is given in Table IV-6. The slump of concrete was 70 mm. The average compressive strength of the concrete at 28 days (tested on 110×220 mm cylindrical specimens) was 45 MPa. The elastic modulus was 32 GPa. The tensile strength was 4.7 MPa, which was tested by splitting test on the cylindrical specimens. The porosity was about 15.2%.

Table IV-6 Concrete proportioning

Mix composition		
Rolled gravel (silica+limestone)	5-15 mm	1109 kg/m^3
Sand	0-5 mm	745 kg/m^3
Portland cement OPC (high performance)		364 kg/m^3
Water		182 kg/m^3

4.3.2 Reinforced Concrete Specimens

The four reinforced concrete specimens studied here were full-size beams (3000×280×150 mm) cast in 2013 and having the same concrete cover depth in order to study the impact of top-casting-induced defects on the corrosion process. These beams were named C beams. They were stored in

an aggressive environment under loading. The dimensions and the reinforcement layout of the concrete beams is shown in Figure IV-48.

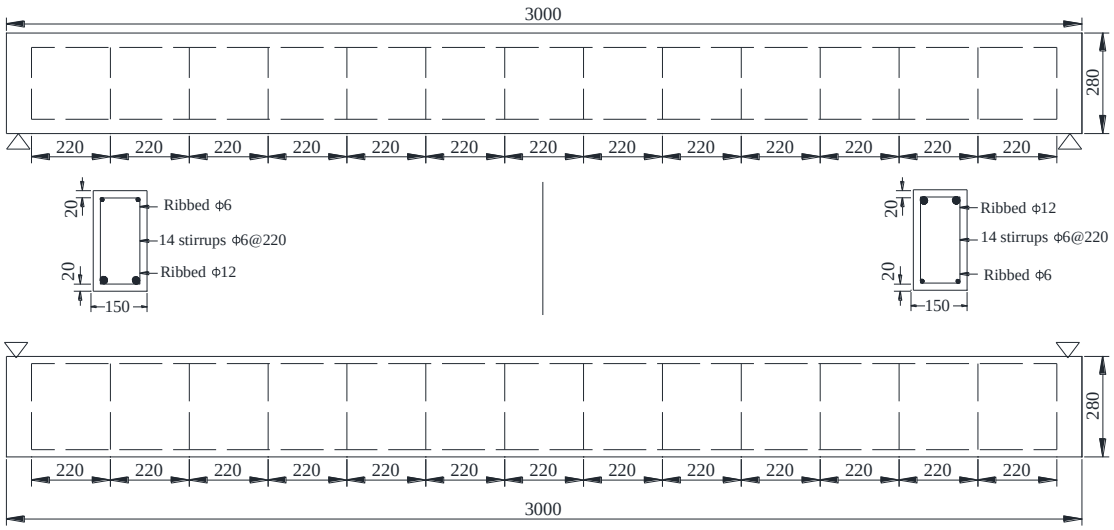

Figure IV-48 Layout of the reinforced concrete beams (all dimensions in mm)

The four beams were divided into two groups according to the casting direction beam C1 and beam C2 were in Group 1 while beam C3 and C4 were in Group 2. Two beams in the same group had the same casting direction but different exposure conditions. In Group 1, all the compressive bars were top-cast steel bars according to the casting direction, which meant that some top-casting-induced defects existed at the compressive bar-concrete interface and the concrete cover of the compressive zone was more porous. In Group 2, both the compressive bars were bottom-cast steel bars according to the casting direction, no water bleeding defects were expected at the compressive bar-concrete interface and the compressive zone was denser than that of Group 1. The casting mode and the exposure direction for all the beams is shown in Figure IV-49. In this figure, the division of each bar into four parts was illustrated, which will be further used to describe corrosion distribution on the steel bar. More details could be found in section 2.7 of this paper.

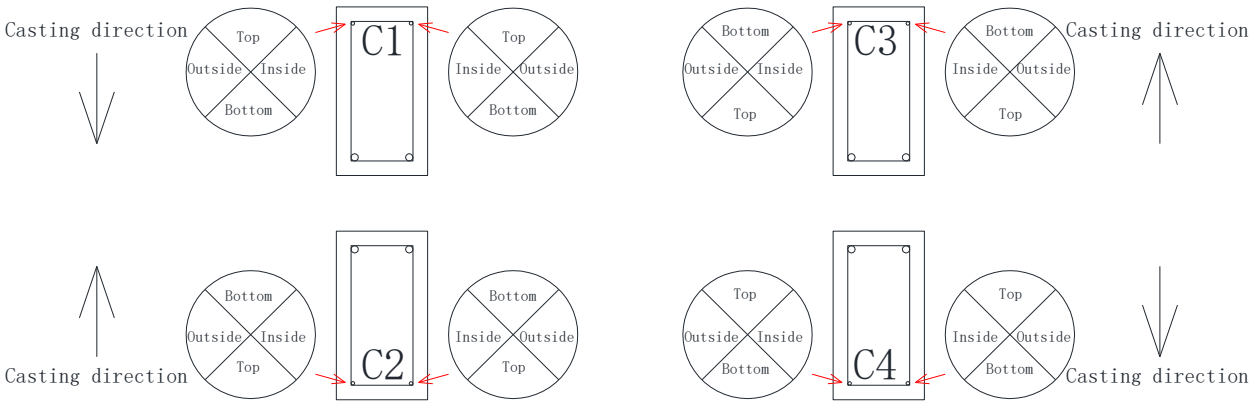

Figure IV-49 Casting mode and division of the compressive bars into four parts

4.3.3 Loading system and exposure conditions

The corrosive environment and the loading mode of all the beams are shown in Figure IV-50. The aggressive environment was a salt fog produced by spraying (35 g/L of NaCl corresponding to the chloride concentration of sea water) in a cycle of 2 days' wetting followed by 5 days' drying. All the beams were loaded in 3-point bending. Two loading values were used Mser 1= 21.2 kN•m (Group 1) and Mser2 = 14.1 kN•m (Group 2). In the loading setup, beam C1 was above beam C2, and beam C3 was above beam C4.

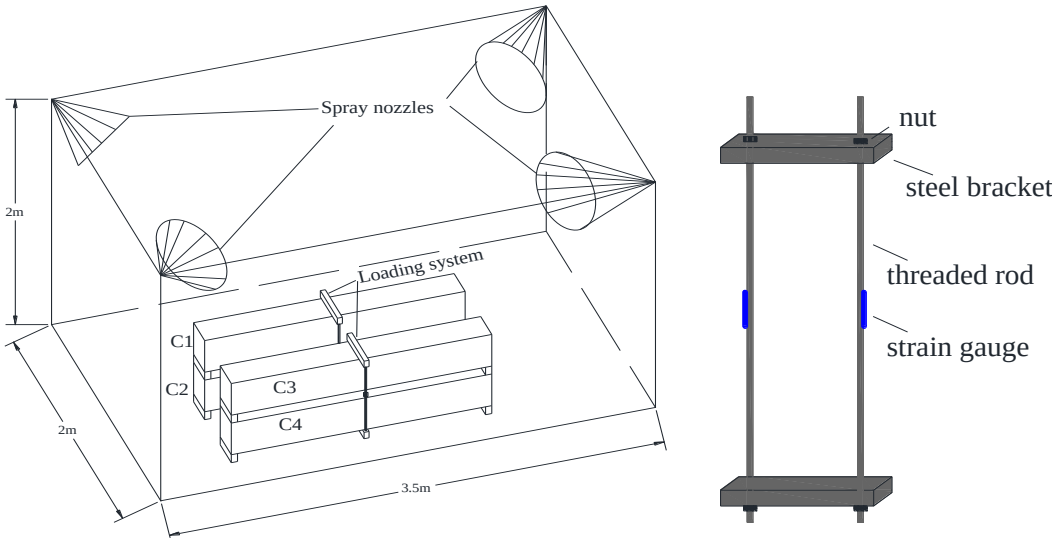

Figure IV-50 Loading system and exposure conditions

4.3.4 Corrosion-induced cracking maps

For beams C1 and C2, the corrosion-induced cracking situation were checked at 8 and 24

months and cracking maps were recorded at 29 months and 38 months respectively. Corrosion-induced cracking situation were checked at 8 and 24 months and cracking maps of beams C3 and C4 were plotted at 29 months and 48 months.

Only the widths of longitudinal corrosion-induced cracks along compressive reinforcement were indicated on the maps. The C-I crack widths were measured with a video microscope having an accuracy of 0.01 mm and a magnification ranging from 25 times to 175 times.

4.3.5 Top-casting-induced defects

After recording the cracking maps of C beams, some parts from C1 and C3 beams were observed with back scattered electron imaging (BSE) in order to characterize the presence of water-bleeding induced defect at the bottom side of re-bars.

4.3.6 Chloride profiles

After the preparation of samples for scatter electron imaging, some concrete powder was taken from these beams for chloride concentration testing. The locations where samples were collected are indicated by circles in Figure IV-53 to Figure IV-56. Each concrete powder sample from the compressive surfaces and sides of the four corroded beams was collected by dry drilling with a German Instruments Rapid Chloride Test RCT sampling device. Chloride ions were extracted with nitric acid at 80℃and the chloride contents were determined by potentiometric titration with $AgNO_3$. The chloride profiles were plotted to a depth of 37.5 mm in beams C1 and C2. For beams C3 and C4, the depth at which concrete powder was collected was up to 35 mm from the concrete surface. In this study, the total chloride content per unit weight of cement was determined.

4.3.7 Corrosion distribution around the perimeter of compressive bar

The corroded reinforcement bars embedded in the beams were extracted and cleaned with Clark's solution (ISO 8407) to remove the corrosion products. As presented in Figure IV-49 Casting mode and division of the compressive bars into four parts, each bar was divided into 4 parts, which were labeled top part, external part, bottom part and internal part according to the casting direction. The corrosion distribution on each part was recorded and the corrosion area ratio of each part was calculated, which will be discussed in section 7.4.5.

4.3.8 Cross-sectional loss due to corrosion

After the re-bars had been cleaned, the weight loss of the steel bars was used to calculate the loss of cross-section due to corrosion. The bars were cut into short pieces of various lengths according to the corrosion pattern (pitting or general corrosion) and corrosion details. The length of each section depended on the corrosion condition along the steel bar and was measured with Vernier calipers having a precision of 0.02 mm. Each short section was weighed on a balance with a precision of 0.01g. The loss of cross-section was then calculated with Equation 1. The original mass of the short sections could be calculated with Equation 2.

$$\Delta As = \frac{Mo-M}{Mo} \times As \qquad \text{Equation 1}$$

$$Mo = \rho \times As \times L \qquad \text{Equation 2}$$

where ρ (g/cm^3) is the density of the steel bar, taken as 7.85 g/cm^3;

L (mm) is the length of each short section;

Δ As (mm^2) is the average loss of cross-section of the corroded bar over the short section length;

As (mm^2) is the nominal cross-section of the steel bar;

M (g) is the residual mass of the short sections of corroded bar;

Mo (g) is the nominal mass of the steel bar.

4.4 Experiment Results and Discussion

4.4.1 Characterization of water-bleed defects at the steel-concrete interface

The interfaces between concrete and compressive bars of C1 and C3 were observed with BSE, the images are presented in Figure IV-51 and Figure IV-52 respectively. The white arrows in the photos mean the casting direction.

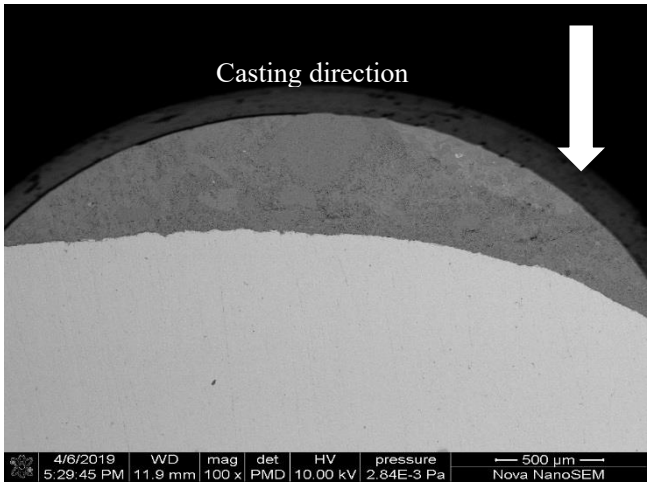

Figure IV-51.1 Top side interface of beam C1

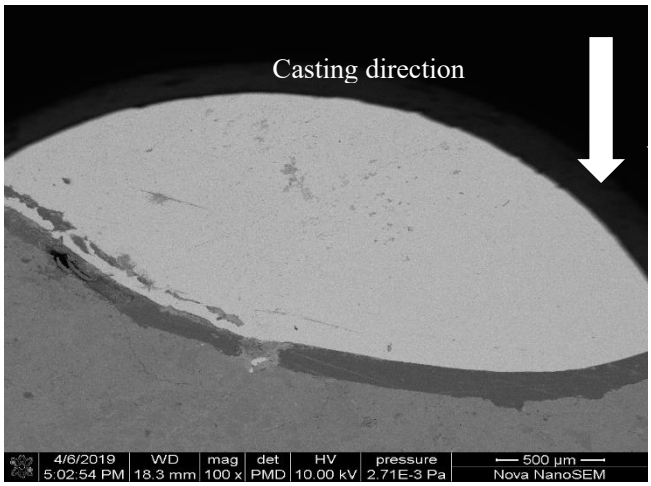

Figure IV-51.2 Bottom side interface Figure of beam C1

Figure IV-51 Characterization of steel-concrete interface of beam C1

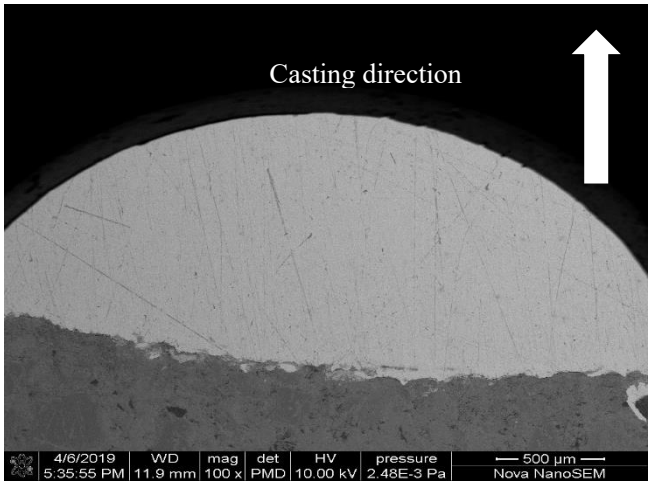

Figure IV-52 1 Top side interface of beam C3

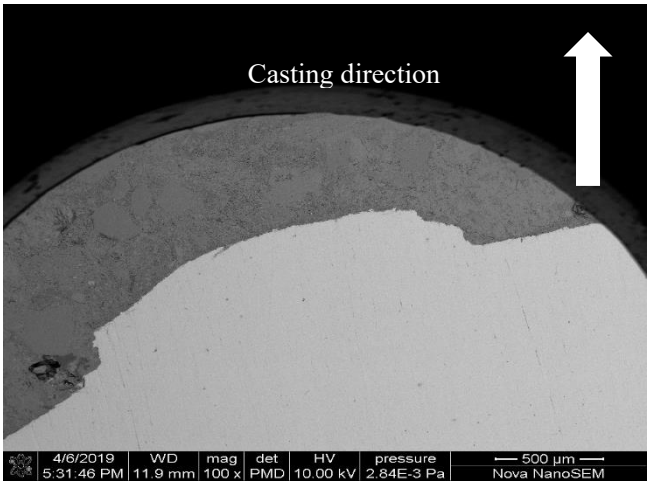

Figure IV-52 2 Bottom side interface of beam C3

Figure IV-52 Characterization of steel-concrete interface of beam C3

The compressive bars of beam C1 were located on the top part of the beam during casting process. As presented in Figure IV-51, we can find an obvious gap with a thickness of about 0.2 mm existing on the bottom side of compressive bar in beam C1. While the steel-concrete interface on the top side of compressive bar in beam C1 was quite dense. For beam C3, the steel-concrete interface on the bottom side of compressive bars was similar as that on the top part, and both steel-concrete interfaces were dense without significant defects.

4.4.2 Effect of top-casting-induced defects on the corrosion-induced cracking in the compressive zone

Observation on the C-I cracks along the compressive bars were recorded (Figure IV-53 to

Figure IV-56). On these maps, the longitudinal red lines correspond to the C-I cracks. The numbers along the red lines correspond to the opening widths of cracks. The arrow located at the right side of each beam shows the casting direction.

For beam C1, first C-I cracks were visible at only 8 months, then C-I cracks spread along the compressive reinforcement and then only small parts of the beams were no affected by C-I cracks at 38 months (Figure IV-53).

For beam C2, first corrosion-induced cracks were visible after 24 months on the front face, and then both front and back face of the beam were affected by corrosion-induced cracks at 38 months (Figure IV-54).

For beam C3, no C-I cracks were found near the compressive zone at 29 months and just a short one was observed on the front side of the compressive area at 48 months (Figure IV-55).

For beam C4, no C-I were recorded all along the experiments until 48 months (Figure IV-56).

Beams C1 and C3 had the same exposure conditions top surface corresponded to compressive surface and corrosion of compressive bars in beam C1 developed faster which could be attributed to the presence of top-casting-induced defects in the steel-concrete interface in case of beam C1 which was not the case for beam C3.

Beams C2 and C4 had the same exposure conditions bottom surface corresponded to compressive surface and corrosion of compressive bars in beam C2 developed faster than in beam C4 which could be attributed to the presence of top-casting-induced defects in the steel-concrete interface in case of beam C2 which was not the case for beam C4.

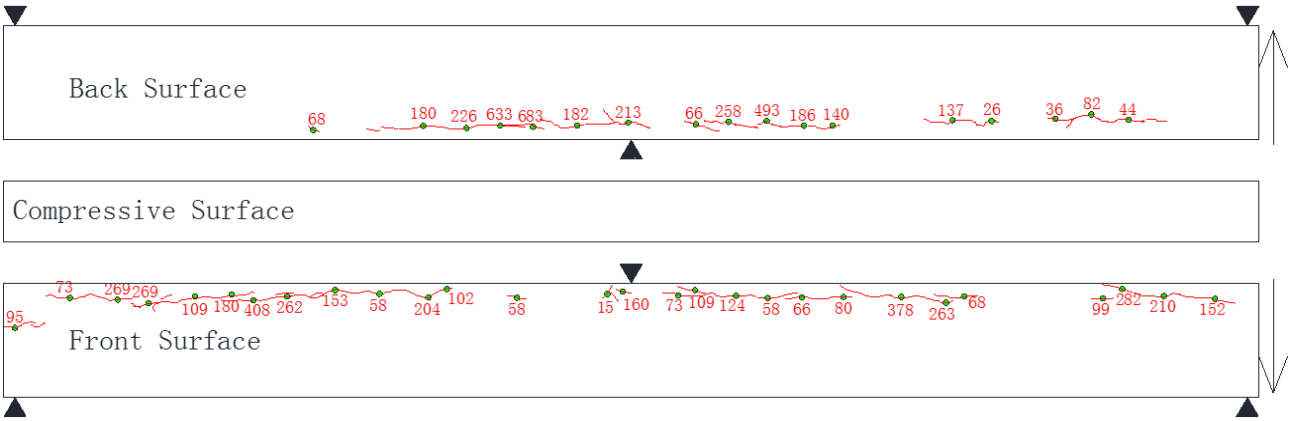

Figure IV-53.1 Cracking maps of beam C1 after 29 months

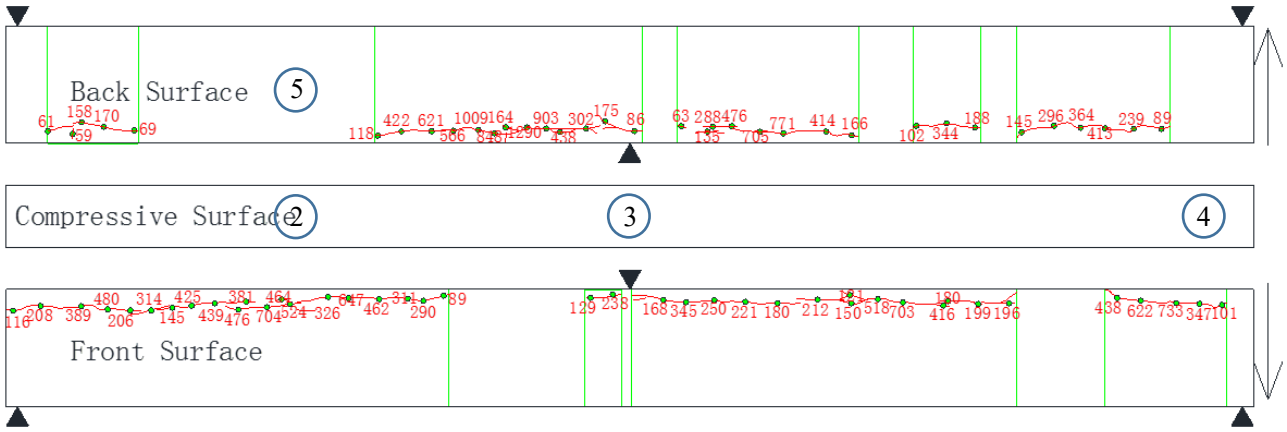

Figure IV-53.2 Cracking maps of beam C1 after 38 months

Figure IV-53 Corrosion-induced cracking maps of beam C1 (crack widths in μm)

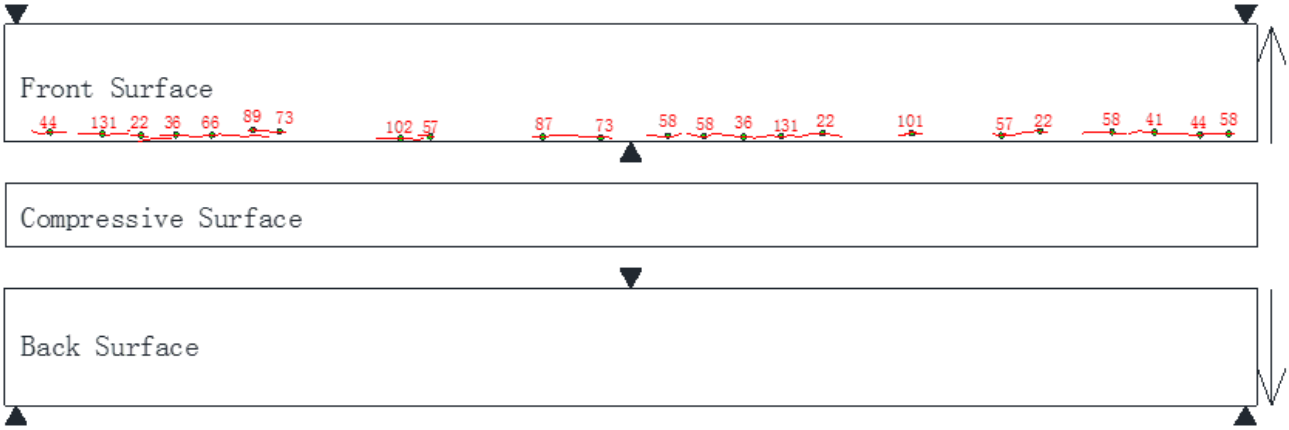

Figure IV-54.1 Cracking maps of beam C2 after 29 months

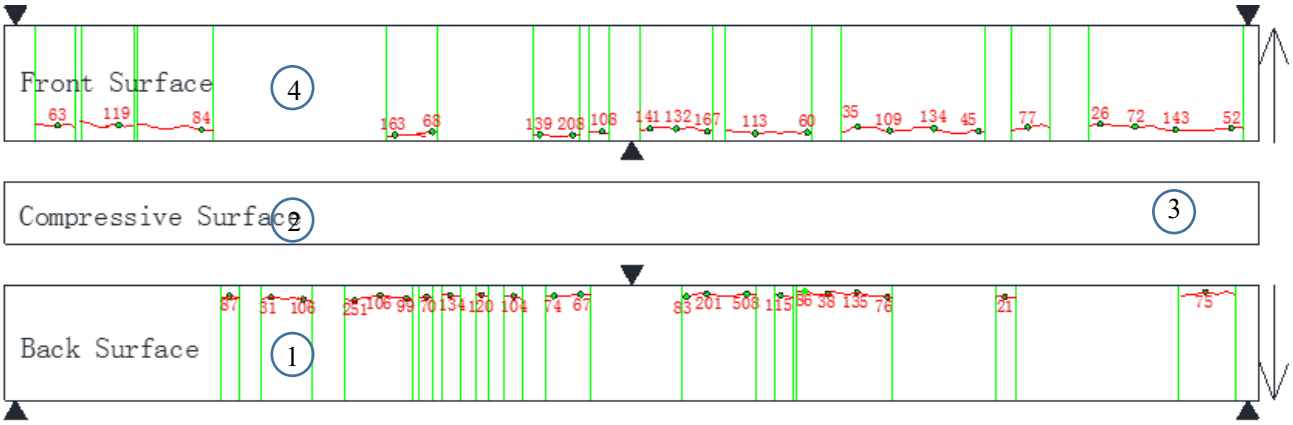

Figure IV-54.2 Cracking maps of beam C2 after 38 months

Figure IV-54 Corrosion-induced cracking maps of beam C2 (crack widths in μm)

Figure IV-55.1 Cracking maps of beam C3 after 29 months

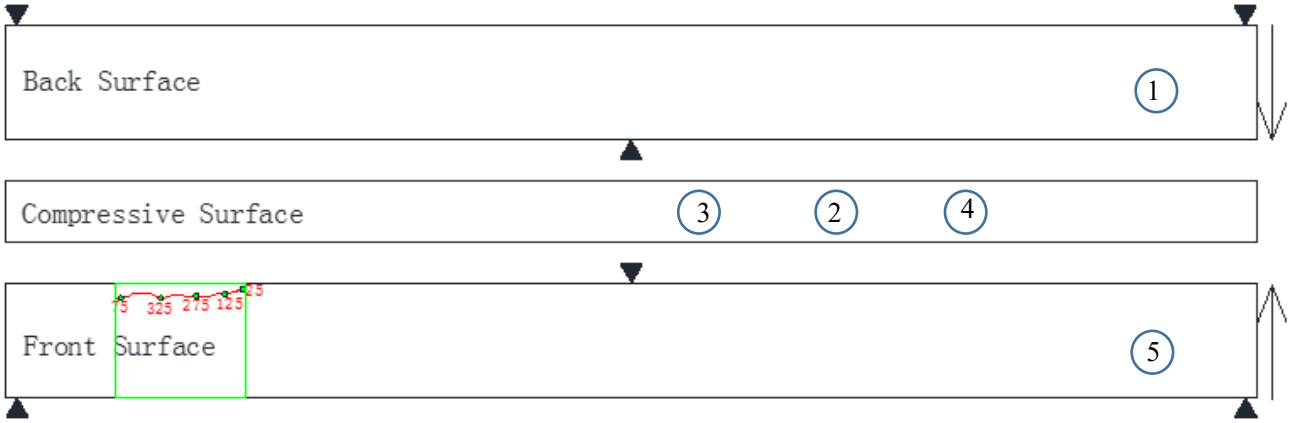

Figure IV-55.2 Cracking maps of beam C3 after 48 months

Figure IV-55 Corrosion-induced cracking maps of beam C3 (crack widths in μm)

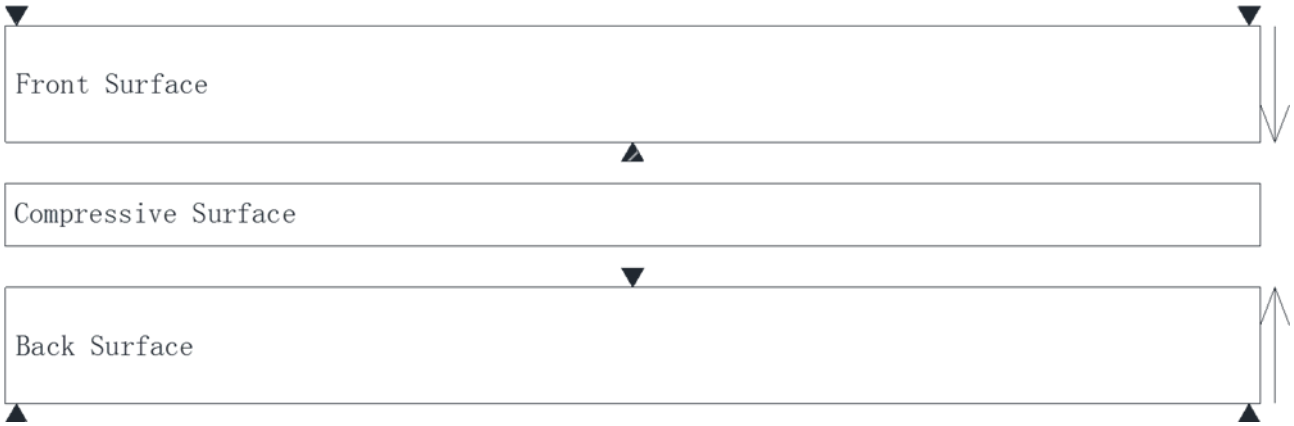

Figure IV-56 Corrosion-induced cracking maps of beam C4 (crack width in μm)

Table IV-7 presents the development of corrosion-induced crack length along compressive bars of C beams at different corroding ages. From Figures 9 and 10, it can be observed that the longest and widest corrosion-induced cracks appeared in the compressive zone of beam C1 and beam C2

and the length development of corrosion-induced cracks was significant during 29 to 38 months of exposure. It should be noted that some tiny corrosion-induced cracks appeared on the front side of C2 after 24 months of exposure. In contrast, if the compressive zone was without defects, as in the compressive zones of beams C3 and C4, the appearance of corrosion-induced cracks was delayed to 48 months for C3 and did not occur for C4 until 48 months. This means that top-casting-induced defects favored the development of corrosion and the appearance of corrosion-induced cracks.

Table IV-7 Length of corrosion-induced cracks of C beams at different corroded ages

	Interfacial state	**Exposure conditions**		**Length of corrosion-induced cracks (mm)**					
			Exposure time (month)	0	8	24	29	38	48
C1	Defects	Top exposure	Front side	0	692.8	1194.5	2140.3	2388.9	
			Bottom side	0	0	897.4	1509.4	1812.6	
C2	Defects	Bottom exposure	Front side	0	0	0	1542.6	1598	
			Bottom side	0	0	0	0	1168.9	
C3	No defects	Top exposure	Front side	0	0	0	0		303
			Bottom side	0	0	0	0		0
C4	No defects	Bottom exposure	Front side	0	0	0	0		0
			Bottom side	0	0	0	0		0

Note Beams C1 and C2 were broken after 38 months of exposure, so the lengths of corrosion-induced cracks were not recorded.

4.4.3 Effect of casting direction and exposure condition on chloride ingress

Figure IV-57 presents the distribution of chlorides at different depths below the compressive and lateral surfaces of the four C beams. The two yellow lines in Figure IV-57 represent the diameter and position of the compressive bar embedded in the concrete beam. The chloride concentration at the location of the compressive bar indicated in Figure IV-58 was calculated according to Figure IV-57.

For the four beams, Figure IV-59 (a) shows a different chloride concentration at the outside and inside parts of the reinforcement of beam from lateral ingress, which exceeded the general

chloride threshold concentration given by ACI and RILEM [25].

Figure IV-58(b) concerns the effect of exposure conditions on the chloride ingress from the compressive surface. Here, the chloride concentration of beam C1 was significantly higher than that of beam C2. This is because the compressive surface of beam C1 was the upper surface exposed to salt spray, whereas the compressive surface of beam C2 was the bottom surface and chlorides could not accumulate at the bottom surface.

The effect of casting direction on the chloride penetration from the compressive surface is shown in Figure IV-58(c). The chloride concentration of beam C1 was slightly higher than that of beam C3. Although they were located at the same position, more chloride ions could penetrate in the compressive zone of beam C1 due to the more porous concrete cover formed by top-casting, while the compressive zone of beam C3 was denser due to bottom-casting.

In Figure IV-58(d), we combined the effect of exposure direction and casting direction by comparing C2 and C3 beams. Results show that the effect of exposure conditions on the chloride penetration from the top exposure compressive surface was more important than the effect of casting direction.

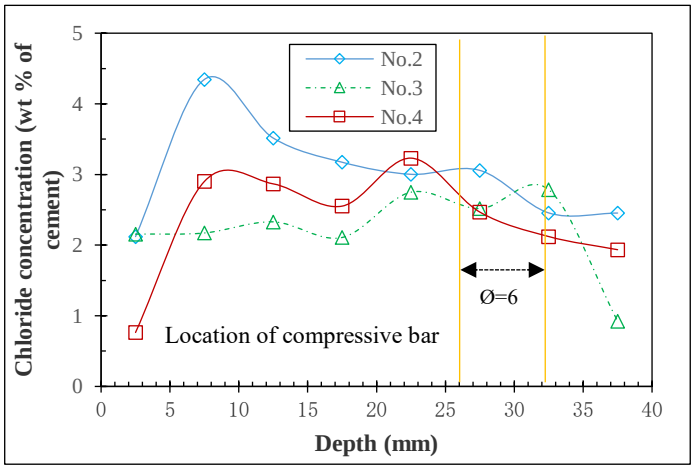

Figure IV-57 (a) Beam C1 compressive surface

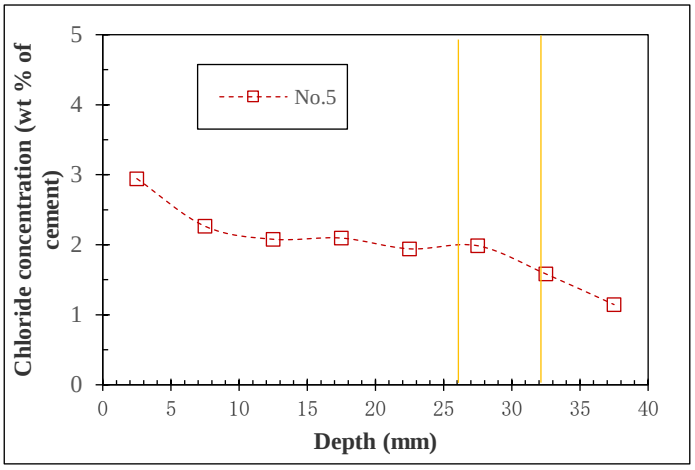

Figure IV-57 (b) Beam C1 lateral surfaces

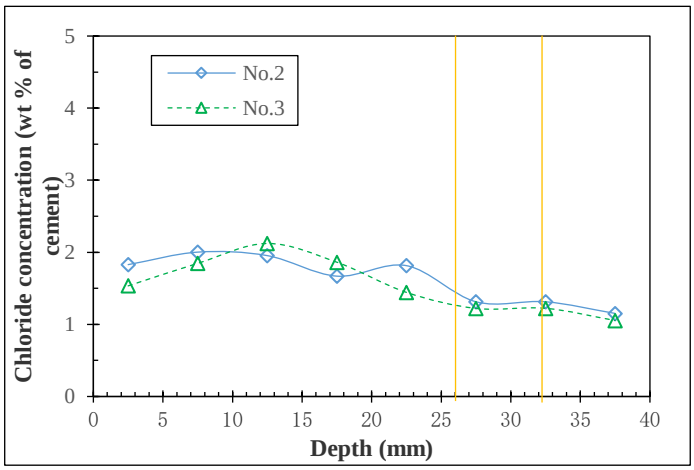

Figure IV-57 (c) Beam C2 compressive surface

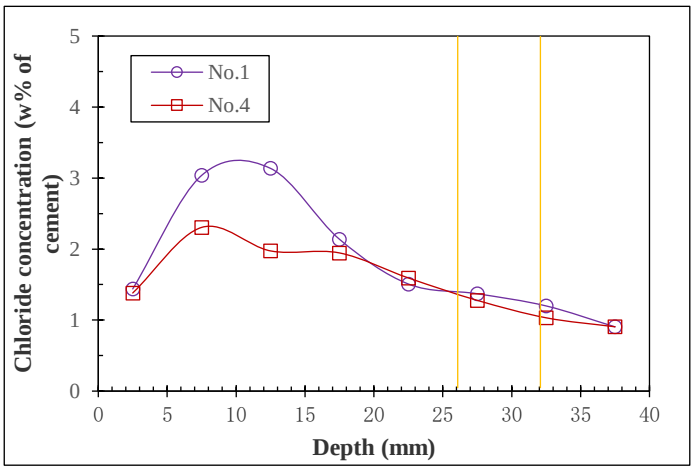

Figure IV-57 (d) Beam C2 lateral surfaces

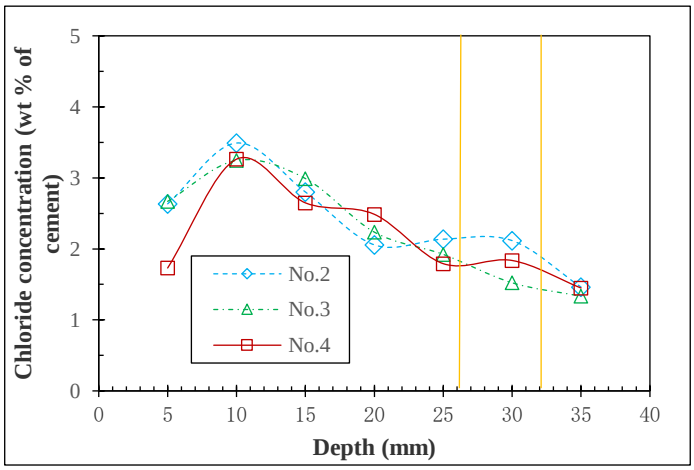

Figure IV-57 (e) Beam C3 compressive surface

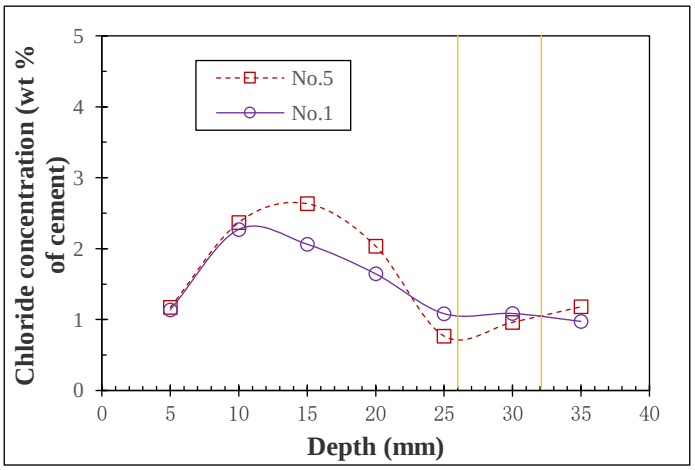

Figure IV-57 (f) Beam C3 lateral surfaces

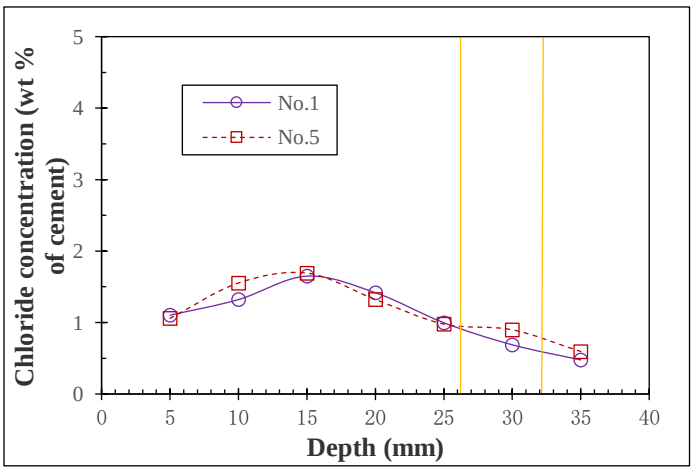

Figure IV-57 (g) Beam C4 lateral surfaces

Figure IV-57 Chloride profiles of beams C1 and C2 for 38 months and C3 and C4 for 48 months

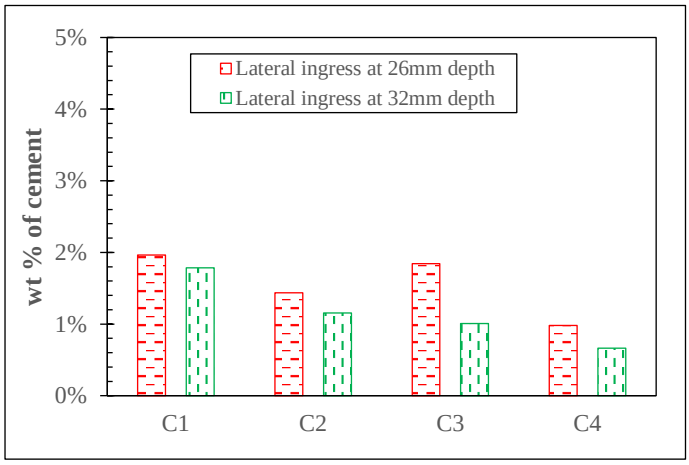

Figure IV-58 (a) Chloride ingress from lateral surfaces

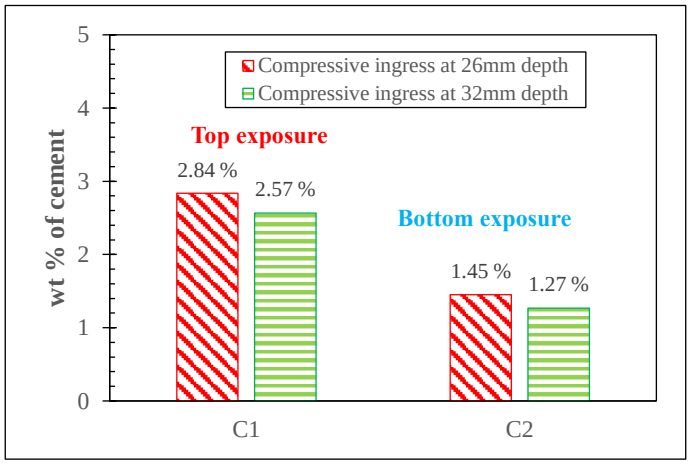

Figure IV-58 (b) Chloride ingress from compressive surface

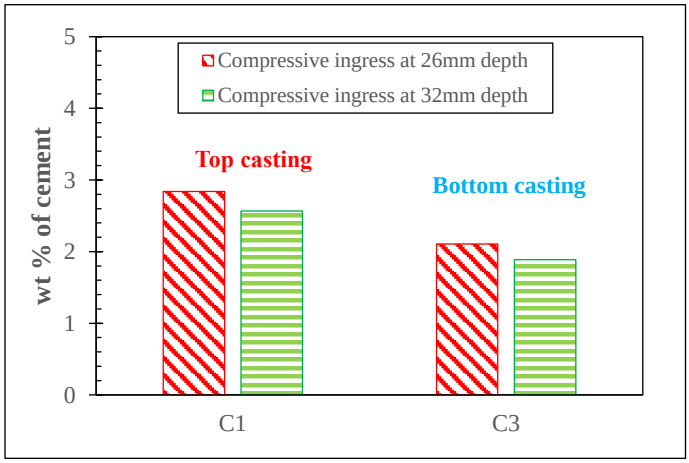

Figure IV-58 (c) Chloride ingress from compressive surface

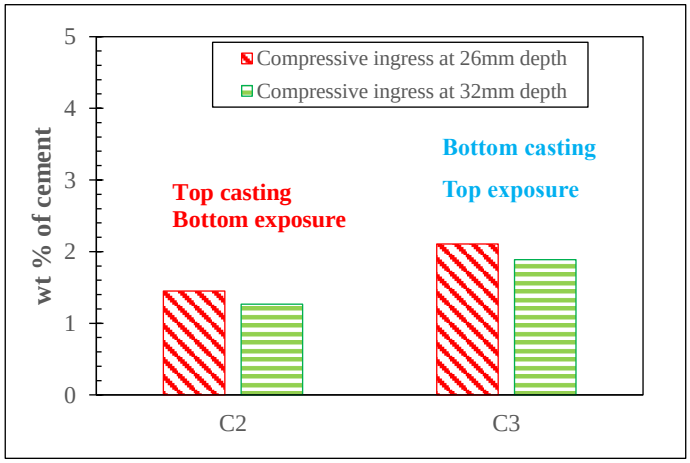

Figure IV-58 (d) Chloride ingress from compressive surface

Figure IV-58 Chloride concentration at the level of the surface of compressive bar according to different exposure and casting directions

4.4.4 Effect of top-casting-induced defects on the cross-sectional loss of compressive bars

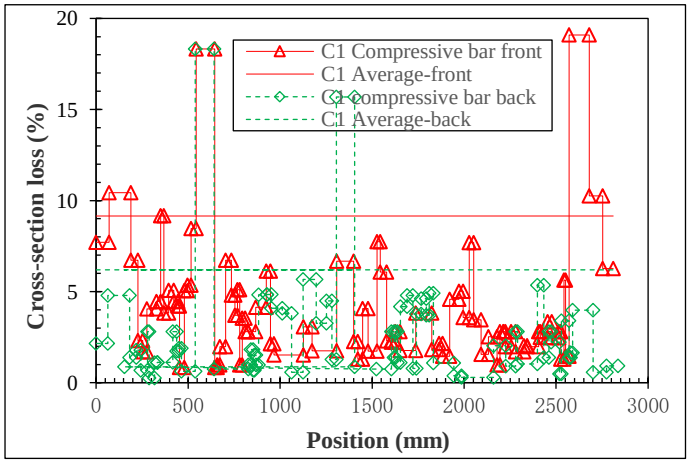

Figure IV-59 (a) Cross-sectional loss of beam C1 at 38 months

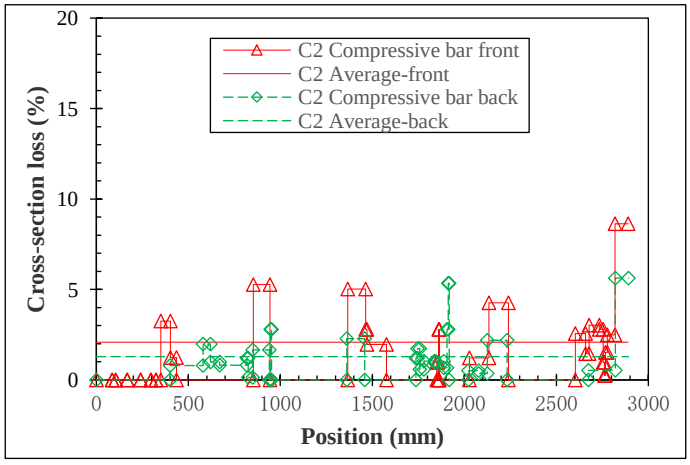

Figure IV-59 (b) Cross-sectional loss of beam C2 at 38 months

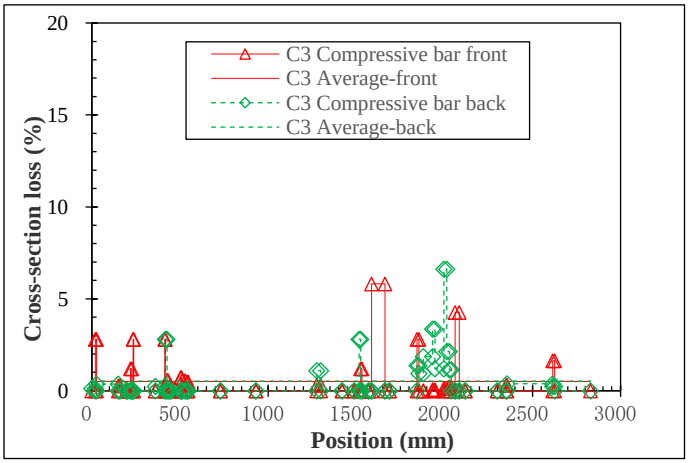

Figure IV-59 (c) Cross-section loss of beam C3 at 48 months

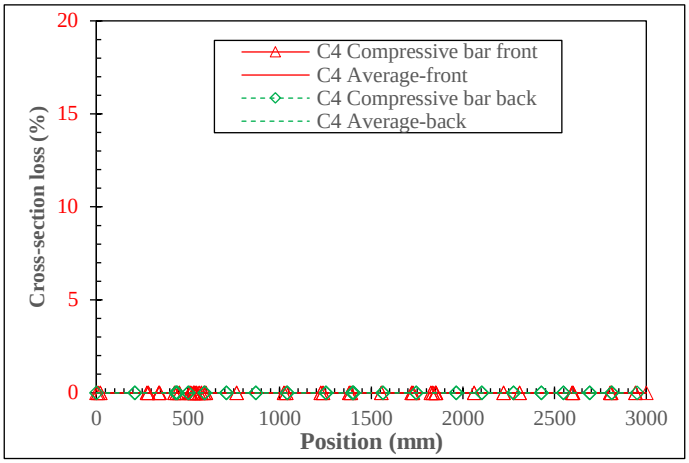

Figure IV-59 (d) Cross-section loss of beam C4 at 48 months

Figure IV-59 Cross-sectional loss of the compressive bars in beams C at different ages

Figure IV-59 shows the loss of cross-section of the compressive bar embedded in each C beam. Figure IV-60, Figure IV-61 and Figure IV-62 present the average and maximum losses of cross-section of compressive bars in relation to different exposure conditions and casting directions.

1). Effect of casting direction For beams C1 and C3, with the same exposure conditions but different casting directions, Figure IV-59(a), Figure IV-59(b), Figure IV-60(a) and Figure IV-60(b), show that the average and maximum loss of cross-section of the compressive bar of beam C1 are significantly higher than those of beam C3 and there is more pitting along the compressive bar of beam C1 than that of beam C3. The same phenomenon can also be found in beams C2 and C4 (Figure IV-60(c) and Figure IV-60(d)), with, again, the same exposure but different casting directions. It can be deduced that, under the same exposure conditions, top-casting defects lead to greater average and maximum loss of cross-section in the compressive bar.

2.) Effect of exposure conditions For beams C1 and C2, with the same casting direction but different exposures, Figure IV-59(a), Figure IV-59(c), Figure IV-61(a) and Figure IV-61(b), show that the average and maximum loss of cross-section of the compressive bar of beam C1 are significantly higher than those of beam C2. Similar results can be found on the compressive bars of beams C3 and C4 (Figure IV-61(c) and Figure IV-61(d)), which also had the same casting direction but different exposures. This means that, for the same casting direction, top exposure conditions lead to more serious cross-sectional loss of compressive bar.

3.) For different casting directions and different exposure conditions, as in beams C2 and C3, it can be seen that beam C2 was subjected to more serious corrosion in terms of distribution of

pitting and average and maximum loss of cross-section of the compressive bar at 38 months, while only some pitting corrosion was found on the compressive bar of beam C3 at 48 months (Figure IV-59(c)). This means that the effect of top-casting-induced defects on corrosion is stronger than the effect of exposure conditions.

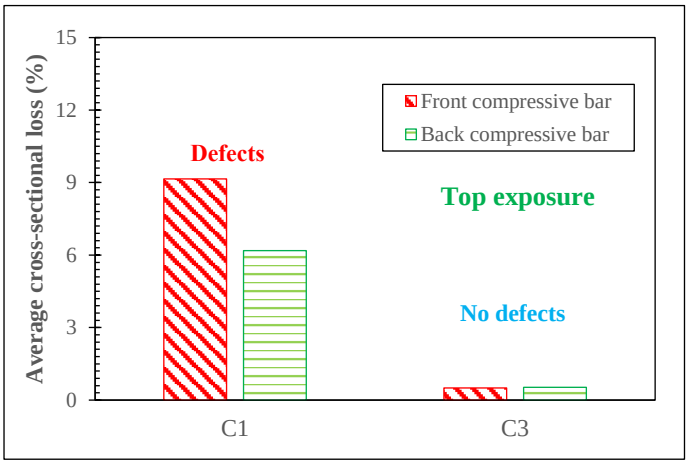

Figure IV-60 (a) Average cross-sectional loss

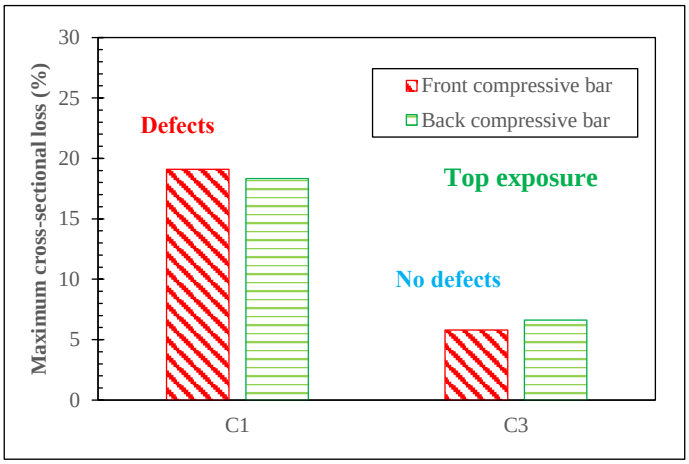

Figure IV-60 (b) Maximum cross-sectional loss

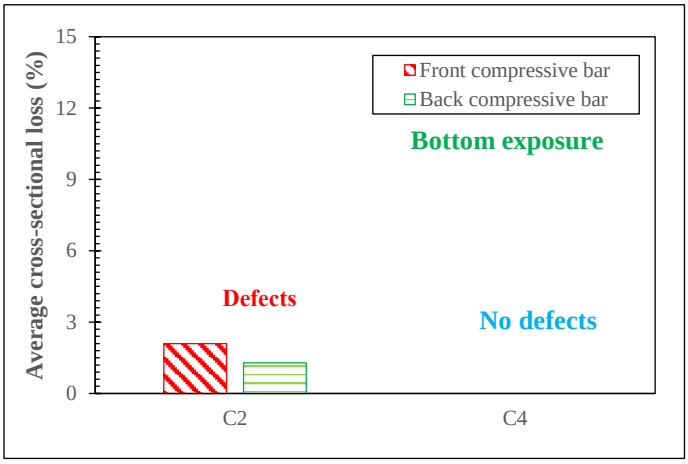

Figure IV-60 (c) Average cross-sectional loss

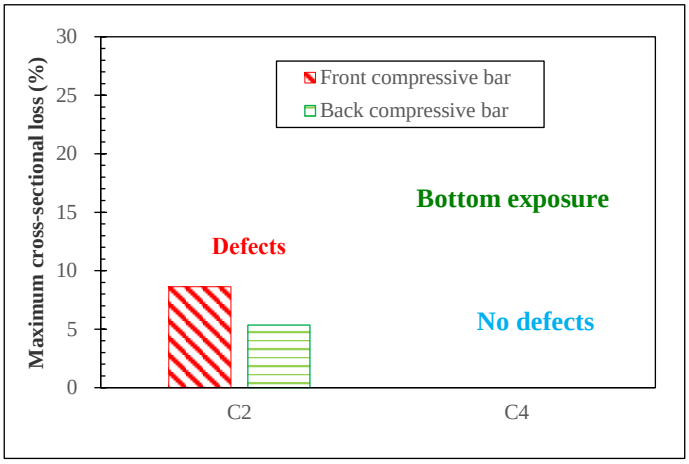

Figure IV-60 (d) Maximum cross-sectional loss

Figure IV-60 Effect of top-casting defects on loss of cross-section of compressive bar

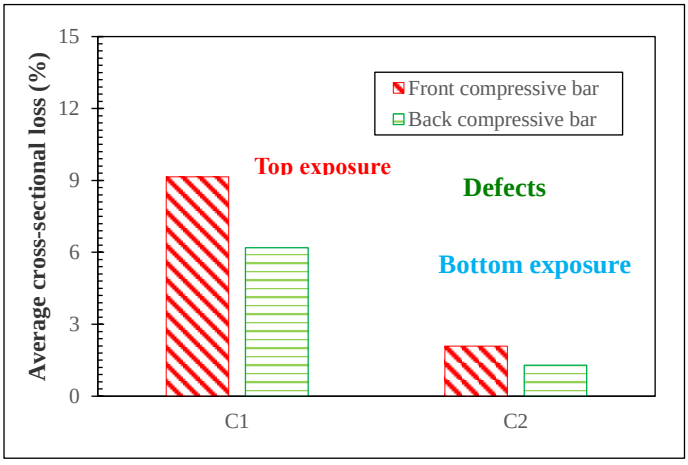

Figure IV-61 (a) Average cross-sectional loss

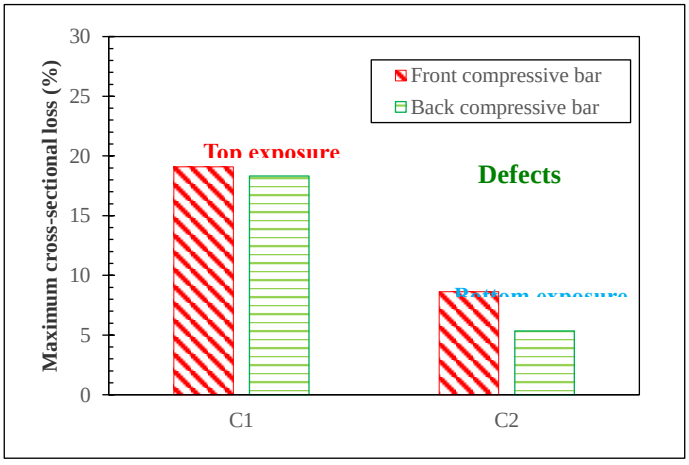

Figure IV-61 (b) Maximum cross-sectional loss

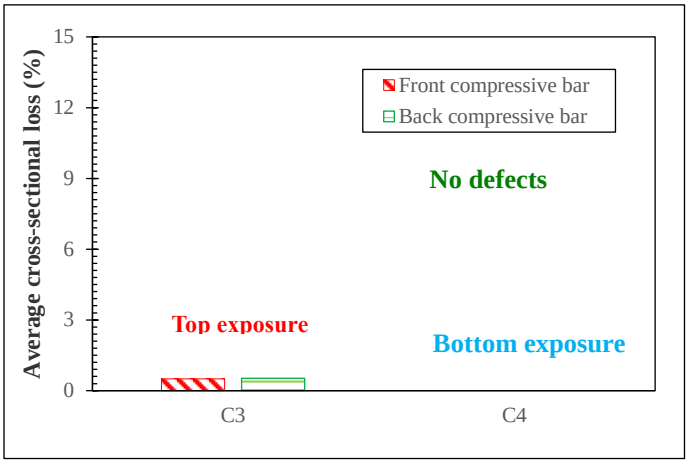

Figure IV-61 (c) Average cross-sectional loss

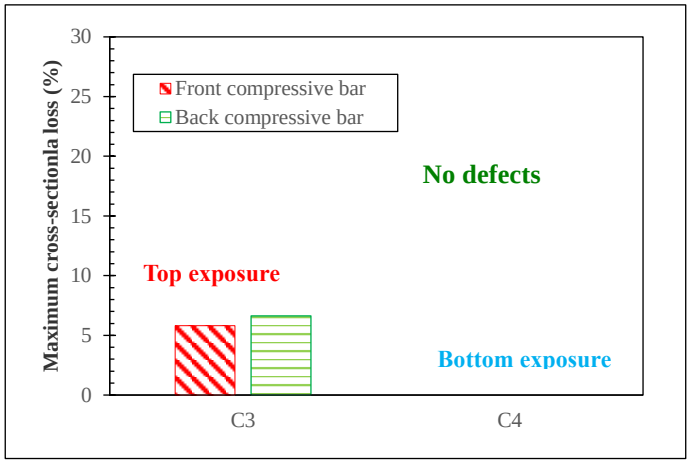

Figure IV-61 (d) Maximum cross-sectional loss

Figure IV-61 Effect of exposure conditions on loss of cross-section of compressive bar

4.4.5 Corrosion propagation along and around the perimeter of the compressive bars

After the initiation of chloride induced corrosion, according to Zhang et al. [26] and François et al. [27], there are 3 steps in the propagation process. In the first step, localized corrosion is the major phenomenon until the appearance of the first corrosion-induced cracks. In the presence of corrosion-induced cracks, corrosion evolves and becomes generalized; this is the second step of the corrosion process. When spalling of the concrete occurs, a third step of propagation begins where generalized corrosion is the major phenomenon in the spalling zone.

According to the cracking maps in Figure IV-53 to Figure IV-56 and the cross-sectional loss in Figure IV-59, we can find that distribution of corrosion on the compressive bars was not uniform. Some parts were still in initiation phase (no corrosion), others are in first propagation state (corrosion occurred but no corrosion-induced cracks were found on the concrete surface) and some are in second propagation state (corroded and some corrosion-induced cracks appeared on the concrete surface). The effect of top-casting-induced defects and the top exposure condition on the development of the chloride-induced corrosion around the perimeter and along the length of the re-bars, is discussed below.

➢ **Corrosion propagation of beams with top-casting-induced defects**

Width of corrosion induced cracks can reflect corrosion degree at a certain extent [27, 28]. Here we analyzed the relationship between corrosion distribution around the perimeter of the compressive bars and the width of corrosion induced cracks. As presented in Section 7.3.4, corrosion

area within a certain length was divided into four parts, including top side, bottom side, outside and inside. Figure IV-62 presented the relationship between crack width and corrosion distribution around the perimeter of steel bars in beam C2. It should be noted that corrosion around the perimeter of steel bars was characterized by the ratio of corrosion area of one quarter around perimeter (top, bottom, outside or inside) within a certain length to the total corrosion area of the compressive bar.

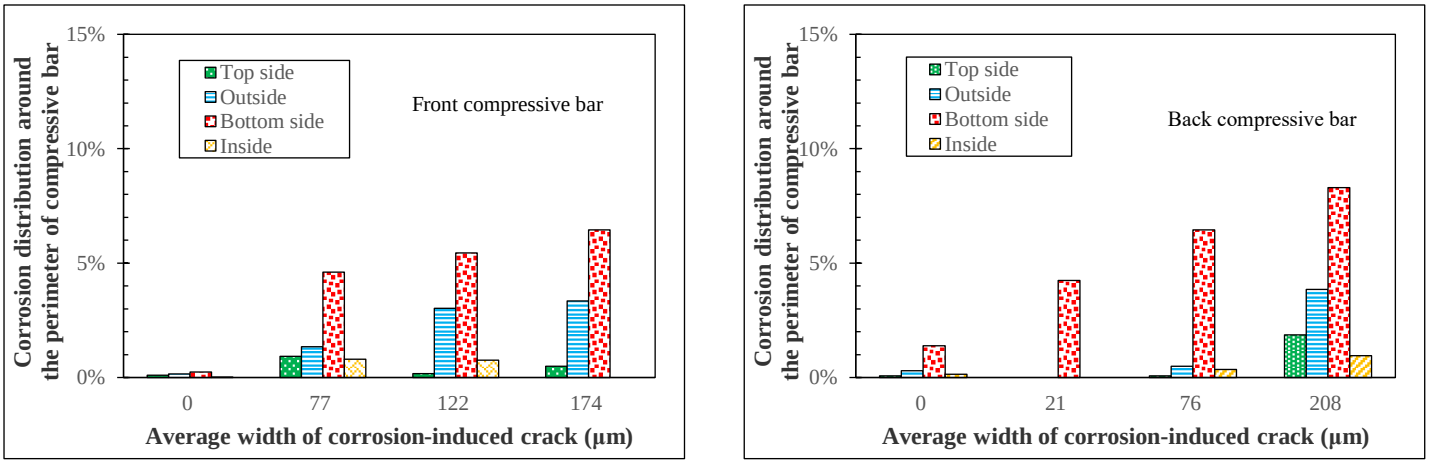

Figure IV-62 Relationship between average width of corrosion-induced cracks and corrosion distribution around the perimeter of compressive bars in beam C2

From Figure IV-62, when there were no corrosion-induced cracks, namely, the value of average width and average length was zero, corrosion always firstly took place on the bottom side with top-casting defects (case of corrosion without corrosion-induced cracks). When corrosion-induced cracks appeared and the crack opening gradually increased, the corrosion develops progressively on the other three sides of compressive bar but the bottom side remains the most attacked by corrosion.

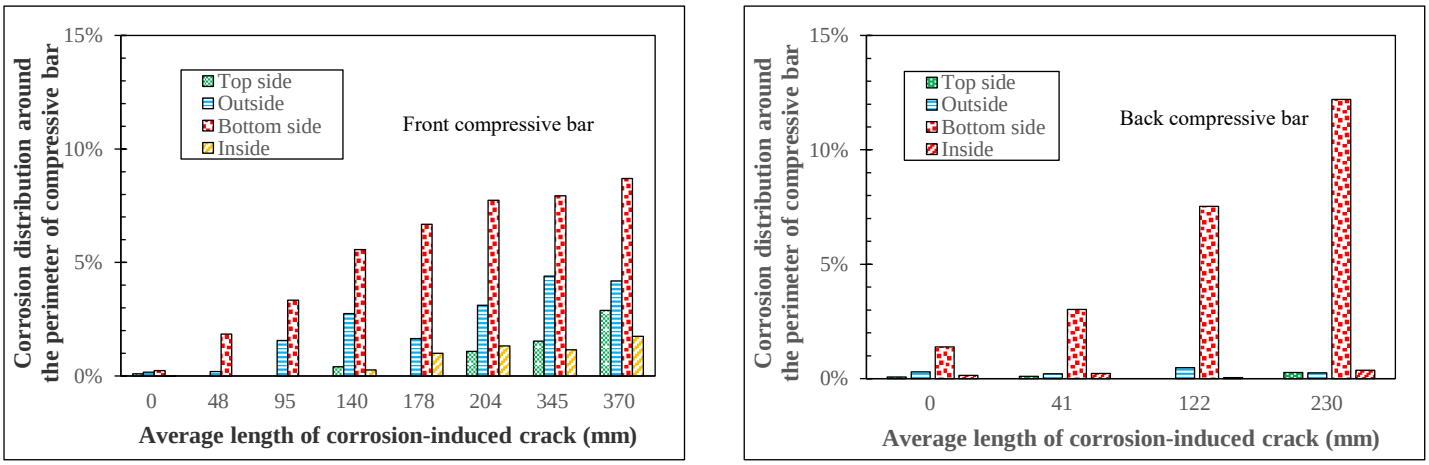

Figure IV-63 Relationship between average length of corrosion-induced cracks and corrosion distribution around the perimeter of compressive bars in beam C2

Figure IV-63 presents the relationship between the lengths of corrosion induced cracks and corrosion distribution around the perimeter of the compressive bars of beam C2. It shows that

corrosion initiated on the bottom side of compressive bar and then gradually evolved from bottom side to other three sides of steel bar accompanying with the development of corrosion induced cracks.

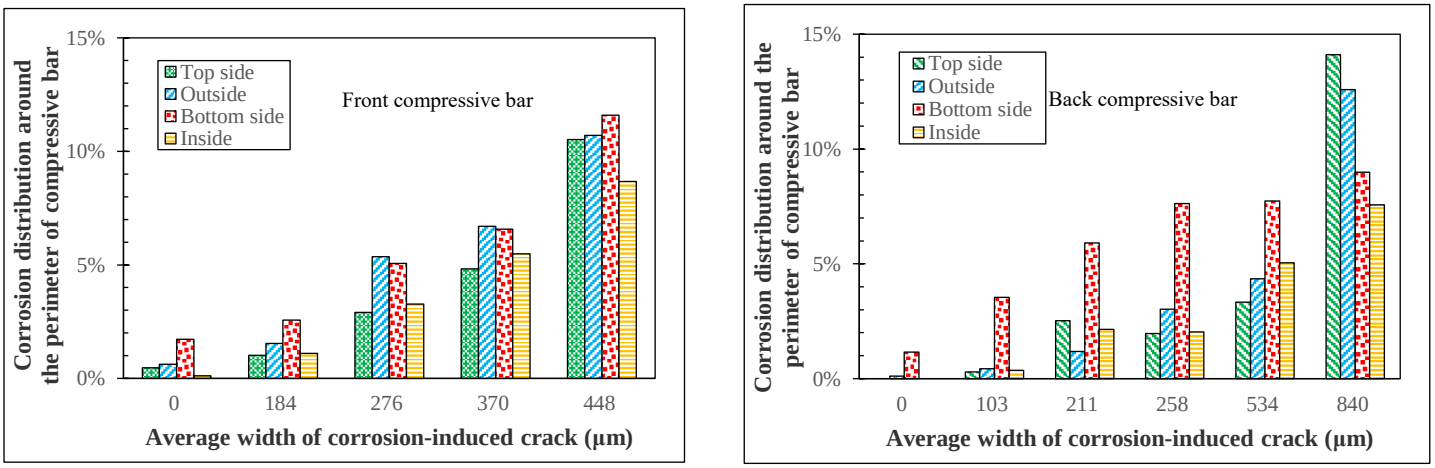

Figure IV-64 Relationship between average width of corrosion-induced cracks and corrosion distribution around the perimeter of compressive bars in beam C1

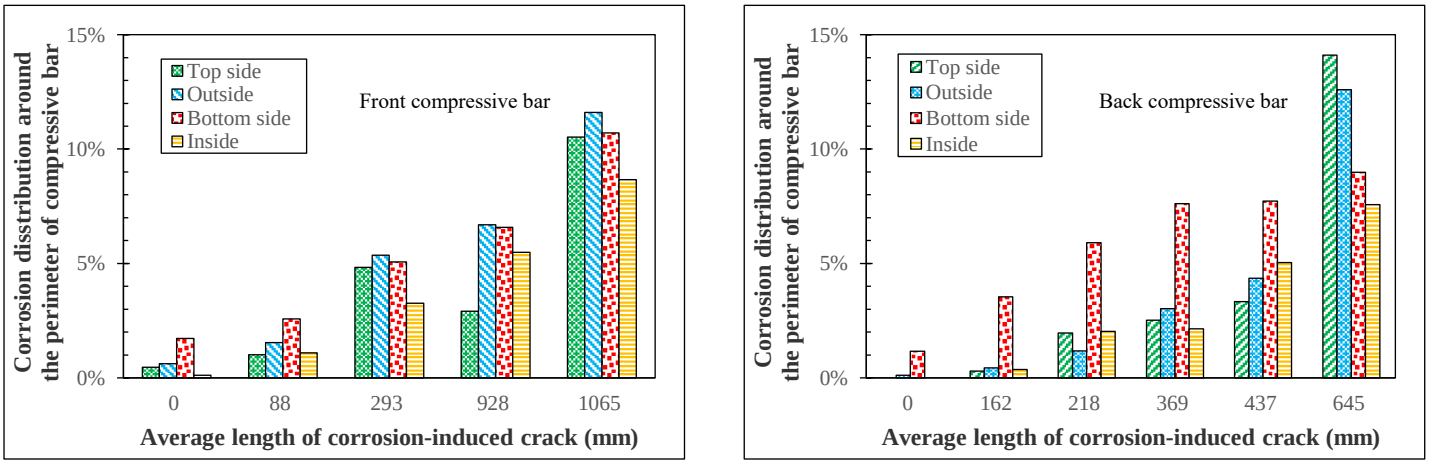

Figure IV-65 Relationship between average length of corrosion-induced cracks and corrosion distribution around the perimeter of compressive bars in beam C1

Same analysis was conducted on beam C1, the relationship between corrosion distribution around the perimeter and the width/length of corrosion induced cracks was presented in Figure IV-64 and Figure IV-65 respectively. Comparing Figure IV-53 and Figure IV-54, it could be found that more corrosion induced cracks were found on beam C1, and the maximum width of corrosion induced cracks on beam C1 was wider than that on beam C2. It means that the corrosion degree of compressive bars in beam C1 was more serious than beam C2. From Figure IV-64 and Figure IV-65, we can conclude that corrosion distribution became more uniform around the perimeter with the corrosion degree increased.

This result means top-casting defects no longer affected the evolution of corrosion process

when the corrosion degree exceeded a threshold value.

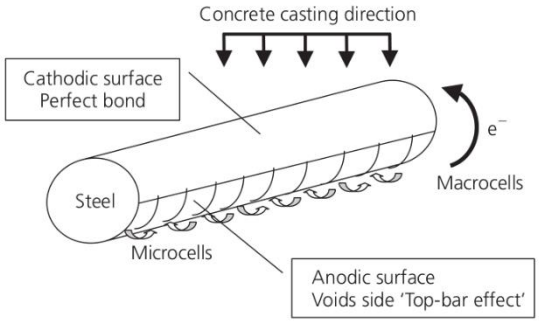

Figure IV-66 Macro-cell formation for re-bars affected by the "top-bar effect" [17]

Some research has confirmed that the corrosion starts at the side of a steel bar with defects [17, 19, 22] due to the difference of micro-environment between the sides of the steel bar with and without defects. In the first step of propagation, the side of the reinforcement bar with defects acts as an anode, while the side of steel bar without defects acts as a cathode (Figure IV-66). So, during the first step of propagation, the corrosion of steel bar takes place on the bottom side relative to the casting direction. With the evolution of corrosion, large amounts of corrosion products are formed. Corrosion products would firstly fill the defects [17]. During this stage, localized corrosion is the dominant process. Then, corrosion products, which have a greater volume than the initial steel, induce tiny corrosion cracking when the resulting tensile stress in the surrounding concrete reaches the tensile strength limit of concrete. This is the start of the second step of propagation, which progressively leads to a generalization of the corrosion around the perimeter of the steel bars in front of corrosion-induced cracks.

➢ **Corrosion propagation in beam without top-casting-induced defects**

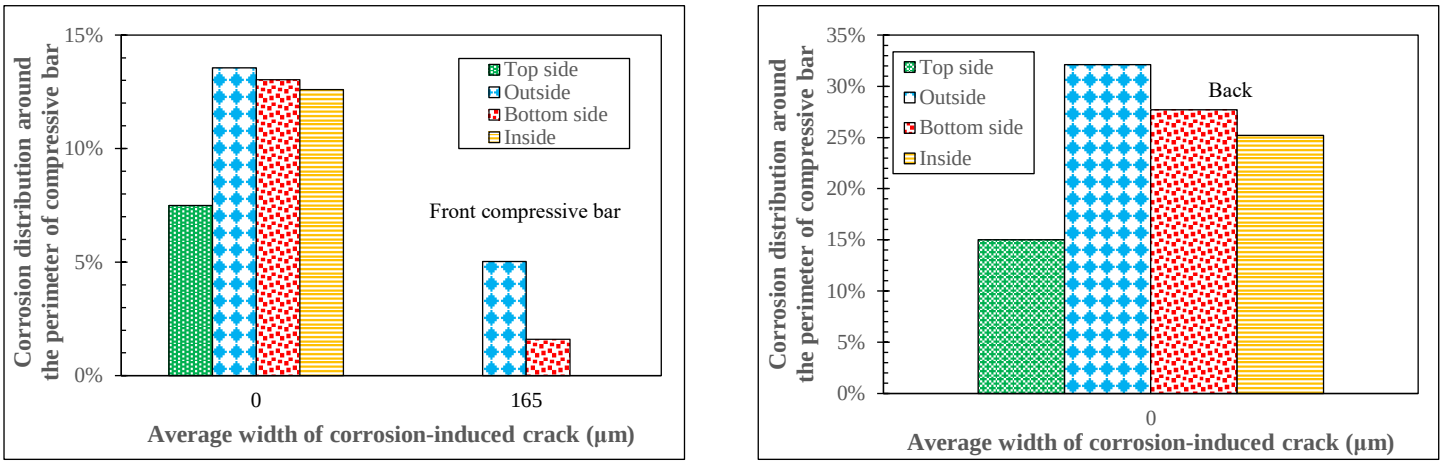

Figure IV-67 Relationship between average width of corrosion-induced cracks and corrosion distribution around the perimeter of compressive bar in beam C3

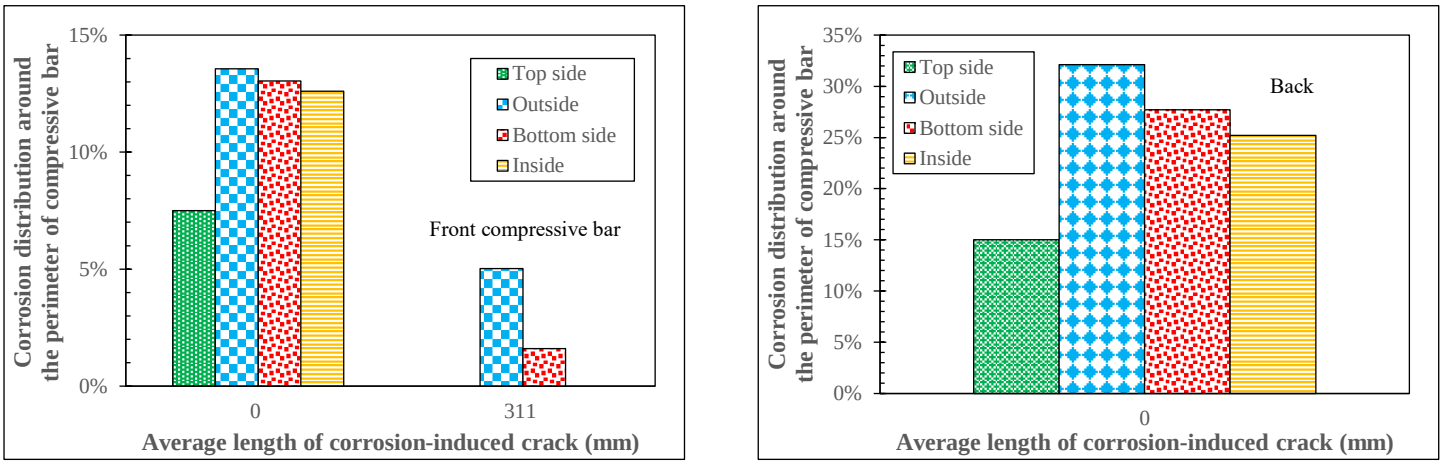

Figure IV-68 Relationship between average length of corrosion-induced cracks and corrosion distribution around the perimeter of compressive bar in beam C3

Without top-casting-induced defects, only C3 beam exhibited some corrosion and some corrosion-induced cracks. No corrosion was found on the compressive bars of beam C4.

Figure IV-67 and Figure IV-68 show that for C3 beam, corrosion developed all along the perimeter of re-bars with a slight tendency to be more pronounced on the outside and bottom sides which are the sides closet to the concrete surfaces (lateral and top) where chloride ingress.

4.5 Conclusion

Four beams with the same concrete cover depth but different casting directions and exposure conditions were investigated. The corrosion-induced cracking maps, chloride profiles of concrete, cross-sectional loss of compressive bars, and corrosion distribution around and along the compressive bars of the four beams were studied and compared with each other. The following

conclusions were drawn

1. Top-casting-induced defects occurred at the bottom part of the reinforcement on the upper part of beams, led to earlier corrosion initiation and first development at the location of the defects.

2. After the appearance of corrosion-induced cracks, corrosion spread all around the perimeter of the reinforcing bars.

3. Without top-casting defects, corrosion initiated and first developed preferentially at the outside surface of reinforcing bars, closer to the concrete surface exposed to chloride environment.

4. Top-casting-induced defects strongly accelerated the corrosion process and reduced the service life of RC structures.

5. Top-casting-induced defects coupled with top surface exposure gave the worst conditions for durability of steel reinforcements in concrete beams.

4.6 References

[1] A. Neville, Chloride attack of reinforced concrete: an overview, Materials and structures, 28 (1995) 63.
[2] L. Bertolini, B. Elsener, P. Pedeferri, E. Redaelli, R.B. Polder, Corrosion of steel in concrete: prevention, diagnosis, repair, John Wiley & Sons2013.
[3] M. Mahmaran, Yaman, Influence of transverse crack width on reinforcement corrosion initiation and propagation in mortar beams, Canadian Journal of Civil Engineering, 35 (2008) 236-245.
[4] C. Arya, F. Ofori-Darko, Influence of crack frequency on reinforcement corrosion in concrete, Cement
Concrete Research, 26 (1996) 345-353.
[5] G. Balabanic, N. Bicanic, A. Duerkovic, The influence of w/c ratio, concrete cover thickness and degree of water saturation on the corrosion rate of reinforcing steel in concrete, Cement and concrete Research, 26 (1996) 761-769.
[6] R. François, G. Arliguie, Influence of service cracking on reinforcement steel corrosion, Journal of Materials in Civil Engineering, 10 (1998) 14-20.
[7] P. Mangat, B. Molloy, Factors influencing chloride-induced corrosion of reinforcement in concrete, Materials and Structures, 25 (1992) 404-411.
[8] A. Michel, A.O.S. Solgaard, B.J. Pease, M.R. Geiker, H. Stang, J.F. Olesen, Experimental investigation of the relation between damage at the concrete-steel interface and initiation of reinforcement corrosion in plain and fibre reinforced concrete, Corrosion Science, 77 (2013) 308-321.
[9] T.U. Mohammed, N. Otsuki, H. Hamada, T. Yamaji, Chloride-induced corrosion of steel bars in concrete with presence of gap at steel-concrete interface, Materials Journal, 99 (2002) 149-156.

[10] M. Otieno, M. Alexander, H.-D. Beushausen, Corrosion in cracked and uncracked concrete,influence of crack width, concrete quality and crack reopening, Magazine of Concrete Research, 62 (2010) 393-404.
[11] J. Ryou, K. Ann, Variation in the chloride threshold level for steel corrosion in concrete arising from different chloride sources, Magazine of Concrete Research, 60 (2008) 177-187.
[12] B. Sangoju, R. Gettu, B. Bharatkumar, M. Neelamegam, Chloride-induced corrosion of steel in cracked OPC and PPC concretes: Experimental study, Journal of materials in civil engineering, 23 (2011) 1057-1066.
[13] A. Scott, M. Alexander, The influence of binder type, cracking and cover on corrosion rates of steel in chloride-contaminated concrete, Magazine of Concrete Research, 59 (2007) 495-505.
[14] W. Sun, Y. Zhang, S. Liu, Y. Zhang, The influence of mineral admixtures on resistance to corrosion of steel bars in green high-performance concrete, Cement and Concrete Research, 34 (2004) 1781-1785.
[15] K.S. Tuutti, Corrosion of steel in concrete, (1982).
[16] T. Vidal, A. Castel, R. François, Corrosion process and structural performance of a 17 year old reinforced concrete beam stored in chloride environment, Cement and Concrete Research, 37 (2007) 1551-1561.
[17] R. Zhang, A. Castel, R. François, Influence of steel-concrete interface defects owing to the top-bar effect on the chloride-induced corrosion of reinforcement, Magazine of Concrete Research, 63 (2011) 773-781.
[18] T.A. Soylev, R. François, Quality of steel-concrete interface and corrosion of reinforcing steel, Cement and Concrete Research, 33 (2003) 1407-1415.
[19] T.A. Soylev, R. François, Corrosion of reinforcement in relation to presence of defects at the interface between steel and concrete, Journal of materials in civil engineering, 17 (2005) 447-455.
[20] A. Kenny, A. Katz, Statistical relationship between mix properties and the interfacial transition zone around embedded rebar, Cement and Concrete Composites, 60 (2015) 82-91.
[21] A. Horne, I. Richardson, R. Brydson, Quantitative analysis of the microstructure of interfaces in steel reinforced concrete, Cement and Concrete Research, 37 (2007) 1613-1623.
[22] W.H. Hartt, J. Nam, Effect of cement alkalinity on chloride threshold and time-to-corrosion of reinforcing steel in concrete, Corrosion, 64 (2008) 671-680.
[23] L. Yu, R. François, R. Gagné, Influence of steel-concrete interface defects induced by top-casting on development of chloride-induced corrosion in RC beams under sustained loading, Materials and Structures, 49 (2016) 5169-5181.
[24] V.H. Dang, R. Francois, Influence of long-term corrosion in chloride environment on mechanical behaviour of RC beam, Engineering Structures, 48 (2013) 558-568.
[25] E. Committee, Eurocode2: Design of concrete structures-Part 1-2: General rules-Structural fire design, ENV 1992-1-2, 1995.
[26] R. Zhang, A. Castel, R. François, Concrete cover cracking with reinforcement corrosion of RC beam during chloride-induced corrosion process, Cement and Concrete Research, 40 (2010) 415-425.
[27] R. François, S. Laurens, F. Deby, 4 - In situ Corrosion Diagnosis, Corrosion and its Consequences for Reinforced Concrete Structures, Elsevier2018, pp. 77-104.
[28] T. Vidal, A. Castel, R. Francois, Analyzing crack width to predict corrosion in reinforced concrete, Cement and concrete research, 34 (2004) 165-174.

5 Corrosion behavior of stirrups in corroded concrete beams exposed to chloride environment under sustained loading

5.1 Abstract

This paper discusses the corrosion behavior of stirrups in two concrete beams under sustained loading, exposed to a chloride environment for 9 years. The cracking maps of concrete beams were recorded after 28 days and after 9 years. The corrosion maps of the stirrups were drawn and the cross-sectional losses of stirrups were measured after destroying the beams. The experimental results show that the horizontal legs of stirrups mainly corroded at the mid span of the tensile zone and at the ends of the compressive zone of the reinforced concrete beams regardless of the exposure conditions, while the opposite horizontal legs were protected. The corrosion of vertical legs of stirrups, which was slight, was not impacted by the load-induced cracks. There was no correlation between stirrups and the main reinforcing steels in the concrete in terms of corrosion. The corrosion behavior of the intersection between stirrups and main bars was controlled by the interfacial conditions between them. The location of cathodic protection area was affected by the corrosion process. In the first stage of corrosion, the area of cathodic protection mainly located at the mid span of top cast rebars in compressive side. In the second period of corrosion, apart from the previous cathode in compressive zone, the location of cathodic protection also located at the ends of bottom cast rebars in tensile zone.

Key words: corrosion; horizontal stirrups; vertical stirrups; intersection of main steel bars.

5.2 Introduction

Steel corrosion results in the deterioration of reinforced concrete structures and constitutes their main durability issue [29].Numerous studies have been published on the corrosion behavior of the main deformed steel rebars embedded in concrete structures and show that the development of corrosion on reinforcement steel bars is controlled by the quality of the steel-concrete interface [1, 9, 13, 14, 16-19, 21, 23, 30-40]. Stirrups, which are regarded as an important part of the reinforcement of concrete structures[41], are used for fixing the location of the main deformed steel bars during the manufacture and installation of the steel frame and for bearing the shear stress during

the service life of the reinforced concrete structure[42]. However, the corrosion behavior of stirrups used in reinforced concrete has received very little research attention.

A common stirrup can be divided into three parts according to the casting direction of the concrete: horizontal legs, vertical legs and corners. The relative orientation of the different legs of the stirrups and the casting direction of the fresh concrete governs the conditions at the stirrup-concrete interface. Some published investigations have confirmed that the steel corrosion behavior is closely related to the interfacial conditions [30, 43]. A study of the characteristics of a steel-mortar interface by Horne et al.[21] indicated that few interfacial defects could be seen surrounding the vertically orientated reinforcing steels and the top side of horizontal steel rebars according to the casting direction but, when the bottom side of the horizontal steel rebar was considered, numerous top-casting defects were found in the steel-concrete/mortar interface, including air bubbles and bleed water voids, which were controlled by the casting height[30, 43-45]. However, hardly any articles concerning the interfacial conditions of the corner part of stirrups have been published. Alhozaimy et al.[46] reported that the concrete at the steel-concrete interface close to the intersections of two bars was more porous than that far from such intersections.

In the case of corrosion of stirrups in concrete, Mohammed et al.[9] indicated that pitting corrosion mainly occurred at the bottom of horizontal legs of stirrups according to the casting direction, while the vertical legs and the top side of horizontal legs were subject to general corrosion. Yu et al.[31] reported that some severe pitting corrosion mainly occurred at the top horizontal legs, corresponding to the tensile surface of the RC beam, especially when the stirrups were located at mid span of the RC beam. A few instances of pitting corrosion were observed at the top half vertical legs, while hardly any pitting corrosion was spotted on the bottom horizontal legs. Alhozaimy et al.[46] found that the stirrup corrosion rate was higher at locations where two bars intersected.

According to the fundamentals of differential metal contact corrosion, the corrosion of the main steel bar is related to the stirrups[47]. Ou Geng[47] considered that, during the period of corrosion, stirrups acted as anodes while the deformed steel bar was regarded as a cathode when electrical contact existed between them. Thus stirrups protect longitudinal deformed steel bar against corrosion. Tong[48] revealed that the corrosion of main reinforcing steels decreased as the diameter of the stirrups increased. In contrast, Mohammed et al. and Otsuki et al. [38, 49] investigated the

chloride-induced corrosion of steel bars with respect to their orientation in concrete and indicated that stirrups helped to accelerate the macrocell corrosion of main steel. However, this report[38] is a subject of some controversy, as François and Castel [36] consider that the conclusions obtained are not necessarily applicable to long-term corrosion processes.

The objective of the present investigation is to study the corrosion behavior of stirrups extracted from two reinforced concrete beams that had been exposed to a chloride environment under sustained load for 9 years. The cracking maps of the reinforced concrete beams were recorded first. Then, the microstructure of the steel-concrete interface was studied and, third, the cross-sectional loss of stirrups and the distribution of corrosion on them were measured and compared. The corrosion behavior of different legs of stirrups is analyzed and, finally, the relationship between stirrups and main reinforcing steels in concrete beams is discussed.

5.3 Experimental program

5.3.1 Reinforced concrete specimens

Two reinforced concrete beams, labelled As01 and As02, were prepared in 2010. Both were cast with the dimensions 3000×280×150 mm. The layout of reinforced concrete beams and the location of the sustained load are shown in Figure IV-69. The red lines in the figure indicate the tensile bars, while the green lines correspond to the compressive bars. The black lines between the compressive bar and tensile bar represent the stirrups.

Figure IV-70 shows the cross-section of the As beams. The thickness of the concrete cover around the stirrups is 40 mm. The diameters of the compressive bar, tensile bar and stirrups used here are 8 mm, 16 mm and 8 mm, respectively.

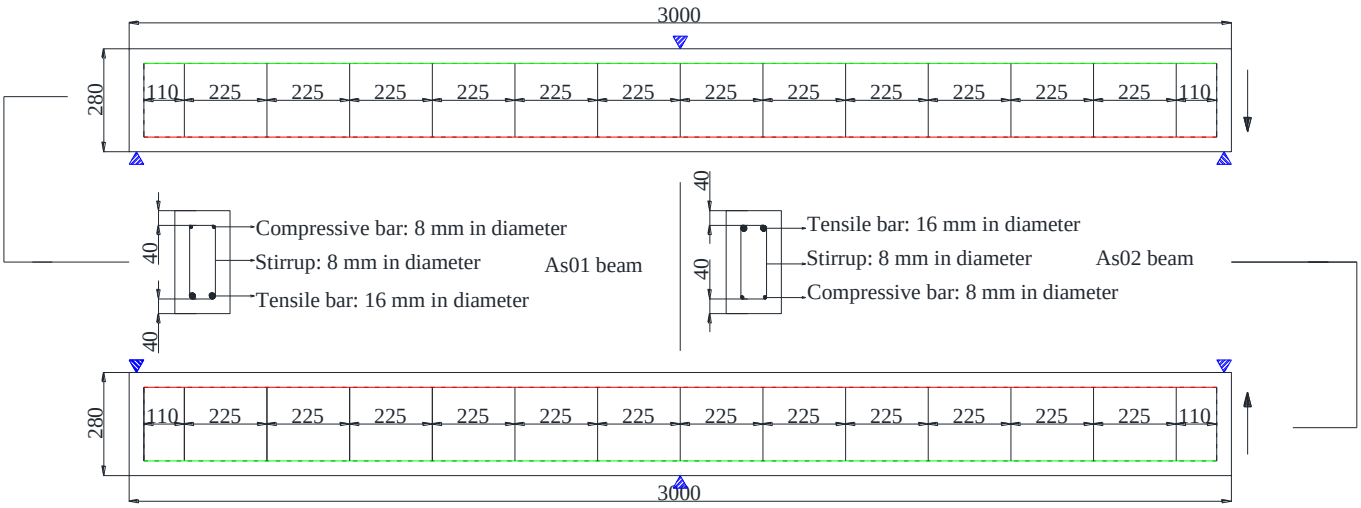

Figure IV-69 Layout of reinforced concrete beams (all dimensions in mm)

(The green lines represent the compressive bars, the red lines the tensile bars and the black lines the stirrups. The arrows represent the casting direction)

5.3.2 Raw materials

Cement (CEM Ⅰ, Grade 52.5 R) manufactured by the Lafarge Cement Group, having a density of 3.15 g/cm^3 and Blaine specific surface area of 415 m^2/kg, was used to prepare the concrete used in this study. The chemical composition is given in Table IV-8.

Table IV-8 Cement chemical composition (%)

	SiO_2	Al_2O_3	Fe_2O_3	CaO	MgO	SO_3	Na_2O
Weight（%）	21.4	6.0	2.3	63.0	1.4	3.0	0.5

The concrete mixture proportions are given in Table IV-9. The slump of the concrete was 70 mm. Its average compressive strength at 28 days (tested on 110×220 mm cylindrical specimens) was 45 MPa, its elastic modulus was 32 GPa and its tensile strength was 4.7 MPa (tested by splitting test on the cylindrical specimens). The porosity was about 15.2%.

Table IV-9 Concrete composition

Mix composition		
Rolled gravel (silica+limestone)	5-15mm	1109 kg/m^3
Sand	0-5mm	745 kg/m^3
Portland cement: OPC (high performance)		364 kg/m^3
Water		182 kg/m^3

5.3.3 Casting and curing of reinforced concrete beams

When these beams were cast, the fresh concrete was placed in the framework in two layers, each approximately half of the height of the mold. An internal vibrator was used to compact the concrete. The casting direction of these beams is indicated in Figure IV-70 by the black arrow near the cross-section of each beam.

In the case of As01, the tensile bars were the bottom cast bars and the tensioned surface was the bottom surface, due to the sustained load. For As02 beams, the tensile bars were also the bottom cast bars according to the casting direction while the tensioned surface due to the sustained load was the top surface. According to the casting direction of As beams, no top-casting defects were expected to appear at the tensile bar-concrete interface.

After casting, both beams were covered with a plastic sheet in order to avoid any shrinkage cracking, then, after demolding, they were cured in the laboratory at ambient temperature for 28 days.

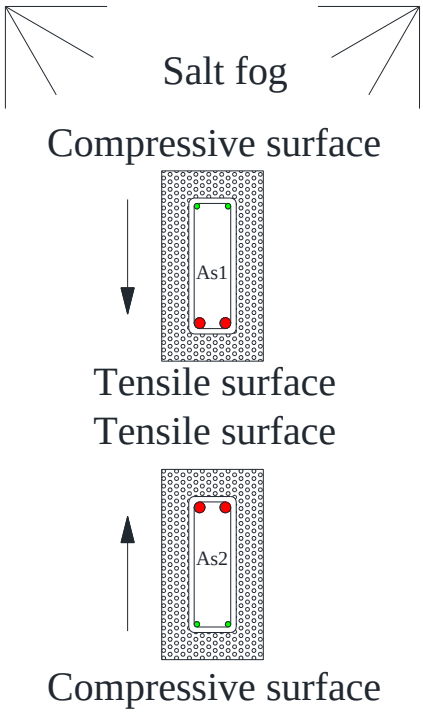

Figure IV-70 Casting direction and location of each reinforced concrete beam

5.3.4 Loading and exposure conditions

The corrosive environment and the loading mode of the beams are shown in Figure IV-71. The

aggressive environment was a salt fog (35 g/L of NaCl, corresponding to the chloride concentration of sea water). Both As beams were loaded together in 3-point bending. The load value, Mser = 20 kN•m was used. The loading device led to beam As01 being located above As02.

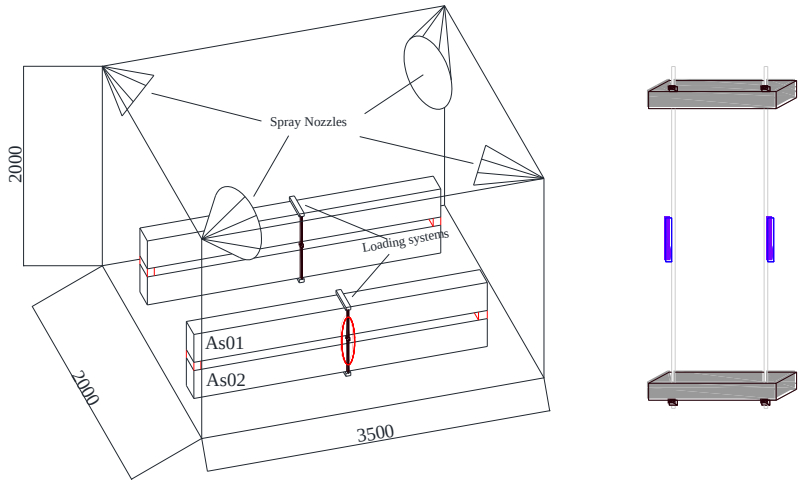

Figure IV-71 Loading system and exposure conditions

5.3.5 Cracking maps

Before the beams were exposed in the chloride chamber, the locations and widths of load-induced cracks were recorded after 28 days of loading. Then, during exposure in the chloride environment, visual inspections were carried out periodically to check if any cracks had been induced by corrosion. Corrosion-induced cracks of the two beams were mapped and the crack widths were measured with a video microscope having an accuracy of 0.01 mm and a magnification ranging from 25 times to 175 times.

5.3.6 Interfacial conditions of steel and concrete

At the end of the experimental work, both top-cast and bottom cast parts of beam As02 were observed with back scattered electron imaging (BSE) in order to characterize the interfacial conditions of steel and concrete.

For the BSE test, steel-concrete interface samples were prepared and dried to constant weight in a vacuum oven at 60 °C. These samples were next placed in a cylindrical mold filled with epoxy resin in a vacuum environment, then ground and polished with 500, 1000 and 3000 grade silicon carbide paper and diamond pastes using a polishing machine. Finally, the samples were dried in a

vacuum oven. Scanning electron microscopy manufactured by Tescan in the Czech Republic was used to analyze the microstructure of the steel-concrete interface.

5.3.7 Loss of diameter of stirrup and main steel rebars

The concrete cover was destroyed and the stirrups were cleaned using Clark's solution (ANSI/ASTM G1-72) in order to remove all the corrosion products.

The average degree of stirrup corrosion was assessed by measuring the diameter loss with a Vernier caliper after complete removal of the corrosion products. The average loss of cross-section was calculated with Equation 1.

$$\Delta \mathrm{As} = \frac{\sum \pi r_i^2 L_i}{L_{total}} \times 100\% \qquad \text{Equation 1}$$

where L_{total} (mm) is the total length of the horizontal leg or vertical leg of the stirrup without the intersection area;

Δ As (mm^2) is the average loss of cross-section of the corroded leg of the stirrup;

L_i (mm) is the length of the corroded area on the leg of the stirrup;

r_i (mm) is the radius of the corroded area on the leg of the stirrup.

The main steel rebars were cut into short pieces of different lengths according to the corrosion pattern (pitting or general corrosion) and corrosion detail. The length of each section depended on the corrosion condition along the steel bar and was measured with Vernier calipers with a precision of 0.02 mm. Each short section was weighed on a balance with a precision of 0.01 g and the loss of cross-section was then calculated with Equation 2. The original mass of the short sections was calculated with Equation 3.

$$\Delta \mathrm{As} = \frac{Mo - M}{Mo} \times As \qquad \text{Equation 2}$$

$$\mathrm{Mo} = \rho \times \mathrm{As} \times \mathrm{L} \qquad \text{Equation 3}$$

where ρ (g/cm^3) is the density of the steel bar, considered to be 7.85 g/cm^3;

L (mm) is the length of each short section;

Δ As (mm^2) is the average loss of cross-section of the corroded bars over the short section length;

As (mm^2) is the nominal cross-section of the steel bars;

M (g) is the residual mass of the short sections of corroded bars;

Mo (g) is the nominal mass of the steel bars.

5.4 Results and discussion

5.4.1 Characterization of the steel-concrete interface

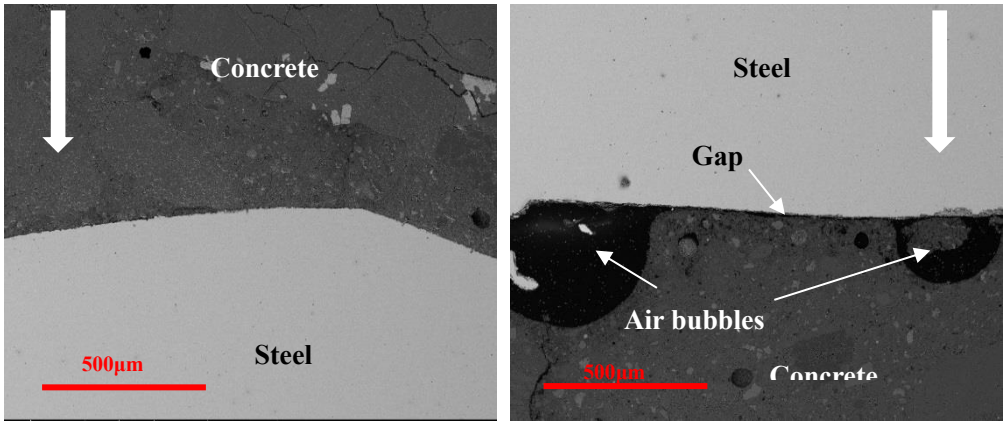

Figure IV-72 Interfacial conditions of top-cast bar

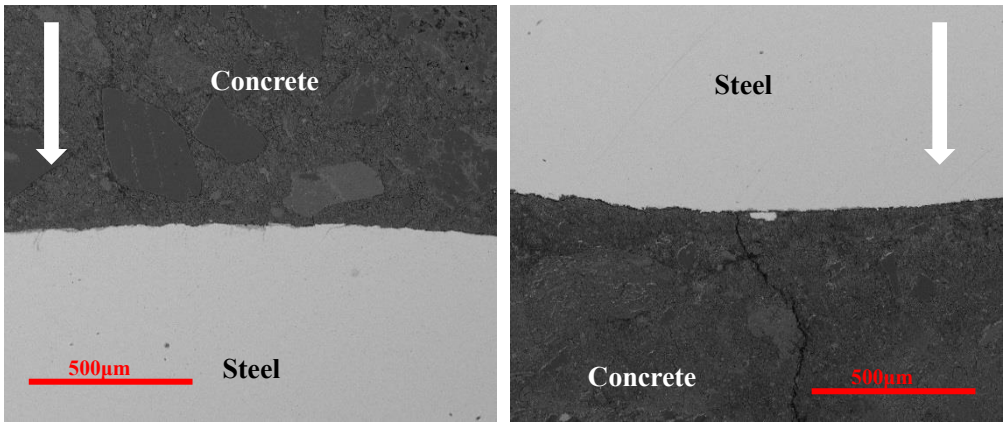

Figure IV-73 Interfacial conditions of bottom-cast bar

The conditions of the steel-concrete interfaces are shown in Figure IV-72 and Figure IV-73. It is obvious that the quality of the top interface of the top-cast bar was perfect, while air bubbles and gaps appeared in the bottom surface of the top-cast bar. However, no defects were found around the bottom-cast steel regardless of whether observations concerned the top side or bottom side according to the casting direction. These results are in accordance with references [40, 45, 50].

5.4.2 Cracking maps of reinforced concrete

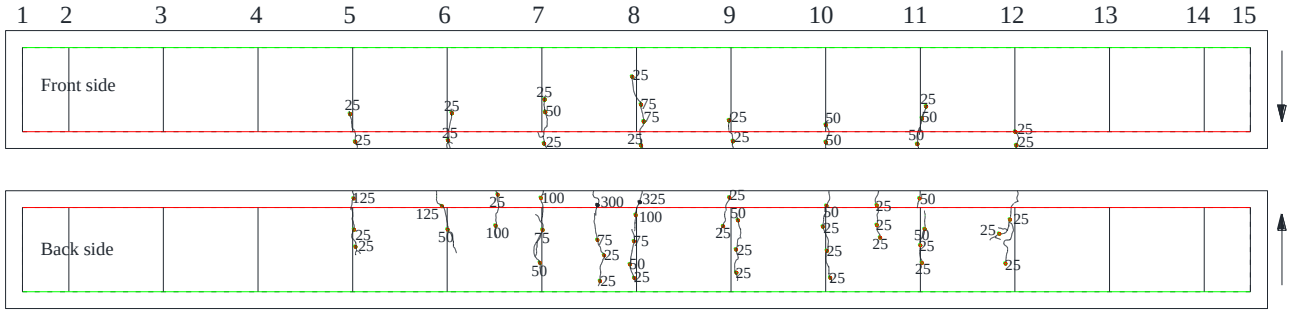

(a) Cracking situation on As01 beam at 28 days

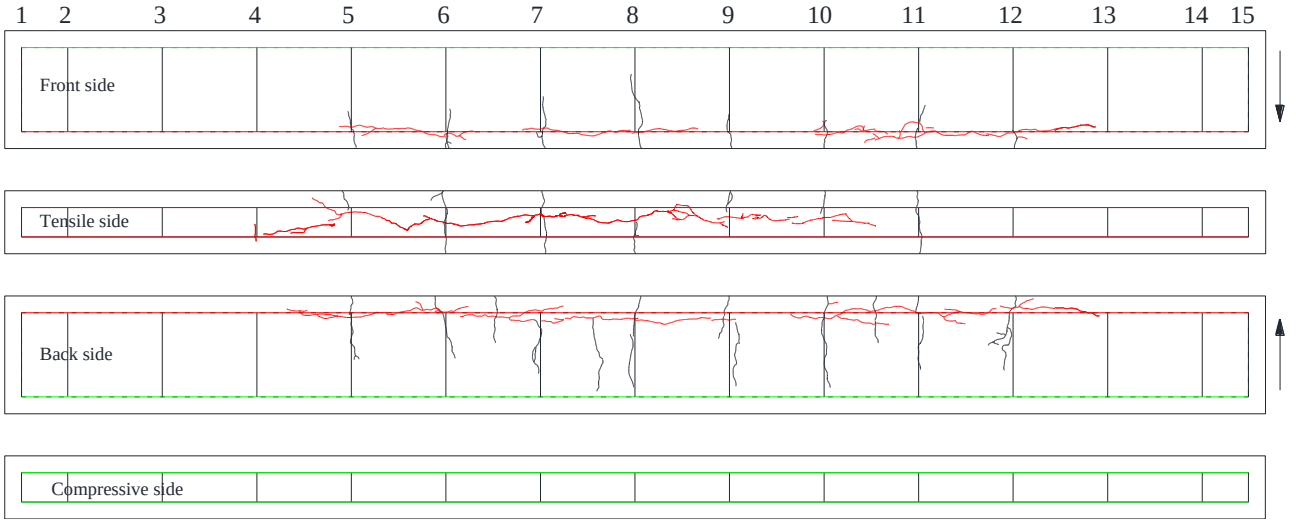

(b) Cracking situation on beam As01 at 9 years

Figure IV-74 Cracking situation on As01

(Red lines, green lines and black lines in cracking map correspond to the tensile bars, compressive bars and stirrups, respectively. Arrows at right indicate the casting direction)

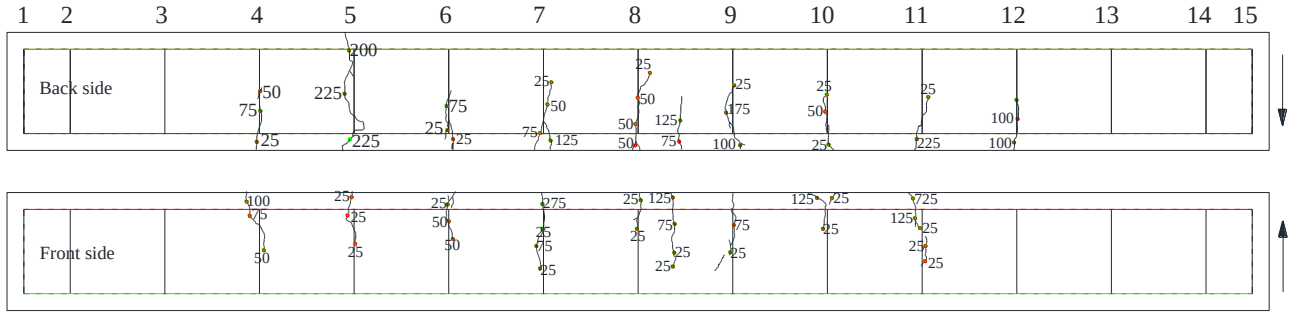

(a) Cracking situation on beam As02 at 28 days

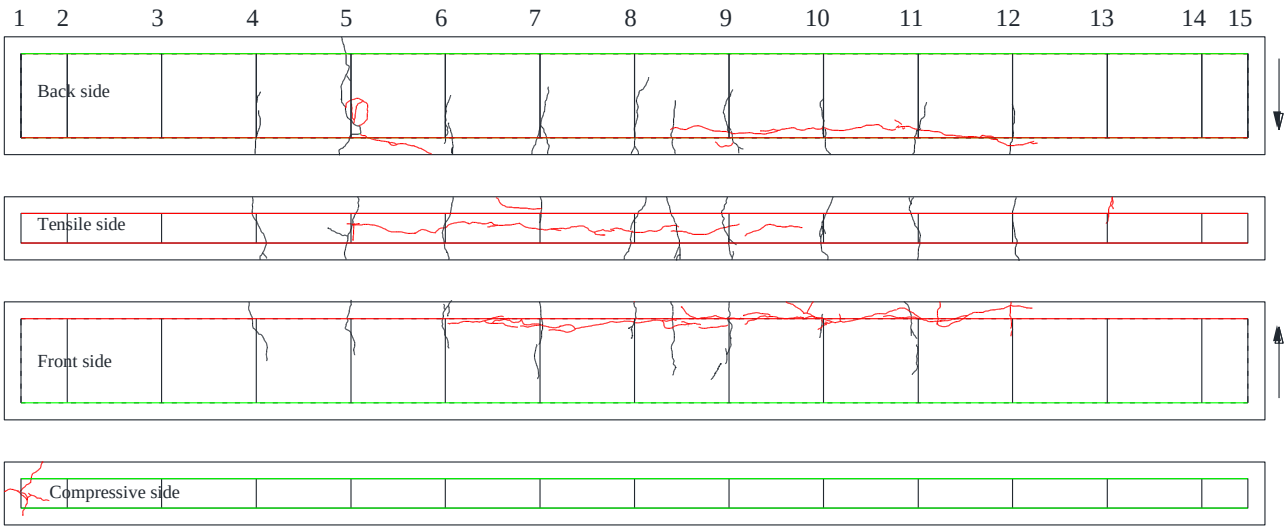

(b) Cracking situation on beam As02 at 9 years

Figure IV-75 Cracking situation on As02

(Red lines, green lines and black lines in the cracking map correspond to the tensile bars, compressive bars and stirrups, respectively. Arrows at right indicate the casting direction)

The cracking maps of beams As01 and As02 are given in Figure IV-74 and Figure IV-75. For both beams, it can be noted that some corrosion-induced cracks were generated near the tensile bars due to corrosion of the main bars. According to the results in Figure IV-74 and Figure IV-75, the corrosion of tensile bars was the consequence of load-induced cracks located in the tensile zone. Yu et al.[31] indicated that corrosion of steel initiated at the crack tip where some chloride ions penetrating through load-induced cracks first encountered steel bars. In the case of the compressive zone, there were hardly any corrosion-induced cracks found in the vicinity of compressive bars after 9 years of exposure. This can be attributed to the relatively thick concrete cover blocking the penetration of chloride ions and thus delaying the corrosion process of steel bars[31], even in the presence of top-casting defects at the compressive steel-concrete interface (in Figure IV-72).

Load-induced cracks appeared along the vertical legs of stirrups, as these places were subjected to stress concentration due to the presence of a stirrup when the external load was applied[6]. In beam As01, they were found from the location of the fifth stirrup to the twelfth stirrup, while in beam As02, load-induced cracks were found from the fourth stirrup to the twelfth stirrup. In comparison with the state of the beams at 28 days, parts of transverse cracks had extended along the vertical legs of stirrups due to the corrosion. However, no new transverse cracks appeared at other stirrups.

5.4.3 Corrosion maps of stirrups

The horizontal leg of a stirrup had an inside part and an outside part (Figure IV-69) according to the thickness of the concrete cover (Figure IV-70). The outside part faced towards the concrete cover, while the inside corresponded to the center of the concrete beam. In Figure IV-76, the red areas correspond to the intersection area of the main steel bar with the stirrup, while the blue zones are non-intersection zones.

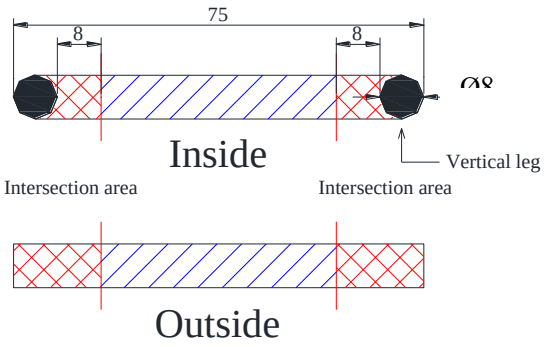

Figure IV-76 Shape of horizontal leg of stirrup

The stirrups were divided into two parts according to the presence of load-induced cracks: a “no load-induced cracks” zone and a “load-induced cracks” zone (see Figure IV-77 and Figure IV-78). The grey areas on the stirrups in the figures correspond to a cross-sectional loss of less than 3%, since the corrosion level of these areas was slight. For other, pitting corrosion the value assessed with the Vernier caliper is given.

From Figure IV-77 and Figure IV-78, it can be seen that the corrosion behavior of the horizontal legs and the vertical legs of stirrups was markedly different. For the horizontal legs, in the no load-induced cracks zone, strong pitting corrosion always occurred at top-cast horizontal legs, whereas the bottom-cast horizontal legs underwent slight pitting or no corrosion. In contrast, in the load-induced cracks zone, most of the bottom-cast horizontal legs suffered from severe pitting corrosion, while slight pitting corrosion mainly occurred on the bottom side of top-cast horizontal legs according to the casting direction. For all the stirrups of As01 in the cracked zone, slight corrosion occurred on the bottom part of top-cast horizontal legs. It could be ascribed to the coupling effect of top-casting induced defects and top exposure.

Vertical legs were mainly affected by slight pitting corrosion (the loss of cross-section was less than 3%), and hardly any rules could be found for the corrosion distribution.

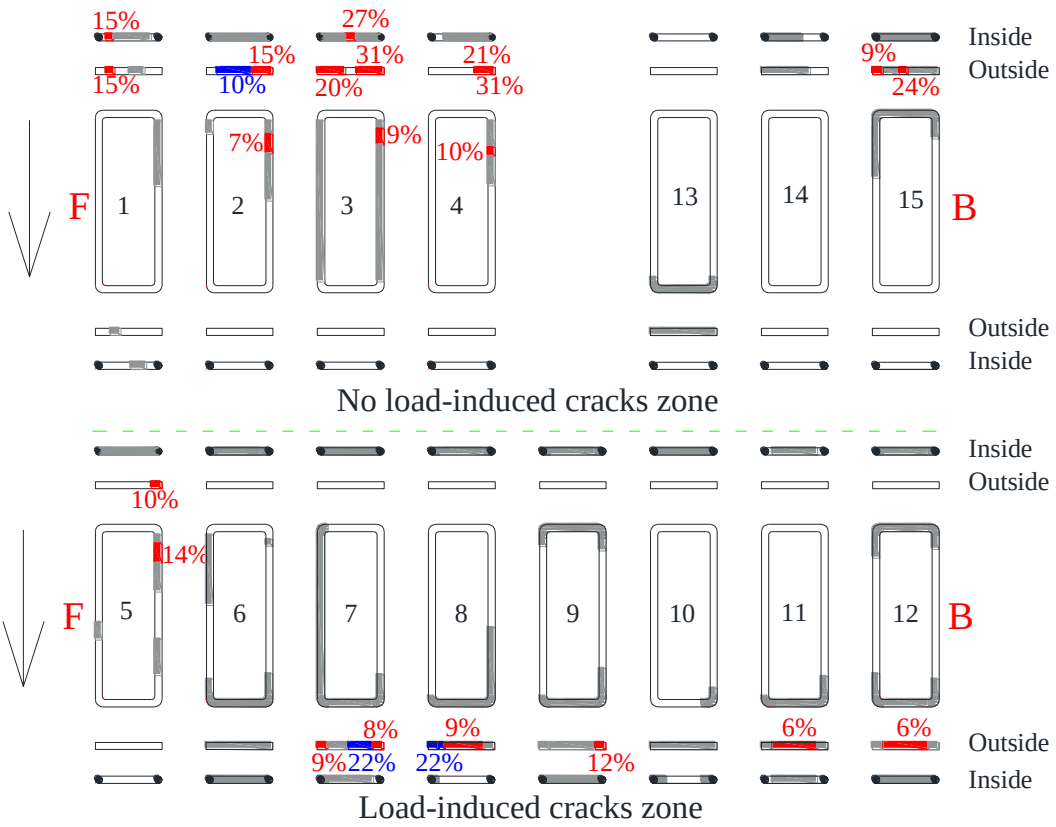

Figure IV-77 Corrosion situation of the stirrups of beam As01

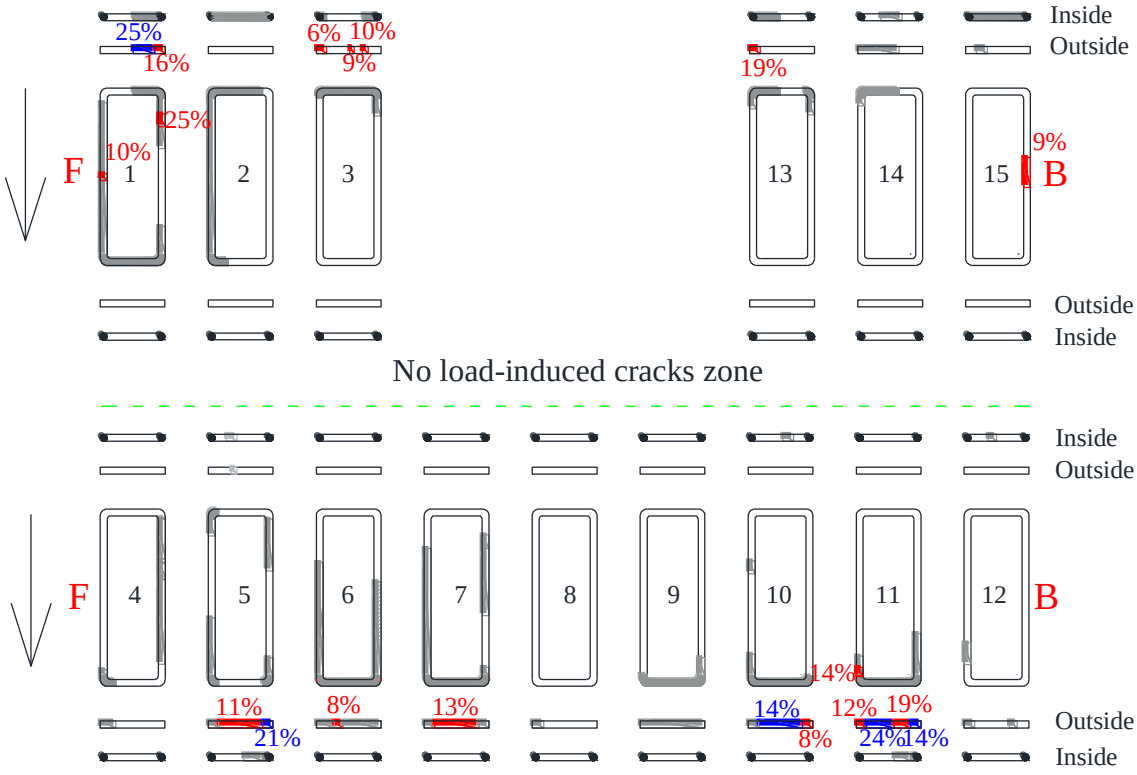

Figure IV-78 Corrosion situation of the stirrups of beam As02

5.4.4 Corrosion on the horizontal legs of stirrups

Figure IV-79 and Figure IV-80 present the corrosion patterns of horizontal legs in both beams before cleaning with Clark's solution. In the compressive zone, corrosion mainly took place at both ends while, in the tensile zone, corrosion mainly occurred at mid span of the beam.

(a) Corrosion of horizontal legs in compressive zone

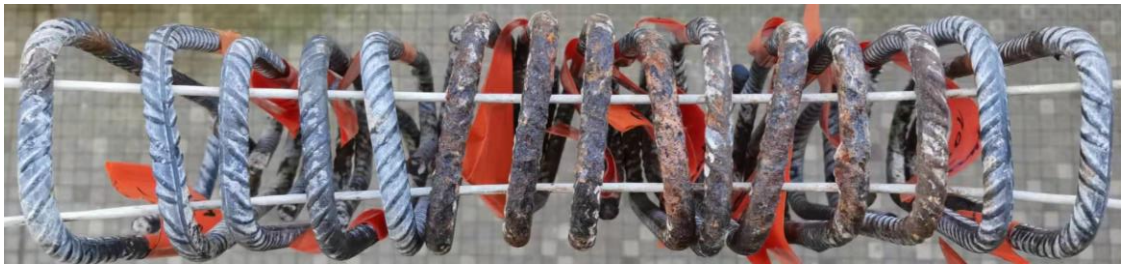

(b) Corrosion of horizontal legs in tensile zone

Figure IV-79 Horizontal legs of stirrups in beam As01

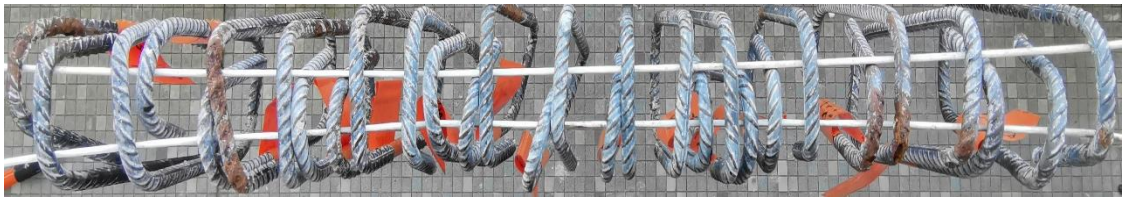

(a) Corrosion of horizontal legs in compressive zone

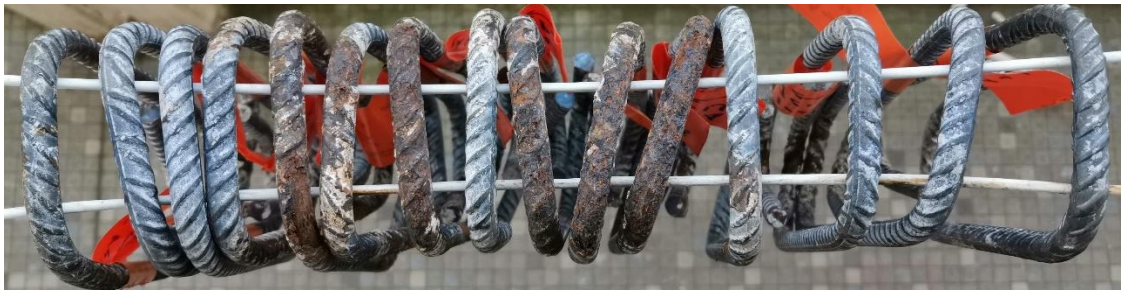

(b) Corrosion of horizontal legs in tensile zone

Figure IV-80 Horizontal legs of stirrups in beam As02

The average corrosion calculated on the basis of Equation 1 for the horizontal legs of stirrups in both reinforced concrete beams is shown in Figure IV-81

The horizontal legs of stirrups in the no induced-cracks zone of the compressive zone suffered severe corrosion while, in the load-induced cracks zone, the horizontal legs were subject to slight

corrosion. The average corrosion of horizontal legs in the compressive zone of beam As01 was higher than that in beam As02 because the compressive side of beam As01 was the top exposure side, on which more chlorides could be received during the exposure period[31, 50].

In the tensile side, corrosion mainly took place on the horizontal legs of stirrups in the load-induced cracks zone. There was hardly any corrosion on the horizontal legs in the no load-induced cracks zone of the tensile side.

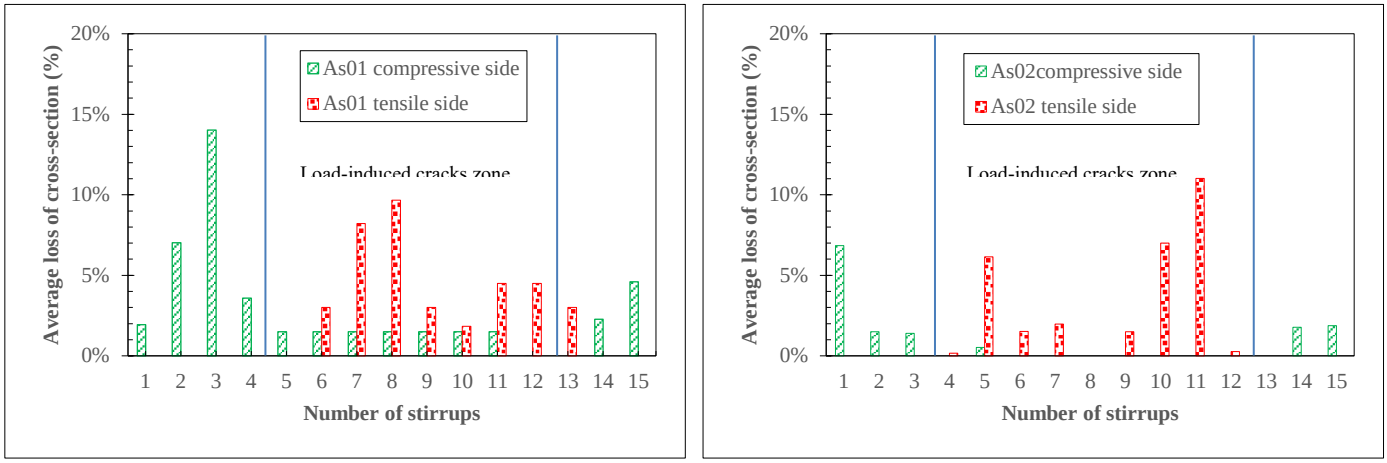

(a) Horizontal legs in As01 (b) Horizontal legs in As02

Figure IV-81 Average loss of horizontal legs of stirrups in As beams

The corrosion distributions on the horizontal legs of stirrups in both beams were recorded and are shown in Figure IV-82 and Figure IV-83.

For the inside of top-cast horizontal legs in the compressive zone of beam As01, slight corrosion can be seen because of top-casting defects (Figure IV-72)[50]. A similar phenomenon can also be found in beam As02. Since the compressive side of As02 corresponds to bottom exposure conditions, the corrosion at the inside of top-cast horizontal legs was weaker than that in As01[50], which was affected by both top-casting and top exposure.

For the outside of the horizontal legs of stirrups in beam As01, severe pitting corrosion mainly took place in the no load-induced cracks zone of the compressive side. However, the outside parts of horizontal legs in the no load-induced cracks zone of the tensile side suffered only slight corrosion. In contrast, in the load-induced cracks zone, the outside of most horizontal legs in the compressive zone was not corroded, while the outside of the corresponding horizontal legs in the tensile zone was subjected to severe pitting corrosion. Similar results were also found for beam As02.

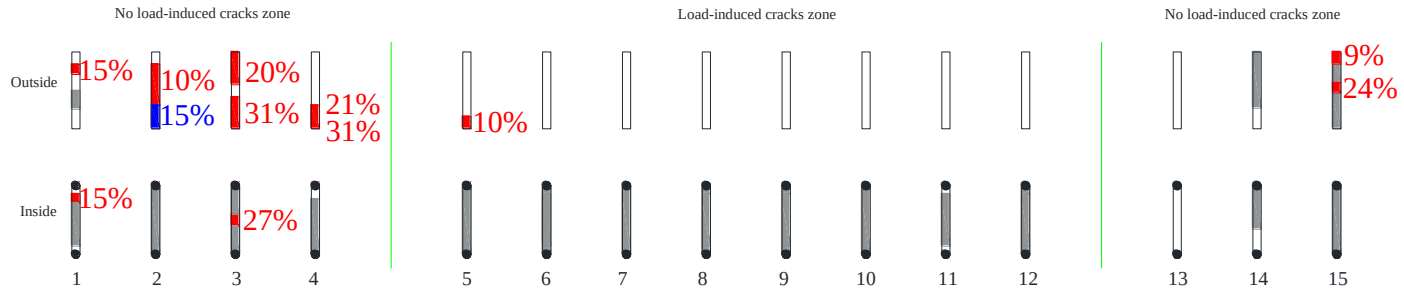

(a) Horizontal legs in compressive zone of beam As01

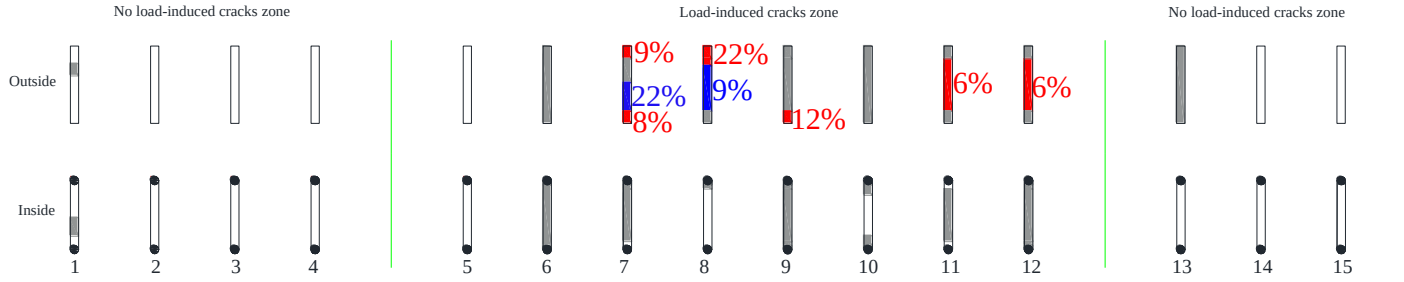

(b) Horizontal legs in tensile zone of beam As01

Figure IV-82 Corrosion distribution on horizontal legs of stirrups in beam As01

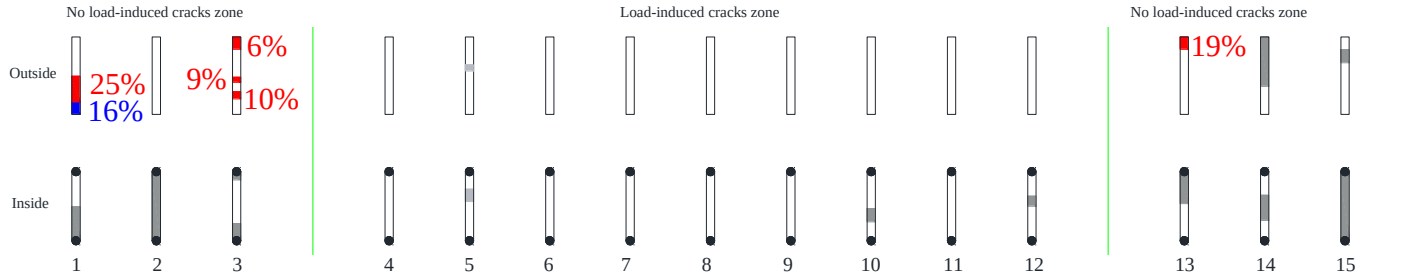

(a) Horizontal legs in compressive zone of beam As02

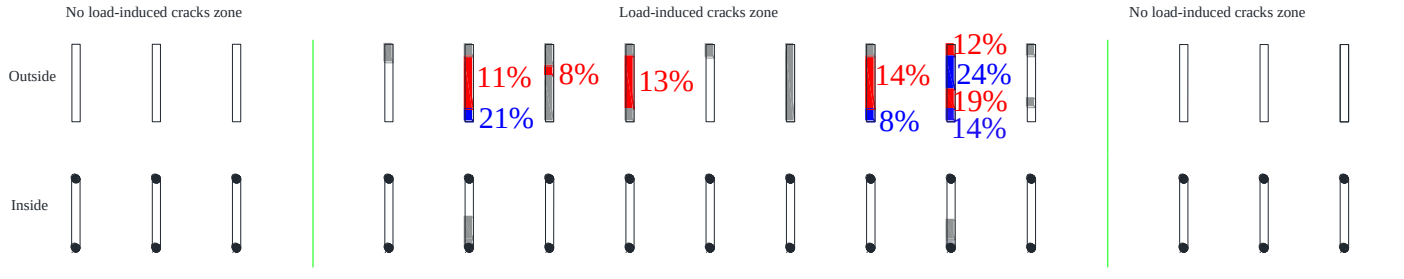

(b) Horizontal legs in tensile zone of beam As02

Figure IV-83 Corrosion distribution on horizontal legs of stirrups in beam As02

In reinforced concrete beams, stirrups electrically connect tensile and compressive rebars, making electrons free to move. The results obtained suggest that the corrosion process of stirrups in an RC beam can be divided into two steps. The relevant schematic illustrations are given in Figure IV-84.

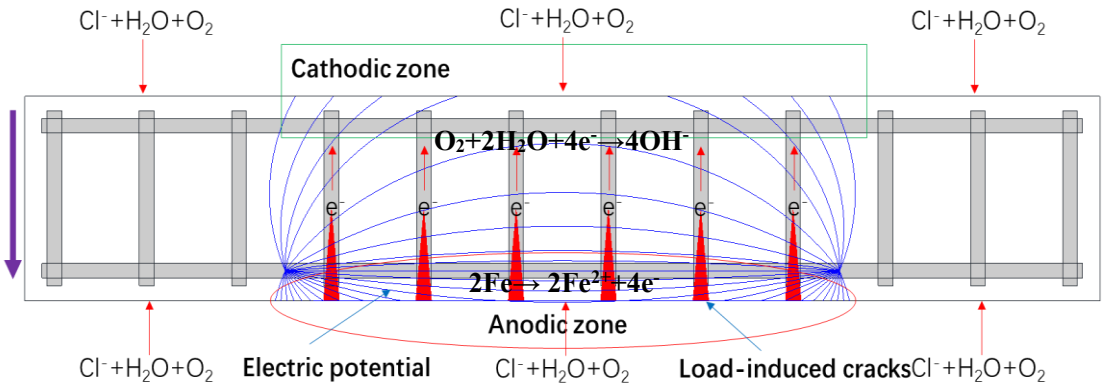

(a) Macrocell corrosion of stirrups in RC in first step of corrosion

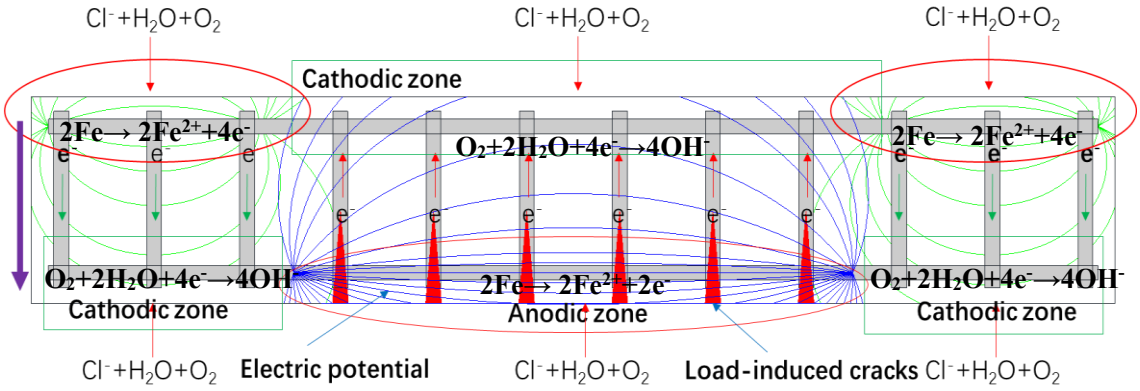

(b) Macrocell corrosion of stirrups in RC in second step of corrosion

Figure IV-84 Macrocell corrosion of stirrups in RC structures in service

(Red triangles mark the load-induced cracks; blue and green curves correspond to the electric potential; purple arrow represents the casting direction)

During the first step, after application of the loading to the RC beam, some load-induced cracks appeared along the vertical legs of stirrups in the tensile zone. In the chloride fog environment, chloride ions and moisture firstly penetrated to the depth of the horizontal legs of stirrups in the tensile zone through the load-induced cracks, attacking the passive layer formed on the outside surface of the horizontal legs of stirrups. Once the passive layer was broken down, corrosion started immediately; the outside of the horizontal legs entered the active stage and acted as the anode. Meanwhile, the other half of the horizontal legs of stirrups in the compressive zone were in a passive state due to the protection of the thick concrete cover. Because of the electrical connection between the two parts, the compressive zone of the stirrups acted as a cathode and was protected, since cathodic zones are more polarized and active close to the anodic zone. Thus, the electrons migrated from the horizontal legs in the tensile zone to the horizontal legs of the compressive zone in the load-induced cracks zone.

Within the corrosion process of the second step, after the chloride ions had penetrated the uncracked concrete cover of the no load-induced cracks zones, because the greater distance from the anodic zone limited the cathodic polarization at the end of the beam, chloride could depassivate the horizontal legs of stirrups and induce a new anodic zone. The corresponding horizontal legs in the tensile zone then acted as the cathodic zone and were protected.

5.4.5 Corrosion on the vertical legs of stirrups

After the external load had been applied, load-induced cracks appeared along the vertical legs of stirrups in the tensile zone. During the exposure period, the vertical legs of the stirrups in the mid spans of the beams were exposed directly to the chloride environment. Otieno et al.[51] consider that the corrosion of steel will be accelerated when the crack widths increase. However, from Figure IV-82 and Figure IV-83, it can be observed that almost all the vertical legs of stirrups suffered from only slight corrosion. The average cross-sectional loss of vertical legs was calculated and is presented in Figure IV-85, where the cross-sectional loss of most vertical legs can be seen to be less than 3.5 %, regardless of whether the zone was a load-induced cracks or a no load-induced cracks zone. So, the load-induced cracks appeared not to affect the corrosion of vertical legs of stirrups.

Similarly to the situation for the horizontal legs of stirrups in the tensile zone, because transverse cracks accelerated the corrosion initiation of steel by providing preferential pathways for aggressive agents, the first corrosion on the vertical legs of stirrups occurred in the load-induced cracks zone[6, 51-53]. Because there were no defects along the vertical legs of the stirrups[9, 21], corrosion developed extremely slowly after its initiation[54]. Therefore, despite the presence of transverse cracks, after corrosion initiation, not only was the corrosion behavior of vertical legs of stirrups similar to that in an uncracked RC beam, but the cross-sectional loss of vertical legs was also similar after 9 years of exposure, regardless of whether a load-induced cracks zone or a no load-induced cracks zone was considered.

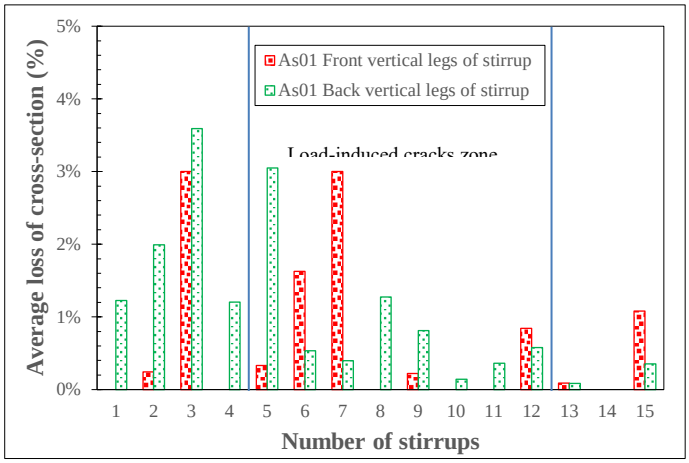

(a) Vertical legs in As01

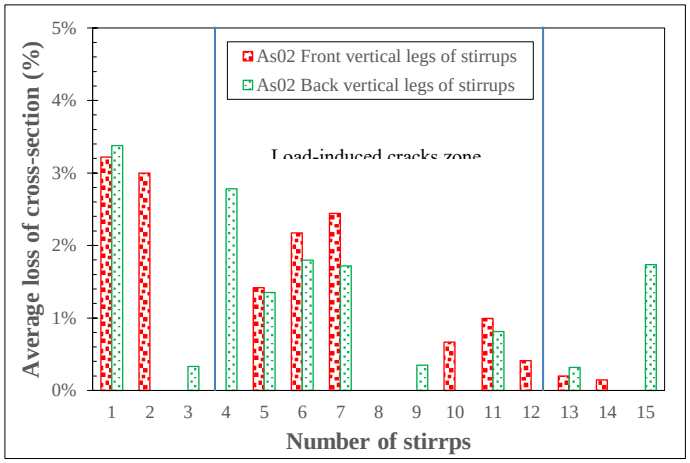

(b) vertical legs in As02

Figure IV-85 Average loss of vertical legs of stirrups in As beams

5.4.6 Effect of stirrups on the corrosion of main deformed steel rebars

According to Figure IV-70, the main reinforcing steels contact the corners of stirrups directly and, therefore, the cross-sectional losses of the main steel rebars and the corners of stirrups were measured. They are shown in Figure IV-86. For the compressive reinforcing steels, corrosion mainly took place at the ends of steel rebars while, in the case of tensile steel rebars, corrosion was mainly concentrated at the mid span of the beam. Thus, along the length of the reinforced concrete beam, the corrosion distribution on the main bars was similar to that on stirrups. It should be noted that the corrosion of the compressive bars in beam As01 and the tensile bars in beam As02 was greater than, respectively, those of beams As02 and As01. These results were attributed to the effect of exposure conditions[40, 50].

According to the theory of differential metal corrosion[47, 55, 56], some researchers [47, 48, 57] consider that stirrups could protect the main steel rebars against corrosion. However, Mohammed et al. and Otsuki et al. [38, 49] have reported that stirrups do not protect the main steel bars but accelerate their corrosion rate. According to the results shown in Figure IV-86, it can be seen that severe corrosion took place on some main steel rebars when the stirrup corners were only slightly corroded, and that some main steel rebars in contact with strongly corroded stirrup corners suffered from only slight corrosion at the intersection site. Therefore, it can be deduced that the corrosion of stirrups was not related to that of the main steel rebars.

When the steel frame is machined, it is inevitable that some gaps will be randomly induced between stirrup and main bar, especially for steel frames that are fastened with iron wire. These gaps

may be partly or wholly filled with cement paste when fresh concrete is cast and vibrated and, when the concrete hardens, various interfacial defects may form at the stirrup-main bar intersection [46], causing different corrosion behavior of stirrups and rebars[43]. Thus, it is impossible to establish a correlation in terms of corrosion between stirrups and the reinforcing steels in contact with them.

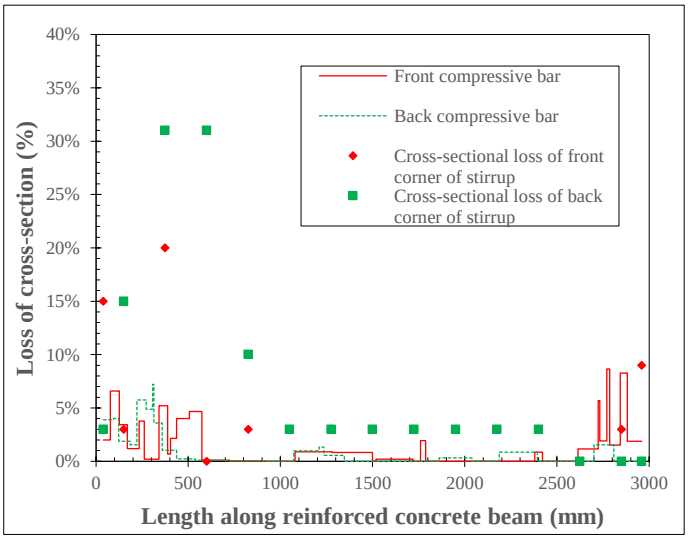

(a) Compressive rebars and stirrups in As01 beam

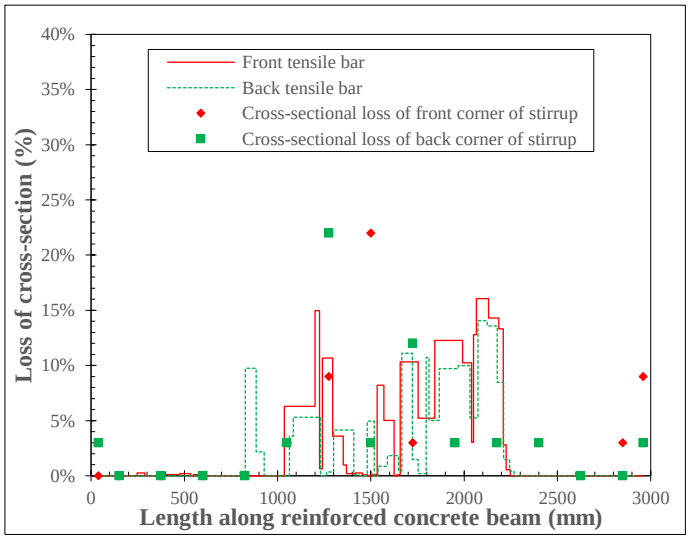

(b) Tensile rebars and stirrups in As01 beam

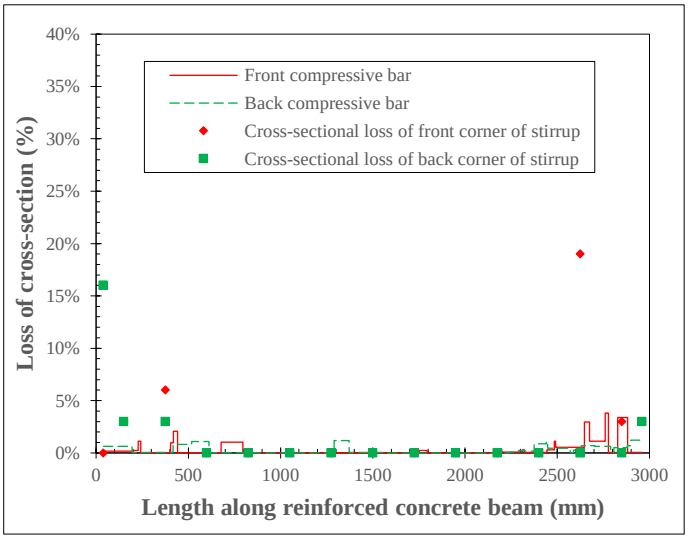

(c) Compressive rebars and stirrups in beam As02

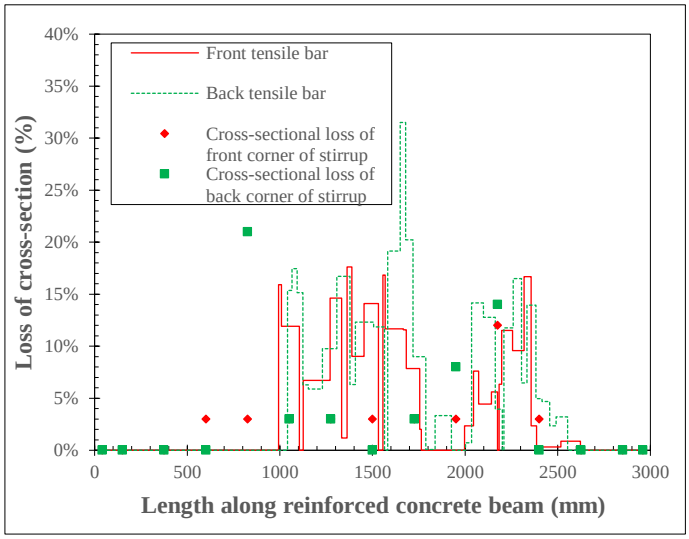

(d) Tensile rebars and stirrups in beam As02

Figure IV-86 Cross-sectional loss of main bars and stirrups in As beams

5.5 Conclusion`

Two reinforced concrete beams, with the same concrete and same cover depth but exposed to different conditions, were investigated. The work particularly studied the corrosion behavior of stirrups in the absence or presence of load-induced cracks formed by sustained loading.

The cracking maps, cross-sectional loss of stirrups, and corrosion distribution around the

stirrups of the two beams were studied and compared with each other. The following conclusions were drawn:

1. For the horizontal legs of stirrups, regardless of the exposure conditions, corrosion always occurred at the mid span of the tensile zone and at the ends of the compressive zone of the reinforced concrete beam, while the opposite horizontal legs were protected.
2. The vertical legs of stirrups mainly suffered from slight corrosion. In spite of the presence of load-induced cracks, after 9 years' exposure to a chloride environment, the average cross-sectional loss of all these vertical legs of stirrups was still less than 3.5%.
3. The stirrups were not related to the main reinforcing steels in terms of corrosion. The corrosion behavior of the intersection between stirrups and main bars was in connection with the interfacial conditions between stirrups and main bars.
4. The areas of cathodic protection on steels in reinforced concrete beam increased with the development of corrosion process. In the first stage of corrosion, cathodic protection mainly took place on the top cast steel rebars in the mid span of compressive zone. In the second period of corrosion, apart from the mid span of compressive zone, the areas of cathodic protection also located at the ends of bottom cast rebars in tensile zone.

5.6 References

[1] A. Neville, Chloride attack of reinforced concrete: an overview, Materials and structures, 28 (1995) 63.
[2] L. Bertolini, B. Elsener, P. Pedeferri, E. Redaelli, R.B. Polder, Corrosion of steel in concrete: prevention, diagnosis, repair, John Wiley & Sons2013.
[3] M. Mahmaran, Yaman, Influence of transverse crack width on reinforcement corrosion initiation and propagation in mortar beams, Canadian Journal of Civil Engineering, 35 (2008) 236-245.
[4] C. Arya, F. Ofori-Darko, Influence of crack frequency on reinforcement corrosion in concrete, Cement
Concrete Research, 26 (1996) 345-353.
[5] G. Balabanic, N. Bicanic, A. Duerkovic, The influence of w/c ratio, concrete cover thickness and degree of water saturation on the corrosion rate of reinforcing steel in concrete, Cement and concrete Research, 26 (1996) 761-769.
[6] R. François, G. Arliguie, Influence of service cracking on reinforcement steel corrosion, Journal of Materials in Civil Engineering, 10 (1998) 14-20.
[7] P. Mangat, B. Molloy, Factors influencing chloride-induced corrosion of reinforcement in concrete, Materials and Structures, 25 (1992) 404-411.

[8] A. Michel, A.O.S. Solgaard, B.J. Pease, M.R. Geiker, H. Stang, J.F. Olesen, Experimental investigation of the relation between damage at the concrete-steel interface and initiation of reinforcement corrosion in plain and fibre reinforced concrete, Corrosion Science, 77 (2013) 308-321.
[9] T.U. Mohammed, N. Otsuki, H. Hamada, T. Yamaji, Chloride-induced corrosion of steel bars in concrete with presence of gap at steel-concrete interface, Materials Journal, 99 (2002) 149-156.
[10] M. Otieno, M. Alexander, H.-D. Beushausen, Corrosion in cracked and uncracked concrete,influence of crack width, concrete quality and crack reopening, Magazine of Concrete Research, 62 (2010) 393-404.
[11] J. Ryou, K. Ann, Variation in the chloride threshold level for steel corrosion in concrete arising from different chloride sources, Magazine of Concrete Research, 60 (2008) 177-187.
[12] B. Sangoju, R. Gettu, B. Bharatkumar, M. Neelamegam, Chloride-induced corrosion of steel in cracked OPC and PPC concretes: Experimental study, Journal of materials in civil engineering, 23 (2011) 1057-1066.
[13] A. Scott, M. Alexander, The influence of binder type, cracking and cover on corrosion rates of steel in chloride-contaminated concrete, Magazine of Concrete Research, 59 (2007) 495-505.
[14] W. Sun, Y. Zhang, S. Liu, Y. Zhang, The influence of mineral admixtures on resistance to corrosion of steel bars in green high-performance concrete, Cement and Concrete Research, 34 (2004) 1781-1785.
[15] K.S. Tuutti, Corrosion of steel in concrete, (1982).
[16] T. Vidal, A. Castel, R. François, Corrosion process and structural performance of a 17 year old reinforced concrete beam stored in chloride environment, Cement and Concrete Research, 37 (2007) 1551-1561.
[17] R. Zhang, A. Castel, R. François, Influence of steel-concrete interface defects owing to the top-bar effect on the chloride-induced corrosion of reinforcement, Magazine of Concrete Research, 63 (2011) 773-781.
[18] T.A. Soylev, R. François, Quality of steel-concrete interface and corrosion of reinforcing steel, Cement and Concrete Research, 33 (2003) 1407-1415.
[19] T.A. Soylev, R. François, Corrosion of reinforcement in relation to presence of defects at the interface between steel and concrete, Journal of materials in civil engineering, 17 (2005) 447-455.
[20] A. Kenny, A. Katz, Statistical relationship between mix properties and the interfacial transition zone around embedded rebar, Cement and Concrete Composites, 60 (2015) 82-91.
[21] A. Horne, I. Richardson, R. Brydson, Quantitative analysis of the microstructure of interfaces in steel reinforced concrete, Cement and Concrete Research, 37 (2007) 1613-1623.
[22] W.H. Hartt, J. Nam, Effect of cement alkalinity on chloride threshold and time-to-corrosion of reinforcing steel in concrete, Corrosion, 64 (2008) 671-680.
[23] L. Yu, R. François, R. Gagné, Influence of steel-concrete interface defects induced by top-casting on development of chloride-induced corrosion in RC beams under sustained loading, Materials and Structures, 49 (2016) 5169-5181.
[24] V.H. Dang, R. Francois, Influence of long-term corrosion in chloride environment on mechanical behaviour of RC beam, Engineering Structures, 48 (2013) 558-568.
[25] E. Committee, Eurocode2: Design of concrete structures-Part 1-2: General rules-Structural fire design, ENV 1992-1-2, 1995.

[26] R. Zhang, A. Castel, R. François, Concrete cover cracking with reinforcement corrosion of RC beam during chloride-induced corrosion process, Cement and Concrete Research, 40 (2010) 415-425.
[27] R. François, S. Laurens, F. Deby, 4 - In situ Corrosion Diagnosis, Corrosion and its Consequences for Reinforced Concrete Structures, Elsevier2018, pp. 77-104.
[28] T. Vidal, A. Castel, R. Francois, Analyzing crack width to predict corrosion in reinforced concrete, Cement and concrete research, 34 (2004) 165-174.
[29] R. François, S. Laurens, F. Deby, Corrosion and Its Consequences for Reinforced Concrete Structures, Elsevier2018.
[30] U.M. Angst, M.R. Geiker, A. Michel, C. Gehlen, H. Wong, O.B. Isgor, B. Elsener, C.M. Hansson, R. François, K. Hornbostel, The steel-concrete interface, Materials and Structures, 50 (2017) 143.
[31] L. Yu, R. François, V.H. Dang, V. L'Hostis, R. Gagné, Development of chloride-induced corrosion in pre-cracked RC beams under sustained loading: Effect of load-induced cracks, concrete cover, and exposure conditions, Cement and Concrete Research, 67 (2015) 246-258.
[32] W.D. Lindquist, D. Darwin, J. Browning, G.G. Miller, Effect of cracking on chloride content in concrete bridge decks, American Concrete Institute, 2006.
[33] P.P. Win, M. Watanabe, A. Machida, Penetration profile of chloride ion in cracked reinforced concrete, Cement and concrete research, 34 (2004) 1073-1079.
[34] C. Lim, N. Gowripalan, V. Sirivivatnanon, Microcracking and chloride ion diffusion of concrete under sustained uniaxial compression, Special Publication, 221 (2004) 893-910.
[35] A. Castel, T. Vidal, R. François, G. Arliguie, Influence of steel-concrete interface quality on reinforcement corrosion induced by chlorides, Magazine of Concrete Research, 55 (2003) 151-159.
[36] R. Francois, A. Castel, Influences of bending crack and water-cement ratio on chloride-induced corrosion of main reinforcing bars and stirrups. Discussion and Closure, ACI Materials Journal, 98 (2001).
[37] A. Castel, R. Francois, G. Arliguie, Chloride diffusion in reinforced concrete beam under sustained loading, Special Publication, 200 (2001) 647-662.
[38] N. Otsuki, S.-i. Miyazato, N.B. Diola, H. Suzuki, Influences of bending crack and water-cement ratio on chloride-induced corrosion of main reinforcing bars and stirrups, Materials Journal, 97 (2000) 454-464.
[39] N. Otsuki, M. Hisada, N.B. Diola, T. Uddin, Experimental study on interfacial transition zones in reinforced concrete, Doboku Gakkai Ronbunshu, 1998 (1998) 155-167.
[40] W. Zhang, R. François, L. Yu, Influence of load-induced cracks coupled or not with top-casting-induced defects on the corrosion of the longitudinal tensile reinforcement of naturally corroded beams exposed to chloride environment under sustained loading, Cement and Concrete Research, 129 (2020) 105972.
[41] P. Bhatt, T.J. MacGinley, B.S. Choo, Reinforced concrete design: Design theory and examples, CRC Press2006.
[42] A.H. Nilson, G. Winter, L.C. Urquhart, O.R. Charles Edward, Design of concrete structures, McGraw-Hill New York, USA1991.
[43] U.M. Angst, M.R. Geiker, M.C. Alonso, R. Polder, O.B. Isgor, B. Elsener, H. Wong, A. Michel, K. Hornbostel, C. Gehlen, The effect of the steel–concrete interface on chloride-induced corrosion

initiation in concrete: a critical review by RILEM TC 262-SCI, Materials and Structures, 52 (2019) 88.
[44] F. Chen, C.-Q. Li, H. Baji, B. Ma, Quantification of steel-concrete interface in reinforced concrete using Backscattered Electron imaging technique, Construction and Building Materials, 179 (2018) 420-429.
[45] T.A. Soylev, R. François, Quality of steel–concrete interface and corrosion of reinforcing steel, Cement and Concrete Research, 33 (2003) 1407-1415.
[46] A. Alhozaimy, R.R. Hussain, R. Al-Zaid, A. Al Negheimish, Investigation of severe corrosion observed at intersection points of steel rebar mesh in reinforced concrete construction, Construction and Building Materials, 37 (2012) 67-81.
[47] O. Geng, Reinforcement corrosion and degradation rate of concrete members China railway publishing house2010.
[48] L. Tong, Research on the damage of concrete and the influence for the longitudinal reinforcement corrosion by stirrup corrosion Structural Engineering, Xi'an University of Architecture and Technology, 2013.
[49] T.U. Mohammed, N. Otsuki, M. Hisada, Corrosion of steel bars with respect to orientation in concrete, ACI Materials Journal, 96 (1999) 154-159.
[50] W. Zhang, L. Yu, R. François, Influence of top-casting-induced defects on the corrosion of the compressive reinforcement of naturally corroded beams under sustained loading, Construction and Building Materials, 229 (2019) 116912.
[51] M. Otieno, M. Alexander, H.-D. Beushausen, Corrosion in cracked and uncracked concrete-influence of crack width, concrete quality and crack reopening, Magazine of Concrete Research, 62 (2010) 393-404.
[52] R. Francois, J. Maso, Effect of damage in reinforced concrete on carbonation or chloride penetration, Cement and Concrete Research, 18 (1988) 961-970.
[53] C. Arya, F. Ofori-Darko, Influence of crack frequency on reinforcement corrosion in concrete, Cement and Concrete Research, 26 (1996) 345-353.
[54] R.M. Ghantous, S. Poyet, V. L'Hostis, N.-C. Tran, R. François, Effect of crack openings on carbonation-induced corrosion, Cement and Concrete Research, 95 (2017) 257-269.
[55] H. Kaesche, Corrosion of metals: physicochemical principles and current problems, Springer Science & Business Media2012.
[56] Y. Dejun, S. Zhuoshen, Metal Corrosion Science, Bering: Metallurgical Industry Press1999.
[57] X. Zhang, S. Wei, W. Qin, Corrosion mechanism analysis of stirrups in concrete structures, Journal of Guangxi University(Natural Science Edition), 28(1) (2003) 10-13.

V. Conclusions and recommendations

1 General conclusions

In this thesis, the effect top-casting-induced defects and cracks on the corrosion behavior of reinforcing steel in concrete under chloride environment in corrosion initiation phase and corrosion propagation phase was investigated, respectively. The corrosion of stirrups used in reinforced concrete exposed under sustained load was analyzed.

In the case of the research on the reinforcing steel corrosion behavior in corrosion initiation, six concrete blocks with top-casting-induced defects and artificial crack were designed. The interfacial conditions of steel-concrete, including the distribution of air bubbles under steel rebar, the density of steel-concrete interface and the cement hydration products in the steel-concrete interface, were analyzed and compared. The chloride penetration in steel-concrete interface was measured. The corrosion current of steel rebars was measured and analyzed.

In the case of the study on the reinforcing steel corrosion behavior in corrosion propagation, four reinforced concrete beams with top-casting defects and load-induced cracks were used. The cracking maps of these beams, chloride profiles, corrosion maps of reinforcing steels were measured and analyzed.

For the investigation of the corrosion behavior of stirrups, two reinforced concrete beams exposed for 9 years were used. The cracking maps of beams, the corrosion maps of stirrups and the diameter loss of stirrups and main rebars were measured and compared.

According to the experimental study, the following conclusions can be drawn

1.1 In the case of the interfacial conditions of steel-concrete

1. The distribution of air bubbles in steel-concrete interface was markedly impacted by casting effect. According to the casting direction, a few of air bubbles was found in the top interface of steel-concrete, which mainly concentrated at the rib foot zone. However, in the bottom interface of steel-concrete, most of air bubbles concentrated at the rib foot area and about one quarter of these air voids appeared on the no-rib zone, while no more than 10% were found at the rib top.
2. Bleed water voids always appeared in the bottom interface of steel-concrete according to the casting direction. For the concrete samples used in this investigation, on the top side, the

interfacial thickness of steel-concrete was less than 25 μm, while, for the bottom part, the thickness was about 125 μm.

3. The cement hydration products in the steel-concrete interface consisted mainly of $Ca(OH)_2$, ettringites and C-S-H gel. The top-cast effect does not impact the type of cement hydration products around the steel rebar, but affects their structures. In the top interface of steel-concrete, no obvious crystals can be found, but some large particles can be spotted at the rib foot and rib top. However, in the bottom interface, some portlandite crystals and ettringite crystals can be observed. The microstructures of the rib foot and rib top were looser and more porous than that of the no-rib zone.
4. Top-casting defects facilitate the transportation of chloride. When top-casting defects coupled with transverse crack, chloride ions quickly penetrate from transverse crack and migrate along the interface of steel-concrete with top-casting defects to the location far from the crack.

1.2 In the case of the corrosion behavior of reinforcing steel in concrete in corrosion initiation

1. Corrosion always initiated at the bottom side of reinforcing steel when the presence of top-casting defects regardless of the presence or absence of an artificial crack, even if a higher concentration of chloride ions was found at the top side of the steel rebar than at the bottom side.
2. Corrosion initiation had no correlation with the distribution of air bubbles in steel-concrete interface, but showed high correlation with the “rib foot” of the steel rebar, as corrosion mainly initiated at the rib foot location.
3. In presence of both artificial cracks and top-casting defects, chlorides ingressed along the bottom part of the steel concrete interface and initiated corrosion at different locations along the rebar. This marked extension of pitting corrosion induced large amounts of corrosion products, which led to the formation of corrosion-induced cracks. As a result, corrosion initiation was followed by corrosion propagation. Top-casting defects associated with direct access for chlorides from the outside, e.g. via an artificial crack or load-induced cracks, is the worst scenario for corrosion and needs special attention from designers to avoid premature deterioration of reinforced concrete structures.

4. With a cover of 21 mm and the presence of top-casting defects, the service life, based on the criterion of appearance of corrosion-induced cracks, is 2.5 longer in the absence of an artificial crack than in its presence. It is expected, and is one perspective of the work, that this difference in service life will increase with larger thickness of the concrete cover.

1.3 In the case of the corrosion behavior of reinforcing steel in concrete in corrosion propagation

1. Despite the chloride ingress to rebars facilitate by cracks, there is no correlation between the opening of load-induced cracks and corrosion development or the loss of cross-section due to corrosion for relatively short-term experiments. No initiation of corrosion at some crack locations could be found in the case of no top-casting-induced defects along the steel bars. Moreover, zones far from service cracks and zones without service cracks (close to the supports) show the same loss of cross section as zones in front of service cracks.
2. Without top-casting-induced defects, there was no correlation between the existence of load-induced cracks and corrosion propagation. Although corrosion was initiated at cracks, it does not propagate, because the cracks heal. With top-casting-induced defects, corrosion initiated at cracks and propagates because of the ingress of chlorides all along the bars due to defects.
3. With top-casting-induced defects, corrosion initiated at cracks and propagates because of the ingress of chlorides all along the bars due to defects. This result could explain much of the controversy concerning cracks reported in the literature as many of the studies were performed on top casting bars. Without top-casting defects, corrosion initiated and first developed preferentially at the outside surface of reinforcing bars, closer to the concrete surface exposed to chloride environment. With top-casting defects,
4. Top-casting-induced defects strongly accelerated the corrosion process and reduced the service life of RC structures. Top-casting-induced defects coupled with top surface exposure gave the worst conditions for durability of steel reinforcements.

1.4 In the case of corrosion behavior of stirrups in corroded reinforced concrete beams

1. For the horizontal legs of stirrups, regardless of the exposure conditions, corrosion always occurred at the mid span of the tensile zone and at the ends of the compressive zone of the

reinforced concrete beam, while the opposite horizontal legs were protected.

2. The vertical legs of stirrups mainly suffered from slight corrosion. In spite of the presence of load-induced cracks, after 9 years' exposure to a chloride environment, the average cross-sectional loss of all these vertical legs of stirrups was still less than 3.5%.
3. The stirrups were not related to the main reinforcing steels in terms of corrosion. The corrosion behavior of the intersection between stirrups and main bars was in connection with the interfacial conditions between stirrups and main bars.
4. The areas of cathodic protection on steels in reinforced concrete beam increased with the development of corrosion process. In the first stage of corrosion, cathodic protection mainly took place on the top cast steel rebars in the mid span of compressive zone. In the second period of corrosion, apart from the mid span of compressive zone, the areas of cathodic protection also located at the ends of bottom cast rebars in tensile zone.

2 Recommendations

This study has achieved the main objectives listed in Chapter Ⅰ of the thesis. Due to the limited scope of the study, further research work should be carried out in the following areas

1. According to the obtained results, corrosion preferentially initiated at the rib zone regardless of the presence or absence of air voids. Apart from the effect of top-casting defects, the character of reinforcing steel, such as the microstructure of steel surface and the rebar geometry, appears to impact the corrosion initiation of reinforcing steel, for these factors may impact corrosion initiation by modifying the steel-concrete interface locally. However, this issue has received very little research attention. Therefore, in order to further understand the corrosion initiation of steel rebar in concrete, it is important to study the effect of the character of steel on corrosion initiation of steel in concrete.
2. It has been found that top-casting defects accelerate the corrosion of steel in concrete. However, the corrosion degree cannot be reliably predicted through the top-casting defects. Thus, the quantitative research on the influence of top-casting defects on corrosion development need to be studied.
3. The impact of top-casting defects on corrosion development was studied in only one type of concretes, further study should be conducted on different types of concrete to improve the interfacial conditions between steel and concrete.